University of Liege
Faculty of Applied Sciences

Modeling brain-state dependent memory consolidation

PhD thesis by **Kathleen Jacquerie** | July 2023

Supervised by

Guillaume Drion

Jury members

Guillaume Drion	University of Liege, Belgium
Pierre Sacré	University of Liege, Belgium
Alessio Franci	University of Liege, Belgium
Jean-Michel Redouté	University of Liege, Belgium
Vincent Seutin	University of Liege, Belgium
Dhruva Raman	University of Sussex, United Kingdom
Julijana Gjiorgjieva	Technical University of Munich, Germany

Academic year 2022-2023

Most of the graphical drawings are done on Adobe Illustrator or PowerPoint by myself. I acknowledge freepik (svstudioart, rawpixel, pch.vector, macrovector) and IA softwares for some artworks and spell checkers.

This thesis was funded by the Funds For Scientific Research (FRS-FNRS).

Abstract

Our brains enable us to perform complex actions and respond quickly to the external world, thanks to transitions between different brain states that reflect the activity of interconnected neuronal populations. An intriguing example is the ever-present switch of brain activity that occurs while transitioning between periods of *active* and *quiet waking*. It involves transitions from small-amplitude, high-frequency brain oscillations to large-amplitude, low-frequency oscillations, accompanied by *neuronal activity switches from tonic firing to bursting*. The switch between these firing modes is regulated by neuromodulators and the inherent properties of neurons. Simultaneously, our brains have the ability to learn and form memories through persistent changes in the strength of the connections between neurons. This process is known as *synaptic plasticity*, where neurons strengthen or weaken connections based on their respective firing activity.

While it is commonly believed that putting in more effort and time leads to better performance when memorizing new information, this thesis explores the hypothesis that taking occasional breaks and allowing the brain to rest during quiet waking periods may actually be beneficial. Using a computational approach, the thesis investigates the relationship between the transitions in brain states from active to quiet waking described by the neuronal switches from tonic firing to bursting, and synaptic plasticity on memory consolidation.

To investigate this research question, we constructed neurons and circuits with the ability to switch between tonic firing and bursting using a conductance-based approach. In our first contribution, we focused on identifying the key neuronal property that enables robust switches, even in the presence of neuron and circuit heterogeneity. Through computational experiments and phase plane analysis, we demonstrated the significance of a distinct timescale separation between sodium and T-type calcium channel activation by comparing various models from the existing literature.

Synaptic plasticity is studied to understand learning and memory consolidation. The second contribution involves a taxonomy of synaptic plasticity rules, investigating their compatibility with switches in neuronal activity, small neuronal variabilities, and neuromodulators.

The third contribution reveals the evolution of synaptic weights during the transition from tonic firing in active waking to bursting in quiet waking. Combining bursting neurons with traditional synaptic plasticity rules using soft-bounds leads to a *homeostatic reset*, where synaptic weights converge to a fixed point regardless of the weights acquired during tonic firing. Strong weights depress, while weak weights potentiate until reaching a set point. This homeostatic mechanism is robust to neuron and circuit heterogeneity and the choice of synaptic plasticity rules. The reset is further exploited by neuromodulator-induced changes in synaptic rules, potentially supporting the Synaptic-Tagging and Capture hypothesis, where strong weights are tagged and converge to a high reset value during bursting.

While burst-induced reset may cause forgetting of previous learning, it also restores synaptic weights and facilitates the formation of new memories. To exploit this homeostatic property, an innovative burst-dependent structural plasticity rule is developed to encode previous learning through long-lasting morphological changes. The proposed mechanism explains late-stage of Long-Term Potentiation, complementing traditional synaptic plasticity rules governing early-stage of Long-Term Potentiation. Switches to bursting enable neurons to consolidate synapses by creating new proteins and promoting synapse growth, while simultaneously restoring efficacy of postsynaptic receptors for new learning. The novel plasticity rule is validated by comparing it with traditional synaptic rules in various memory tasks. The results demonstrate that switches from tonic firing to bursting and the novel structural plasticity enhance learning and memory consolidation.

In conclusion, this thesis utilizes computational models of biophysical neurons to provide evidence that the switches from tonic firing to bursting, reflecting the shift from active to quiet waking, play a crucial role in enhancing memory consolidation through structural plasticity. In essence, this thesis offers computational support for the significance of taking breaks and allowing our brains to rest in order to solidify our memories.

These findings serve as motivation for collaborative experiments between computational and experimental neuroscience, fostering a deeper understanding of the biological mechanisms underlying brain-state-dependent memory consolidation. Furthermore, these insights have the potential to inspire advancements in machine learning algorithms by incorporating principles of neuronal activity switches.

Short Abstract

This thesis explores the interplay between switches in brain states associated with neuronal switches from tonic firing to bursting into memory consolidation driving by synaptic plasticity. It investigates the neuronal mechanisms underlying these switches and their impact on memory formation. By modeling neurons and circuits using a conductance-based approach, the thesis demonstrates the importance of a timescale separation between sodium and calcium channel activation for robust switches. A taxonomy of synaptic plasticity rules is provided, evaluating their compatibility with neuronal activity changes and neuromodulators. The thesis also reveals a homeostatic reset in synaptic weights during the transition from tonic firing to bursting, which is robust to heterogeneity. This reset is utilized in the Synaptic-Tagging and Capture hypothesis, enhancing memory consolidation. Additionally, a burst-dependent structural plasticity model is proposed, explaining long-lasting changes in synapse morphology and protein generation during bursting activity. The combination of bursting switches and structural plasticity improves learning and memory consolidation. It has the potential to inspire further research in experimental neuroscience and machine learning.

Acknowledgment

”A PhD is like a marathon...” This is the sentence my supervisor told me at the beginning of my project. However, I would like to correct him by saying that ”A PhD is like a trail race”, with its steep climbs and challenging descents, where the path is often unpredictable. Without the invaluable help of the individuals mentioned below, I would not have crossed the finish line.

First and foremost, I express my sincere gratitude to my supervisor, Guillaume Drion, whose support is immeasurable. He introduced me to the field of computational neuroscience, which marked an irreversible turning point in my career and personal life. From the beginning to the end, he guided me on this journey. He taught me the importance of reliability and integrity in research. He constantly pushes the boundaries to strengthen my research. He was the best coach I could have had during this trail. I understand that I must have been energy-consuming for him, with our never-ending meetings, listening to all my rehearsals, and commenting on my rainbow-colored graphs. However, I can honestly say that I have always cherished those moments and had a great time. I am grateful for the freedom he granted me. My PhD experience would not have been the same without the conferences and trips he allowed me to undertake. I would like to thank him for believing in me since my master’s degree. He is a true inspiration with his strong character and perseverance. I sincerely hope for many years of collaboration ahead.

Next, I extend my thanks to Pierre Sacré, whom I dragged into in my project. His help was invaluable, and I learned a great deal from him, from his meticulous attention to detail to his kindness. I am proud of the lab that Guillaume and Pierre are constructing, where neuroscience and engineering harmoniously converge, at the University of Liege.

In addition to my supervisor, my PhD journey would not have been the same without the help of Caroline Minne. She started as my master student, became a colleague, and is now a cheerful friend. I would also like to express my gratitude to all my nine master students, who were talented and enthusiastic young women. Their projects not only contributed to my research but also allowed me to enjoy supervising research projects and developing my teaching skills. It has encouraged me to continue pursuing an academic career.

I would also like to acknowledge Vincent Seutin, who assisted me in entering the field of experimental neuroscience. His infectious joy for life was always uplifting, and he provided valuable advice to further connect my project to electrophysiology. He taught me patch-clamp techniques, and the experiments would have not been possible without his team members, Laura Robaye and Laura Vandries, in the lab. In the GIGA Neuroscience, I cannot miss the opportunity to thank Kevin Jehasse, an amazing and fun collaborator who I am confident will become a brilliant electrophysiologist. I would also like to thank Sofian, for generously dedicating his time to bridge the gap between computational and experimental reality in my project.

I extend my appreciation to the jury members who took the time and energy to thoroughly review my dissertation, as well as all the members of the thesis committee who provided valuable advice throughout this work.

I also received tremendous support from the amazing neuroscientists I met outside of Liege at conferences, as well as the incredible members from MCN who have now become collaborators and even more, friends. I am excited to attend more Experiential Methods in Computational Neuroscience (ExMCN) conferences.

Besides research, I had the privilege of being accompanied by fantastic people in various projects such as Pot’ingé, the ReD, and MT180. These people have helped me learn a lot in shaping the person I aspire to become and grow awareness on questions such as ecology and feminism.

Finally, I would like to express my sincere gratitude to my mother and, especially, my sister Geraldine, for their unwavering support during the most challenging moments. Geraldine has been a constant source of inspiration in my life, with her courage and positive outlook on every situation. Her presence has provided me with strength and encouragement throughout my PhD. And last but not least, my friends - some who have been with me since the beginning, like Ségolène, Mariel, Marie, and Manon, and others who joined more recently, like Robin, Lola, Marie, and Lara for bringing boundless joy, laughter, and authenticity into my life. I cannot conclude without mentioning Sven. He helped me to become a better and stronger version of myself.

This long trail was filled with joy, smiles, and fascinating discoveries. I am excited to run new races carrying with me the invaluable skills and knowledge I have acquired throughout my PhD.

- A la vie.

Contents

Acronyms

5-HT serotonin. 7, 8

ACh acetylcholine. 7, 8, 15, 20

AdEx Adaptive Exponential Integrate-and-Fire. 37

ADP After Depolarizing Potential. 16

AMPA alpha-amino-3-hydroxy-5-methyl-4-isoxazolepropionic acid. 38

AMPAr AMPA receptors. 9, 24–26, 28–30, 115

BDNF brain-derived neurotrophic factor. 31

BPAP Back-Propagating Action Potential. 37, 42

BTDP Burst-Time Dependent Plasticity. 31, 47

CaM calcium/calmodulin complex. 28, 29

CaMKII calcium-calmodulin-dependent protein kinase II. 28, 29, 44

cAMP cyclic adenosine monophosphate. 29

CaN calcineurin. 28, 29

CREB cAMP-response element binding protein. 29, 31

DA dopamine. 7–9, 15, 20

E-LTD Early Long Term Depression. 29

E-LTP Early Long Term Potentiation. 28–31, 57, 58, 104, 111, 113–115

early-weight early-phase synaptic weight. 104–107, 110, 114–116

early-weights early-phase synaptic weights. 104, 106, 113, 118

ECoG electrocorticography. 9, 12

EEG Electroencephalogram. 9, 12, 13

EPSC Excitatory Postsynaptic Current. 24–26, 33

EPSP Excitatory Postsynaptic Potential. 7, 24–26, 37, 42

fMRI functional Magnetic Resonance Imaging. 9

GABA gamma-aminobutyric acid. 7, 9, 38

Glu glutamate. 7, 9, 20

HA Histamine. 7–9, 20

HH Hodgkin and Huxley. 38, 39

IEGs immediate early genes. 31

IF Integrate-and-Fire. 37

IPSP Inhibitory Postsynaptic Potential. 7

L-LTD Late Long Term Depression. 30

L-LTP Late Long Term Potentiation. 28–31, 44, 57, 104, 106, 111, 113–116

late-weight late-phase synaptic weight. 104–107, 110, 115, 116

late-weights late-phase synaptic weights. 104, 113, 117, 118

LFP Local Field Potential. 9, 12, 13

LTD Long Term Depression. 25, 28

LTP Long Term Potentiation. 25, 27–29, 31

MEA Multi-electrode array. 10, 12

MEG Magnetoencephalography. 9

NA noradrenaline. 7, 8, 20

NMDA N-methyl-D-aspartate. 39

NMDAr NMDA receptors. 9, 24–26, 39

NREM Non Rapid Eye Movement. 14, 15

PET Positron Emission Tomography. 9

PKA Protein Kinase A. 29, 31

PP1 protein phosphatase 1. 28, 29

PRP plasticity related products. 31, 57, 114

PSD postsynaptic density. 25, 104, 105

QIF Quadratic Integrate-and-Fire. 37

REM Rapid Eye Movement. 14, 15

RF receptive field. 108, 119, 123

SNR Signal-to-Noise Ratio. 107, 108, 113, 118

SPB Spikes Per Burst. 16

STC Synaptic Tagging and Capture. 31, 57, 59, 114

STD Short-Term Depression. 47

STDP Spike-Time Dependent Plasticity. 26, 31, 32, 44, 45, 57

STG stomatogastric ganglion. 22

STN stomatogastric nervous system. 22, 23

TTX Tetrodotoxine. 32

VDCC voltage dependent calcium channels. 24

CHAPTER 1

Introduction

When memorizing new information, it is commonly assumed that the more effort and time we invest, the better our performance will be. However, it turns out that taking occasional breaks associated with a restful brain may be precisely what we require. In my thesis, we investigate this hypothesis using a computational approach. We developed a biophysical neural network capable of simulating various brain states, including active learning and quiet waking states. This network can modify its connections to encode new memories. Our results suggest that during periods of quiet waking, neurons collectively engage in bursting activity, which facilitates the consolidation of memories.

This thesis introduces a computational framework that combines models of biophysical neurons operating in different brain states with models of synaptic plasticity for learning and memory. This innovative approach offers valuable insights into biophysics and has the potential to drive advancements in machine learning algorithms for artificial neural networks.

1.1 Thesis motivation

Our brain can be seen as a symphony orchestra, with billions of individual neurons as musicians, each playing their instruments, listening, and adapting to one another's sounds. Just as the orchestra can produce different compositions, our brain operates in various states known as *brain states*. During the *active state*, the orchestra performs a lively and dynamic symphony, associated with alertness, attention, and cognitive engagement. In contrast, *quiet waking* transitions the orchestra into a softer and more introspective melody, characterized by reduced consciousness. Environmental stimuli, emotional states, neuromodulation, and internal processes influence these switches between compositions.

Indeed, brain states reflect the activity of interconnected neuronal populations. Switches from active waking to quiet waking are characterized by fast transitions from small-amplitude, high-frequency brain oscillations to large-amplitude, low-frequency oscillations in the thalamo-cortical system (McGinley et al., 2015). This reflects the switches from *tonic firing*, where neurons individually respond to incoming stimuli, to *bursting*, when neurons exhibit collective activity followed by periods of silence.

Learning and memory, captivating processes in neuroscience, enable organisms to acquire, store, and retrieve information. Learning involves acquiring new knowledge and skills through experiences, while memory is the ability to retain and recall previously acquired information. We constantly rely on these capabilities in our daily lives, whether it is navigating from our home to our work, recognizing people, or speaking multiple languages, for example. The foundation of learning and memory lies in interconnected neurons forming a network. These neurons possess a crucial property called *synaptic plasticity*, that enable them to form and modify connections with each other (Lamprecht and LeDoux, 2004). Synaptic plasticity, driven by intricate molecular and cellular processes, can be simplified by Hebb's postulate : "neurons that fire together, wire together" (Hebb, 1949). Thus, neuronal firing activities play a vital role in learning and memory.

This leads us to question how switches in brain states, specifically from active waking to quiet waking, influence memory consolidation. Despite the significant interest in learning and memory, research has predominantly focused on active waking, with tonic firing, forming new connections or consolidating existing ones. By contrast, quiet waking, with synchronized bursting neurons, has received less investigation. However, considering that animals and humans are not continuously engaged in memory tasks and frequently experience moments of reduced consciousness, it sheds light on the potential role of quiet waking in memory consolidation. While less engaged in learning or active information processing,

quiet waking could support the cellular and molecular mechanisms underlying memory consolidation.

To investigate this hypothesis, we employ mathematical and engineering approaches. By constructing circuits using biophysical neuron models, we explore the interplay between switches in neuronal activities, from tonic firing to bursting, and synaptic plasticity in the context of memory consolidation.

1.2 Thesis outline

This thesis is rooted in computational neuroscience, with the goal of being accessible to the whole spectrum of neuroscience from biology to machine learning. The two first chapters establish a foundation for both fields. **Chapter 2** reviews basic neuroscience concepts, such as neurons, synaptic transmission, neuromodulation and the biological framework for brain states and synaptic plasticity. It offers insights into distinct brain states, specifically focusing on the transitions from active to quiet waking. These transitions are attributed to the behavior of neurons within the population as they switch between tonic firing and bursting activities. Simultaneously, learning and memory processes are facilitated by synaptic plasticity, a neuronal property that involves the adjustment of connections between neurons. Synaptic plasticity can be categorized into early-phase and late-phase mechanisms, each relying on distinct underlying processes. **Chapter 3** provides the framework for modeling neurons with conductance-based models and extends it to circuits. It also explains the implementation of the different traditional synaptic plasticity rules associated with the early-phase of plasticity. Modeling synaptic plasticity relies on several features such as neuron model, region, and network size, among others. It categorizes the different types of traditional synaptic rules such as phenomenological and calcium-based rules. Finally, it introduces models of structural plasticity, associated with late stages of plasticity.

Chapters 4 to **7** detail the contributions of my PhD thesis.

Chapter 4 discusses the implementation of neuron models that switches neuronal activities from tonic firing to bursting and are compatible with neuronal and circuit variability. By conducting computational experiments and employing phase-plane analyses, this study investigates six published models at the cellular and circuit levels to uncover a specific cellular property that guarantees robust switches. This property is intricately linked to the kinetics of membrane proteins, known as ion channels, which play a crucial role in regulating neuronal activity. To ensure the development of robust models, it is vital to faithfully incorporate the specific dynamics of these proteins into computational models.

Chapter 5 delves into the state-of-the art in synaptic plasticity models. Based on a taxonomy of different categories of models, we aimed to emphasize the similarities and the discrepancies between them. It also questions the robustness of these rules in the face of neuronal and circuit perturbations in the presence of switches in neuronal activities. It specifically focuses on qualitatively testing the response of two categories of synaptic plasticity rules, namely phenomenological and calcium-based rules, when subjected to small perturbations.

Chapter 6 tackles the core of this thesis and combines the model of biophysical neurons and synaptic plasticity models. It monitors the evolution of the synaptic connections between neurons during switches from active learning, associated with tonic firing to quiet waking, associated with bursting. Using computational experiments and mathematical analyses, it compares several models of synaptic plasticity and tests the effect of neuronal variability and network heterogeneity. It unravels the role of interplay between active waking and quiet waking associated with a transition from tonic firing to bursting with traditional synaptic plasticity.

Chapter 7 investigates how quiet waking with the collective bursting activity can promote memory consolidation. A novel burst-driven structural plasticity is presented to propose a mechanism to enhance memory consolidation during quiet waking. Using various memory tasks, combinations of different switches in neuronal activities and the different rules are compared.

Chapter 8 summarizes the thesis and its limitations and it proposes future perspectives. **Chapter 9** briefly discusses my side projects. This last chapter is followed by **Supplementary Materials**. The roadmap of my PhD thesis is depicted in the following illustration, which is divided into chapters. Each chapter begins with a gray box that offers a concise overview of the context and the chapter's significance within the overall thesis. Additionally, it refers to the published output associated with that particular chapter.

Chapter 2
Background
in neuroscience

Brain-state

Active state | Quiet state

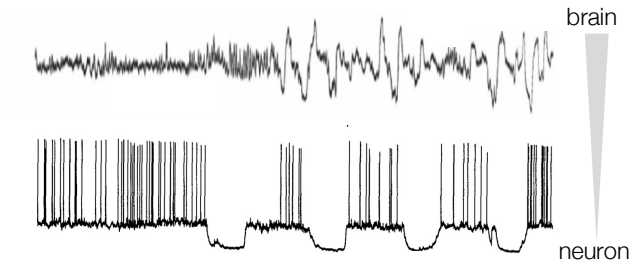

tonic | burst

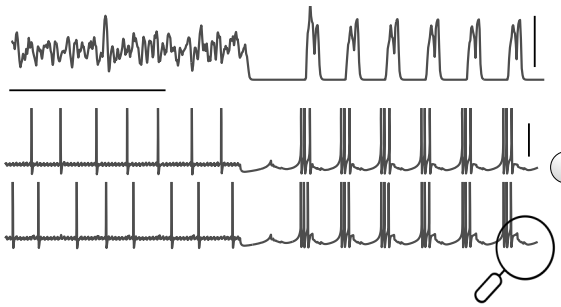

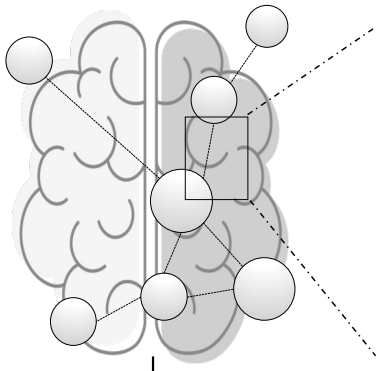

Memory

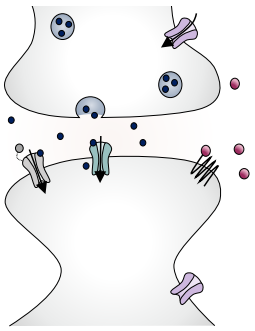

synaptic plasticity

Chapter 3

Modeling neurons & circuits | Modeling synaptic plasticity rules

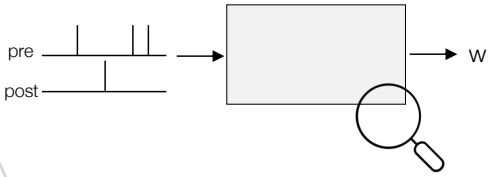

Chapter 4

Neuronal property required for robust switches to plasticity and variability

Chapter 5

Are current synaptic plasticity robust to neuronal variabilities?

Chapter 6

Interplay between switches
from tonic firing to bursting & synaptic plasticity

- ❑ Different rules are compared
- ❑ Mathematical analyses of the effect of bursting on synaptic plasticity

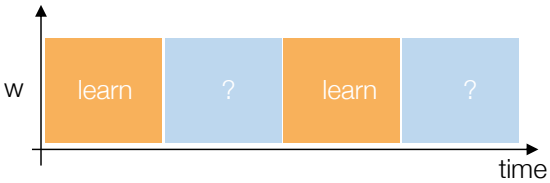

Bursting drastically affects memory consolidation

Chapter 7

- Creation of a burst-driven novel plasticity rule
- Comparison with traditional synaptic plasticity rules in many configurations of switches with and without burst on various memory tasks

Chapter 8

Brain-state dependent memory consolidation for

Experimental neuroscience

Artificial intelligence

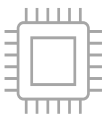

Neuromorphic engineering

1.3 Thesis contributions

The main results of the thesis can be found in the following publications. Contributions to conferences with posters and talks are available on my ORBI profile `https://orbi.uliege.be/profile?uid=p179634`.

. Kathleen Jacquerie, Caroline Minne, Juliette Ponet, Nora Benghalem, Pierre Sacré, Guillaume Drion (2022). Switches to rhythmic brain activity lead to a plasticity-induced reset in synaptic weights.
Biorxiv preprint
`doi:10.1101/2022.07.15.500198`

. Kathleen Jacquerie, Caroline Minne Guillaume Drion (2022). Neuromodulation of synaptic plasticity rules avoids homeostatic reset of synaptic weights during switches in brain states.
COSYNE March, 2022, poster (Lisbon, Portugal).
`https://hdl.handle.net/2268/288490`

. Kathleen Jacquerie and Guillaume Drion (2021). Robust switches in thalamic network activity require a timescale separation between sodium and T-type calcium channel activations.
PLoS Computational Biology.
doi:10.1371/journal.pcbi.1008997

. Kevin Jehasse, Kathleen Jacquerie, Alice de Froidmont, Camille Lemoine, and Thierry Grisar, Katrien Stouffs, Bernard Lakaye and Vincent Seutin (2021). Functional analysis of the F337C mutation in the CLCN1 gene associated with dominant myotonia congenita reveals an alteration of the macroscopic conductance and voltage dependence.
Molecular Genetics and Genomic Medicine, e1588
doi:10.1002/mgg3.1588

. Kathleen Jacquerie (2021). Introduction aux signaux et systèmes : Fascicule d'exercices (ULiege Manual for students).
Pre-print ULiege server.

. Kathleen Jacquerie and Guillaume Drion (2019). A cellular mechanism makes switches in brain states compatible with synaptic plasticity.
COSYNE March, 2019, poster (Lisbon, Portugal)
`https://hdl.handle.net/2268/246930`

CHAPTER 2

Background in Neuroscience

This chapter offers a comprehensive background in neuroscience. The initial section revisits fundamental concepts, providing clear definitions and outlining the roles of key elements in this thesis, including neurons, ion channels, synapses, and neuromodulators. It then delves into an exploration of brain states, elucidating the reasons for their transitions and their link to neuronal activities. The intriguing relationship between brain states and neuromodulation is also discussed. The final segment of this chapter centers around synaptic plasticity, providing a detailed explanation of its various mechanisms.

2.1 Elementary concepts of neuroanatomy, neurons, and neuromodulators

2.1.1 Neuroanatomy

Our brain is the organ that controls our motor skills, our memory, our emotion, our breathing, or most process that governs our body and our mind (Purves, 2014). It receives and emits chemical and electrical signals throughout our body to react to the external world, to drive our behavior, and to build our consciousness. This organ is divided in several structures performing different functions (Figure 2.1A). For example, the *cortex* is the outer part of the brain and is responsible for a variety of functions including movement, emotion, and sensory perception among others. The main part of the cortex is the *neocortex* and the rest is called allocortex. In the neocortex, cortical neurons are organized in six layers stacked on each other. They can also be studied in columns. It is divided into different regions associated with different functions. For example, the frontal cortex is involved in decision-making while the occipital cortex processes visual information. The *thalamus* is located deep in the brain and acts as a relay station for sensory information. It receives signals from the body and sends them to the appropriate region in the cortex. It is involved in regulating consciousness, sleep, and arousal. The *hippocampus* is a seahorse-shaped structure made of allocortex and located in the temporal lobe of the brain and is primarily involved in the formation and consolidation of memories. It is also involved in spatial navigation, which is the ability to navigate and remember the locations of objects in our environment. This thesis briefly mentions several structures crucial to understand the brain's functioning, such as the basal ganglia, striatum, brainstem, locus coeruleus, basal forebrain, nucleus basalis of Meynert, amygdala, raphe nuclei, substantia nigra, ventral tegmental area, and hypothalamus. Their location and roles are briefly described in Supplementary Material B. Like the components of a factory, these structures are interconnected and work together to sustain life. A deficiency in any of these parts can lead to pathological behaviors and disrupt the brain's proper functioning. Therefore, studying neuroanatomy and coordination between these structures has been crucial in developing therapeutic solutions.

2.1.2 The basics of neuron structure and function

Our brain is composed of more than 86 billion of neurons (Herculano-Houzel, 2009). These fundamental units process the information between the body and the brain. Neurons are excitable cells that are triggered by chemical or electrical signals, and they establish communication among themselves through the generation of electrical signals called *action potentials*. Each neuron consists of three main parts: the *dendrites*, which collect the incoming signals, the *soma*, known as the cell body, which integrates these signals and the *axon*, which transmits the response by releasing a neurotransmitter at its terminal part.(Figure 2.1B).

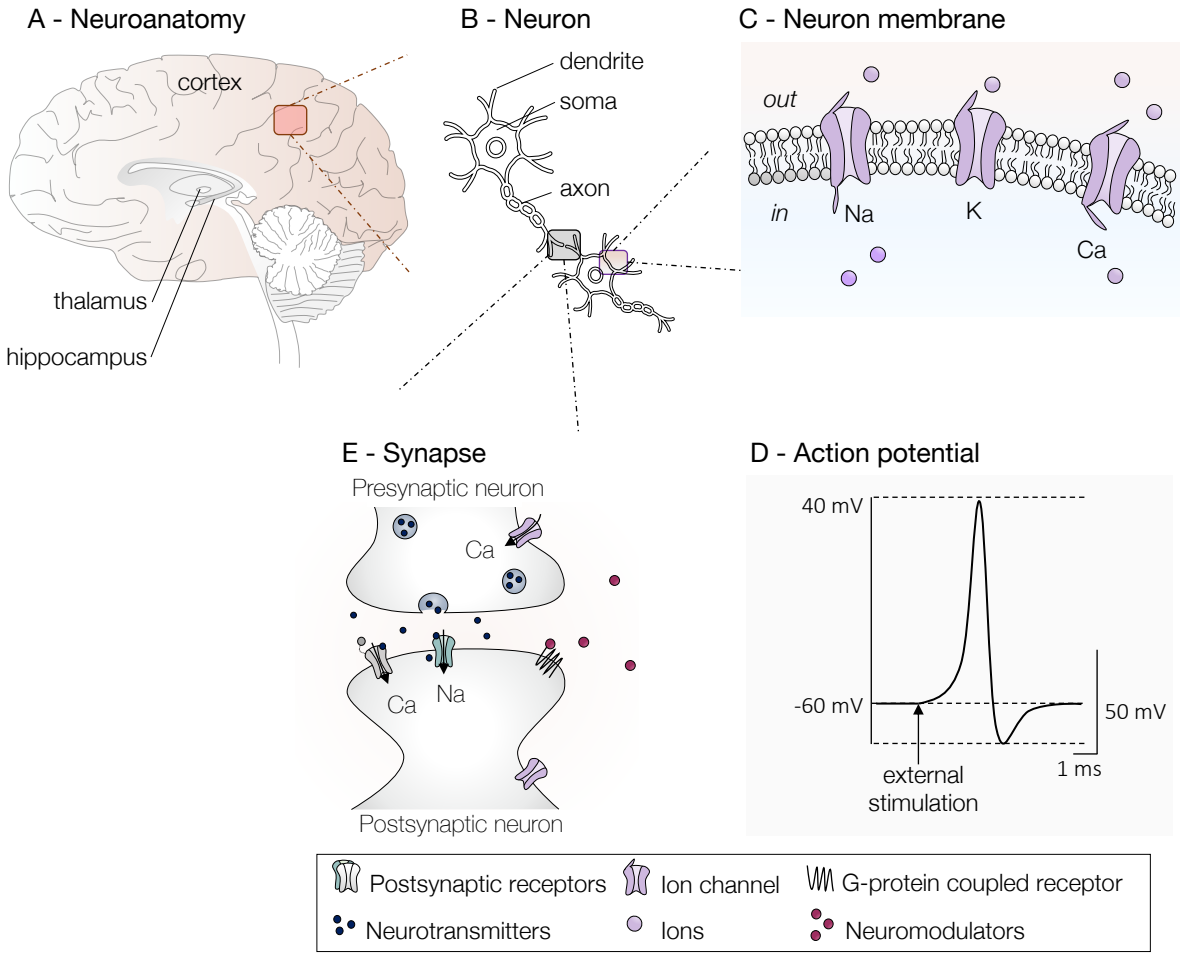

Figure 2.1: Hierarchical Structure of the Brain and the Neuronal Action Potential. A. The brain is composed of distinct structures, each with a unique function. **B.** The neuron receives information from the dendrites, processes it in the soma, and sends the response along the axon. **C.** Ion exchange through ion channels in the neuron's membrane, generating the membrane potential. **D.** The all-or-nothing rise in the membrane potential is called the action potential, which is used to transmit information to other neurons. **E.** The synapse is the region where the pre- and postsynaptic neurons connect and communicate via neurotransmitters. The electrical signal is transformed into neurotransmitter release that binds to postsynaptic receptors. Inspired from (Bear et al., 2016; Drion, 2013)

Neurons share similar components with classical cells such as the plasma membrane that separates the intra- and extracellular compartments (Drion, 2013; Hille, 2001). This membrane is permeable to small molecules and water, but almost fully impermeable to ions and large molecules (Figure 2.1C). *Ion channels*, which are particular proteins embedded in the membrane, allow the flow of ions through the membrane. They are selective to a given type of ions such as sodium (Na^+), potassium (K^+), calcium (Ca^{2+}), or chloride (Cl^-) and they regulate the concentration of these ions across the membrane. Therefore, the concentration of positive and negative ions on both sides of the membrane and its permeability generate an electrical potential called the *membrane potential*. Without any external signal, the neuron is at its resting potential around -60 mV in a majority of cases, which is maintained by the balance of ion concentration and ion channel activity.

When a neuron receives a stimulus such as stress, pressure, electrical current, or chemical transmitters, ion channels open, allowing the flow of ions through the membrane, causing a change in the potential (Bear et al., 2016). The neuron responds to this change, by altering its membrane potential. A positive applied current is making the memrane potential less negative, known as *depolarization*, while a negative applied current reduces the membrane potential, known as *hyperpolarization*. A sufficient depolarization from the resting potential causes the all-or-nothing rise in the membrane potential, corresponding to the *action potential* or *spike*. This also reflects the cell *excitability*.

2.1.3 Ion Channels: their structure and role in neuron excitability

Ion channels are membrane proteins that allow the flow of ions following their gradient concentration. For example, ions channels allowing calcium flow are called calcium channels. These gateways have specific opening and closing mechanisms that are regulated by complex processes. They can be dependent on the membrane voltage or the calcium

concentration. They open or close at different timescales. Their kinetics are critical in the regulation of the membrane potential and govern neuron excitability. Ion channels are commonly characterized by gates, which include activation and inactivation gates, representing intricate molecular subunits. Neurons can produce a variety of responses thanks to the interplay between the different ion channels that have various gating kinetics and voltage-dependency.

2.1.4 The mechanism of action potential generation

The most familiar neuronal response is the action potential (Figure 2.1D). At rest, the membrane potential is around −60 to -70mV (Purves, 2014; Bear et al., 2016). The resting membrane potential is established through the uneven distribution of ions between the intracellular and extracellular environments, as well as the varying permeability of the membrane to different ion species. When the neuron receives an excitatory input, it depolarizes. If the input is weak, the neuron will go back to its resting state. If the input is strong, it activates the choreography of ion flows that build up the action potential. Sodium channels are voltage-dependent. They allow sodium ions to enter which further depolarizes the membrane voltage. Due to the voltage dependency, more ions are entering and it causes positive feedback. It creates a rapid depolarization known as the rising phase of the action potential. As the membrane reaches its peak, the voltage-dependent potassium channels open allowing potassium to exit the cell. It leads to a repolarization, which occurs on a slower timescale. The membrane voltage may transiently become more hyperpolarized than the resting state, a phenomenon known as hyperpolarization. This is facilitated by the closure of ion channels, the gradual inactivation of certain voltage-dependent potassium channels, and the action of ion pumps (Byrne et al., 2014).

This choreography is governed by the dynamics of sodium and potassium channels. At rest, sodium and potassium activation gates are closed and sodium inactivation gate is open. The excitatory stimulus causes the depolarization of the membrane voltage that causes the fast opening of the sodium activation gate resulting in sodium ion influx. The potassium activation gate is opening but on a slower timescale resulting in potassium ions release after the initial influx of Na+. In parallel, the sodium inactivation gate slowly closes stopping the sodium ion flux. The neuron hyperpolarizes causing the sodium channel activation gate and the potassium channel activation gate to close due to their voltage-dependency and sodium channel inactivation to open again.

Now that the mechanisms of action potential generation are detailed, the remaining question is how this electrical signal is transmitted to other neurons.

2.1.5 The Synapse: from action potential to neurotransmitter release

An action potential is generated at the axon initial segment, then it propagates along the axon. It reaches the axon terminal called the *synapse* and it triggers the release of chemical substances, called the neurotransmitters, to the target neurons (Figure 2.1E). The electrical signal is transformed into a chemical signal. There also exists an electrical synapse called gap junction. Its physiological relevance is limited in adult brains and therefore this thesis focuses on the chemical ones (Heidelberger et al., 2014).

The membrane of the presynaptic terminal is depolarized by the arrival of the action potential. This opens the voltage-gated calcium ion channels, allowing calcium to enter the presynaptic terminal and trigger a signaling cascade. Synaptic vesicles fuse with the membrane of the presynaptic neurons and release the stored neurotransmitters in the synaptic cleft. These neurotransmitters bind to the postsynaptic neuron receptors. It generates the opening or closing of these receptors translated by depolariz tion or hyperpolarization of the postsynaptic membrane potential that respectively define an Excitatory Postsynaptic Potential (EPSP) or an Inhibitory Postsynaptic Potential (IPSP).

2.1.6 The neuromodulators: from the definition to the projecting circuit and their main roles

Neurotransmitters vs Neuromodulators: understanding the distinction

Neurotransmitters are chemical substances released by neurons to targeted neurons. Different types exist: noradrenaline (NA), also called norepinephrine, acetylcholine (ACh), serotonin (5-HT), dopamine (DA), Histamine (HA) glutamate (Glu) and gamma-aminobutyric acid (GABA). They target postsynaptic receptors in order to convey the electrochemical signal. In this way, they perform the synaptic transmission.

Neuromodulators are a subset of neurotransmitters with a more diffuse release compared to the targeted action of the neurotransmitters during the synaptic transmission. Neuromodulators bind to G protein-coupled receptors and alter the cellular or synaptic properties of the neurons. Instead of carrying fast information as performed by neurotransmitters, they can modulate the synaptic transmission over a long period of time by modifying the electrical behavior of the pre- or the postsynaptic neurons.

As a brief reminder, two main classes of receptors exist(Purves, 2014). The *ionotropic receptors*, also called neurotransmitter-gated or ligand-gated channels, directly open ion channels as soon as neurotransmitters bind to the protein. The *metabotropic receptors* are membrane receptors that trigger a cascade of intracellular events using a second messenger signal. They are indirectly linked to ion channel regulation.

Box 1 - Fun fact about histamine and allergies

Allergies occur when the immune system misidentifies harmless substances as threats, triggering histamine release and causing symptoms like sneezing, itchy eyes, congestion, and wheezing. Antihistamines alleviate symptoms by blocking histamine receptors, including those involved in regulating sleep, which can lead to drowsiness. This drug example highlights the wide-ranging effects of neuromodulators.

Overview of major neuromodulators and their functions in the brain

Neuromodulators play fundamental roles in our brains, and their actions are diverse. However, due to their diffuse effects, it can be challenging to identify their key functions. Moreover, they often work together, as demonstrated by research (Gu, 2002; Avery and Krichmar, 2017; Nadim and Bucher, 2014). The following is a brief, non-exhaustive overview of the main neuromodulators, categorized according to the location of their generating neurons, their projection regions, and their primary functions.

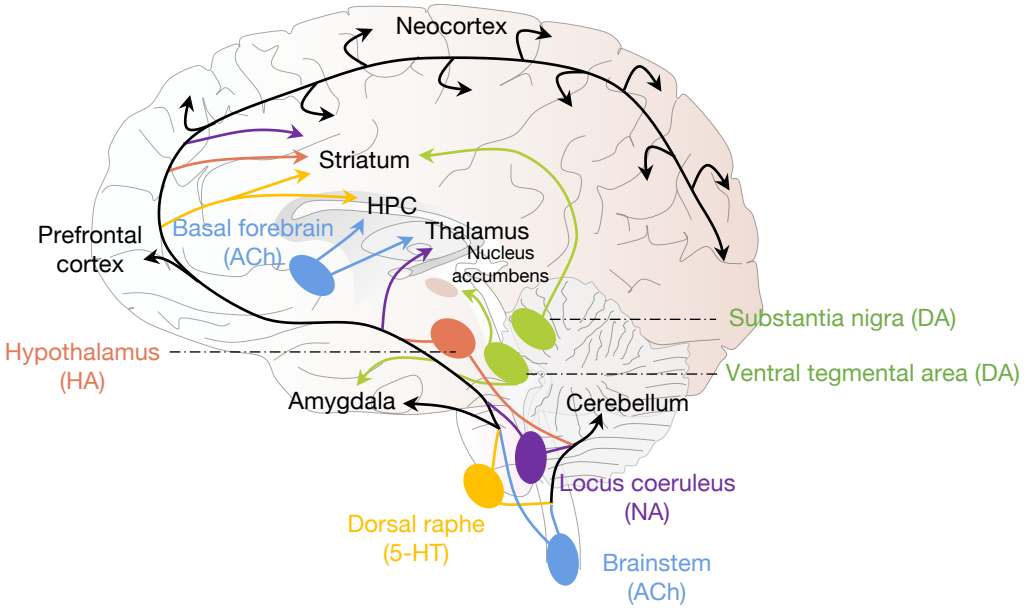

Figure 2.2: Major neuromodulatory pathways in the human brain. Each pathway is indicated by a colored oval representing the schematic location of the neuromodulatory neurons projecting into different brain areas, as shown by the arrows. The noradrenergic (NA) pathway is drawn in purple, the cholinergic (ACh) pathway is in blue, the serotonergic (5-HT) pathway is in yellow, the dopaminergic (DA) pathway is in green, and the histaminergic (HA) pathway is in red. HPC means hippocampus. Inspired from (Bear et al., 2016; Mei et al., 2022)

- noradrenaline (NA): Noradrenergic neurons are located in the locus coeruleus located in the pons. They project to the cortex, the cerebellum, the hippocampus, the thalamus, the striatum and the hypothalamus. They are related to arousal and they mediate vigilance and alertness (Figure 2.2, purple).

- acetylcholine (ACh): Cholinergic neurons are mainly located in two regions either in the basal forebrain or in the nucleus basalis of Meynert and the brainstem. They are innervating the neocortex, the thalamus, the hippocampus and the amygdala among others. There are two types of receptors: nicotinic (ionotropic) and muscarinergic (metabotropic). They regulate arousal, attention and play a role in learning, memory (especially spatial memory), mood control, and behavior control (Figure 2.2, blue).

- serotonin (5-HT): Serotonergic are found in the raphe nuclei of the brainstem. They project to the cortex, hypothalamus, striatum, hippocampus, and amygdala. Their roles are related to reward, cost assessment or coping with the environment as well as learning, memory or sleep (Figure 2.2, yellow).

- dopamine (DA): Dopaminergic neurons are located in the midbrain, in the substantia nigra and the ventral tegmental area. They project to the striatum but also to nucleus accumbens, amygdala, hypothalamus and cortex. This neuromodulator is well-known as the pleasure chemical and its role in the reward system. It also plays a key role in movement, cognition, motivation, and neuroendocrine control. These dopaminergic pathways play a critical role in diseases such as Parkinson and schizophrenia and Alzheimer's disease (Figure 2.2, green).

- Histamine (HA): Histaminergic neurons are mainly located in the tuberomammillary nucleus (in the hypothalamus). They have widespread projections in various brain areas including the cortex (Gu, 2002). Histamine plays a role in wake-sleep regulation, arousal, motor activity, learning, stress, aggression, pain perception, self-stimulation, reinforcement and other processes listed in (Gu, 2002) (Figure 2.2, red).

- glutamate (Glu): Glutamate is the most abundant excitatory neurotransmitter in the nervous system. Neurons generating glutamate are distributed in the brain. The receptors are AMPA receptors (AMPAr) (α-amino-3-hydroxy-5-methyl-4-isoxazolepropionic acid receptor) or NMDA receptors (NMDAr) (N-methyl-D-aspartate). They play multiple roles, for example they are involved in the regulation of sleep (Watson et al., 2011).

- gamma-aminobutyric acid (GABA): GABA is the most inhibitory neurotransmitter. It helps to maintain homeostasis by maintaining an excitatory-inhibitory balance. Neurons synthesizing GABA are widely distributed in the brain. GABA receptors are either ionotropic, called $GABA_A$ receptors, or metabotropic, called $GABA_B$.

2.1.7 Tools for Investigating the Brain: from Behavior to Single Neuron Activity

Neuroscience research relies on a variety of techniques to investigate the function and structure of the brain. These techniques vary in their spatial and temporal resolutions, invasiveness, and technical demands. In the early stage of neuroscience, scientists had no other options than opening the brain and observing the organ, the anatomy, and practicing surgery (Buzsáki, 2009). Nowadays, with the development of new technologies, reading the brain from large scale to micro scale is much easier (Figure 2.3). Here is a non-exhaustive list of the different techniques commonly used in neuroscience:

- Behavior:
  Observing behavior is a simple and technically undemanding method for gaining insights into human or animal functioning. It can yield valuable information about decision-making, memory retrieval, and sexual behavior among others. Researchers may passively observe behavior or request that participants perform specific tasks.

- Brain imaging - using metabolic activity as an indirect measure of the neuronal activity

  - functional Magnetic Resonance Imaging (fMRI):
    Neural activity induces changes in metabolic processes such as blood flow or oxygen supply. This non-invasive technique indirectly measures brain activity in different brain regions by detecting variations in blood oxygenation levels. The temporal resolution is not accurate enough to measure rapid changes in brain activity.
  - Positron Emission Tomography (PET):
    Similar to fMRI, it is a non-invasive imaging technique using radioactive tracers to measure metabolic activity such as the glucose uptake or occupation of receptors for example.

- Electroencephalogram (EEG):
  The EEG is a non-invasive technique using surface electrodes on the scalp. These electrodes record summed activity of large populations of neurons in large brain areas such as the population activity of cortical neurons. It is commonly used to study brain rhythms that are associated with different cognitive states (Figure 2.4, top).

- Magnetoencephalography (MEG):
  MEG measures magnetic fields generated by the neural activity in the brain. Like EEG, it is a non-invasive technique that provides the overall activity of large populations of neurons. It is commonly used to record deeper structures such as the thalamus and the brainstem.

- electrocorticography (ECoG):
  The ECoG is an invasive technique to record the population activity of neurons in a large area (order of millimeters square) by placing a grid of electrodes directly at the surface of the brain. It records the superficial layer of the brain (Figure 2.4, second recording). It has more spatial precision than the EEG.

- Local Field Potential (LFP):
  Extracellular recording of a population activity of neurons in a localized area of the brain, typically using micro-electrodes. It reflects the collective activity of populations with a better precision than EEG or ECoG. It is often used to study neuronal synchrony (Figure 2.4, center).

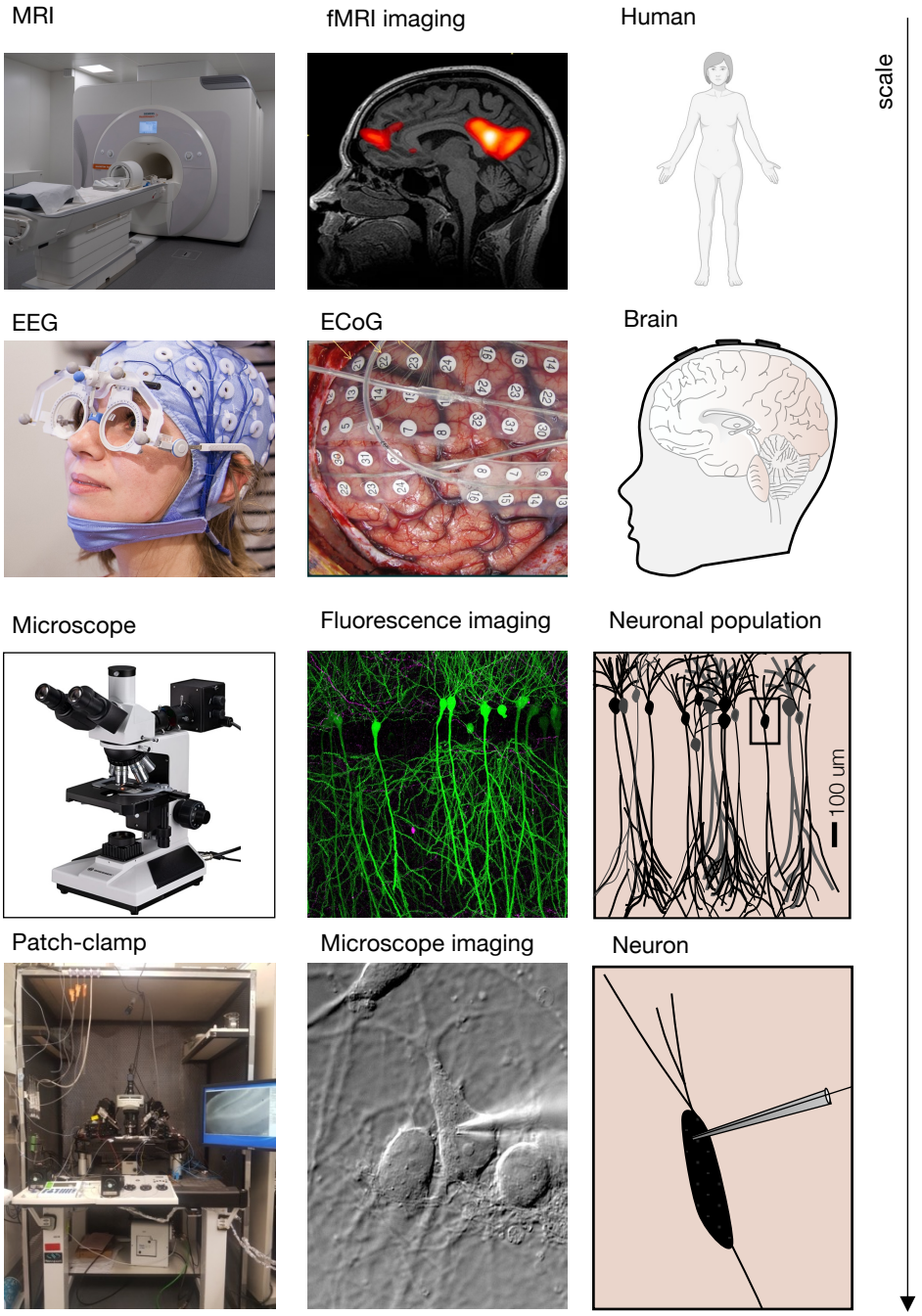

Figure 2.3: Experimental techniques to study brain activity from whole brain imaging to cellular recording. **MRI** is a type of scan using magnetic fields to provide an image of the whole brain (fMRI imaging). **EEG** records the electrical activity of the brain via electrodes on the scalp. **ECoG** is similar but the electrodes are placed at the surface of the brain. **Microscope** is a device to observe very small objects. **Fluorescence imaging** helps to differentiate elements on a petri dish. **Patch-clamp** set up with microscopes, electrodes, and pipettes to record the electrical activity of a neuron. The **microscope imaging** shows the pipette on a neuron. Images for MRI (URL, e), fMRI scan (URL, b), Human (Biorender), EEG (URL, g), ECoG (Greiner et al., 2016), Microscope (URL, c), Fluorescence imaging (Bloss et al., 2018), Patch-clamp (URL, d), Microscope imaging (URL, a). Schematics were drawn by myself.

- Multi-electrode array (MEA):
  A cluster of sensors able to simultaneously record the activity (action potentials) of hundreds of neurons (Figure 2.4, center).

- Single neuron recording (Figure 2.4, bottom)
    - extracellular recording: by placing an electrode in the extracellular medium, this technique allows for the recording of sharp variations in the potential but not the membrane potential itself. It is useful for recording neuronal firing.
    - intracellular recording: a sharp pipette is inserted inside the neuron and is connected to an amplifier to record the electrical activity of individual neurons.
    - patch-clamp: a glass pipette is used to create a continuity between the pipette and the membrane. This allows currents flowing through ion channels (voltage-clamp). By maintaining a constant applied current (current-clamp), it allows variation of membrane potential with high precision. This technique provides a high temporal and spatial resolution but it is invasive and technically demanding.
- Microscope imaging:
  To observe the anatomy of the brain, surgery, dissection and microscope provide inside about the morphology of the different structures of the brain from organs to proteins.
    - Optical imaging: by using a fluorescent substance, calcium concentration can be monitored during the brain or neuronal activity.
    - Calcium Imaging: in vivo, fluctuations of the calcium concentration can be measured in tens of neurons simultaneously using fluorescent dyes.
    - Voltage-Sensitive Dye Imaging: Similarly to calcium imaging, it uses fluorescent dyes to measure changes in the membrane potential of neurons.
    - Two-photon imaging: it is a type of microscopy to record neuronal activity by measuring fluorescence. This device provides a good temporal resolution and a superb spatial resolution (dendritic spines can be visualized).
    - Optogenetics: This technique permits targeting and controlling the activity of particular cells by using light-sensitive proteins that are genetically engineered.

Each of these techniques has its advantages and disadvantages concerning their spatial or temporal resolutions and their invasiveness. Researchers must carefully choose the appropriate methods to answer their research questions.

Box 2 - ***in-vitro*, *in-vivo*, *ex-vitro* and *in-silico***

These terms are sometimes confusing. Here is a brief reminder:
- *in-vitro*, translated in glass: the experiments take place in a test tube.
- *in-vivo*, translated in life: the experiments take place in the living organism.
- *ex-vivo* refers to the experiments taking place in a tissue that has been extracted from an animal or human and is kept alive.
- *in-silico* refers to silicon chips used in computers: the experiments are performed on computers and via virtual simulations.

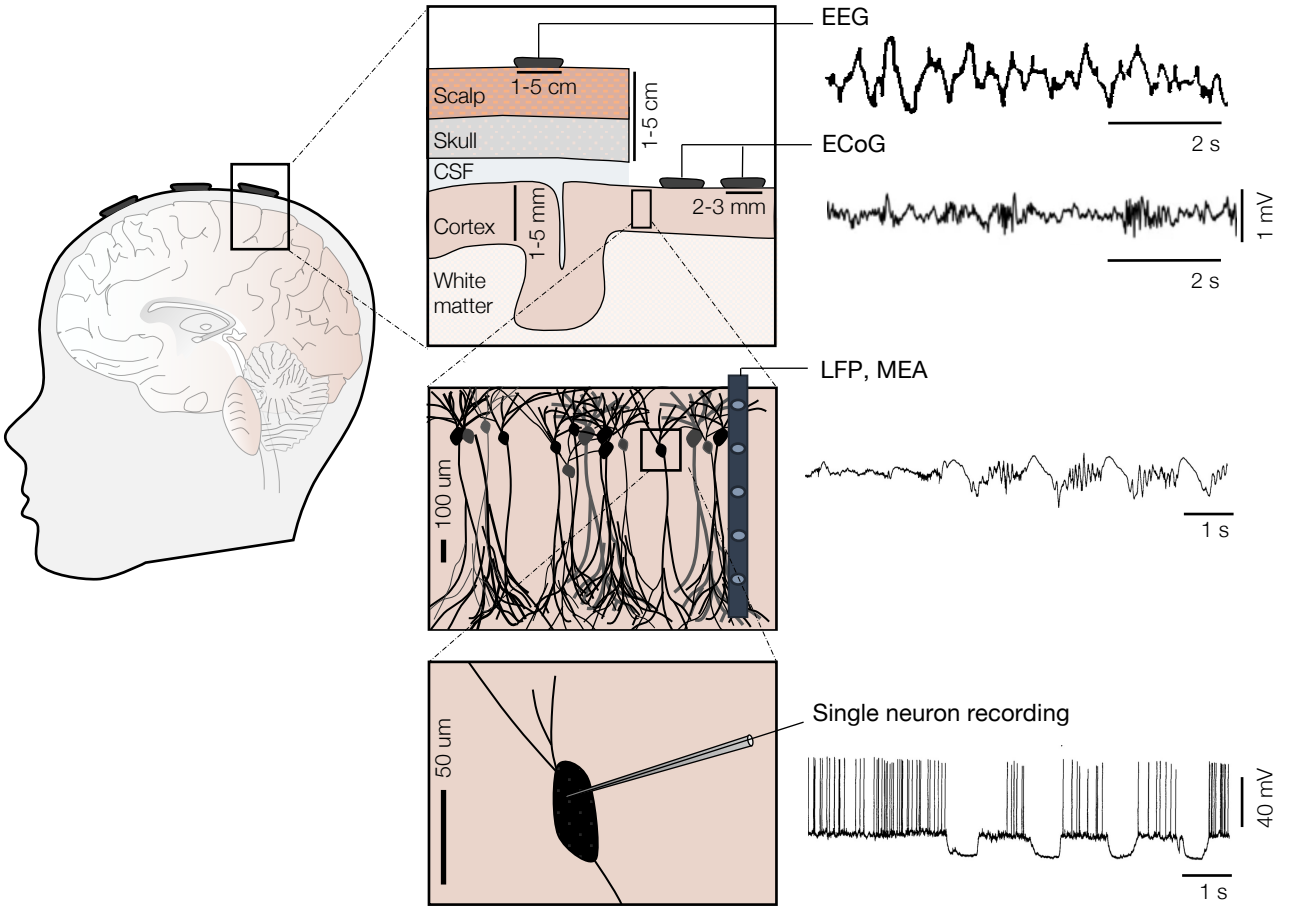

Figure 2.4: Schematic of the measurements from the neuronal population to a single neuron activity. EEG is recorded at the scalp via electrodes and shows brain waves. ECoG is similar except that the electrode is directly at the surface of the brain. LFP are obtained via deep brain electrodes or using Multi-electrode array (MEA). The recording of a single neuron is obtained via small pipettes (here patch clamp recording, more precisely current-clamp). Inspired from (Hagen et al., 2018) and recordings taken from EEG (McCormick and Bal, 1997), ECoG (Konerding et al., 2018), LFP and Single (Contreras and Steriade, 1995).

2.2 Understanding brain states: from brain activity to neuronal activity

2.2.1 Brain state identification

Our everyday life is sequenced by different states. During the night, we sleep and dream, and then we wake up and begin the day. We are capable of walking, looking around, and rapidly reacting to our environment. We can also engage in complex actions, think, and remember. These transitions between states are commanded by our brain (Bradley et al., 2022).

A *brain state* mirrors the overall activity pattern of the neuronal population that can vary depending on the context. Indeed, the brain is made of interconnected neurons that communicate with each other, receive information and process it. Ongoing neural activities give rise to rich patterns that can be observed at different scales; from molecule and cell levels to microcircuits or networks up to the whole brain. Capturing brain states at a given spatial scale requires appropriate techniques: from neuronal recordings with a pipette to population activity with LFP or EEG. The fluctuations between brain states occur at various timescales (Figure 2.5). At one extreme, brain states change over at hundreds of milliseconds during sharp shifts of attention, fast memory retrieval, or when several action potentials are generated in response to sensory stimuli, such as a change in light intensity. Intermediately, brain states are fluctuating in the range of hours with wake-sleep cycles. In the extreme case, brain states evolve throughout brain development or during long-term changes in behavior, such as skill acquisition or recovery from injury.

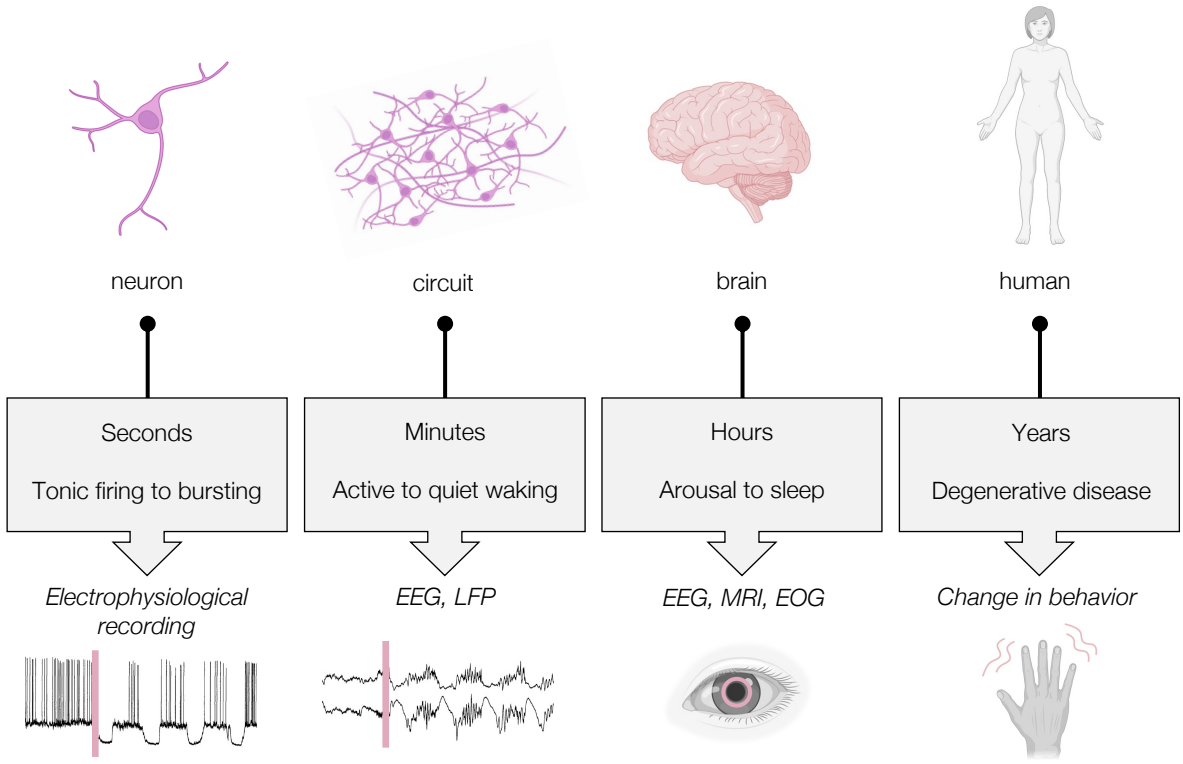

Figure 2.5: Brain states can be studied from the neuronal level to the human level. (left to right) Neurons switch their electrical activity (e.g. switch from tonic firing to bursting) in the range of millisecond to second timescale. A circuit is composed of several neurons, and a change in their electrical activity is reflected in the circuit rhythm (e.g. switch from small-amplitude, large-frequency LFP oscillation to large-amplitude, slow oscillation). Brain states reflect the activity of neuronal and circuit population (from arousal to sleep, the brain has a different activity that can be recorded by changes in pupil diameter or EEG oscillations among others. Brain states can occur throughout aging with pathological transitions observed in small behavioral changes (e.g. tremors in neurodegenerative disease increase with aging). Recordings from (Contreras and Steriade, 1995) and artworks from Biorender.

I follow the scientific definition provided in (Bradley et al., 2022; Zagha, 2014) telling that a brain state is "a recurring set of neural conditions that is stable for a behaviourally significant period of time. This set of neural conditions is often reflected in distinct patterns of ongoing activity but can also be revealed by neural responses to stimuli."

Distinct brain states are characterized by distinct neural signatures mostly defined by the frequency and the spatiotemporal patterns of the LFP (Kringelbach and Deco, 2020). They are often associated with identifiable cognitive or motor states. In addition, other features such as the breathing speed, the muscle tone, the eye movement, the pupil diameter, the heartbeat might help to distinguish the brain states (Reimer et al., 2014; McGinley et al., 2015).

Classification and characteristics of brain waves in different states

Figure 2.6 reveals a large variety of brain waves that were classified based on the frequency content in the EEG or LFP oscillations (Tyree and Luis De Lecea, 2017; Buzsáki, 2009):

- gamma oscillations at 30 to 100Hz - associated with an engaged consciousness.
- beta oscillations at 12 to 30Hz - associated with active waking, concentration, and mental alertness.
- alpha oscillations at 8 to 12Hz - associated with quiet waking, resting, relaxed, and calm state of mind.
- theta oscillations at 4 to 8Hz - associated with sleep and deep relaxation.
- delta oscillations at 0.5 to 4Hz - associated with deep sleep, the slowest brain waves.

The familiar example of sleep helps to get more insight into the fluctuations in brain states (McGinley et al., 2015; Molnár et al., 2021). Classically, deep sleep is characterized by a large-amplitude and low-frequency signal with no eye movement and reduced muscle tone, referred as Non Rapid Eye Movement (NREM), associated with a succession of delta and theta oscillations. By opposition, waking is associated with small-amplitude faster frequency fluctuations, associated with a mixture of alpha and beta oscillations. These two stages are often described respectively as a global synchronization dominated by low-frequency content or global desynchronization. The term Rapid Eye Movement (REM) is often encountered for the dream stage that looks similar to the waking state except for paralyzed muscle tone and rapid-eye-movements are observed.

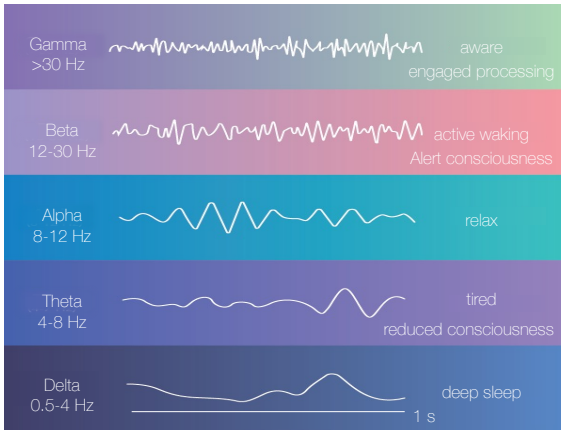

Figure 2.6: Brain wave oscillations and the associated state of arousal. Fast oscillations are related to engaged processing and slow oscillations correspond to deep sleep. Image from (URL, f)

This simplistic distinction between waking and sleep has been challenged and the concept of *active waking* and *quiet waking* have been introduced. During quiet waking, larger amplitude, lower frequency oscillations are observed for example in the somatosensory, visual, and auditory cortical regions. These oscillations are suppressed as soon as humans or animals enter active waking due to for example motion or attention shift (McGinley et al., 2015).

Fluctuations in brain states

The brain's evolution during a given action or mindset is a fascinating phenomenon, as is understanding how the transition between different states occurs. For instance, when we are meeting someone important, our heart rate increases, our hands sweat, and our body temperature rises, all of which are orchestrated by the brain operating in an alert state. Various pathways, such as brain circuitry, movement-related factors, and breathing, influence the transition between states (Tantirigama et al., 2020). However, neuromodulation is the major factor that affects the transition. Figure 2.7 provides insight into the close relationship between brain states and neuromodulators. The cocktail of chemical substances is constantly fluctuating. During active waking, the brain has a high concentration of noradrenaline, acetylcholine, serotonin, dopamine, and histamine. These concentrations decrease in quiet waking and are very low during Non Rapid Eye Movement (NREM) sleep.

Several diseases, such as schizophrenia, epilepsy, autism, Alzheimer's, and Parkinson's disease, dramatically alter brain states (Uhlhaas and Singer, 2006; Kühn et al., 2004; Cannon et al., 2014). Parkinson's disease, for instance, is often recognized by motor dysfunctions such as arm tremors, which are explained by a drastic change in the expected brain state.

The mechanisms underlying switching between brain states are not yet fully understood. Studying the interplay between neuromodulation and switches in brain states at the cellular level can provide insight into these mechanisms.

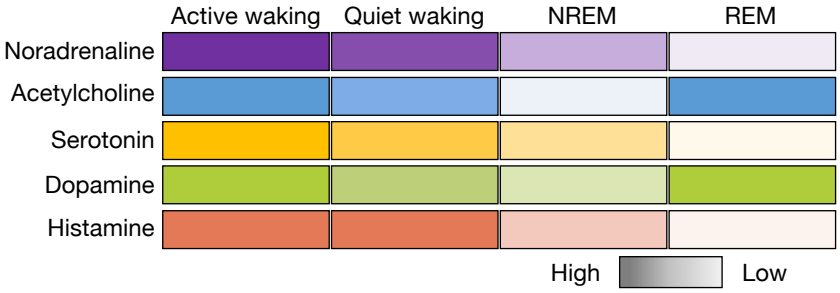

Figure 2.7: A visual representation of the fluctuations in neuromodulators present during different brain states. Active waking is characterized by a high quantity in the five major neuromodulators. This abundance is reduced in quiet waking and even more in NREM. By contrast,REM has a ACh and DA level. Inspired by (Tyree and Luis De Lecea, 2017).

2.2.2 Neuronal activity reflects the brain state

The diversity of neurons in the brain is what allows for the myriad of brain states that we experience. Neurons come in different morphology, shapes and sizes, and possess unique types of ion channels which allow them to generate electrical signals and communicate with other neurons. Their different neuronal properties allow them to generate firing patterns. The term *firing pattern* refers to the specific sequence of action potentials the neuron generates over time. It depends on the neuron itself as well as the timing and the intensity of the received stimulus. The term neuronal excitability is also often met in literature and refers to the ability of a neuron to generate an action potential in response to a stimulus.

Classification of neuronal firing patterns

Figure 2.8 uncovers the existence of the different firing patterns often encountered in biology. This is a non-exhaustive list and description of these patterns (Komendantov et al., 2019; Izhikevich and Hoppensteadt, 2004):

- *tonic firing*: the neuron produces a succession of action potentials in response to an external stimulus or a sustained input (also called tonic spiking, regular spiking).
- *bursting*: the neuron generates a sequence of clustered action potentials occurring at high frequency separated by silent periods (Kucyi and Davis, 2017).
- *plateau potential*: the neuron can maintain its spiking activity for a relatively long period of time after the occurrence of an excitatory stimulation, it is a form of bistability (Marder, 2003).
- *pacemaking*: the neuron generates a constant succession of action potentials at a fixed frequency independently of any external input, only by relying on its intrinsic properties.
- *rebound bursting*: a burst of action potentials in response to a hyperpolarization input after its end.
- *adapting spiking*: the neuron generates a succession of action potentials with a gradual decrease in its firing rate over time in response to a constant stimulus.

For example, the Blue Brain project engages in a gargantuan challenge: the reconstruction and simulation of a column of the neocortex. They model different cell types classified based on their morphology and their firing patterns (Markram et al., 2015). Conversely, in the context of my thesis, we decided to focus my interest on two firing patterns: tonic spiking and bursting.

Bursting: definition, characteristics, shape, and mechanisms of generation

Already investigated 25 years ago, this firing pattern was defined by ”clusters that often last at most 25 ms and contain several action potentials from two to 6 at a high frequency (about 200 Hz)” (Lisman, 1997). The interest in this particular firing pattern has continued to grow.

Brain regions containing neurons able to burst
Bursting is observed in several brain regions (Shao et al., 2021; Zeldenrust et al., 2018) such as in the cortex, mostly in pyramidal neurons; in the hippocampus, in the pyramidal neurons in CA1 region; the thalamus, in the thalamocortical and neurons of the reticular nucleus; in the hypothalamus, in gonadotropin-releasing hormone (GnRH) neurons; in the cerebellum, in Purkinje and granules cells; in the brainstem and in the ventral tegmental area, in dopaminergic neurons (Figure 2.9, top-left). It is also observed outside the brain and in different species such as in pre-Botzinger complex with

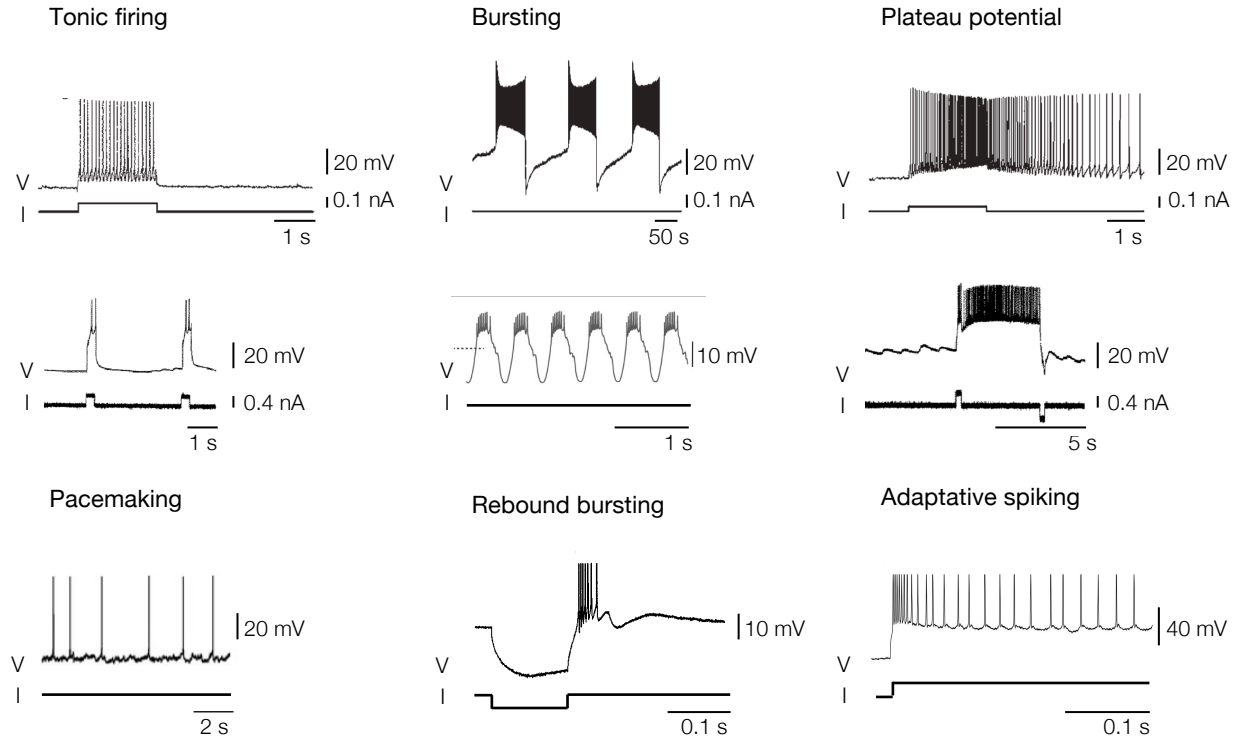

Figure 2.8: The most often encountered neuronal firing patterns. **Tonic firing**: neuronal response to an input signal by generating successive action potential (top: dorsal horn from (Marder, 2003); bottom: dorsal gastric neuron in (Weimann et al., 1993)). **Bursting**: several action potentials are generated followed by a quiescent period (top: dorsal horn from (Marder, 2003); bottom: lateral pyloric neuron in (Marder and Rue, 2021)). **Plateau potential**: the spiking activity is maintained after the stimulation (top: dorsal horn from (Marder, 2003); bottom: dorsal gastric neuron in (Weimann et al., 1993)). **Pacemaking**: continuous spiking activity at the same frequency without any input (respiratory neuron in (Ramirez et al., 2011)). **Rebound bursting**: bursting in response to a hyperpolarization input (thalamic neuron in (McCormick and Bal, 1997)). **Adaptative spiking**: the spiking frequency decreases over time (visual system interneuron in (Gabbiani and Krapp, 2006). V is the membrane potential and I is the input current.

the respiratory neurons; in stomatogastric ganglion in crustaceans with the anterior bursting neuron; in abdominal ganglion in aplysia with the neuron R15; in circuit involved in central pattern generator (Grillner and Kozlov, 2021) and in pancreatic beta cells (Jeong, 2012).

Bursting is characterized by several features
Bursting can be described by different features (Van Pottelbergh et al., 2018; Drion et al., 2012) (Figure 2.9, top-right):

- The *active period* is the duration composed of the succession of action potentials, called the burst or spike train.
- The *quiescent period* is the silent period between the spiking period, also called the intraburst interval.
- the *interburst period* is the timing between two distinct bursts of action potentials. The *interburst frequency* is the inverse of the interburst period.
- the *intraburst period* is the timing between two action potentials inside the burst, also called the inter-spike interval. It can vary within the burst. The *intraburst frequency* is the inverse of the intraburst period.
- the *duty cycle* is the ratio between the intraburst period and the interburst period.
- the number of *Spikes Per Burst (SPB)*.
- the *spike latency* is the delay between the start of the depolarization and the start of the spike train.
- the *plateau* potential: the burst of action potentials occurs at a more depolarized potential than the hyperpolarized state. It allows to identify an up and down state in the firing pattern. We note that this name is also used as a type of firing pattern.
- the *After Depolarizing Potential (ADP)* the burst is finished by a small depolarization bump before hyperpolarizing.

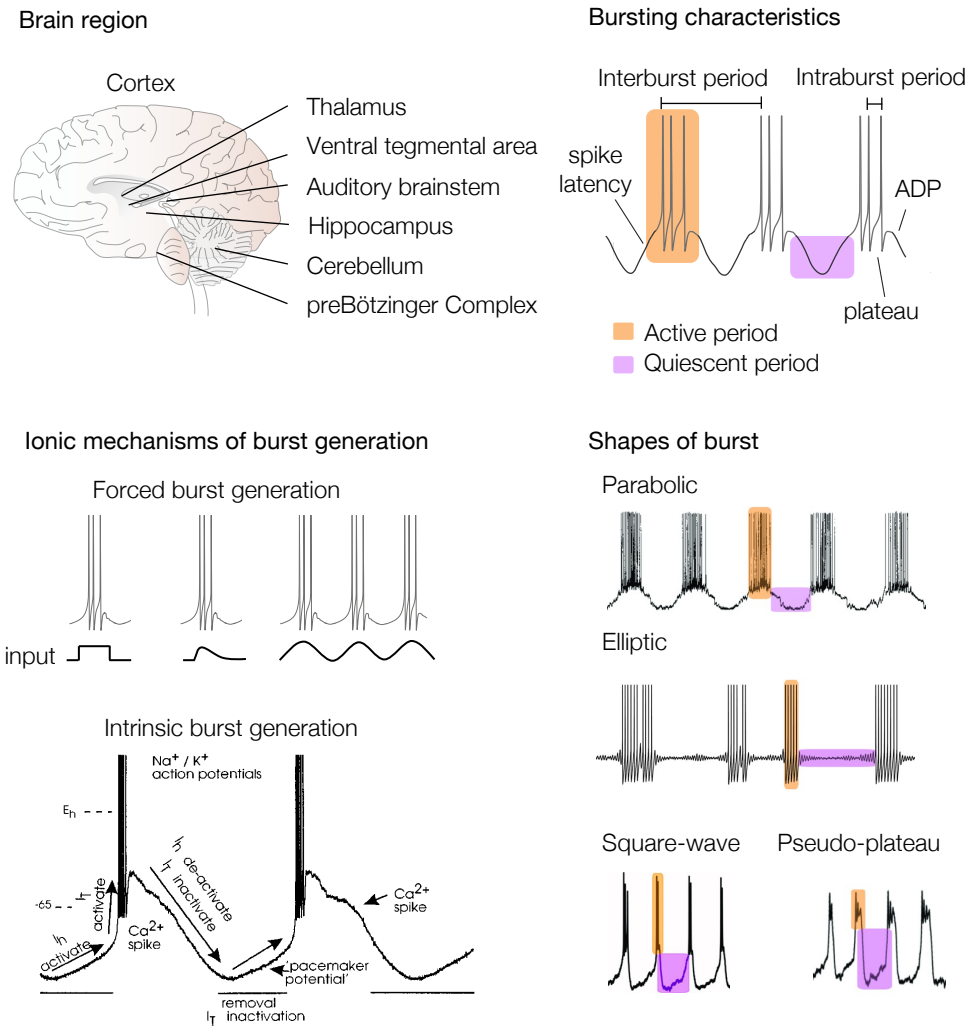

Figure 2.9: Bursting: definition, characteristics, shape, and mechanisms of generation. Bursting neurons are found in various brain regions (Zeldenrust et al., 2018). It is characterized by several features and it can take several shapes (Desroches et al., 2022). The burst generation can be forced due to external input or it can be generated by the interplay of different ionic currents (McCormick and Bal, 1997).

Bursting can take several shapes

Bursting can display different signatures that are described by the oscillations (Desroches et al., 2022; Drion et al., 2012; Van Pottelbergh et al., 2018; Smith et al., 2000) (Figure 2.9, bottom-right):

- the *parabolic bursting*: the train of spikes is at a noticeable depolarized state with respect to the hyperpolarized membrane voltage. It is observed in Aplysia R15 for example (Adams, 1985; Turrigiano et al., 1995)
- the *elliptic bursting*: the neuron discharges continuously during the active period and stops without a noticeable plateau potential. It is observed in pancreatic beta-cells (Bertram et al., 2008) but it is more often encountered in mathematical models.
- the *square wave bursting*: the burst is a bit more depolarized compared to the parabolic bursting observed in sensory neurons.
- the *pseudo-plateau bursting*: a strong plateau potential is observed and the amplitude of the successive action potentials is decreasing.

Mechanisms behind bursting

Two categories of burst generation are considered according to (Jeong, 2012; Jeong et al., 2012) (Figure 2.9, bottom-left):

- *forced burst generation*: the burst is the consequence of stimulation with a current that drives the neuron above or below the action potential threshold. This current can be the result of either an external simulation via an electrode

- for example, a square-wave signal current or synaptic input. In the case of synaptic input, either the neuron is normally spiking but a periodic inhibitory provokes intervals of silence or the neuron is silent and receives periodic excitatory synaptic input causing the clusters of action potentials (Figure 2.9)

- *intrinsic burst generation*: the neuron is able to burst due to the different ion channels. Their opening and closing kinetics orchestrate the intrinsic generation of bursting such that intrinsic currents depolarize the neuron until it reaches its firing threshold, allowing the occurrence of several action potentials. Then, the neuron hyperpolarizes on an ultraslow timescale. This sequence is repeated due to the interaction of the different ion channels. Experimental neuroscientists have been trying to identify the ionic currents necessary for this autonomous pattern generation. The T-type calcium channels have been recognized to play a critical role in many cases (Cain and Snutch, 2010) (Figure 2.9) .

Neurons can switch between firing patterns

Neurons are fundamental units of the brain; their varieties in morphology, roles and now their firing patterns is at the basis of the complexity and power of our brain. Figure 2.8 reveals the richness in neuronal firing patterns. But most surprisingly, one neuron can switch from a firing pattern to another firing pattern. It is mainly caused by the modulation of ion channel properties. Several factors can modulate these properties such as:

- neuromodulation (like dopamine, serotonin or acetylcholine): neuromodulators alter the ion channels for example by blocking or recruiting them, changing their densities, altering their kinetics (Steriade et al., 1993).

- synaptic input: an inhibitory input can switch a neuron from regular spiking to bursting by activating some ion channels that were previously inactivated.

- environmental changes: temperature and pH among others are external factors that can modify the ion channels (Hedrick and Waters, 2012; Haley et al., 2018).

- other mechanisms such as a change in the resting potential or changes in the extracellular concentration of potassium (Fröhlich and Bazhenov, 2006).

Switches from tonic spiking to bursting

Mechanisms at the cellular level
The thalamic neuron has been a nice support for many years to understand what are the key mechanisms of the transition from tonic spiking to bursting (McCormick and Bal, 1997; Cain and Snutch, 2010) (Figure 2.9, bottom-left). This neuron is mainly driven by a sodium current, several types of potassium currents, a T-type calcium current and a hyperpolarization-activated current (H current). At a depolarized state, the neuron is governed by the dynamics of the sodium and potassium channels generating a succession of action potentials. Due to a change in the neuromodulatory state, for example, the neuron is hyperpolarized which results in calcium channel activation. They open at a slow timescale generating a calcium influx that depolarizes the neuron. A fast sodium current and a delayed rectifier potassium current produce action potentials. Simultaneously, calcium channels close on an ultraslow timescale. The neuron hyperpolarizes, and no more action potential is generated. The hyperpolarization-activated is activated and redepolarizes the neuron to activate the whole process again.

To switch from tonic spiking to burst, the neuron must be hyperpolarized to ensure the de-inactivation of calcium channels. As explained earlier in the mechanisms of switches, this can be achieved by applying an external hyperpolarizing current or neuromodulators that affect the ion channel properties and set the neuron in a hyperpolarized state.

Switching from tonic spiking to bursting is not only associated with transitions from wakefulness to sleep
This section explains the relationship between this switch at the neuronal level and the switch in brain state with the associated behavioral state (Takahashi et al., 2006).

The switch from tonic spiking to bursting is often associated to the transition from wakefulness to sleep. Indeed, during wakefulness, neurons are reacting to incoming signals and discharge accordingly in tonic spiking (Figure 2.10A). This is translated at the population level by a small, high-frequency signal. Transitioning to sleep, neurons are bursting and a synchronization of the activity is created resulting in a large, low-frequency LFP signal (McCormick and Bal, 1997). It is often referred to active (*up*) and inactive (*down*) periods occurring at low frequency. Tonic mode was thought to be the default mode during wakefulness to relay the information while bursting mode was associated with a blocking of the information from the external mode.

But more and more evidence confirms that bursting occurs during wakefulness (Fanselow et al., 2001; Steriade et al., 2001; Zagha, 2014; Reimer et al., 2014). Some recordings were even obtained in monkey (Guillery and Sherman, 2002) while in the past it was mainly on rodents and cats. Bursting plays a role in the information processing during waking

behavior (Sherman, 2001; Ramcharan et al., 2000). For example, this is illustrated by the presence of slow oscillatory activity during quiet waking with the absence of movement (Figure 2.10B). As soon as the animal walks or moves its whisker, the slow rhythmic activity is suppressed as shown respectively in (Polack et al., 2013) and (Lee and Dan, 2012). These two states are also referred to as *synchronized state* when the collective activity of neurons provokes this slow oscillation, and *desynchronized state* when neurons are spiking in tonic without being synchronized. "While the slow oscillation was once thought to be restricted to periods of slow wave sleep, animal studies now suggest that it may occur in the waking state, particularly during periods of inattentiveness or drowsiness" (McCormick and Salkoff, 2015).

These switches in wakefulness have an impact on sensory processing (Steriade et al., 2001). This bidirectional switch allows us to meet changing behavioral demands (Crandall et al., 2015).

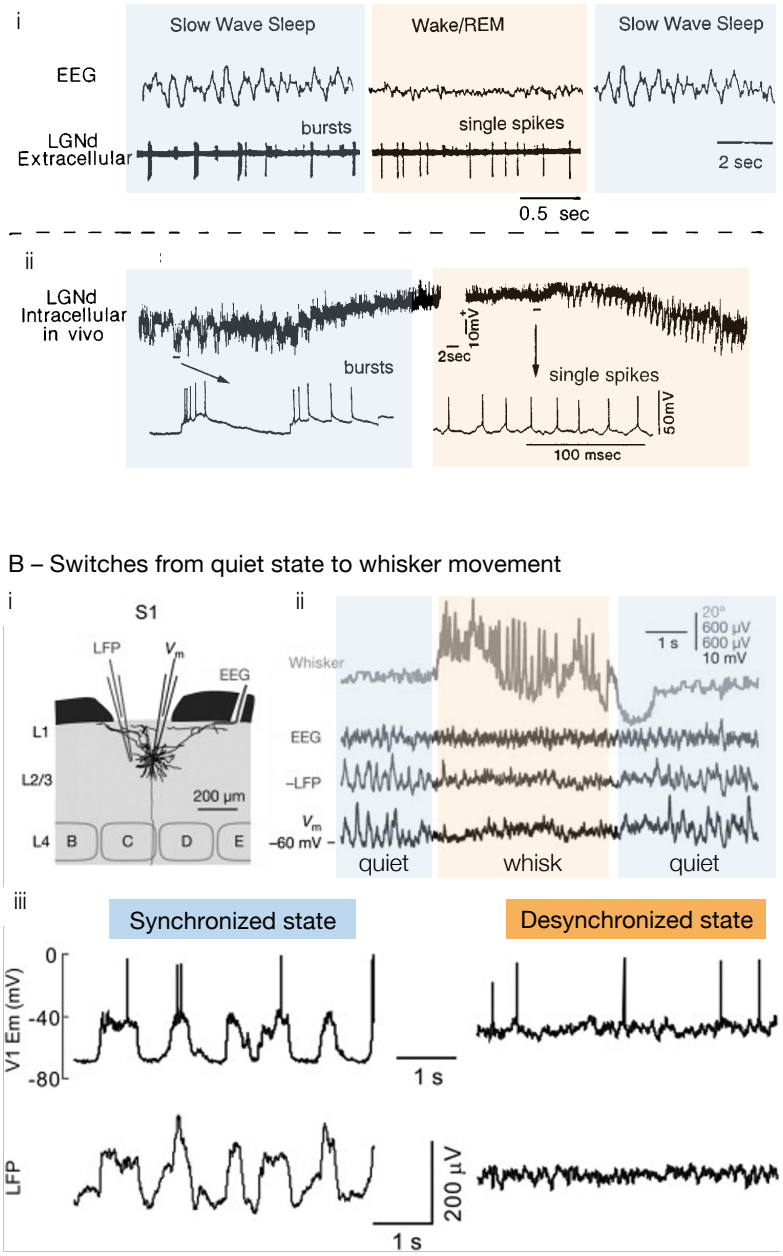

Figure 2.10: Switches from tonic firing to bursting are associated with different brain state transitions. A. EEG signal switches from large-amplitude, low-frequency oscillation to small-amplitude, large-frequency oscillation during sleep to wake transition (McCormick and Bal, 1997). **B.** A similar oscillations shift is observed when a rodent starts to move its whisker as observed in the EEG signal and neuronal recording. Bursting is associated to a synchronized state between neurons. Tonic is associated to a desynchronized state (Lee and Dan, 2012)

Examples from thalamic neurons, dopaminergic neurons, sensory processing, and neurological diseases
Thalamic neurons have been presented in the previous section as one of the useful support to investigate switches from tonic firing to burst and vice-versa. Figure 2.11C and D show single-cell neuronal recordings of this switch associated to the transition from wakefulness to sleep. But this switch occurs in other regions (Figure 2.11A), is initiated by different factors (Figure 2.11B) and is associated with diverse switches in brain states and behavior. Several examples are shown in Figures 2.11E to M.

Cortical neurons are also switching under changes in neuromodulators (ACh, NA, HA and Glu) during wake-sleep cycles (Figure 2.11E). The switch from regular spiking to bursting is observed in paradoxal sleep and palatable food consumption (Dahan et al., 2007; Ji et al., 2009).

Midbrain opaminergic neurons have two modes of discharge: pacemaking or bursting (Tsai et al., 2009; Johnson et al., 1992). Without stimulation, the neuron is in pacemaking mode (Figures 2.11J, K). It fires at a small frequency around 1 Hz. Under special conditions, such as NMDA current or ion channel blocker (e.g. apamin), neurons are bursting (Figures 2.11J, K). The release of DA in this case is much larger and called phasic. It is associated in some of these neurons with what is called "positive error in reward prediction", meaning that the animal obtains a reward that is larger than anticipated (Schultz, 2007).

Similarly, respiratory neurons switch from pacemaking to bursting under the control of noradrenaline (Figure 2.11I).

Switches in neuronal firing can be induced by movement initiation. For example, interneurons transition from bursting activity to regular tonic firing as soon as an animal moves on a treadmill (Figure 2.11G). In Xenopus, motor neurons are tonically firing during swimming, but switching to bursting is associated with a state where the animal struggles (Figure 2.11H).

With the current climate crisis, understanding the effect of temperature on the brain has become increasingly urgent. For instance, under certain conditions, an increase in temperature can switch neurons from bursting to tonic firing (Figure 2.11L).

Neurons are sensitive to drugs. (Cichon et al., 2023) observed that ketamine can trigger 'non-ordinary brain states' by suppressing the spontaneous activity of some neurons and activating some silent ones (Figure 2.11M). The brain enters a particular mode in which it is disconnected from the external environment but still performing internal subjective experiences (Cichon et al., 2023; Yang et al., 2018).

We have the ability to switch from hearing to listening. It is translated by a switch in brain states mirroring the switch in neuronal activity in the auditory cortex and other brain regions (De Franceschi and Barkat, 2021). It is confirming that sensory inputs in this case sound is processed in different manners depending on the neuronal firing patterns. This state-dependent sensory processing also occurs in the olfactory cortex (Murakami et al., 2005). Response to smells is bigger while neurons are spiking compared to the weaker response while neurons are in low-frequency rhythm.

Some diseases are marked with pathological brain states. As mentioned earlier, Parkinson or Alzheimer diseases (PD or AD) are well-known examples of abnormal brain oscillations compared to normal conditions. In normal conditions, neurons in the subthalamic nucleus (STN) neurons and globus pallidus (GP) neurons are in tonic activity - characterized by a small amplitude, high-frequency content at the population level (Figure 2.11F). In abnormal conditions (in PD), the STN and GP are in low-frequency rhythmic bursting (Bevan, 2002; Beurrier et al., 1999). In the context of dystonia - a neurological disease that causes the muscles to contract involuntarily, Purkinje cells that were tonically spiking in control conditions exhibit an abnormal high-frequency bursting (Fremont et al., 2014).

For pain processing, depending on the operation mode of the neuron: the pain is differently processed by our brain. In spiking mode, the innocuous stimuli are associated with acute nociception, while the generation of plateau potentials, by increasing the excitability of deep dorsal horn neurons plays a role in central sensitization (Marder, 2003). The electrical traces of the different operating modes are shown in Figure 2.9,top row). To illustrate with a simple example, the contact with a needle can be interpreted by three sensations: either pain is only felt when the needle touches the skin (spiking mode), or pain persists after the needle removal (plateau potential mode) or pain is abnormally felt even without stimulus (bursting mode). There are also examples in the context of anxiety, depression epilepsy, schizophrenia, and addiction among others. Better understanding the modification of discharge patterns could help to develop therapeutic treatments.

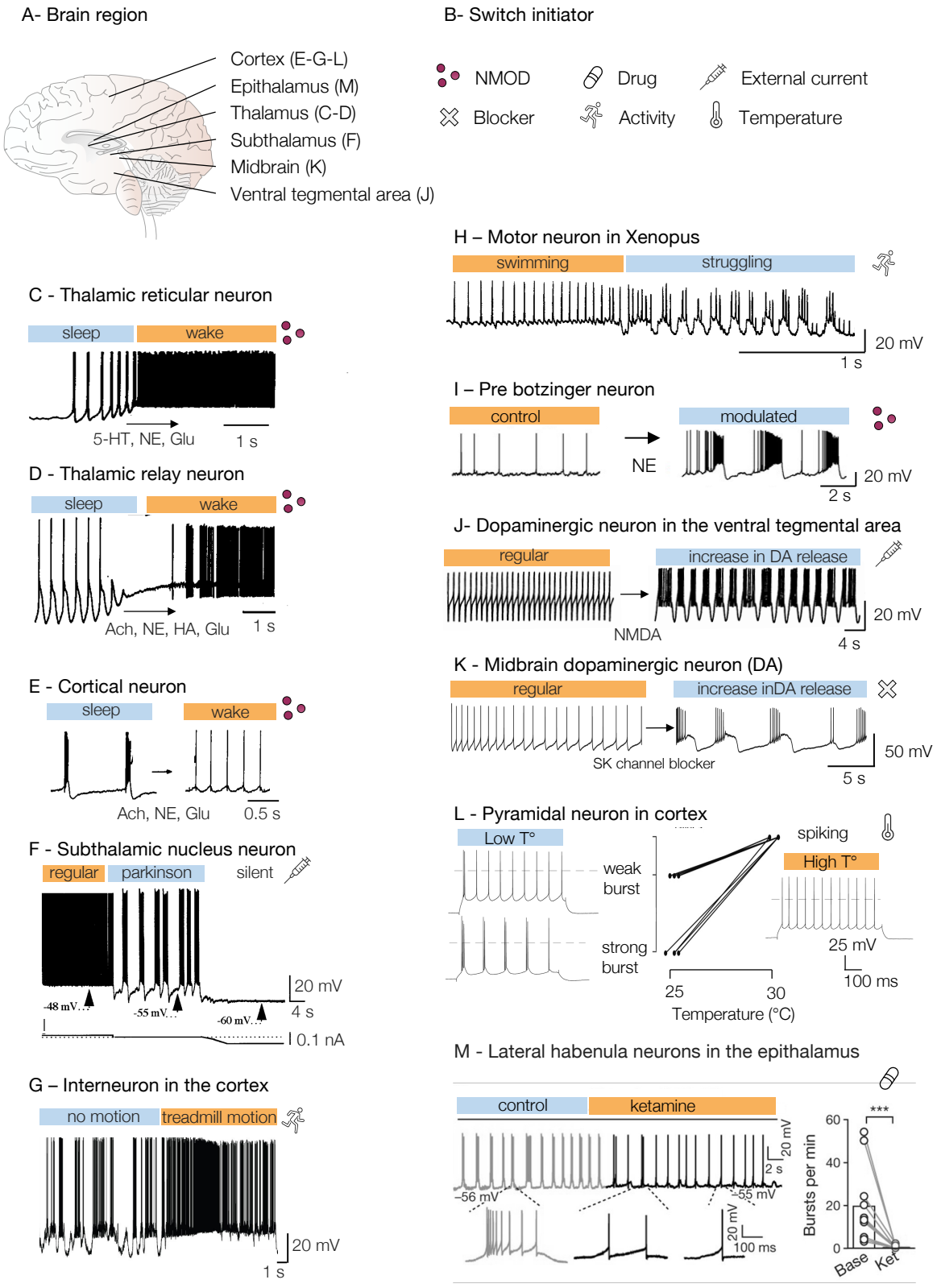

Figure 2.11: Neurons are switching from tonic firing to burst in various brain regions, caused by several factors and associated to several brain states. A. Switches are observed in a myriad of regions. **B.** Several types of switch initiators exist. **C-M** Examples of switches from tonic firing to bursting (or vice-versa) in different neuron types, under different initiators. Recordings (C,D,E) from (McCormick and Bal, 1997) , (F) from (Beurrier et al., 1999), (G) from (Polack et al., 2013), (H) from (Soffe, 1993), (I) from (Ramirez et al., 2011), (J) from (Johnson et al., 1992), (K) from (Ji et al., 2009), (L) from (Hedrick and Waters, 2012), (M) from (Yang et al., 2018). ACSF = artificial cerebrospinal fluid

2.3 Understanding the multimodal roles of neuromodulators in neural processing

Neuromodulators are powerful substances in our brain that control and enable rapid reactions. Their mechanisms are complex due to their diffuse projection and broad operating modes (see Section 2.1.6). They are responsible for configuring circuits that reflect different behaviors (Marder et al., 2014). Figure 2.2 illustrates the challenges in studying the effects of neuromodulators, as their actions are coordinated and they have multiple targets, posing a significant struggle in understanding their impact. A recent review by (Shine et al., 2021) sheds light on the fact that investigating neuromodulation spans from the microscale, e.g. with modifications in neurotransmitters and recruitment or suppression of ion channels, to the macroscale, e.g. with changes between different behaviors such as stress response or transition from wakefulness to sleep. In the context of this thesis, we are interested in switches from tonic firing to bursting, reflecting for example switches from active to quiet waking as detailed in the previous section. How are neuromodulators able to generate robust switches? How can we investigate this question despite the brain complexity, the variability between neurons, the history of the circuit, and the experiences?

A breakthrough strategy to investigate neuromodulation is to focus on small circuits, as done in the impressive work of Professor Eve Marder. The stomatogastric nervous system (STN) of crustaceans has been her experimental and computational playground (Figure 2.12A). It controls stomach movement, and its circuit is well-defined. The identification of the different neurons inside the stomatogastric ganglion (STG) can be achieved through extracellular recording of the lateral ventricular nerve (lvn). The lateral pyloric (LP) neuron, pyloric (PY) neuron, and the pyloric dilator (PD) neuron successively burst, generating a triphasic rhythmic pattern (Figure 2.12A). Studying wild-caught animals from the ocean provides valuable insights into neuroscience, as these animals exhibit significant variabilities in their neuronal properties while still displaying similar behaviors.

Figure 2.12B shows that while recording neurons in two different animals have similar firing patterns, the intrinsic properties can vary largely between animals. For example, Figure 2.12B (right) reveals that different potassium currents largely vary between different animals.

Neuromodulators have been investigated for their various actions over the last 30 years, but we will highlight four key findings (Nadim and Bucher, 2014; Marder and Bucher, 2007):

- Different neuromodulators may have a converging action on the same voltage-gated ion channels (Figure 2.12C).
- Individual neuromodulators may have different actions on a neuron by altering different physiological mechanisms. These modulators can produce different forms of pyloric rhythms (Figure 2.12D).
- One neuromodulator may affect different voltage-gated ion channels. Figure 2.12E shows that dopamine (DA) modulates different types of currents in the same neuron.
- Neurons and synapses are affected by neuromodulators (see more in Chapter 2.1.6).

The study of neuromodulators raises important questions about how they are able to alter multiple parameters while maintaining network output. Specifically, how do neuromodulators tune circuits to produce different rhythms that reflect different behaviors? This balance between stability and flexibility is a fundamental aspect of circuit function. Furthermore, the robustness and predictability of neuromodulators is particularly intriguing given the variability in intrinsic parameters observed across animals (Marder et al., 2014). Recent studies suggest that neuromodulators achieve stability by tuning both inward and outward currents simultaneously, thus achieving the same result in different animals. These findings shed light on the complex mechanisms by which neuromodulators regulate neural circuits and highlight the need for further investigation into their role in neural processing (Goaillard and Marder, 2021).

Box 3 - Why do we study crustaceans to understand human brains?

Studying the nervous systems of small animals offers a simpler and more accessible approach compared to larger animals or humans, yet their functions are remarkably similar. For instance, the first action potential was recorded in a squid (Hodgkin and Huxley, 1952), and the results have been replicated in our own brains. The crustacean circuit is particularly advantageous due to its simplicity, which allows for easy identification of neurons and key players such as neuromodulators and peptides. This provides a powerful foundation for deriving general principles of neural function.

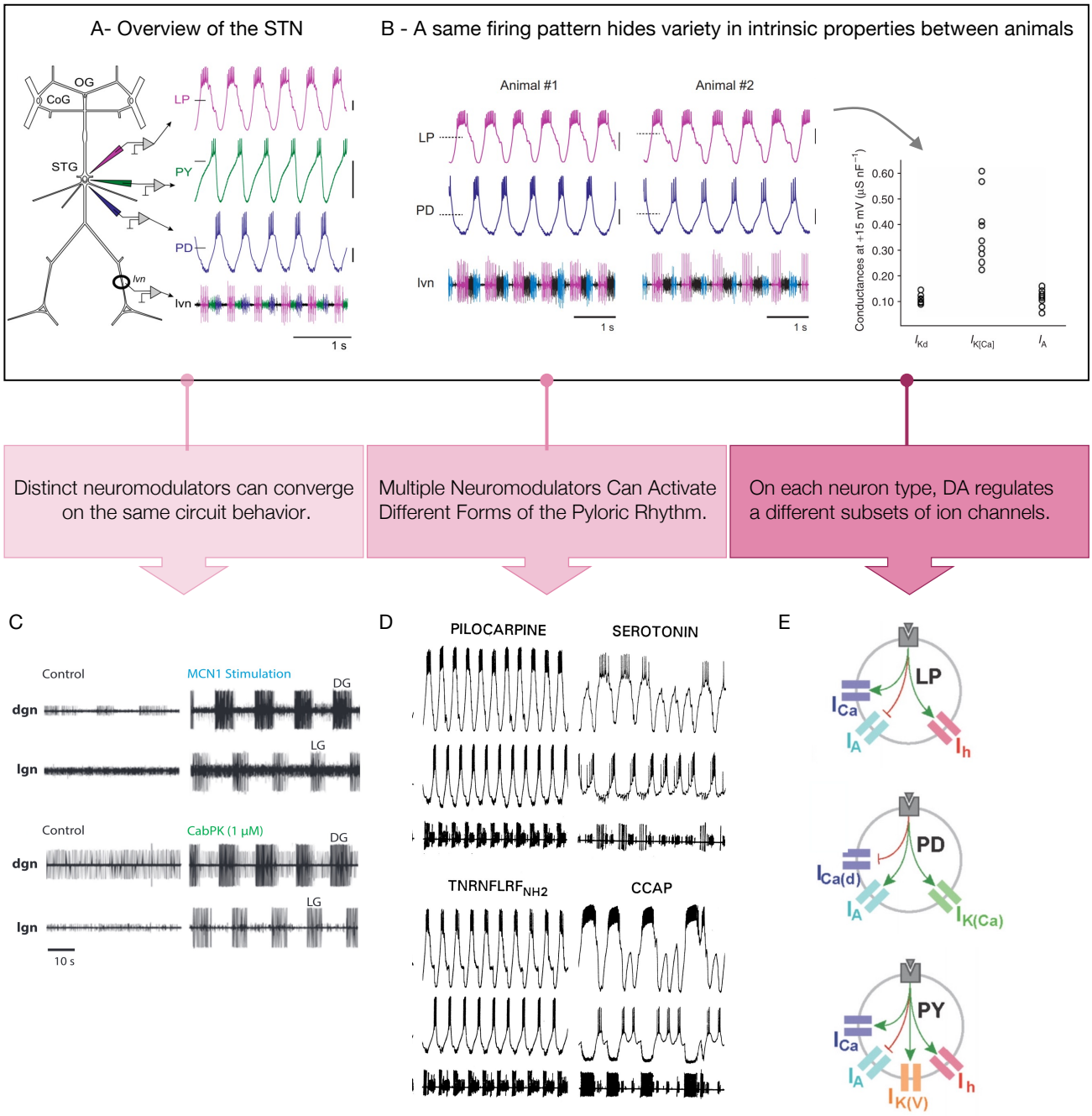

Figure 2.12: Neuromodulators have complex actions on the nervous systems. A. Schematic of the stomatogastric nervous system (STN) and the bursting neurons (Marder and Rue, 2021). **B.** Animals have similar activities (Marder and Rue, 2021) but different intrinsic properties (Schulz et al., 2006). **C.** A similar rhythm can be retrieved by applying different neuromodulators (Marder et al., 2014). **D.** Different neuromodulators activate different rhythms (Marder, 2012). **E.** Neuromodulators have different actions on different neurons. (Marder and Bucher, 2007)

2.4 Synaptic plasticity

2.4.1 Synapse: definition, structure, and functioning

The term *synapse* originates from Greek sunapsis, from 'sun' that means together and 'hapsis' that means joining, in total it gives joining together. It corresponds to the junction where information is transmitted between two neurons. It consists of the presynaptic terminal, the gap between the two neurons (synaptic cleft) and the postsynaptic neurons that contains receptors.

Synaptic transmission corresponds to the ability of neurons to transmit information between each other. An action potential generated at the presynaptic neurons reaches the axon terminal and it is converted into a chemical signal that corresponds to neurotransmitter release. These neurotransmitters bind to the postsynaptic neurons that generate a response. The *synaptic strength* refers to the magnitude of this synaptic response that can be recorded as an Excitatory Postsynaptic Potential (EPSP) or Excitatory Postsynaptic Current (EPSC) (for excitatory synapse). In the literature, the terms synaptic strength and synaptic efficiency are interchangeable, while the synaptic strength reflects the response magnitude, the *synaptic efficiency* specifically describes how effectively a synapse transmits information.

The synaptic strength can be increased or decreased and it is what makes our brain plastic and able to adapt the connections between neurons. Before exploring all the plasticity mechanisms, a more accurate description of the synaptic transmission and the synapse is required.

Synaptic transmission

The information transmission consists of three main steps as shown in Figure 2.13: (i) the action potential at the presynaptic neuron triggers glutamate release, (ii) glutamate binds to the postsynaptic receptors, (iii) the postsynaptic receptors allow the flow of ions inside the postsynaptic neurons that generate a change in the postsynaptic membrane voltage.

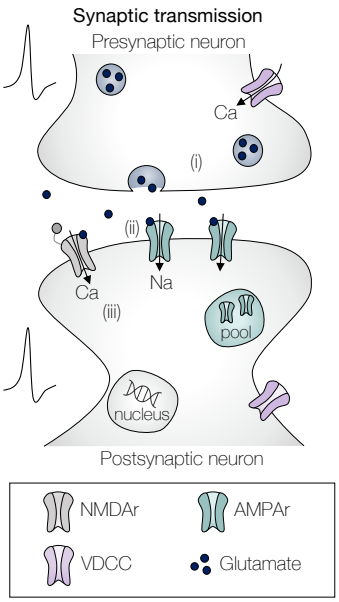

Figure 2.13: Molecular mechanisms of synaptic transmission. (i) Presynaptic membrane depolarization triggers the release of neurotransmitter release in the synaptic cleft. (ii) Neurotransmitters bind to postsynaptic receptors. (iii). Postsynaptic receptors allow the flux of ions inside the postsynaptic neuron. Inspired from (Lamprecht and LeDoux, 2004; Bear et al., 2016).

(i) The membrane depolarization at the presynaptic neuron terminal allows calcium to enter the terminal through voltage-dependent N or P/Q calcium channels which triggers a signaling cascade. Synaptic vesicles containing neurotransmitters fuse with the membrane and release the stored neurotransmitters in the synaptic cleft

(ii) Glutamate binds to two postsynaptic receptors that are implicated in distinct roles in both synaptic transmission and synaptic plasticity. The first of these receptors is AMPAr, an ionotropic receptor that opens when glutamate binds to it. Once activated, sodium and to a lesser extent potassium ions primarily flow through the membrane, depolarizing the postsynaptic membrane voltage. The second type of receptor is the NMDAr, which is a receptor that opens under two conditions, namely when simultaneous binding of glutamate and a co-agonist (glycine or d-serine) occurs and when a membrane depolarization (e.g. induced by AMPAr activation) removes magnesium ions that otherwise block the channel. This receptor is primarily selective for calcium ions, but also allows sodium and potassium ion flow.

(iii) Both AMPAr and NMDAr work together to mediate synaptic transmission. Glutamate released from the presynaptic neuron binds to both receptors, but only opens the AMPAr, resulting in ion flow and membrane depolarization. This depolarization triggers the removal of the magnesium, allowing NMDAr to open, as the two activation conditions are fulfilled. The NMDAr are often called coincidence detectors as their activation requires a presynaptic activity causing glutamate release and a postsynaptic activity causing depolarization to remove the magnesium block. Calcium flows into the postsynaptic neurons, as well as sodium enters and potassium exits.

As we will see in more details below, calcium plays a crucial role in the process of synaptic plasticity and it is why it is really important to understand how and why it enters the postsynaptic neuron. Another source of calcium entering the postsynaptic neurons is voltage dependent calcium channels (VDCC) such as L-type or T-type among others (Lamprecht and LeDoux, 2004). These calcium channels can amplify the depolarization.

Finally, the postsynaptic neuron response to the presynaptic neuron action potential can be measured by the Excitatory Postsynaptic Potential (EPSP) or Excitatory Postsynaptic Current (EPSC) (Citri and Malenka, 2008).

Dendritic spines play an important role in synaptic plasticity

As just described, postsynaptic receptors are the principal actors in synaptic transmission. They are mainly located at a particular region of the postsynaptic neurons: on the *spine*.

The dendritic spine is a small protrusion at the surface of the dendrite that receives input from other neurons (Figure 2.14A). It consists of a thin neck and a spine head. The dendritic spines contain receptors, channels, signaling molecules, which are useful for its spine functional role, and protein scaffolds, which provide the spine structure (Bozelos and Poirazi, 2017). These receptors, basically AMPAr and NMDAr, are concentrated at the tip of the spine in a visually distinct site called the postsynaptic density (PSD) (Bonilla-Quintana and Rangamani, 2022).

The spine morphology is characterized by several geometric features: the length and the width of the neck, the volume of the head, and the surface area of the PSD. These features are correlated with the number of postsynaptic receptors (Borczyk et al., 2019).

Based on these features, spines can be classified into three categories (Figure 2.14B): filopodia is a finger-like spine, thin spine, mushroom spine, and stubby spine. Logically, spines with a larger head represents a stronger connection between the pre- and the postsynaptic neurons (Bonilla-Quintana and Rangamani, 2022; Lamprecht and LeDoux, 2004). The spin shape relies on the spine cytoskeleton, composed among others by *actin* filaments.

The spine has the ability to compartmentalize calcium influx that empowers it with the ability to segregate different inputs.

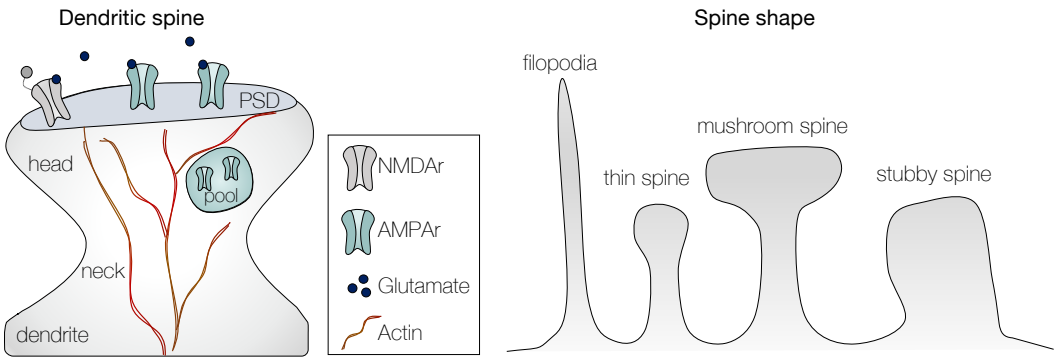

Figure 2.14: Schematic of a dendritic spine and its different shapes. A. A dendritic spine is composed of a neck and a head. The region where postsynaptic receptors are concentrated is called postsynaptic density (PSD). Actin participates in the spine shape. **B.** Spines can take several shapes defined by the neck width and the head volume. Inspired from (Bonilla-Quintana and Rangamani, 2022)

2.4.2 Plasticity: from early to late change

How do neurons adapt their synaptic strengths with each other or in other words, how does synaptic plasticity work? Scientists have been trying to answer these questions for decades (Takeuchi et al., 2014). Ramon y Cajal proposed theoretical hypotheses about the change in synaptic transmission in the nineteenth century (Cajal, 1888). Followed by Donald Hebb that brought attention to plasticity with his famous quote ”Cells that fire together, wire together” (Hebb, 1949). Experiences on Aplysia provided some of the first evidence that synaptic strength changes in response to stimuli (Kandel, 1979). In parallel, (Bliss and Lømo, 1973) introduced the notion of Long Term Potentiation (LTP) and Long Term Depression (LTD), as forms of long-lasting synaptic plasticity. LTP involves a persistent increase of synaptic strength, while LTD involves a persistent decrease of synaptic strength (Lamprecht and LeDoux, 2004).

Nowadays, research on synaptic plasticity is exploding; from understanding the molecular mechanisms to the formation of new networks. It confirms that synaptic plasticity can be described by many forms and mechanisms and that is also region-dependent. It can span from milliseconds to hours, days, and even longer (Citri and Malenka, 2008). We will first recall what are the different quantitative measures of plasticity, the different tools used to record plasticity and what are the most encountered plasticity-induced protocols. Then, we will enter the core of the plasticity mechanisms from short-term plasticity to longer-lasting synaptic changes.

Quantification of synaptic plasticity

There are several ways to quantify how synaptic transmission is modified (Cirelli, 2017). Here is a non-exhaustive list:

- at the structural level: change in spine size, axon to spine interface (ASI), spine volume, spine width;
- at the molecular level: change in the number of synaptic receptors such as AMPAr or NMDAr;
- at the electrophysiological level: change in Excitatory Postsynaptic Potential (EPSP) or Excitatory Postsynaptic Current (EPSC), by comparing the amplitude (Bi and Poo, 1998) or the change in slope (Frey et al., 1993) or other consequences.

Tools to measure synaptic plasticity

Synaptic change can be monitored at the structural level by modern imaging technologies; by tracking the evolution of the spine morphology. Changes in EPSP or EPSC are recorded by electrophysiological recording for example via electrodes in the postsynaptic neurons (Abraham et al., 2019). The advantages and disadvantages of the different techniques are discussed in (Glasgow et al., 2019).

Plasticity-induced protocols

Experimentalists record one of the parameters mentioned above to define a basal control condition (w_0). Then, perform a plasticity-induced protocol. After the protocol, the same parameter is measured and the ratio provides the synaptic change (Δw). Figure 2.15 explains the different steps achieved in electrophysiology to provide experimental data after a plasticity-induced protocol (Bi and Poo, 1998)

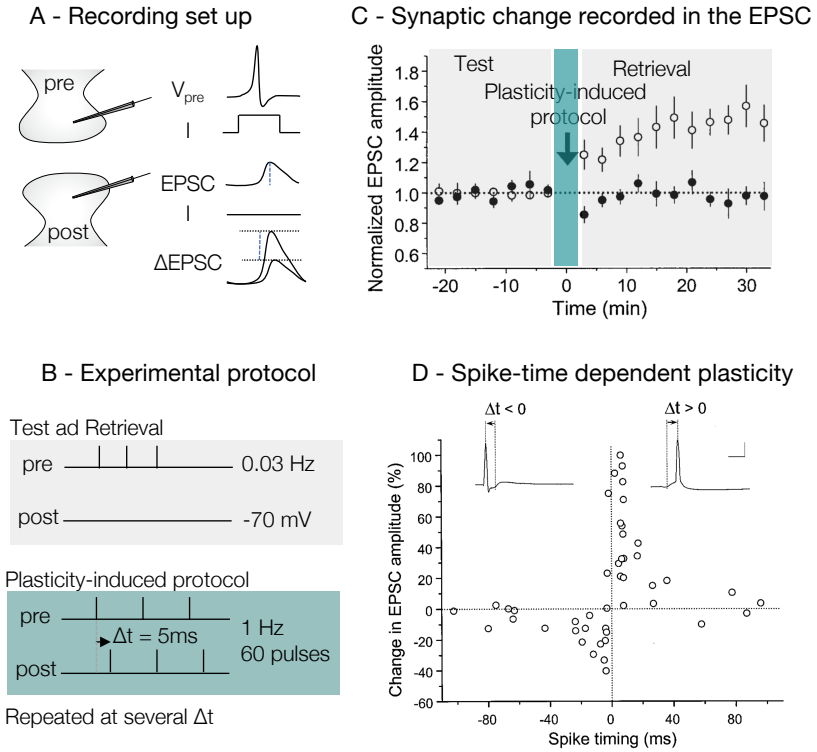

Figure 2.15: Components of a classical spike-time dependent plasticity protocol. **A.** Control conditions with pre- and post-synaptic activities trigger the recording of changes in synaptic transmission (e.g. via EPSC). **B.** (top) Test protocol measures initial synaptic strength via response to presynaptic pulses. (bottom) The plasticity-induced protocol involves 60 pulses at 1Hz in both neurons with a controlled time-lag (Δt) referred to as the Spike-Time Dependent Plasticity (STDP) protocol. **C.** Experimental data obtained for Δt = 5 ms. **D.** Experimental data for different time-lags. Figures C-D are adapted from (Bi and Poo, 1998).

Figure 2.16 (top) provides an overview of the most common plasticity-induced protocols performed in the last years (Krieg and Triesch, 2014). The strategy is to test the effect of one parameter on the synaptic strength: such as the presynaptic frequency, the time-lag between two pre and postsynaptic spikes (Δt), the postsynaptic membrane voltage V_{post} among others.

- the *rate protocol* records the synaptic strength after stimulating the presynaptic neuron at a given frequency while the postsynaptic neuron is not modulated ($\Delta w = F(f_{\text{pre}})$) (Dudek and Bear, 1992; Frey and Morris, 1998; Gerstner, 2011) (Figure 2.16A).

- The *Spike-Time Dependent Plasticity* protocol is largely used; both the pre- and postsynaptic neurons are stimulated at a low frequency (0.1 or 1Hz) with a certain time-lag Δt ($\Delta w = F(\Delta t)$ (Debanne et al., 1994; Bi and Poo, 1998; Markram et al., 1997; Abbott and Nelson, 2000; Gerstner et al., 1996) (Figure 2.16B).
- The membrane *voltage* of the postsynaptic neuron is depolarized by the experimenter while presynaptic fibers are stimulated at a given frequency ($\Delta w = F(V_{\text{post}}, f_{\text{pre}})$ (Bi and Poo, 1998; Artola et al., 1990; Sjöström et al., 2001; Ngezahayo et al., 2000; Artola and Singer, 1993) (Figure 2.16C).
- The *frequency*-dependent protocol consists in generating spikes at a given pairing frequency (f_{pairing}) with presynaptic spikes preceding postsynaptic spikes by 10 ms (or post-pre with a time delay written -10 ms) ($\Delta w = F(f_{\text{pairing}})$ with $\Delta t = \pm 10$ms)(Sjöström et al., 2001) (Figure 2.16D).
- *More complex* induction protocols are also used. Triplet and quadruplets are similar to the STDP protocol, with three or four spikes generated instead of two (Wang et al., 2005; Froemke and Dan, 2002; Froemke et al., 2006; Wittenberg and Wang, 2006). Postsynaptic 'bursts': repetitive action potentials in a short period of time of 1, 2, or 3 spikes paired with one single presynaptic spike induced experimentally (Nevian and Sakmann, 2006; Debanne et al., 1994; Froemke et al., 2006) (Figure 2.16E).

More details on plasticity-induced protocols are available in (Inglebert et al., 2021; Krieg and Triesch, 2014; Harnett et al., 2009). More factors can influence the result of the synaptic plasticity such as the synaptic location (Froemke and Dan, 2002; Sjöström and Häusser, 2006) and the initial synaptic strength (Ngezahayo et al., 2000).

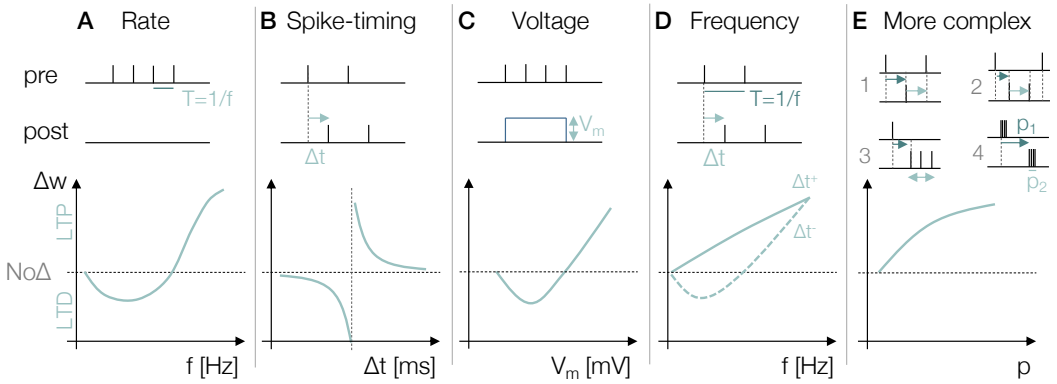

Figure 2.16: Schematic of commonly used plasticity induction protocols. A. Rate-based protocol compares the postsynaptic response for varying presynaptic firing frequencies f. **B.** Spike-timing dependent protocol tests the effect of a time-lag Δt between pre- and postsynaptic spike timing at a fixed frequency. **C.** Voltage-based plasticity protocol tests the impact of the postsynaptic membrane voltage V_m during presynaptic spiking. **D.** Frequency-dependent plasticity protocol studies the impact of pre- and postsynaptic spiking frequencies f for two different time-lags (Δt^+ and Δt^-). **E.** More complex protocols include the triplet 1, quadruplet 2, theta burst 3, or burst-dependent 4 protocol characterized by one or several parameters (symbolized by p_1, p_2, etc.). Inspired by (Clopath, 2019)

Short-term plasticity

Short-term plasticity refers to changes in the synaptic transmission that occurs over a period ranging from milliseconds to several minutes. There are two types of short-term plasticity: facilitation and depression. Briefly, *facilitation* involves an increase in the synaptic strength due to the rapid succession of action potentials at the presynaptic neuron (Castro-Alamancos and Connors, 1997). This activity leads to a buildup of calcium, which in turn affects the exocytosis of synaptic vesicles resulting, in the change in probability of the neurotransmitter release (Citri and Malenka, 2008). In contrast, *depression* involves a decrease of the synaptic strength caused by the depletion of neurotransmitter stores at the presynaptic terminal (Heidelberger et al., 2014).

Short-term plasticity is often correlated with mechanisms in the presynaptic neurons because each synapse is characterized by a probability of release of the vesicles, and, depending on this parameter, synapses can undergo various changes. By contrast, longer changes in the synaptic plasticity preferentially occur at the postsynaptic neuron.

Long-term plasticity: definition and classification

Long Term Potentiation (LTP) was shown experimentally (exactly 50 years ago) by(Bliss and Lømo, 1973) as a long-term increase in the synaptic strength following a brief, high-frequency stimulation or other induction protocol (Baltaci et al., 2019). Nowadays, we define LTP more globally as an activity-dependent long-lasting increase in the synaptic strength (Abraham et al., 2019; Citri and Malenka, 2008). Forty years ago, LTP was already divided into two categories

depending on the generation of new proteins or not as shown experimentally in (Frey et al., 1993; Krug et al., 1984) by using inhibitors of protein synthesis.

- Early Long Term Potentiation (E-LTP) [1] refers to the early phase of long-term change, which is independent of protein synthesis, without any structural change of the synapse. It lasts up to 1-3h.
- Late Long Term Potentiation (L-LTP) refers to the late phase, which is dependent on de-novo protein synthesis (with the activation of transcription factors) and structural change of the synapse.

Conversely, the concept of Long Term Depression (LTD) refers to a long-lasting decrease in the synaptic strength. In the quest to unrevealing the mechanisms behind these long-term changes, the next section explains the causal steps starting from the entry of calcium to persistent changes in the synapse.

Mechanisms of early long-term potentiation (E-LTP) and depression (E-LTD)

We need to zoom in at the molecular level to understand the machinery. Calcium enters the postsynaptic neuron and binds to calmodulin, forming the complex known as calcium/calmodulin complex (CaM). This complex acts as a dynamic calcium sensor, depending on the concentration, it triggers different processes that either lead to Long Term Potentiation (LTP) (for elevated calcium influx) or Long Term Depression (LTD) (for intermediate calcium influx) (Kotaleski and Blackwell, 2010; Feldman, 2012; Seibt and Frank, 2019). Figure 2.17 details their mechanisms.

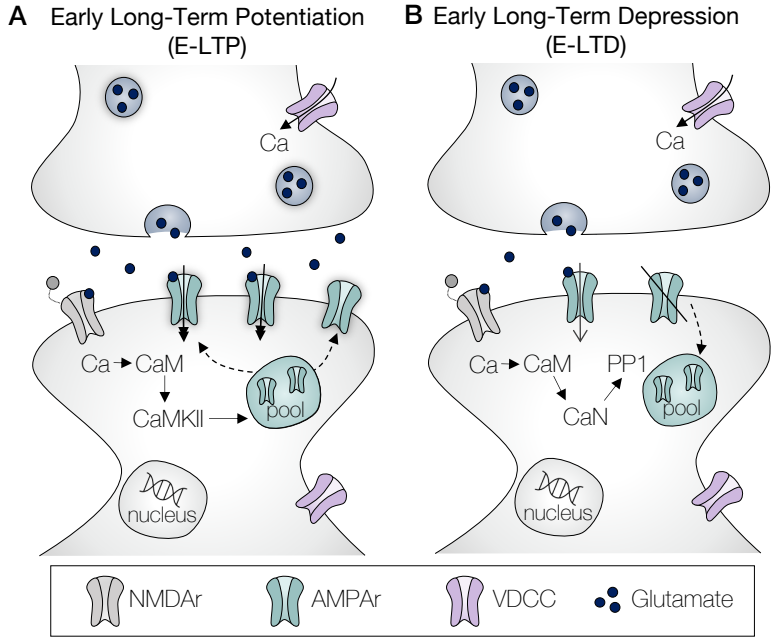

Figure 2.17: Mechanisms of Early phase of Long-Term Plasticity. A. Large calcium influx activates CaM that in turn phosphorylates CaMKII. This reaction increases the postsynaptic receptor efficacy and triggers the insertion of new AMPAr from a pool, causing E-LTP. **B.** A intermediate calcium influx activates triggers calcineurin (CaN) activation, which in turn activates the protein phosphatase 1 (PP1). In total, it decreases receptor efficacy and removes AMPAr from the membrane. Inspired by (Lamprecht and LeDoux, 2004).

Early Long Term Potentiation (E-LTP)

In the case of elevated calcium influx following high frequency stimulation, the calcium/calmodulin (CaM) complex triggers calcium/calmodulin-dependent protein kinase, known as CaMK (Figure 2.17A). A *kinase protein* has the property to regulate other proteins by attaching phosphate groups, a process known as phosphorylation, which causes a functional change in the targeted protein (Bear et al., 2016; Seibt and Frank, 2019). In the context of synaptic plasticity, CaMKII, a member of the CaMK family, is known to phosphorylate a variety of proteins, including ion channels, neurotransmitter receptors, and synaptic scaffolding proteins. One of its most important targets is the AMPAr. As previously explained, it is the primary mediator of fast excitatory synaptic transmission in the brain. Elevated calcium influx quickly activates CaMKII, which potentiates the synapse in two manners:

- (i) increase in existing AMPAr efficiency via phosphorylation leading to a better synaptic transmission.

[1] In literature, the acronym E-LTP might be also used for Excitatory Long Term Plasticity or potentiation by contrast to inhibitory plasticity. In the context of my thesis, E-LTP is only for Early Long Term Potentiation.

- (ii) insertion of new AMPAr into the postsynaptic membrane - a process known as fast AMPAr trafficking. Indeed, some vesicles queue near the membrane, and in response to CaMKII activation, the vesicles containing newly synthetized AMPAr fuse with the membrane and deliver new AMPAr to the synapse, via exocytosis, causing the swelling of the spines (Seibt and Frank, 2019). AMPAr can be recruited from extrasynaptic regions.

The Early Long Term Potentiation (E-LTP) is independent of de-novo protein synthesis and morphological change of the spine.

Early Long Term Depression (E-LTD)
In the case of moderate calcium influx, the calcium/calmodulin complex (CaM) preferentially triggers a calcium/calmodulin-dependent protein phosphatase, known as calcineurin (CaN) (Figure 2.17B). A phosphatase protein is an enzyme that removes phosphate from target proteins. This, in turn, activates a protein phosphatase 1 (PP1), which inhibits the action of CaMKII by dephosphorylating it (Citri and Malenka, 2008).

As previously explained, calcium is crucial for synaptic plasticity, which raises the question of how the same signal can trigger *both* LTP and LTD ? The key difference lies in the level of NMDAr activation, and it is important to remember that the different types of calcium response selectively activate different types of enzymes that have an opposing effect. LTP and LTD reflect the bidirectional regulation of phosphorylation and of the number of AMPAr in the synapse.

Mechanisms of late long-term potentiation (L-LTP) and depression (L-LTD)

The LTP that lasts longer and induces changes in the spine morphology is called Late Long Term Potentiation (L-LTP). It is distinguished from E-LTP by the fact that it induces changes in its protein synthesis. Figure 2.18 illustrates the mechanisms.

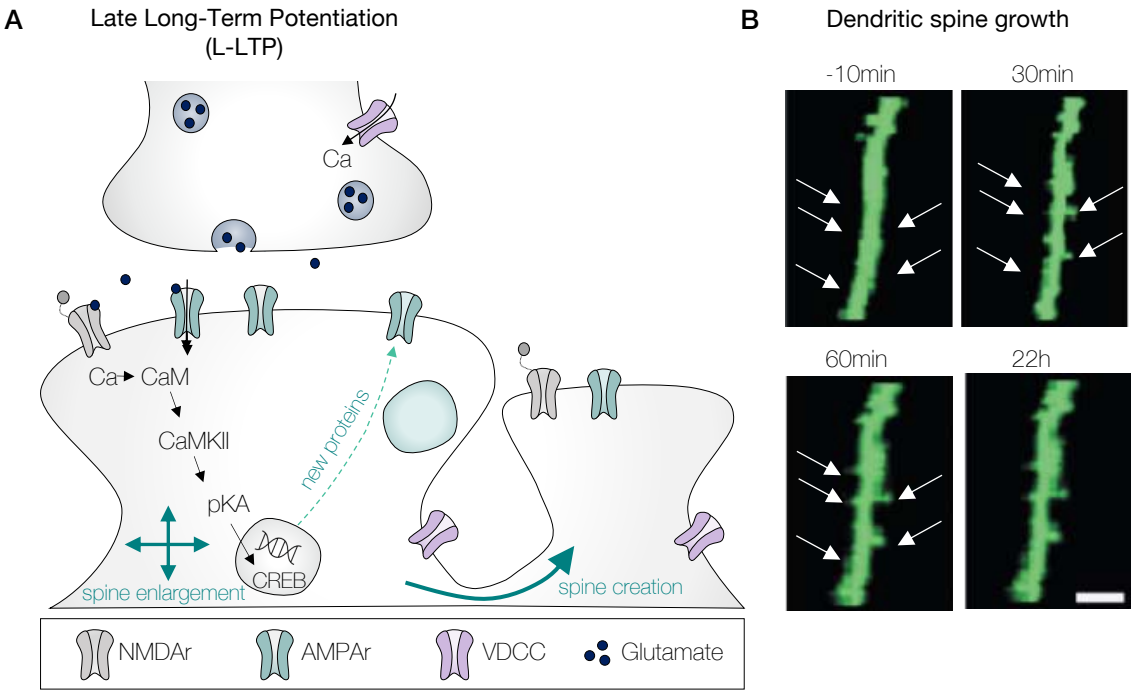

Figure 2.18: Mechanisms of late long-term potentiation with the associated morphological changes. A. Activity-dependent calcium influx triggers signaling molecules that lead to the generation of new proteins, insertion of new AMPAr at the membrane, spine enlargement, and spine creation. **B.** Clear visualization of spine growth over a long period, obtained by two-photon microscopy. White bar represents 3 μm (Engert and Bonhoeffer, 1999). Inspired by (Lamprecht and LeDoux, 2004).

On a longer timescale, the rise of calcium level that activates CaMKII or CaMKIV (another member of the CaMK family) in turn activates cyclic adenosine monophosphate (cAMP) (Golbert et al., 2017). This intracellular signaling molecule activates the production of Protein Kinase A (PKA) (Figure 2.18A). Then, the latter enters the nucleus and activates transcription factors such as cAMP-response element binding protein (CREB) that regulate gene expression. These transcription factors can induce the expression of genes that encode new proteins, including AMPAr and growth factors. After the synthesis of new AMPAr, they are trafficked to the synapse, via slow AMPAr trafficking. Additionally, the growth factors modify the synapse morphology and the cytoskeleton is impacted by modifying some support-proteins such as *actin*. Altogether, this process contributes to the long-term morphological change such as enlargement of the spine

head (larger surface, increased head volume, wider and shorter neck), growth of the dendritic spines (polymerization of actin filament), insertion of new receptors that have specifically just been synthesized (by contrast to the fast trafficking of receptors from the already available vesicle pools discussed in the E-LTP), formation of new synapses, rearrangement of the actin cytoskeleton and changes in the distribution of neurotransmitter receptors (receptor clustering).

Figure 2.18B shows microscope imaging of a dendritic shaft and its spines over time. The generation of new protrusions and the increase in the volume of existing spines are depicted (Lamprecht and LeDoux, 2004). The complementary process of Late Long Term Depression (L-LTD) triggers another signaling cascade that promotes the removal and inhibition of AMPAr and the shrinkage of the spine (Bliss and Cooke, 2011).

This level of details is sufficient for the purpose of my thesis. For more information on the intracellular signaling pathways in (Berridge, 2014; Citri and Malenka, 2008; Kotaleski and Blackwell, 2010; Bading, 2013; Heidelberger et al., 2014; Golbert et al., 2017; Seibt and Frank, 2019; Feldman, 2020).

Summary and clarification of the diverse concepts involved in synaptic plasticity

In my pursuit of understanding how neurons alter their connections with each other, first synaptic transmission is reviewed. Next, short-term and long-term changes are distinguished, and then long-term changes are classified into two categories based on the generation of new proteins: early and late processes. The causal steps that mediate lasting changes at the synapse are also detailed.

Figure 2.19 presents a schematic overview of what we will refer to as *traditional synaptic plasticity* and *structural plasticity*. The terminology in this field can be overwhelming, but we aim to summarize the various concepts concisely and present the hypothesis of my thesis.

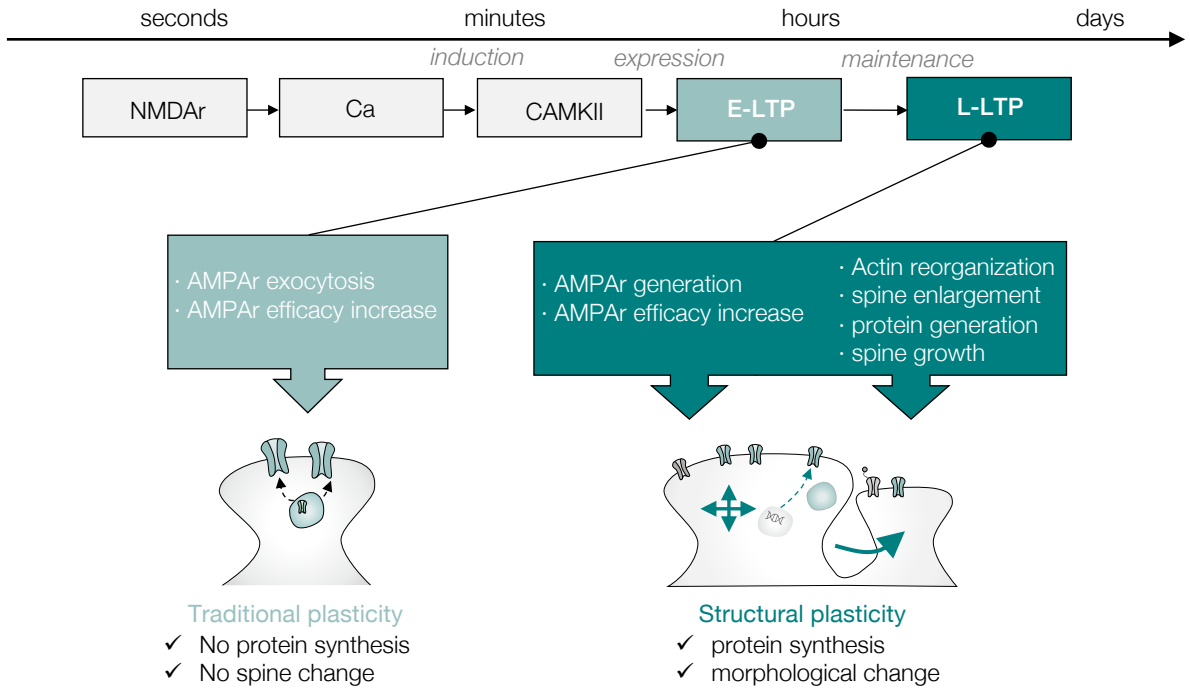

Figure 2.19: Summary of different concepts of synaptic plasticity across different timescales. The influx of calcium into the postsynaptic neurons during the induction phase triggers a signaling cascade that leads to the expression of early-phase LTP (E-LTP), also known as traditional synaptic plasticity. This process enhances the efficacy of postsynaptic receptors and allows for exocytosis. In contrast, late-phase LTP (L-LTP), also known as structural plasticity, is associated with long-lasting structural changes in the synapse. Adapted from (Bonilla-Quintana and Rangamani, 2022).

The process known as Early Long Term Potentiation (E-LTP), or *LTP expression* (Heidelberger et al., 2014), involves the exocytosis of new AMPAr from the vesicle pool and an increase in the efficacy of existing receptors, without any protein synthesis or spine morphological changes (Lamprecht and LeDoux, 2004). In computational neuroscience, it is often associated with the *traditional plasticity*.

In contrast, Late Long Term Potentiation (L-LTP), or *LTP maintenance* (Heidelberger et al., 2014), involves an increase in the number of receptors in a given spine, changes in the efficacy of existing receptors, and even more characterizing of this phase, the morphological changes in the spine (Lamprecht and LeDoux, 2004). The generation of new proteins mediates this process, and in computational neuroscience, it is often modeled by the *structural plasticity*.

We would like to highlight that in both situations, AMPAr are likely to be inserted or removed from the postsynaptic

membrane but the insertion mechanism is different dependent on the LTP category. During E-LTP, new receptors are inserted at the postsynaptic membrane from pools of available receptors. By contrast, for L-LTP, the insertion of new receptors requires first its production thanks to protein synthesis.

2.4.3 Synaptic-tagging and capture hypothesis: a mechanism that binds E-LTP and L-LTP

The Synaptic Tagging and Capture (STC) hypothesis is a theory proposed to link the early and late phases of synaptic plasticity, where new proteins must be synthesized and the synapse changes its morphology. This theory can be divided into different steps (Figure 2.20). First, the synaptic potentiation generates a local *tag*. Then, plasticity related products (PRP) are activated or synthesized. The third step consists of the capture of these products by tagged synapses. Last, the synaptic strength is stabilizing (Redondo and Morris, 2011; Ding et al., 2022). In essence, the synaptic tagging and capture hypothesis suggests that the early phase of plasticity sets the stage for the late phase, providing a mechanism to link the two processes (Baltaci et al., 2019; Abraham et al., 2019).

Several candidates have been suggested as tags: CaMKII, f-actin, and protein kinase A (PKA). For PRP, calcium signals or transcriptional activators have been often identified more precisely, immediate early genes (IEGs), brain-derived neurotrophic factor (BDNF), Arc and a protein kinase C called PKMζ (Bin Ibrahim et al., 2022).

Neuromodulation potentially affects the result of STC. Some researches hypothesize that neuromodulators, like dopamine, play a role. "DA receptor activation can lead to enhanced somatic and dendritic protein synthesis essential for the establishment of lasting plasticity and memory (...). This function is mediated by PKA, extracellular-signal-regulated kinase (ERK), CaMKIV, and cAMP response element-binding protein CREB" (Takeuchi et al., 2014; Redondo et al., 2010).

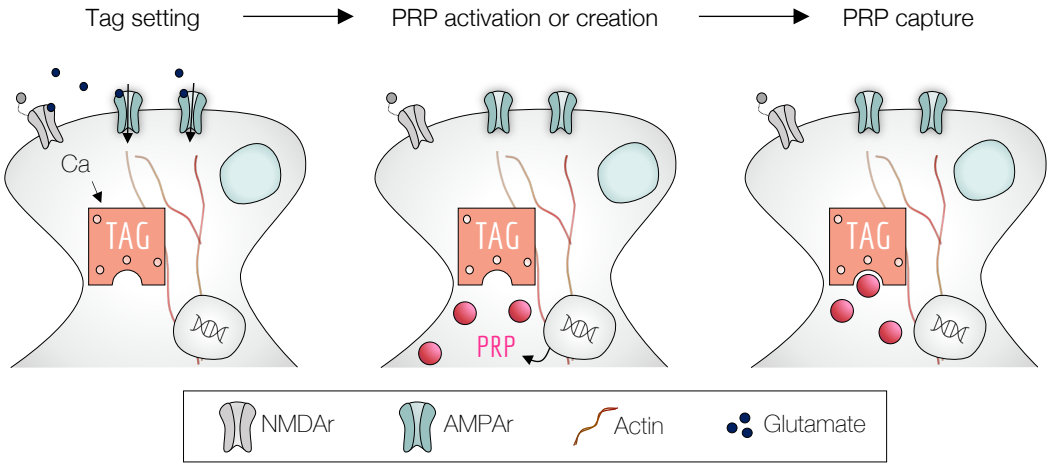

Figure 2.20: Molecular mechanisms behind the hypothesis of Synaptic Tagging and Capture (STC) hypothesis. Synaptic potentiation leads to a tag setting (left) and the synthesis and activation of plasticity related products (PRP) (center). For maintenance of LTP, PRP must be captured by tagged synapse (right). Inspired by (Redondo and Morris, 2011)

2.4.4 Beyond Hebbian Plasticity: the many faces of synaptic plasticity

Many researches on synaptic plasticity have been influenced by Hebb's postulate, "Neurons that fire together, wire together" (Hebb, 1949). In the previous section, we have detailed the potential mechanisms of synaptic plasticity, where the receptor quantity are altered, and postsynaptic dendrites undergo structural changes. Initially, the focus has been on the change in synaptic transmission when the presynaptic and the postsynaptic neurons spike to reproduce experimentally the Hebb's postulate. This type of plasticity is called *Hebbian plasticity*, where strong inputs increase the synaptic strength while weak inputs decrease it, creating a positive feedback mechanism (Fauth and Tetzlaff, 2016). However, many factors can impact the result of synaptic plasticity leading to different types of plasticity referred to as 'Neohebbian plasticity' (Brzosko et al., 2019; Baltaci et al., 2019; Citri and Malenka, 2008; Lisman et al., 2011).Figure 2.21 provides an overview of experiments showing neohebbian plasticity recordings.

Burst-Time Dependent Plasticity is a type of synaptic plasticity that considers the effect of a bursting regime in the pre- and postsynaptic neurons (Figure 2.21A). A presynaptic neuron burst before a postsynaptic depolarization results in a decrease in synaptic strength. As is the case in STDP, the evolution of the synaptic change as a function of the time-lag (or burst latency) can be extracted (Figure 2.21A, bottom) (Butts et al., 2007).

Metaplasticity refers to the plasticity of synaptic plasticity, meaning that the mechanism itself is plastic. It enhances or suppresses the induction of Hebbian plasticity, depending on the previous history of synaptic activity, as shown in Figure 2.21C. The response at $t = 40$ minutes is slower if the neuron has experienced plasticity earlier. This fine-tunes the response of Hebbian plasticity to stimuli based on prior experience (Abraham and Bear, 1996; Abraham, 2008).

Intrinsic plasticity refers to changes in the excitability of individual neurons, independent of changes in synaptic strength (Daoudal and Debanne, 2003; Debanne et al., 2019; Sehgal et al., 2013; Debanne, 2010). Neurons can adapt the number of ion channels or regulate other molecular mechanisms, as shown in Figure 2.21D. In the control condition (WT), the neuron generates an action potential, and under ion channel blockers, the output pattern remains the same, but some ionic currents have been modified. This mechanism provides an elegant solution for the neuron to retain information without changing the wiring configuration with its neighbor and maintaining the same activity (Marder and Taylor, 2011).

Neuromodulated synaptic plasticity is a type of synaptic plasticity affected by neuromodulators. Figure 2.21E shows that dopamine shifts the classical STDP from the depression-potentiation kernel to the potentiation-potentiation kernel (Zhang and Linden, 2003). The cellular mechanisms underlying neuromodulation of synaptic plasticity are various (Brzosko et al., 2019). First, the neuronal spiking regime can be altered, for example by tuning ion channels. Then, neuromodulation can affect the postsynaptic receptors. Finally, it can regulate the intracellular signaling cascade governing synaptic plasticity (Frey et al., 1993; Lisman et al., 2011; Lerner and Kreitzer, 2011).

Heterosynaptic plasticity refers to changes in synaptic strength induced by activity at neighboring synapses, rather than at the synapse being studied (Chen et al., 2013). In Figure 2.21F, stimulation of the postsynaptic neuron can lead to "heterosynaptic changes at synapses that were not active during the induction" (Chen et al., 2013). This can be depression or potentiation. One current hypothesis supports the impact of calcium diffusion on the dendritic spine, where the amount of calcium will drive potentiation or depression. It may also be noted that the latter explanation is called localization or distance-dependent plasticity (Letzkus et al., 2006).

Homeostatic plasticity, on the other hand, is a type of plasticity that serves to maintain stable neural activity in the face of changing input (Figure 2.21B). If a neuron's activity increases due to excessive stimulation, it down-regulates its excitability to bring neural activity back to a normal level. Conversely, if a neuron's activity decreases (e.g. action potential generation is blocked by TTX), it up-regulates its excitability to increase neural activity. Homeostatic plasticity ensures that the neural network remains stable and balanced, and can be seen as a negative feedback mechanism (Turrigiano et al., 1994).

In addition to the types of plasticity described earlier, namely intrinsic, metaplastic, and heterosynaptic, each of these types can also exhibit homeostatic characteristics (Magee and Grienberger, 2020; Fauth and Tetzlaff, 2016). Neurons can adjust their intrinsic properties to regulate their firing activity, thereby maintaining a constant level of activity (called homeostatic intrinsic plasticity). Similarly, the plasticity threshold of Hebbian plasticity can be modulated to prevent excessive changes in synaptic strength and to maintain stable neural activity (called homeostatic metaplasticity). Another mechanism of homeostatic plasticity involves neighboring synapses that can regulate their strength to counterbalance an excessive increase in one synapse on the dendrite, ensuring that neural network activity remains balanced (called homeostatic heterosynaptic plasticity).

Overall, memory stored in our synapses is dynamically regulated. Ongoing plasticity of connections empowers animals and humans to live, learn and react in a dynamic environment (Abraham et al., 2019). There is more and more evidence that memory is not fixed forever on a given network, naming for example memory drift (Rule et al., 2019), or that memory can be initiated in one region and consolidated in another region, as suggested by the active system memory consolidation hypothesis (Born et al., 2006).

Overall, these different types of plasticity are likely to work together making the understanding a real challenge. Further studies on plasticity at the molecular, neuronal, and population levels are necessary to gain a better understanding of learning and memory, and eventually provide guidance for related diseases.

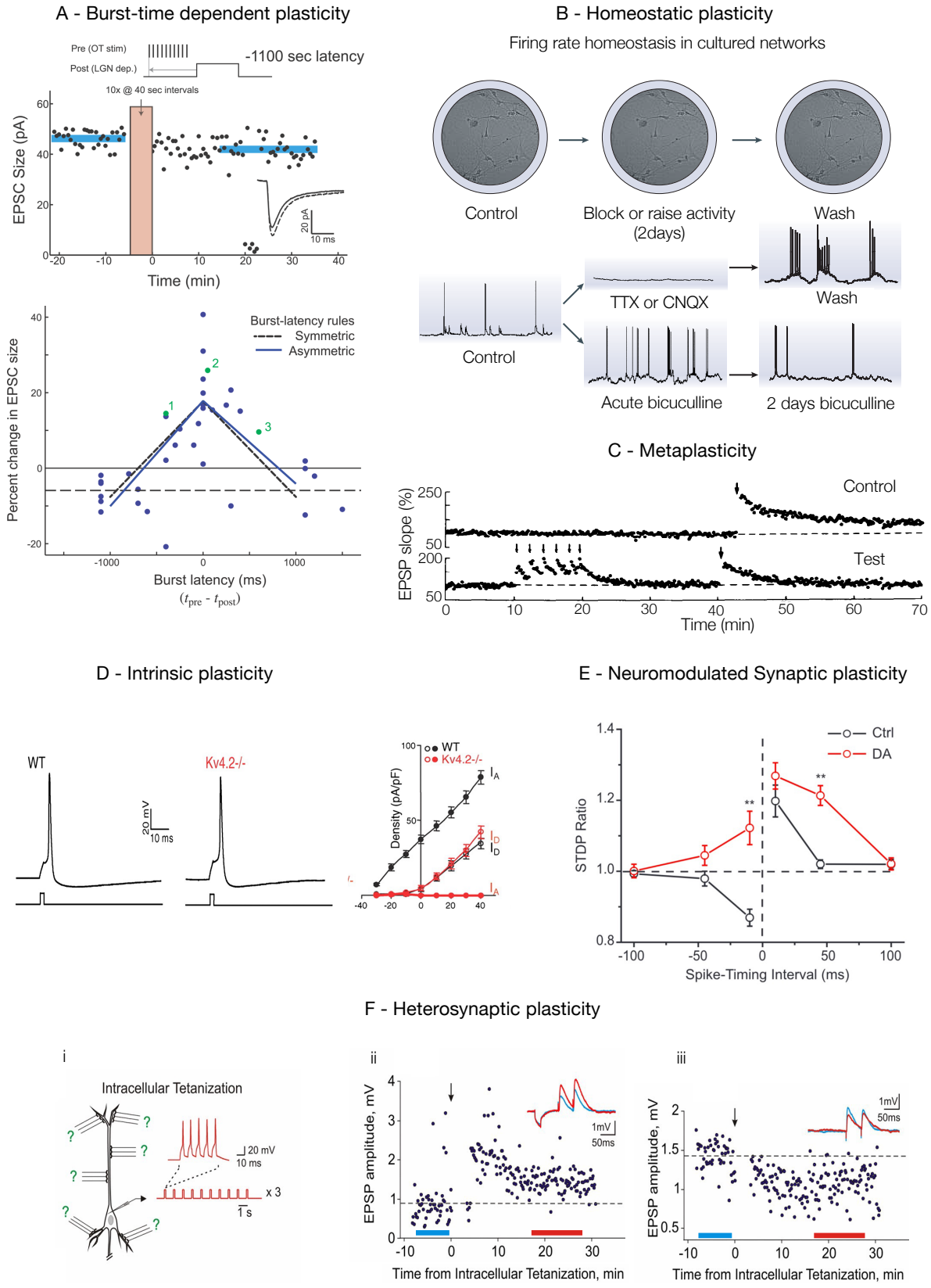

Figure 2.21: Different types of synaptic plasticity experimentally observed. **A.** (top) Evolution of the EPSC amplitude during the burst-time dependent plasticity protocol (with a latency of 1100s) and (bottom) its plasticity change as function of the burst latency (Butts et al., 2007). **B.** Increase or decrease the neuronal activity counterbalanced by homeostatic plasticity (Turrigiano and Nelson, 2004). **C.** Earlier episodes of plasticity affect the result of plasticity (Abraham and Bear, 1996). **D.** Blocking an ion channel (center) does not affect the electrophysiological signature of the neuron because the neuronal intrinsic property adapts as shown by a upregulation of another current (left) - a process called intrinsic plasticity (Marder, 2011). **E.** Neuromodulators affect the outcome of traditional synaptic plasticity (Zhang and Linden, 2003). **F.** (i) Inducing plasticity in one synapse can affect neighboring synapses, (ii) by causing potentiation or (iii) depression (Chen et al., 2013).

CHAPTER 3

Modeling neuron and synaptic plasticity with principles of computational neuroscience

This chapter serves as an in-depth introduction to computational neuroscience, catering to researchers across the spectrum from experimental to theoretical neuroscience. With the goal of accessibility in mind, it covers fundamental principles of the models employed throughout this work. As the thesis is entitled "Modeling brain-state dependent memory consolidation", the chapter focuses on two main areas: brain states and memory.

Brain states, as previously described, explores the behavior of interconnected neurons. This chapter begins with the presentation of various neuron models and subsequently delving into circuit-level modeling. Different techniques for modeling switches between tonic firing and bursting, associated to switches from different brain states, are discussed. Then, a comprehensive understanding of the neuronal and circuit models employed in this thesis is provided.

Then, the chapter dives into modeling synaptic plasticity, which is a key aspect of memory. It starts by outlining the essential features of synaptic plasticity models, followed by an exploration of various models used to capture traditional synaptic plasticity rules associated with early long-term memory changes. A solid taxonomy of traditional synaptic plasticity rules concludes this systematic review. Once again, the synaptic plasticity rules utilized in this thesis are extensively described. Finally, the chapter moves from early to late changes, presenting models of structural plasticity, which contribute to a more comprehensive understanding of memory consolidation.

The different simulations are done in Julia and the codes are open source on my GitHub: `github.com/KJacquerie/Thesis`.

3.1 Modeling neuron

Modeling the membrane voltage, labeled V_m, by an equation is a crucial step in the quest of investigating the neuron activity and is, therefore, a fundamental component of this thesis. In this section, we present an overview of modeling and review the various types of models described in the literature to establish a foundational understanding of this subject matter.

3.1.1 Modeling a neuron as an electrical circuit with voltage-dependent ion channels

A neuron is often described as an equivalent RC circuit. Its phospholipid bilayer membrane is not permeable to ions, it acts as a capacitance defined by C_m producing a capacitance current I_C:

$$I_C = C_\mathrm{m} \dot{V}_\mathrm{m}$$

The ion channels allow the flow of ions. The global activity of all the same ion channels is modeled as a conductance that is non-linearly dynamically regulated. The ion channels are often voltage-dependent, modeled by voltage-dependent activation and inactivation gates. Ion flows through the channel following the concentration gradient until the membrane potential reaches its ion reversal potential E_ion. Altogether, the current flowing through the channel is described by the Ohm's law:

$$I_\mathrm{ion} = g_\mathrm{ion}(V_\mathrm{m} - E_\mathrm{ion})$$

where E_{ion} is the reversal potential also called Nernst potential and g_{ion} is the equivalent ion channel conductance. The conductance can vary between 0 when all the channels are closed up to the maximal conductance $\bar{g}_{\text{ion}}$ when all the channels are open. The maximal conductance depends on the density of the ion channel at the membrane. The opening and closing of the ion channels are regulated by activation and inactivation gates respectively modeled by m_{ion} is the activation variable and h_{ion} is the inactivation variable. And so the current flowing through an ion channel is

$$I_{\text{ion}} = \bar{g}_{\text{ion}} m_{\text{ion}}(V_{\text{m}}) h_i(V_{\text{m}})(V_{\text{m}} - E_i)$$

These gates are voltage-dependent and are governed by the following dynamics:

$$\tau_{x_{\text{ion}}}(V_{\text{m}})\dot{x}_{\text{ion}} = x_{\text{ion},\infty}(V_{\text{m}}) - x_{\text{ion}}$$

where x corresponds to either the activation or inactivation gate, $\tau_{x_{\text{ion}}}$ is the voltage-dependent time-constant and $x_{\text{ion},\infty(V_{\text{m}})}$ is the voltage-dependent steady state value, which is the fraction of open ion channels at the steady state at a given value of V_{m}. These two voltage-dependent variables are often defined by sigmoidal functions.

Modeling neurons as a RC circuit with voltage-dependent conductances was a huge breakthrough in computational neuroscience brought by Hodgkin and Huxley seventy years ago (Hodgkin and Huxley, 1952). It provided a strong framework to simulate an action potential, through the interaction between sodium and potassium channels that are activated at different timescales and values of the membrane potential. This interplay is embedded in the differential equations describing the time constants and the gating variables of the different ion channels. These equations were fitted on electrophysiological recordings.

Altogether, Kirchoff's current law is applied on the capacitance current, the sum of all the ion currents and the external applied current I_{app}

$$I_C + \sum_i I_{\text{ion}} = I_{\text{app}}$$

Finally, the evolution of the membrane potential is defined by

$$C_{\text{m}}\dot{V}_{\text{m}} = -\sum_i I_{\text{ion}} + I_{\text{app}} \tag{3.1}$$

This framework has been extensively used over the past few decades. Like any model, it has its advantages and disadvantages. Each ion channel is described by one or two differential equations for the gates, which significantly increases the computing time but offers valuable biophysical insights. The various parameters have to be fitted according to the neuron type, which presents a challenging degree of freedom (Prinz et al., 2003).

Box 4 - Model of Hodgkin and Huxley: a turning point in computational neuroscience

The model relies on its intricate sets of non-linear differential equations and parameters derived from World War II era experiments. In Hodgkin's obituary, Huxley said: (Huxley, 2001) "To my surprise, the "Hodgkin– Huxley equations" that we published have survived with relatively little modification, although at the time I thought that they were very provisional and would soon be superseded".

This unexpected twist showcases the irony of scientific discovery, where what was thought to be temporary turns out to be timeless, forever shaping our understanding of neuronal behavior and electrical signaling (Sepulchre, 2020).

3.1.2 Modeling neuronal spiking activity

The conductance-based model offers a detailed framework for accurately predicting the evolution of the membrane voltage. However, if one is only interested in spike timings, using this model can be computationally expensive. The choice of an appropriate neuron model depends on the application, research question, and desired level of detail.

This section presents a non-exhaustive list of computational models used to describe neuron activity, divided into five categories: conductance-based model, integrate-and-fire model, event-based model, rate-based model and more complex models grouped under the category of 'Others' (Figure 3.1). For further details, refer to (Gerstner et al., 2014).

- Conductance-based model
  The voltage of the neuron's membrane, denoted as V_{m}, can be described using the Hodgkin and Huxley formalism (Hodgkin and Huxley, 1952) as shown in equation (3.1). The number of ion channels present in the neuron depends on its type and location and can be modeled as a single-point neuron or as multiple compartmental models. The timing of a neuron's spike can be determined by tracking the point at which its membrane voltage crosses a certain threshold.

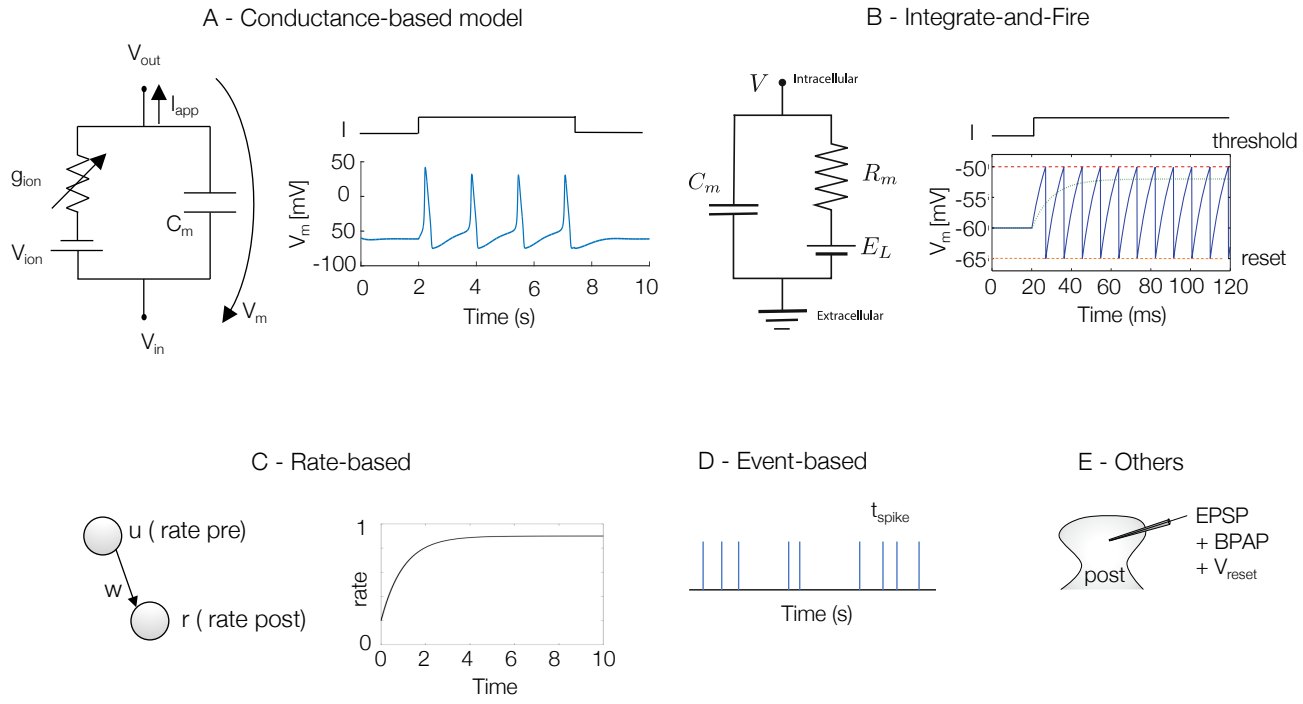

Figure 3.1: Schematic of the different types of neuron models. **A.** A Conductance-based model details the different ion channel contribution and model the membrane as a capacitance. **B.** An Integrate-and-Fire (IF) only models the subthreshold dynamics by a RC circuit (Fourcaud-Trocmé, 2014). **C.** A rate-based model provides the postsynaptic rate as function of the weighted presynaptic rate (Neuromatch, 2021). **D.** The model only considers the neuron spike. **E.** Other models exist with more detailed description of neuronal activity.

- Integrate-and-Fire (IF)
  This implementation aims to describe the shape of the action potential until it reaches its threshold, also called the subthreshold dynamics and it skips the detail concerning the fast increase of the membrane voltage. It lies on the equivalence of the RC circuit by modeling the charge of a capacitance. Its generic equation is

$$C_{\mathrm{m}}\dot{V}_{\mathrm{m}} = -g_{\mathrm{leak}}(V - E_{\mathrm{leak}}) + I_{\mathrm{app}} \qquad \text{if } V_{\mathrm{m}} = V_{\mathrm{th}}, \text{ then } V = V_{\mathrm{rest}}$$

  where g_{leak} is the fixed ohmic leak conductance to account for all ion channels, E_{leak} Nernst potential. For a sufficient applied current I_{app}, the membrane potential V_{m} increases until a threshold value V_{th}. Then, it is reset to the resting state V_{rest}. The potential increases again until the reset and so on. There are several types of IF models detailed in [(Gerstner et al., 2014)]. This formulation is faster compared to conductance-based model but lacks biological details. Variations of IF are encountered in computational models such as the Quadratic Integrate-and-Fire (QIF) or Adaptive Exponential Integrate-and-Fire (AdEx) among others.

- Event-based
  The membrane voltage is not explicitly or as precisely described as in a conductance-based model or an IF model. The spike timing activity is given as a *train of spikes*. Computationally, it can be a simple vector of time associated with each spike time. It is directly injected through a term $\delta(t - t_{\mathrm{spk}})$. The simulation only uses the spike trains to drive its model.

- Rate-based
  The firing rate equation is:

$$\tau\dot{r} = -r + F(I)$$

  where τ is the decay time constant, r is the rate of the neuron in Hz and $F(I)$ is the function the input current. It assumes that the activity of the neuron can be described by its average firing rate. It is simpler than IF. It is often used in large-scale models (Neuromatch, 2021).

- Others
  This category gathers diverse models such as multiple-timescale adaptable models with threshold Lappalainen et al. (2019), models considering only Back-Propagating Action Potential (BPAP), EPSP or models converting spike time into exponential decaying term to mimic the membrane voltage fluctuation. More biological details can be

added to deliver an equation of neuron activity. Therefore, this category permits to encapsulate models that are not perfectly following the more common design of conductance-based, integrate-and-fire, event-based and rate-based implementation.

3.2 Modeling neuronal circuit and network

This thesis adopts the conductance-based paradigm to model neurons, and this section provides a detailed explanation of connecting neurons within this framework. Connecting neurons is a straightforward process, drawing upon the electrical circuit analogy of neurons. Synaptic currents are represented simply as input currents, facilitating the modeling of synaptic connections.

$$C_{\mathrm{m}}\dot{V}_{\mathrm{m}} = -\sum_{i} I_{\mathrm{ion},i} + I_{\mathrm{app}} + I_{\mathrm{syn}}.$$

In this thesis, we consider three synaptic currents driven by different postsynaptic receptors: AMPA, $\mathrm{GABA_A}$ and $\mathrm{GABA_B}$.

There are different manners to describe synaptic currents (Destexhe and Marder, 2004). In my thesis, I follow the Hodgkin and Huxley (HH) formalism such that the postsynaptic receptors allow the flow of ions following the gradient concentration when the channel gate is open. The synaptic currents are defined by:

$$\begin{aligned} I_{\mathrm{AMPA}} &= \bar{g}_{\mathrm{AMPA}}\, s_{\mathrm{AMPA}}(V_{\mathrm{m}} - 0) \\ I_{\mathrm{GABA_A}} &= \bar{g}_{\mathrm{GABA_A}}\, s_{\mathrm{GABA_A}}(V_{\mathrm{m}} - E_{\mathrm{Cl}}) \\ I_{\mathrm{GABA_B}} &= \bar{g}_{\mathrm{GABA_B}}\, s_{\mathrm{GABA_B}}(V_{\mathrm{m}} - E_{\mathrm{K}}) \end{aligned}$$

where $\bar{g}_{\mathrm{AMPA}}$, $\bar{g}_{\mathrm{GABA_A}}$ and $\bar{g}_{\mathrm{GABA_B}}$ are the synaptic conductances.

AMPA receptor reversal potential is set to 0 mV, $\mathrm{GABA_A}$ receptor reversal potential is set to chloride reversal potential ($E_{\mathrm{Cl}} = -70\,\mathrm{mV}$) and $\mathrm{GABA_B}$ receptor reversal potential is set to potassium reversal potential ($E_{\mathrm{K}} = -85\,\mathrm{mV}$).

The gating variables of the synaptic receptors are s_{AMPA}, $s_{\mathrm{GABA_A}}$ and $s_{\mathrm{GABA_B}}$ are variables whose dynamics depend on the activity of the presynaptic neuron. As the presynaptic neuron spikes, it releases neurotransmitters that bind to the receptors and open the receptors. To shortcut all the biological reactions, the gating variable dynamics are simply governed by the presynaptic activity. In my thesis, I use the presynaptic membrane potential:

$$\begin{aligned} \dot{s}_{\mathrm{AMPA}} &= 1.1\, T_{\mathrm{m}}(1 - s_{\mathrm{AMPA}}) - 0.19\, s_{\mathrm{AMPA}} \\ \dot{s}_{\mathrm{GABA_A}} &= 0.53\, T_{\mathrm{m}}(1 - s_{\mathrm{GABA_A}}) - 0.18\, s_{\mathrm{GABA_A}} \\ \dot{s}_{\mathrm{GABA_B}} &= 0.016\, T_{\mathrm{m}}(1 - s_{\mathrm{GABA_B}}) - 0.0047\, s_{\mathrm{GABA_B}} \end{aligned}$$

with transmitter concentration T_{m} depends on the presynaptic membrane voltage and the dynamics follow the formalism described in (Destexhe et al., 1994), that is,

$$T_{\mathrm{m}}(V) = \frac{1}{1 + \exp\left[-(V-2)/5\right]}.$$

The numerical values (1.1, 0.19, 0.53, 0.18, 0.016 and 0.0047) are rate parameters to mimic the kinetics of the synaptic receptors. These values originated from (Destexhe et al., 1994). The smallest, the slowest the kinetics. For $\mathrm{GABA_B}$, the kinetics is slower which is coherent with the metabotropic nature of this receptor.

The literature presents alternative models for synaptic receptor gating variables. Instead of translating the presynaptic membrane potential into a change in the gating variable, some models use the presynaptic spiking time. For instance, the fraction of open postsynaptic receptor channels, represented by $[O]$, is a function of the presynaptic spiking time and the concentration of transmitters $[T]$. This model considers the following equations (Wei et al., 2016):

$$[\dot{O}] = \alpha_{[O]}(1 - [O])[T] - \beta_{[O]}[O]\ [\dot{T}] = A_T \mathbb{I}(t_0 + t_{\mathrm{max,T}} - t)\mathbb{I}(t - t_0)$$

In these equations, t_0 represents the time of receptor activation, A_T and $t_{\mathrm{max,T}}$ represent the amplitude and duration of the neurotransmitter pulse, and $\beta_{[O]}$ and $\beta_{[O]}$ represent the rate constants of receptor opening and closing, respectively. The function $\mathbb{I}$ is a Heaviside step function. Another implementation involves integrating the presynaptic spiking time (Hill and Tononi, 2005). The synaptic gating variable increases with a fast term and decreases following a slow decay, mimicking the opening and closing of the gate (also called dual exponential response).

The aforementioned equations highlight the vastness of the field of computational neuroscience. The process of modeling the dynamics of synaptic receptors requires making decisions, which can vary depending on factors such as the desired level of detail and time efficiency.

A fourth synaptic current can be encountered; the synaptic current through NMDAr. Its implementation using the HH formalism requires an additional term modeling the effect of the magnesium blocker:

$$I_{\mathrm{NMDA}} = \bar{g}_{\mathrm{NMDA}} B(V_{\mathrm{m}}) s_{\mathrm{NMDA}} (V_{\mathrm{m}} - 0)$$

where $B(V_{\mathrm{m}})$ is a sigmoidal function dependent on the postsynaptic membrane potential. In my thesis, the presence of NMDAr is modeled following (Graupner and Brunel, 2012) to ease the implementation of synaptic plasticity rule see Section 3.5.4. In Supplementary Material D, different manners to model NMDA are listed.

3.3 Modeling switches between tonic firing and bursting: techniques encountered in the literature

The preceding sections have provided an overview of neuron modeling and how to connect them together to build circuits and networks. In this section, I will describe several methods for inducing a switch in neuronal activity from tonic firing to bursting, which is the primary focus of my thesis. Then, I will present the characteristics of my circuit in this regard.

One common practice is to modify intrinsic and synaptic mechanisms (Esser et al., 2009; Krishnan et al., 2016; Wang, 2010; Rasmussen et al., 2017). In conductance-based modeling, ion channel and synaptic conductances are altered (Figure 3.2). Examples encountered in the literature include increasing the potassium leak conductance to mimic the varying action of acetylcholine during different brain states, thus inducing switches from tonic firing to bursting (González et al., 2020). Muscarinic receptor activation is sometimes modeled by changes in certain sodium conductances (Hill and Tononi, 2005), and the activation curve of the H-current can also be shifted (Wei et al., 2016) (Figure 3.2B(ii)). Other conductances that may be modified include those of T-type calcium channels, calcium-activated potassium channels, and H-current channels. The external potassium concentration may also be altered (Bacak et al., 2016). Modifying synaptic conductances is also an option (Figure 3.2). This practice raises questions about the compatibility and interaction of this switching technique and synaptic plasticity, as synaptic conductances can encode learning and memory while simultaneously being tuned to another value to drive the shift in neuronal activity. Another method is to hyperpolarize the neuron to de-inactivate T-type calcium channels (as explained in Figure 2.9) (Drion et al., 2019).

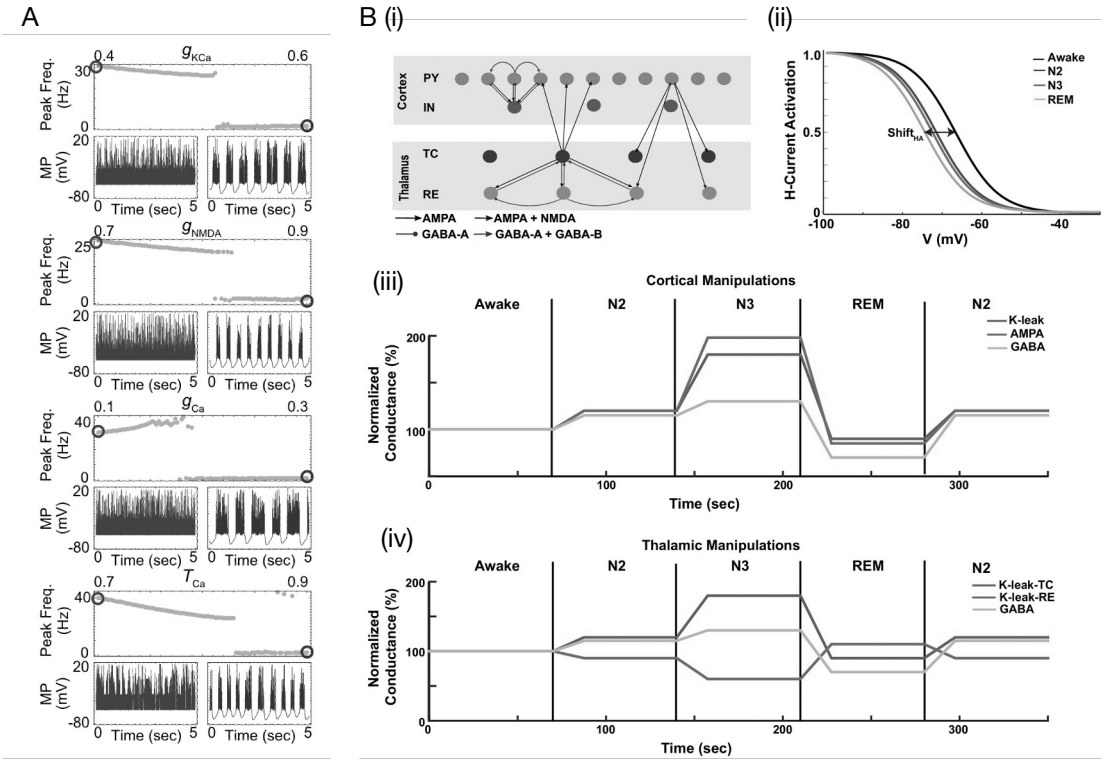

Figure 3.2: Models of switches in firing activity in biophysical neuron and circuit models. A. A switch from tonic firing to bursting is induced by a change in conductances. **B.** A thalamocortical network (i) is able to switch is neuronal activity by modifying H-current gating variable (ii) or by tuning the potassium leak conductance, the AMPA or GABA conductances depending on the state. Tonic firing is encountered in wake and REM) and bursting in sleep (N2-N3). Image A from (Tatsuki et al., 2016) and B from (Wei et al., 2016)

In reduced models, switches in neuronal activity are achieved by changing parameters that shift the shape of the

nullclines. For more information, refer to (Izhikevich and Hoppensteadt, 2004; Van Pottelbergh et al., 2018; Franci et al., 2014).

3.4 Neurons and circuits models coded in this thesis

3.4.1 Neurons are conductance-based models able to switch

The neuron model in this thesis follows a conductance-based formalism from (Drion et al., 2018). formalism such as:

$$C_{\mathrm{m}}\dot{V}_{\mathrm{m}} = -I_{\mathrm{Na}} - I_{\mathrm{K,D}} - I_{\mathrm{Ca,T}} - I_{\mathrm{K,Ca}} - I_{\mathrm{H}} - I_{\mathrm{leak}} + I_{\mathrm{app}},$$

where

- $I_{\mathrm{Na}} = \bar{g}_{\mathrm{Na}}\, m_{\mathrm{Na}}^3\, h_{\mathrm{Na}}\ (V_{\mathrm{m}} - E_{\mathrm{Na}})$ is a transient sodium current,
- $I_{\mathrm{K,D}} = \bar{g}_{\mathrm{K,D}}\, m_{\mathrm{K,D}}^4\ (V_{\mathrm{m}} - E_{\mathrm{K}})$ is a delayed-rectifier potassium current,
- $I_{\mathrm{Ca,T}} = \bar{g}_{\mathrm{Ca,T}}\, m_{\mathrm{Ca,T}}^3\, h_{\mathrm{Ca,T}}\ (V_{\mathrm{m}} - E_{\mathrm{Ca}})$ is a T-type calcium current,
- $I_{\mathrm{K,Ca}} = \bar{g}_{\mathrm{K,Ca}}\, m_{\mathrm{K,Ca}}([\mathrm{Ca}^{\mathrm{T}}])\ (V_{\mathrm{m}} - E_{\mathrm{K}})$ is a calcium-activated potassium current,
- $I_{\mathrm{H}} = \bar{g}_{\mathrm{H}}\, m_{\mathrm{H}}\ (V_{\mathrm{m}} - E_{\mathrm{H}})$ is a hyperpolarization-activated cation current,
- $I_{\mathrm{leak}} = \bar{g}_{\mathrm{leak}}\ (V_{\mathrm{m}} - E_{\mathrm{leak}})$ is a leak current,
- I_{app} an external applied current,

and where m (resp. h) represents the activation (resp. inactivation) variable of the ion channel i. More details about the different ion channels and the parameters used are provided in Supplementary Materials D.

Figure 3.3 shows a simulation of the neuron model. It corresponds to a current-clamp experiment. The applied current is decreased at 500ms which hyperpolarizes the neuron. It switches from tonic firing to bursting. A short transient behavior is noticed after the hyperpolarization.

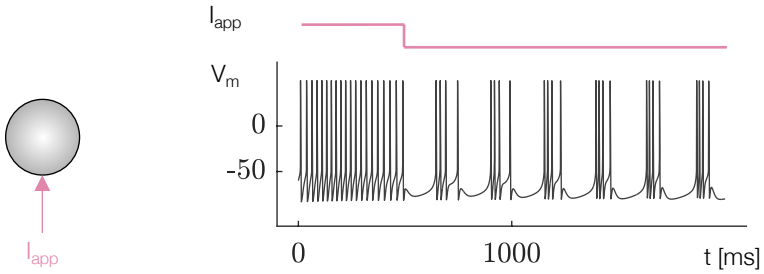

Figure 3.3: Simulation of a neuron switching from tonic firing to burst due to a hyperpolarizing current step. The membrane voltage V_{m} is expressed in mV.

3.4.2 Circuit with excitatory and inhibitory neurons

First, we consider a circuit consisting in two conductance-based model neurons: an excitatory glutaminergic neuron (E) and an inhibitory GABA neuron (I). we illustrate two situations; either the two neurons are reciprocally connected or the inhibitory neuron is synapsing to the excitatory neuron only (Figure 3.4).

In the first situation, depolarizing the inhibitory neuron drives it in tonic spiking that in turn sets the excitatory neuron in a hyperpolarized state. At 1000ms, a brief depolarizing pulse is injected in the excitatory neuron that produces one burst. Then, the inhibitory neuron is hyperpolarized. It switches the circuit in bursting (Figure 3.4A). In the second situation, the connectome is changed. We reproduce the same protocol but with different parameters for the synaptic conductances and the ion channel conductances. The excitatory is less hyperpolarized meaning that a brief applied current triggers an action potential (Figure 3.4B).

These two small computational experiments are simply illustrating different connectomes and switches in neuronal activities.

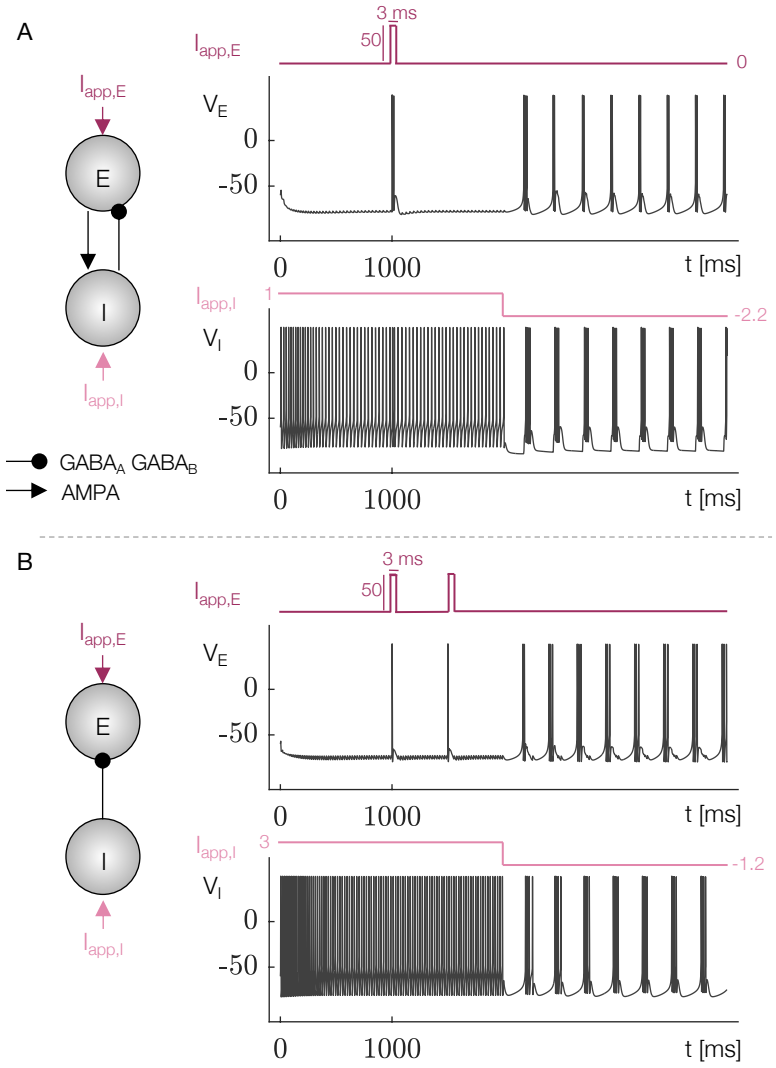

Figure 3.4: Simulation of a two-neuron circuits able to switch from desynchronized to synchronized state. A. Reciprocal connectome: An inhibitory neuron (I) synapses GABA currents to an excitatory neuron (E) which in turn synapses AMPA currents. **B.** Feadforward connection from the inhibitory neuron to the excitatory neuron. In both situations, hyperpolarization of the inhibitory neuron switches the circuit in synchronized bursting state.

3.5 Modeling synaptic plasticity

The section is a part of the perspective paper under progress to question the interaction between existing synaptic plasticity rules and switches in neuronal activity. I had the opportunity to present this work at the Annual Conference of the Belgian Society for Neuroscience in 2021 in Brussels for a talk presentation `https://hdl.handle.net/2268/291895`.

The first part of the perspective paper is a description of synaptic plasticity implementation and the diverse modeling choices. The second part is a taxonomy of the different rules often encountered in the literature, classified in a systematic manner. The third part is presented in Chapter 5 to test well-known synaptic plasticity rules for small neuronal activity switches or perturbations.

Therefore, the following chapter can be seen as a booklet for novices in modeling synaptic plasticity which can be used as a tutorial to understand the different notions to consider while looking for a synaptic plasticity rule.

Neurons have the ability to change their connections with each other based on their activities. Modeling synaptic plasticity consists in creating a model seen as a black box, that uses the pre- and postsynaptic activities as inputs and provides the synaptic strength as output. It is a challenging task because it requires several model decisions, called model features, such as the choice of the brain region, the network size, the neuron model and the definition of the synaptic strength (Figure 3.5A). Then, the core of the challenge is to create the dynamics that govern the evolution of the synaptic strength, *i.e.* the synaptic plasticity rule itself.

3.5.1 Model features

The region of interest

First of all, synaptic plasticity varies depending on the brain *region* (Figure 3.5B). It has been commonly modeled for neurons in the hippocampus (Abarbanel et al., 2003; Van Rossum et al., 2000), the cortex (Chen et al., 2013), the striatum (Nakano et al., 2010; Jedrzejewska-Szmek et al., 2017) or the thalamus (Gjorgjieva et al., 2009). But thanks to the freedom in computational models, a neuron can be adaptable by changing its parameters as done in (Graupner and Brunel, 2012; Clopath et al., 2010) or we can describe an 'abstract neuron' meaning that the associated brain region or the neuron type is not accurately defined and the parameters have been not fitted on experimental data. It is useful to study more general phenomena and to study plasticity using the spike train only for example (Karmarkar and Buonomano, 2002; Liu et al., 2015)

The network size

The second feature is the *network size* (Figure 3.5B). Plasticity can be studied locally by considering only at the postsynaptic site (Graupner and Brunel, 2012; Pfister and Gerstner, 2006). The presynaptic neuron in that case is considered only by its spiking activity for example or by its membrane voltage. It is also common to see a large number of presynaptic neurons projecting to a postsynaptic neuron (Chen et al., 2013; González-Rueda et al., 2018). Thanks to the computer efficiency improvement, the network size can be increased from small networks of 10 neurons to a very large network of thousands of neurons (Chindemi et al., 2022). Similarly, memory engrams rise interest and can be studied in interconnected networks (Delamare et al., 2022).

The neuron model

The third important feature is the computational model of the neuron, which must accurately reproduce its electrical activity (Figure 3.5B). The most commonly used models have been introduced in Section 3.1.2 and include the conductance-based model (Hartley et al., 2006; Gerkin et al., 2010), the integrate-and-fire model and its derivatives (Bush and Jin, 2012; Izhikevich, 2007), the event-based model (Shouval et al., 2002), and rate-based models (Delamare et al., 2022). More complex implementations, such as the description of the Back-Propagating Action Potential (BPAP) and the Excitatory Postsynaptic Potential (EPSP), have been developed, among others (Kumar and Mehta, 2011). Although there are many other computational models of neuron activity, we will limit the discussion to these five approaches. For further information, refer to (Gerstner et al., 2014).

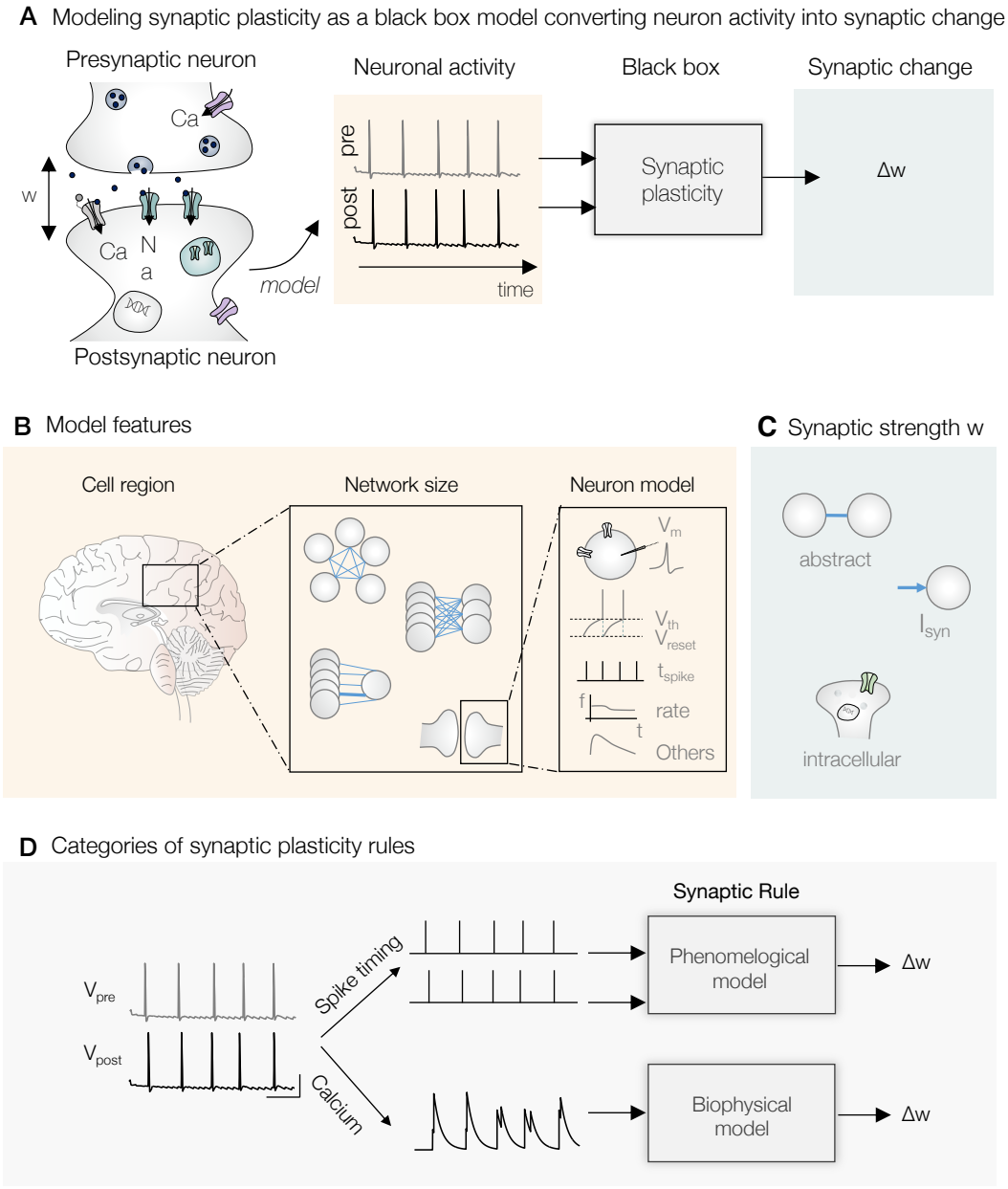

Figure 3.5: Synaptic plasticity model is seen as a black box converting neuronal activity into synaptic change and requires several modeling choices (from neuron, circuit and rules). A. Schematic of the black box concept for synaptic plasticity. **B.** To model the neuronal activity, the region of interest, the network size, the type of neuron model must be clearly defined. **C.** There exists several definition of the synaptic strength that will lead to different variable that we encapsulate in w for sake of simplicity. **D.** There are two main categories of synaptic plasticity rules; phenomenological models convert spike timing into synaptic change and biophysical models use calcium.

The definition of the synaptic strength

The last feature is the *definition of the synaptic strength w* (Figure 3.5C). We highlight three widespread forms.

- Abstract
  The weight w is simply a variable updated by the synaptic plasticity rule and it is not interfering in other model equations. It is encountered in more theoretical papers. We call it an abstract definition (Shouval et al., 2002; Gerkin et al., 2010).

- I_{syn}
  The term w is present in the model and weights the synaptic input. In an Integrate-and-Fire model or in a conductance-based model, the synaptic current is written $I_{\text{syn}} = wF_{\text{syn}}$ where F_{syn} is either a function of the spiking time $\delta(t_{\text{spk}})$ or pre- or postsynaptic membrane voltage $I_{\text{syn}} = \bar{g}_{\text{syn}}(V - E_{\text{syn}})$ such as $\bar{g}_{\text{syn}} = w\bar{g}_{syn}$ (resp. $w\bar{g}_{\text{AMPA}}, w\bar{g}_{\text{NMDA}}$). In more mathematical models, it weights the synaptic activity as done in (Tetzlaff et al., 2013).

- Intracellular
  The strength is quantified by biological quantities, for example the change in the concentration of phosphorylated CaMKII or the concentration of active and phosphorylated AMPAr (Saudargienė and Graham, 2015).

3.5.2 Traditional synaptic plasticity rules

Modeling of synaptic plasticity is trendy these recent years. Browsing the literature to find a synaptic rule adapted to your research can be very challenging. The number of publications providing models of synaptic rules has been increasing over years. The rules can be declined following a very abstract equation to a huge set of detailed plasticity signaling reactions. A myriad of reviews detail models of synaptic plasticity rules since the last 20 years (Morrison et al., 2008; Citri and Malenka, 2008; Feldman, 2012, 2020; Shouval, 2007; Sjöström and Gerstner, 2010; Manninen et al., 2010; Lisman and Spruston, 2010; Markram et al., 2011, 2012; Van Rossum and Shippi, 2013; Fusi and Abbott, 2007; Senn and Group, 2020; Magee and Grienberger, 2020; Chrol-Cannon and Jin, 2014). In the following section, we recall the notion of synaptic plasticity rule and we explain the most encountered models.

Categories of synaptic plasticity rules

Once the region, the network, the neuron and the definition of the synaptic strength have been established, the next primordial step is the implementation of the synaptic plasticity rule. It is translated by an equation describing the evolution of the weight w throughout time $\dot{w}$. The synaptic rule can be seen as the *black box* converting pre and postsynaptic activity as input (A_{pre} and A_{post}), which are implemented for example by the spike times, the firing frequency of the pre- and postsynaptic neurons or the calcium concentration and providing the synaptic change as output (Figure 3.5A) The generic equation is:

$$\dot{w} = F(A_{\text{pre}}, A_{\text{post}})$$

Two main categories of synaptic rules are distinguished (Shouval, 2007; Graupner, 2017; Clopath, 2019)(Figure 3.5D):

- *Phenomenological models* estimate the synaptic strength change by translating the relationship between neuronal activity and the synaptic plasticity. This category of model expresses mathematically the relation between the pre- and post spike times ($t_{\text{pre}}, t_{\text{post}}$), the firing frequency ($f_{\text{pre}}, f_{\text{post}}$) or the neuronal activity to estimate the change in synaptic strength. This approach focuses on abstract equations able to fit experimental data rather than describing all molecular processes underneath.

- *Biophysical models* using biological variables to drive the induction and expression of synaptic plasticity such as calcium concentration or a cascade of kinase activation for example. Indeed, calcium is a good indicator of voltage, frequency, and action potential variation (Feldman, 2012).

The following sections explains their implementations. This method of classification and model description was iniated in (Clopath, 2019).

Synaptic plasticity rule limitations

In the context of this thesis, our research is restricted to excitatory synaptic plasticity and inhibitory synaptic plasticity is put aside. For more details, refer to (Wu et al., 2022). Models of plasticity in the field of machine learning and artificial intelligence such as backpropagation for example are out of scope.

I am interested in articles that investigate the change in synaptic strength due to neuronal activity in order to understand learning, memory formation, and memory consolidation. The types of synaptic plasticity models consider in the following section are related to E-LTP, *i.e.* only change in postsynaptic receptors efficacy and insertion of new receptors via fast trafficking as described in Section 2.4.2. Later, section 3.5.5 details models of L-LTP, also refered as structural plasticity.

Fitting the parameters of the black box on experimental data

To create a model, one must choose values for various parameters. To parameterize a synaptic plasticity rule, a common practice is to replicate a plasticity-inducing protocol, as illustrated in Figure 2.16. The goal is to fit the experimental points, the two most often encountered dataset is the STDP provided by (Bi and Poo, 1998) (Figure 2.15) or the frequency-dependent plasticity protocol provided by (Sjöström et al., 2001).

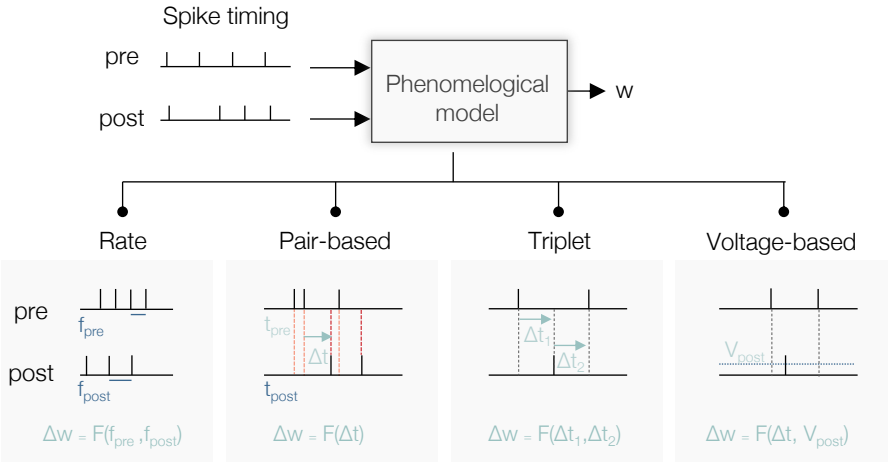

Figure 3.6: Summary of the four main phenomenological models referred as rate-based model (Oja, 1982), pair-based model (Song et al., 2000), triplet model (Pfister and Gerstner, 2006) and voltage-based (Clopath and Gerstner, 2010).

Phenomenological models

In phenomenological models, four pioneered synaptic rules were established in the last 20 years: Rate-based, pair-based, triplet, and voltage-based as illustrated in Figure 3.6 (Gerstner, 2011; Feldman, 2012, 2020).

In line with the Hebbian principle (Hebb, 1949), first models of synaptic plasticity consider only the *rate* of pre- and postsynaptic neurons (f_{pre}, f_{post}) to determine the sign and magnitude of plasticity [model:Oja (1982); Bienenstock et al. (1982); Udakis et al. (2020)]. The *Pair-based* model often called the *Spike-Time Dependent Plasticity (STDP)* [review: Abbott and Nelson (2000); Morrison et al. (2008))] suggests the equation to fit the experimental data resulting from the plasticity-induction protocol (Bi and Poo, 1998). The pre and postsynaptic neurons are spiking at given frequency and the synaptic change depends on the spiking time lag Δt. It has been used in several studies since 20 years [model: Van Rossum et al. (2000); Song et al. (2000); Capone et al. (2019)]. The classical depression-potentiation kernel has been shown to change depending on the region or the animal [review: Abbott and Nelson (2000)]. It has been exploited for example in (Liu et al., 2015) A comprehensive history of STDP is established in [review: Markram et al. (2011); Feldman (2020)]. This rule is constrained by some limitations (Babadi and Abbott, 2016). The *triplet* rule considers the effect of spike triplets such as pre-post-pre or post-pre-post [model: Froemke and Dan (2002); Pfister and Gerstner (2006); Costa et al. (2015); Gjorgjieva et al. (2011)]. *Voltage-based* rules take into account the spike-timing in pre- and postsynaptic neurons as well as the membrane voltage of the postsynaptic neurons [model: Brader et al. (2007); Clopath et al. (2010)] in order to reproduce a larger variety of experimental protocols (Sjöström et al., 2001; Artola et al., 1990; Nevian and Sakmann, 2006).

Table 3.1 provides an overview of the four categories and their equations.

Calcium-based models

This part of the review only covers computational models using calcium as the key driver of the synaptic rule. Modeling of calcium dynamics is detailed in Section D. These rules provide equations explaining the calcium influx dependency. Either kinase or phosphatase proteins are activated leading to an increase or decrease of the strength (Meriney and Fanselow, 2019). This phenomenon is implemented into the synaptic rule with different levels of complexity depending on the model. We highlight three pioneered rules (Figure 3.7: sigmoid, threshold, and process).

First, the synaptic change is governed by a *sigmoid* function of the calcium level: $\tau_w([\text{Ca}])\dot{w} = \text{sig}([\text{Ca}]) - [\text{Ca}]$. A low calcium level does not change the synaptic weight (or at an extremely slow timescale). An intermediate level triggers slow depression while a high calcium level triggers fast potentiation. It reproduces the phosphatase and kinase action. This rule was pioneered by the calcium control hypothesis from (Shouval et al., 2002). The governing rule was further developed throughout time [model: Karmarkar and Buonomano (2002); Kumar and Mehta (2011); Shouval and Kalantzis (2005); Shah et al. (2006); Cai et al. (2007); Carlson and Giordano (2011); Rackham et al. (2010)]. It was used in several applications such as task orientation in place cells or to investigate the effect of the dendritic properties [model: Yu et al. (2008); Iannella et al. (2014); O'Donnel et al. (2011); Franks and Sejnowski (2002)]. The comparison with phenomenological models such as pair-based on triplet is established in (Shouval, 2011).

Next, the sigmoid function describing the continuous relationship between calcium concentration and synaptic change was simplified by (Graupner and Brunel, 2012) into a two-*thresholds* calcium levels triggering depression and potentiation. The comparison with phenomenological models is established in (Graupner et al., 2016). It was used in several studies

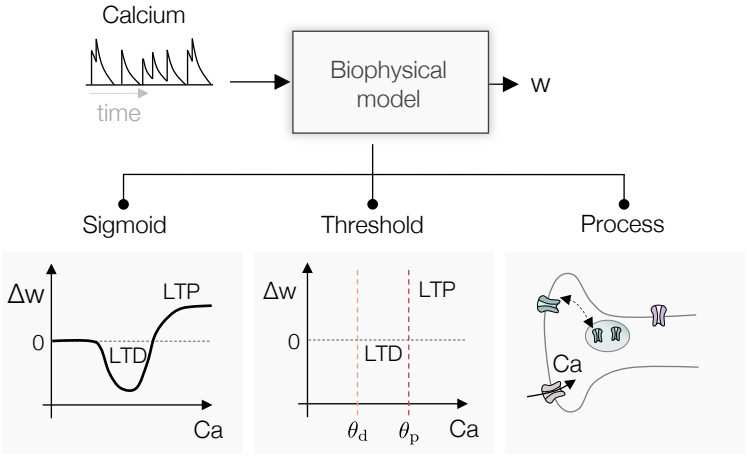

Figure 3.7: Summary of the three main biophysical models modeling the synaptic change according to a sigmoidal function of calcium (Shouval et al., 2002), or by two thresholds calcium levels (Graupner and Brunel, 2012) or by modeling biological details and signaling cascade triggered by calcium (Abarbanel et al., 2003).

for various regions such as the cerebellum or striatum and diverse applications such as memory formation in large-scale networks, [model: (Bouvier et al., 2016; Chindemi et al., 2022; Olcese et al., 2010; Standage et al., 2014; Higgins et al., 2014; Inglebert et al., 2021; Deperrois and Graupner, 2020; Lappalainen et al., 2019; Jedrzejewska-Szmek et al., 2017)].

A third approach uses intermediate steps that first convert calcium influx into intermediate signals and the change in these signals affects the synaptic weight such as $\dot{w} = F(P), \dot{P} = F([\text{Ca}])$ where P quantifies phosphorylation and dephosphorylation processes [model: (Abarbanel et al., 2003; Rubin et al., 2005; Badoual et al., 2006; Hartley et al., 2006; Graupner and Brunel, 2007; Gerkin et al., 2010; Bush and Jin, 2012; Houben and Keil, 2020; Kornijcuk et al., 2020; Saudargienė and Graham, 2015; Ebner et al., 2019)]. The level of details in calcium-driven varies a lot and it helps to provide a degree of freedom to explore the effect of biological factors, for example, the contribution of endoplasmic reticulum [model: (Kubota and Kitajima, 2008; Urakubo et al., 2008; Mahajan and Nadkarni, 2019)].

This review limits its investigation to articles that are only using a small number of intermediate signals and excludes papers proposing detailed mechanisms of the effect of calcium influx on the strength by more intermediates, for example, an interesting model is presented in (Mäki-Marttunen et al., 2020; Kotaleski and Blackwell, 2010). Other reviews like (Graupner and Brunel, 2010; Griffith et al., 2014) further examine and compare, calcium data, models depending only on calcium concentration, or implement biochemical signaling cascades beyond calcium.

Table 3.1 provides an overview of the four categories and their equations.

Model	Mechanism	Description	Reference
	Phenomenological models		
Rate-based	$\dot{w} = F(f_{\text{pre}}, f_{\text{post}})$	f_{pre}: presynaptic neuron firing frequency f_{post}: postsynaptic neuron firing frequency	Bienenstock et al. (1982) Oja (1982)
Pair-based	$\dot{w} = F(\Delta t) = \begin{cases} A^+ \exp(-\Delta t/\tau^+) & \Delta t > 0 \\ -A^- \exp(\Delta t/\tau^-) & \Delta t < 0 \end{cases}$	A^+, A^-: potentiation and depression parameters Δt: timelag between postsynaptic and presynaptic neuron spiking times	Song et al. (2000) Van Rossum et al. (2000)
Triplet	$\dot{w} = F(\Delta t_1, \Delta t_2)$	$\Delta t_1, \Delta t_2$ timelag between three spikes	Pfister and Gerstner (2006)
Voltage-based	$\dot{w} = F(\Delta t, V_{\text{post}})$	Δt: timelag between pre- and postsynaptic spike times V_{post}: postsynaptic membrane voltage	Clopath et al. (2010)
	Biophysical models		
Sigmoid	$\tau_w([\text{Ca}])\dot{w} = \text{sig}([\text{Ca}]) - [\text{Ca}]$	$\tau_w([\text{Ca}])$: calcium dependent time constant sig([Ca]): steady-state value with a sigmoid dependency on calcium	Shouval et al. (2002)
Threshold	$[\text{Ca}] < \theta_d : \dot{w} = 0$ $[\text{Ca}] \in \left[\theta_d, \theta_p\right] : w \nearrow$ $[\text{Ca}] > \theta_p : w \searrow$	θ_d: depression threshold θ_p: potentiation threshold	Graupner and Brunel (2012)
Process	$\dot{w} = F(P)$ $dP/dt = F([\text{Ca}])$	P: process variable $F([\text{Ca}])$: function of calcium signal	Abarbanel et al. (2003)

Table 3.1: Overview of synaptic plasticity rule mechanisms for phenomenological models or biophysical models. Each category is decomposed into its pioneered rules. The mechanisms for the synaptic change $\dot{w}$ are provided with a brief description.

Extended models

The previous synaptic rules are well-known in the literature but it was shown that they cannot explain all the various complex synaptic processes as introduced in Section 2.4.4. Here, we present models describing complementary synaptic mechanisms: (i) short term plasticity, (ii) burst-dependent plasticity, (iii) homeostasis, (iv) metaplasticity, (v) intrinsic plasticity, (vi) heterosynaptic plasticity, (vii) neuromodulated-plasticity and (viii) combinations of synaptic rules. The overview of the extensed models is shown in Figure 3.8.

(i) *Short-Term Depression (STD)* explains that after an action potential, presynaptic resources such as vesicles transporting neurotransmitters are depleted and need to recover to their initial value before being able to act again [review: Zucker and Regehr (2002)]. It is well known as the Markram-Tsodyks model [model: Markram et al. (1997)]. It is common to encounter synaptic plasticity rules including short-term depression in the model because it is modeled with a variable that decays on a fast timescale to mimic the decrease in available presynaptic resources after a spike transmission [model: Zenke et al. (2015); Chen et al. (2013); Olcese et al. (2010); Shah et al. (2006); Cai et al. (2007); Deperrois and Graupner (2020); Carvalho and Buonomano (2011); Hansel and Mato (2013)].

(ii) The *Burst-Time Dependent Plasticity (BTDP)* focuses on the timing of pre- and postsynaptic bursts of activity instead of single-spikes as done in STDP. It permits integration of the effect of high-frequency burst in the synaptic rule. The burst is often encapsulated as a single unit and the synaptic weight is modified dependening on the pre and postsynaptic burst time lag [model: Gjorgjieva et al. (2009); Delattre et al. (2015); Payeur et al. (2020)].

(iii) Hebbian learning rules often lead to a runaway of synaptic strengths (Babadi and Abbott, 2016). As simplified in (Fauth and Tetzlaff, 2016), strong inputs lead to strong connections, similar as positive feedback mechanisms. Once the synaptic strengths are modified by a learning rule it can affect the neuronal activity. To counterbalance this problem, *homeostatic plasticity* refers to compensatory processes operating at various spatial and temporal scales *allowing stabilization of neuronal activity* [review: Turrigiano and Nelson (2004); Karabanov et al. (2015); Meriney and Fanselow (2019); Desai (2003)]. More information on the biological explanations is given in (Shepherd et al., 2006).

If the target neuronal activity is the firing rate: the concept of homeostasis postulates that the connections between neurons should be either scaled up or down respectively as the firing rate decreases or increases [review (Desai and Walcott, 2016)]. From a modeling point of view, two processes are implemented. First, the *synaptic scaling* or *normalization* can be implemented via a multiplicative or substractive modifications of the synaptic weights (Oja, 1982). It aims to scale *all* synaptic weights onto the postsynaptic neuron by preserving the changes induced by Hebbian plasticity (Fauth and Tetzlaff, 2016). The second way is described by (Turrigiano et al., 1994; Turrigiano and Nelson, 2004). The different synapses or intrinsic conductances (see later for intrinsic plasticity) in concert to maintain a target firing activity. It is different that 'simply' dividing all the values by a same factor (as done in synaptic scaling).

If the target neuronal activity is the intracellular calcium level to maintain homeostasis, [model: (O'Leary et al., 2014)] developed a homeostatic rule regulating the synaptic conductances as well as the ion channel conductances. In [model: Yeung et al. (2004)], the NMDA conductance is regulated leading to regulation of the calcium influx through the NMADr.

(iv) *Metaplasticity* is often called "plasticity of synaptic plasticity" and states that previous activity at the synapse can influence LTP or LTD [review: Abraham and Bear (1996); Abraham (2008); Abraham et al. (2019); Meriney and Fanselow (2019); Deisseroth et al. (1995); Yger and Gilson (2015); Lee and Kirkwood (2019)]. It can be seen as a modulation of the synaptic rule itself at a larger timescale. In [model: (Zenke et al., 2013; Benuskova and Abraham, 2007)], synaptic rule parameters vary as a function of the moving firing rate. Metaplasticity was also investigated in calcium-based models [model: Yu et al. (2008); Anirudhan and Narayanan (2015)].

At this stage, the different terms can be confusing because metaplasticity can be homeostatic or not. If the metaplasticity is homeostatic; the synaptic rule changes itself with the aim of maintaining a target activity (Karabanov et al., 2015). Metaplasticity that is not homeostatic simply refers to a modification of the synaptic plasticity rule parameters.

(v) Until now, we have presented plasticity rules that affect the synaptic connection between neurons. However, activity-dependent modification of intrinsic neuronal excitability performed by change of neuronal membrane properties, more specifically the number, distribution or activity of various ion channels located throughout the neuron is another mode of memory formation and storage [review: Debanne et al. (2019); Caverzasio et al. (2018); Daoudal and Debanne (2003); Zhang and Linden (2003); O'Leary et al. (2015)]. This mode is called *intrinsic plasticity* (Titley et al., 2017). Two of the pioneered papers in this field are (LeMasson et al., 1993; Liu et al., 1998).

Once again, intrinsic plasticity can be homeostatic as summarized in [review: Williams et al. (2013); Turrigiano and Nelson (2000)] and modeled in [model: Honnuraiah and Narayanan (2013); O'Leary et al. (2014)]. Another implementation of intrinsic plasticity in a integrate-and-fire model is achieved by tuning the firing threshold [model: Wu et al. (2020)]. In rate-based model, intrinsic plasticity tunes the excitability threshold [model: Delamare et al. (2022)]. In [model: Sehgal et al. (2013)], one rule implements the intrinsic plasticity that exhibits metaplasticity.

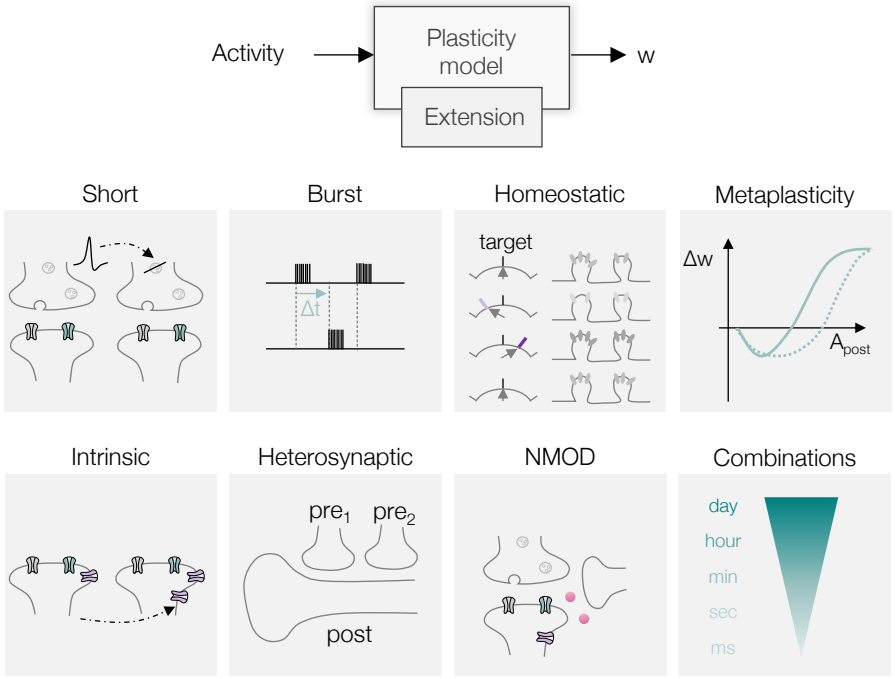

Figure 3.8: Schematic of more complex models of plasticity. **Short**-term dependent plasticity often focuses on presynaptic neurotransmitter release. **Burst**-time dependent plasticity often considers the burst as a whole unit. **Homeostatic** plasticity gathers all the processes that regulate the neuronal activity to its target value. **Metaplasticity** models the plasticity of the plasticity rule itself. **Intrinsic** plasticity refers to the change in neuronal properties rather than a change in synaptic properties. **Heterosynaptic** plasticity considers changes at neighboring synapses. **Neuromodulated** plasticity models the impact of neuromodulators on plasticity. It is often encountered in papers that **combined** several types of plasticity.

(vi) The classical view of synaptic plasticity is built on both presynaptic and postsynaptic neuron activation for plasticity induction. The rules previously described are input-specific and can be categorized as *homosynaptic* plasticity. However, at the same postsynaptic neuron, *heterosynaptic plasticity* refers to changes at synapses that are not presynaptically active during the induction protocol, in other words, the synaptic change is induced by activity in neighboring synapses [review: Meriney and Fanselow (2019); Timofeev and Chauvette (2019)]. Calcium in one synapse can trigger a change in the neighboring synapses [review: Bannon et al. (2016); Chistiakova et al. (2014); Froemke (2015)]. Thus, heterosynaptic plasticity is generated by the same protocols, operates at the same timescale and shares similar mechanisms with homosynaptic plasticity. It offers a solution for competition and stabilization by providing rapid normalization of synaptic strength over individual cells and multi-cellular networks. From a computational point of view, the synaptic strength is driven as already explained by the pre- and postsynaptic neuronal activity as well as the neighboring activity (phenomenological manner) or by affecting modeling the calcium fluctuation coming from the pre, post and neighboring synapses (biophysical manner) [model: Chen et al. (2013); Field et al. (2020); Hiratani and Fukai (2017); Li et al. (2016); Fiete et al. (2010)].

(vii) Experimental studies have more recently investigated the interaction of *neuromodulation* and synaptic plasticity [bio: Seol et al. (2007); Zhang et al. (2009); Salgado et al. (2012); Pawlak and Kerr (2008); Nadim and Bucher (2014)]. The effect of the different neuromodulators on synaptic plasticity is very complex. To name a few, neuromodulatory inputs gate STDP rules via modification of neuronal excitability and spiking dynamics or alteration of intracellular signaling cascades implied in synaptic plasticity [review: (Brzosko et al., 2019; Frémaux and Gerstner, 2015; Pawlak, 2010)]. There are two often encountered ways to derive neuromodulated-synaptic plasticity, either by neuromodulating the STDP or by using a three-factor rule.

The first one is inspired by neuromodulated-STDP. While adding neuromodulators during the STDP protocol, the kernel is shifted [model: (Pedrosa and Clopath, 2017; González-Rueda et al., 2018; Legenstein et al., 2008; Brzosko et al., 2017)]. It is very easy to implement this technique on computational models, the potentiation and depression parameters of the STDP kernel are just changed. It faithfully reproduces experimental data as shown in Figure 2.21E.

The second technique relies on the creation of a mathematical framework called a "*three-factor rule*" [review: Marder (2012); Frémaux et al. (2013); Brzosko et al. (2019); Frémaux and Gerstner (2015); Schultz (2006); Foncelle et al. (2018); Gerstner et al. (2018)]. This three-factor rule two signals: the 'eligibility' trace $e(t)$ and a modulatory trace $m(t)$ (Gerstner et al., 2018; Izhikevich, 2007). The evolution of the weight is obtained by $\dot{w} = e(t)m(t)$. The eligibility trace often follows a typical hebbian learning rule and therefore is driven by the pre- and the postsynaptic activity. Regarding to the modu-

latory signal, it is often modeled as a third signal. The change in the eligibility trace $e(t)$ "is not directly visible and does not automatically trigger a change of the synaptic weight. An actual weight change is implemented only if a third signal, e.g., a phasic increase of neuromodulator activity or an additional input" as explained in (Gerstner et al., 2018). More details on the mathematical implementation are available on (Izhikevich, 2007; Legenstein et al., 2008; Gerstner et al., 2018; Frémaux and Gerstner, 2015; Pawlak, 2010; Madadi Asl et al., 2018). This framework is attractive for reward-based learning, surprise-based learning and novelty-based learning [model: Nakano et al. (2010); Zannone et al. (2018); Ang et al. (2021); Schultz (2006)]. The website (URL, h) gathers numerous models of neuromodulated-synaptic plasticity rules.

(viii) Synaptic plasticity is complex occurring at different places and at different timescales. It is likely that one rule alone is not enough to have the whole picture of the different mechanisms. Therefore, several papers *combine different synaptic rules* at different timescales and include hebbian or homeostatic mechanisms altogether [model: Honnuraiah and Narayanan (2013); Bannon et al. (2017); Fauth and Van Rossum (2019); Zenke et al. (2015); Farries and Fairhall (2007); Wu et al. (2020); El Boustani et al. (2012); Nere et al. (2013); Vignoud et al. (2018)].

Table 3.2 briefly presents the implementation of these different extensions and their mechanisms. It extended the work presented in (Clopath, 2019).

Type	Mechanism	Description	Reference
Short-term	$\tau_{ST}\dot{X}_{ST} = 1 - X_{ST}$	X_{ST}: presynaptic resource, τ_{ST}: resource recovery time-constant	Zenke et al. (2015) Zucker and Regehr (2002)
Burst	$\dot{w} = F(\Delta t^{\text{burst}})$	Δt^{burst}: relative pre and post-synaptic burst timelag	Gjorgjieva et al. (2009)
Homeostasis	scaling: $w = w/w_{\max}$	$w_{\max}$: maximum weight	Turrigiano (2012)
	target activity: $\dot{w}$ prop. $A_{\text{tgt}} - A$	x : weight or ionic conductance A_{tgt}: target activity A: current activity	Williams et al. (2013) Desai and Walcott (2016)
Metaplasticity	$\tau_w\dot{w} = F(\theta)$ $\tau_\theta\dot{\theta} = F(A_{\text{post}})$	θ: threshold between depression and potentiation A_{post}: postsynaptic activity	Abraham and Bear (1996)
Intrinsic	$\dot{g}_{\text{ion}} = F(A)$	g_{ion}: neuron-related variable (ion channel conductance, excitability,...) A: current activity	LeMasson et al. (1993)
	IF: V_{th}	adapt the threshold	Wu et al. (2020)
	rate-based	tune the excitability	Delamare et al. (2022)
Heterosynaptic	$\dot{w_{kj}} = F(A_i, A_j, A_k)$	$A_{i,j}$: activity of presynaptic neuron i or j A_k: activity of neighboring postsynaptic neuron k	Chen et al. (2013) Field et al. (2020)
Neuromodulated	$\dot{w} = \begin{cases} \eta A^+ \exp(-\Delta t/\tau^+) & \Delta t > 0 \\ -\eta A^- \exp(\Delta t/\tau^-) & \Delta t < 0 \end{cases}$	η regulates the STDP kernel	Pedrosa and Clopath (2017)
	$\dot{w} = e(t)m(t)$	$e(t)$: eligibility trace $m(t)$: modulatory signal	Izhikevich (2007)
Combination	$\dot{w} = F(\text{rule}_1, \text{rule}_2)$	Combinations of different synaptic rules at different timescales	Zenke et al. (2015) Fauth and Van Rossum (2019)

Table 3.2: Overview of the more complex models of synaptic plasticity rules. The mechanisms of each rule is described with a conceptual equation.

3.5.3 Taxonomy of traditional synaptic plasticity rules

Developing mathematical equations for synaptic plasticity poses a significant challenge, as evidenced by the numerous models utilized to investigate learning, memory formation and consolidation, and to elucidate the biophysical mechanisms underlying plasticity, all in the pursuit of a better understanding of the signaling cascade. With the abundance of scientific articles available, it can be a daunting task to determine whether a proposed synaptic rule can be applied to a particular problem. This raises several questions, such as how to model neurons and which category of rules should be employed.

To facilitate the search for information, we have created a taxonomy of articles systematically investigating synaptic plasticity rules described in the past 25 years. The objective of this review is to *categorize* the existing models based on their rules and their computational features or model practices. This non-exhaustive classification has been compiled into Excel sheets following the structure provided in Table 3.3.

A. Model features

Region	Network size	Neuron model	Synaptic strength
Hippocampus (H)	One pre- to one postsynaptic neuron (1-1)	Conductance-based (cond)	Abstract weight (abstract)
Cortex (C)	Several pre to one postsynaptic neuron (L-1)	Integrate-and-Fire (IF)	Weighted synaptic input (Isyn)
Striatum (S)	Network/memory assembly (Network)	Event-based implementation (event)	Biological description (Intracellular)
Thalamus (T)		Rate-based (rate)	
Adaptable neuron parameters (adaptable)		EPSP, BPAP, ... (Others)	
Abstract neuron (abstract)			

B. Synaptic plasticity rules

Phenomenological rule	Calcium-based rule	Extended plasticity rule
Rate	Sigmoid	Short-term
Spike-Time	Threshold	Burst-dependent
Triplet	Process	Homeostatic
Voltage-dependent		Metaplasticity
		Intrinsic
		Heterosynaptic
		Neuromodulated
		Combinations

Table 3.3: Criteria for the taxonomy of synaptic plasticity rules. **A.** Classification of model features shared in computational models of synaptic plasticity. The label in brackets are found in the excel sheet. **B.** Classification of synaptic plasticity rules.

Box 5 - How to Navigate in the Jungle of Synaptic Plasticity Models?

The preliminary step is choosing your application and defining the different model features presented in Figure 3.5B).

Then, to aid scientists in selecting appropriate synaptic plasticity rules in computational neuroscience, here is the following guidance we developed. First, make the distinction between Hebbian and Homeostatic plasticity. Hebbian plasticity increases the connections between two neurons with correlated activity, while homeostatic plasticity maintains target neuronal activity.
To implement Hebbian or Homeostatic plasticity, choose a phenomenological (rate, pair-based, triplet, or voltage-based) or calcium-based rule (sigmoid, threshold, or process). This rule will modify the synaptic weight based on the pre- and postsynaptic activity or calcium activity, respectively.
You can add other mechanisms to modify:
- The intrinsic properties, such as models of intrinsic plasticity. It can drive Hebbian or homeostatic changes.
- The neighboring synaptic weights with models of heterosynaptic plasticity. Once again, it can be a hebbian or homeostatic mechanism.
- The initial plasticity rule can also be modified with metaplasticity.
- Neuromodulators can affect several steps of the plasticity mechanisms, participating in Hebbian learning or homeostatic regulations.

Additional details can be added as needed, for example, extended versions that may incorporate burst activity, which has been described with burst-dependent plasticity models, or short-term plasticity. Many rules exist for various applications, and multiple mechanisms can be combined.

3.5.4 Synaptic plasticity rules coded in this thesis

With the large number of synaptic plasticity rules already discussed in the literature, we wanted to explore and compare their behaviors during switches in neuronal activity. The two first models in the phenomenological category and the two first in the calcium-based category are selected. The following part details the model concept, the equations and the parameters.

Pair-based model

• Concept
This model is based on (Morrison et al., 2008; Song et al., 2000; Van Rossum et al., 2000). To reproduce the classical STDP window, the pair-based model is implemented using synaptic traces, respectively x and y for the pre- and postsynaptic cells:

$$\frac{dx}{dt} = -\frac{x}{\tau_x} + \delta\left(t - t_{\text{pre}}\right)$$
$$\frac{dy}{dt} = -\frac{y}{\tau_y} + \delta\left(t - t_{\text{post}}\right).$$

τ_x, τ_y are decaying timeconstants associated with the synaptic traces, t_{pre} (resp. t_{post}) representing the spike timing of the presynaptic (resp. postsynaptic) neuron , *i.e.* each time $t = t_{\text{pre}}$ (resp. $t = t_{\text{post}}$), and the $\delta(t)$ is a dirac function, *i.e.* $\delta(t - t_{\text{pre}}) = 1$ when $t = t_{\text{pre}}$.
The weight change relative to the STDP window was then computed using the following equations, with explicit hard bounds defined such as $0 < w < 1$:

$$w(t) \rightarrow \begin{cases} w(t) + A^+ x(t), & \text{at } t = t_{\text{post}}, \\ w(t) - A^- y(t), & \text{at } t = t_{\text{pre}}, \end{cases}$$

or using soft bounds :

$$w(t) \rightarrow \begin{cases} w(t) + A^+ (1 - w) x(t), & \text{at } t = t_{\text{post}}, \\ w(t) - A^- w y(t), & \text{at } t = t_{\text{pre}}, \end{cases}$$

where $A^+ > 0$, $A^- > 0$ (Morrison et al., 2008; Song et al., 2000; Van Rossum et al., 2000).

BOX 6 - Hard-bounds vs Soft-bounds

To avoid synaptic runaway, there are two modeling methods to constraint the synaptic weight change.
• Using **hard-bounds** models that synaptic changes do not scale with the synaptic strength. Upper and lower "boundaries are imposed as hards constraints" (Gütig et al., 2003). It is also referred as **additive model** (Song et al., 2000).
• Using **soft-bounds** models that "linear attenuation of potentiating and depressing synaptic changes as the corresponding upper or lower boundary is approached" (Gütig et al., 2003). It is also referred as **multiplicative model** (Van Rossum et al., 2000). Inspired by biology, stronger synapses are less likely to potentiate.

• Parameters:
Table 3.4 provides an overview of the different parameter values:

A^+	A^-	τ_x	τ_y
0.0096	0.0053	16.8	33.7

Table 3.4: Pair-based parameters from (Bi and Poo, 2001), data fitted on spike-timing dependent induced plasticity protocol done on the hippocampus.

• Simulation:
We extended the circuit presented in Section 3.4.1 with a four-cell circuits with an inhibitory neuron synapsing $GABA_A$ and $GABA_B$ currents on 3 excitatory neurons. Two presynaptic neurons are synapsing AMPA currents on a postsynaptic

neuron. This small circuit can be seen as a building block in larger network observed in several brain regions, for example in the thalamus or in the cortex (Sherman and Guillery, 1996; Destexhe and Marder, 2004; McCormick and Bal, 1997).

The inhibitory neuron is depolarized during the first 3 seconds at 3 nA/cm^2 then hyperpolarized at - 1.2 nA/cm^2. External currents are applied to excitatory neurons to drive them to fire at a desired mean frequency f_0. These currents are provided as pulses which last 3ms with an amplitude of 50nA/cm^2. The pulse train at a frequency f_0 is generated over a duration T. At this stage, an exact duration $T_0 = 1/f_0$ separates each pulse. Note that the train is shifted by a random delay uniformly drawn from the range $[0, T_0[$. Then, in order to model neuronal variability, a random shift drawn from a normal distribution $\mathcal{N}(0, 0.1T_0)$ is added to each pulse instant. This pulse train drives the neuron into spiking (can be called spike train).

Figure 3.9 shows the recordings of the membrane voltage of the different neurons in the circuit (left). The synaptic traces are also shown for the two presynaptic neurons and the postsynaptic neurons (right). At the bottom, membrane voltages and synaptic traces are zoomed in to show two situations: a presynaptic neuron spikes after a postsynaptic neuron causing a small diminution of w (post-pre). Conversely, a presynaptic neuron spikes before a postsynaptic neuron causes a small increase (pre-post). Switching to burst due to a small hyperpolarization of the inhibitory neuron generates a slow oscillatory oscillation in the synaptic traces which is further investigated in Chapter 6.

Triplet model

• Concept:
Similarly to pair-based model, the triplet model was implemented using trace variables following (Pfister and Gerstner, 2006):

$$\begin{aligned}
\frac{dx_1(t)}{dt} &= -\frac{x_1(t)}{\tau^+} + \delta\left(t - t_{\text{pre}}\right) \\
\frac{dx_2(t)}{dt} &= -\frac{x_2(t)}{\tau_x} + \delta\left(t - t_{\text{pre}}\right) \\
\frac{dy_1(t)}{dt} &= -\frac{y_1(t)}{\tau^-} + \delta\left(t - t_{\text{post}}\right) \\
\frac{dy_2(t)}{dt} &= -\frac{y_2(t)}{\tau_y} + \delta\left(t - t_{\text{post}}\right),
\end{aligned}$$

where t_{pre} (resp. t_{post}) is the timing of a presynaptic spike (resp. postsynaptic). The full model implemented by (Pfister and Gerstner, 2006) takes into account weight change due to pre-post, with the constant A_2^+, inducing potentiation or post-pre pairs, with the constant A_2^-, inducing depression (similar to the classical pair-based model, with $x_1(t)$ and $r_2(t)$ as the presynaptic and postsynaptic traces, respectively with their respective time constant τ^+ and τ^-).

The improvement over the classical pair-based model is that a triplet of spikes is also considered. Thanks to previously introduced traces y_2, decaying with a time constant τ_y, and x_2, decaying with τ_x, pre-post-pre triplets are treated (associated with the constant A_3^-, inducing depression) as well as post-pre-post triplets (associated with the constant A_3^+, inducing potentiation). Weight change goes as follows, with hard bounds (Pfister and Gerstner, 2006) defined such as $0 < w < 1$:

$$w(t) \to \begin{cases} w(t) + x_1(t)\left[A_2^+ + A_3^+ o_2(t-\epsilon)\right], & \text{at } t = t_{\text{post}}, \\ w(t) - o_1(t)\left[A_2^- + A_3^- x_2(t-\epsilon)\right], & \text{at } t = t_{\text{pre}}, \end{cases}$$

or using soft bounds Graupner et al. (2016):

$$w(t) \to \begin{cases} w(t) + x_1(t)(1-w)\left[A_2^+ + A_3^+ o_2(t-\epsilon)\right], & \text{at } t = t_{\text{post}}, \\ w(t) - o_1(t) w\left[A_2^- + A_3^- x_2(t-\epsilon)\right], & \text{at } t = t_{\text{pre}}, \end{cases}$$

ϵ is a small positive constant to ensure that the weight is updated before the detectors x_2 or y_2
• Parameters:

	Model	A_2^+	A_3^+	A_2^-	A_3^-	$\tau_x(ms)$	$\tau_y(ms)$
(C)	Minimal model	0	$6.5e^{-3}$	$7.1e^{-3}$	0	0	114
(H)	Minimal model	$5.3e^{-3}$	$8e^{-3}$	$3.5e^{-3}$	0	0	40

Table 3.5: Triplet parameters from (Pfister and Gerstner, 2006) fitted on cortical data (Sjöström et al., 2001) (C) and hippocampal data (Wang et al., 2005) (H). $\tau^+ = 16.8$ ms and $\tau^- = 33.7$ ms were always the same.

	Model	A_2^+	A_3^+	A_2^-	A_3^-	τ_x	τ_y
(C)	Minimal model	0	0.0165746	0.00826477	0	0	56.38

Table 3.6: Triplet parameters from (Graupner et al., 2016). Fitted on (Sjöström et al., 2001) (C). $\tau^+ = 16.8$ ms and $\tau^- = 33.7$ ms were the same as pair-based model.

• Simulations:
The model provides similar results as the pair based in tonic spiking as it is fitted on the same plasticity-induced protocols (Sjöström et al., 2001; Bi and Poo, 1998). More synaptic traces are used to take into account the configuration pre-post-pre and post-pre-post.

Calcium-based

• Concept
Calcium dynamics plays a key role in designing calcium-based rules. We consider the linear calcium dynamics suggested by (Graupner and Brunel, 2012; Graupner et al., 2016).

The presynaptic and postsynaptic spike contributions add linearly. Indeed, calcium enters from NMDA receptors and voltage-dependent calcium channels. Instead of describing the whole calcium, the phenomenological effect on the calcium variation is considered. At each pre or postsynaptic spike (respectively named as t_{pre} and t_{post}), the calcium immediately rises and then exponentially decays characterized by a calcium decay time constant equal to τ_{Ca}.

$$\frac{dc_{\text{pre}}}{dt} = -\frac{c_{\text{pre}}}{\tau_{\text{Ca}}} + C_{\text{pre}} \sum_i \delta(t - t_{\text{pre},i} - D),$$
$$\frac{dc_{\text{post}}}{dt} = -\frac{c_{\text{post}}}{\tau_{\text{Ca}}} + C_{\text{post}} \sum_j \delta(t - t_{\text{post},j}),$$

where C_{pre} and C_{post} are the presynaptically and postsynaptically evoked calcium amplitudes. The parameter, D is a time-delay between the presynaptic spike and the corresponding postsynaptic calcium transient occurrence that accounts for the slow rise time of the NMDAr-mediated calcium influx (Graupner and Brunel, 2012; Graupner et al., 2016).

The total calcium amplitude $[\text{Ca}](t)$ driving the synaptic change is given by: $[\text{Ca}](t) = c_{\text{pre}}(t) + c_{\text{post}}(t)$. The time-evolution for several pre- and postsynaptic spiking activity is written such as (Graupner et al., 2016):

$$[\text{Ca}](t) = \sum_i C_{\text{pre}} \exp\left(\frac{t - t_{\text{pre},i} - D}{\tau_{\text{Ca}}}\right) + \sum_j C_{\text{post}} \exp\left(\frac{t - t_{\text{post},j}}{\tau_{\text{Ca}}}\right).$$

The resting calcium concentration is set to zero. The calcium concentrations are dimensionless. Both simplification is acknowledged because the synaptic rules are adapted in accordance. If a resting calcium concentration is wanted, the thresholds of potentiation and depression will be adapted.

We use the breakthrough calcium-dependent synaptic rule was suggested by Michael Graupner and Nicolas Brunel in (Graupner and Brunel, 2012) and slightly modified in (Graupner et al., 2016). The model implements two opposing calcium-triggered pathways leading to increases or decreases in synaptic strength. Indeed, potentiation and depression are activated above calcium thresholds. This elegant formalism is described by the following equation:

$$\tau_w \dot{w} = \gamma_{\text{p}}(1 - w)\Theta([\text{Ca}] - \theta_{\text{p}}) - \gamma_{\text{d}} w \Theta([\text{Ca}] - \theta_{\text{d}}) \tag{3.2}$$

where τ_w is the time constant associated with synaptic change. It is composed of two terms, the first one corresponds to potentiation with the potentiation rate equal to γ_{p} and the second term is associated with the depression with the depression rate γ_{p}. The two variables θ_{d} and θ_d are respectively the threshold of potentiation and depression. The expression $\Theta([\text{Ca}] - \theta_{\text{p}})$ is equal to 1 if $[\text{Ca}] - \theta_p$ is greater to 0, *ie.* the calcium is larger than the threshold of potentiation named θ_p. Otherwise, if $[\text{Ca}] < \theta_p$, the expression is equal to 0. Similarly, $\Theta([\text{Ca}] - \theta_d)$ is equal to 1, if $[\text{Ca}] > \theta_{\text{d}}$, otherwise it is equal to 0. The parameter values, presented in Table 3.7 (Graupner et al., 2016), are chosen to ensure the model accurately reproduces the experimental data (Sjöström et al., 2001). The time constants are given in milliseconds, while the remaining units are dimensionless and adjusted to match the experimental observations.

• Simulations
The same circuit as described for the pair-based model is used (Figure 3.10). The time-evolution of membrane voltage of the different neurons is qualitatively the same as in the previous simulation because the neurons have the same properties. Figure 3.10(right) shows the detailed calcium fluctuations associated with the presynaptic neuron and postsynaptic neuron

activities and the corresponding sums. Once again, it highlights the huge difference in the signals driving the synaptic weight change during tonic firing and bursting.

• Some variations of these models have been tested for the computational experiments done in Chapter 6 with different fitted parameters. The model designed by (Shouval et al., 2002) is compared in that same chapter. Its detailed modeling is available in Supplementary Material E.

τ_{Ca}	C_{pre}	C_{post}	D	τ_w	θ_{p}	θ_{d}	γ_{p}	γ_{d}
22.2721	0.8441	1.62138	9.53708	520761.29	2.009289	1	597.08922	137.7586

Table 3.7: Parameters of the calcium-based from (Graupner et al., 2016) fitted on (Sjöström et al., 2001)

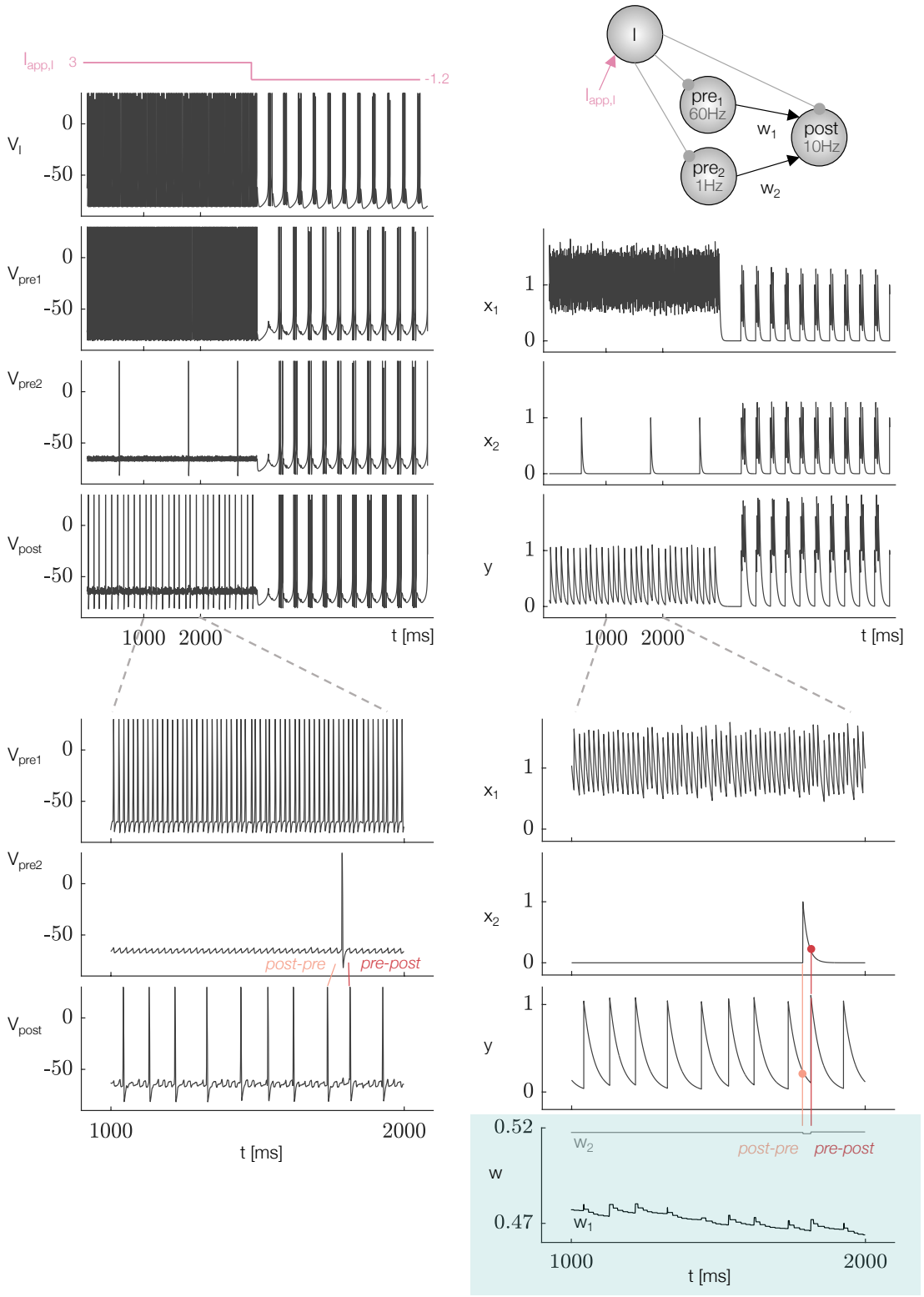

Figure 3.9: A small circuit exhibiting a switch from tonic firing to bursting, with synaptic weights driven by a pair-based rule. (left) Time-evolution of the membrane voltage of the different neurons. Their tonic firing frequencies are given in the circuit schematic (top-right).

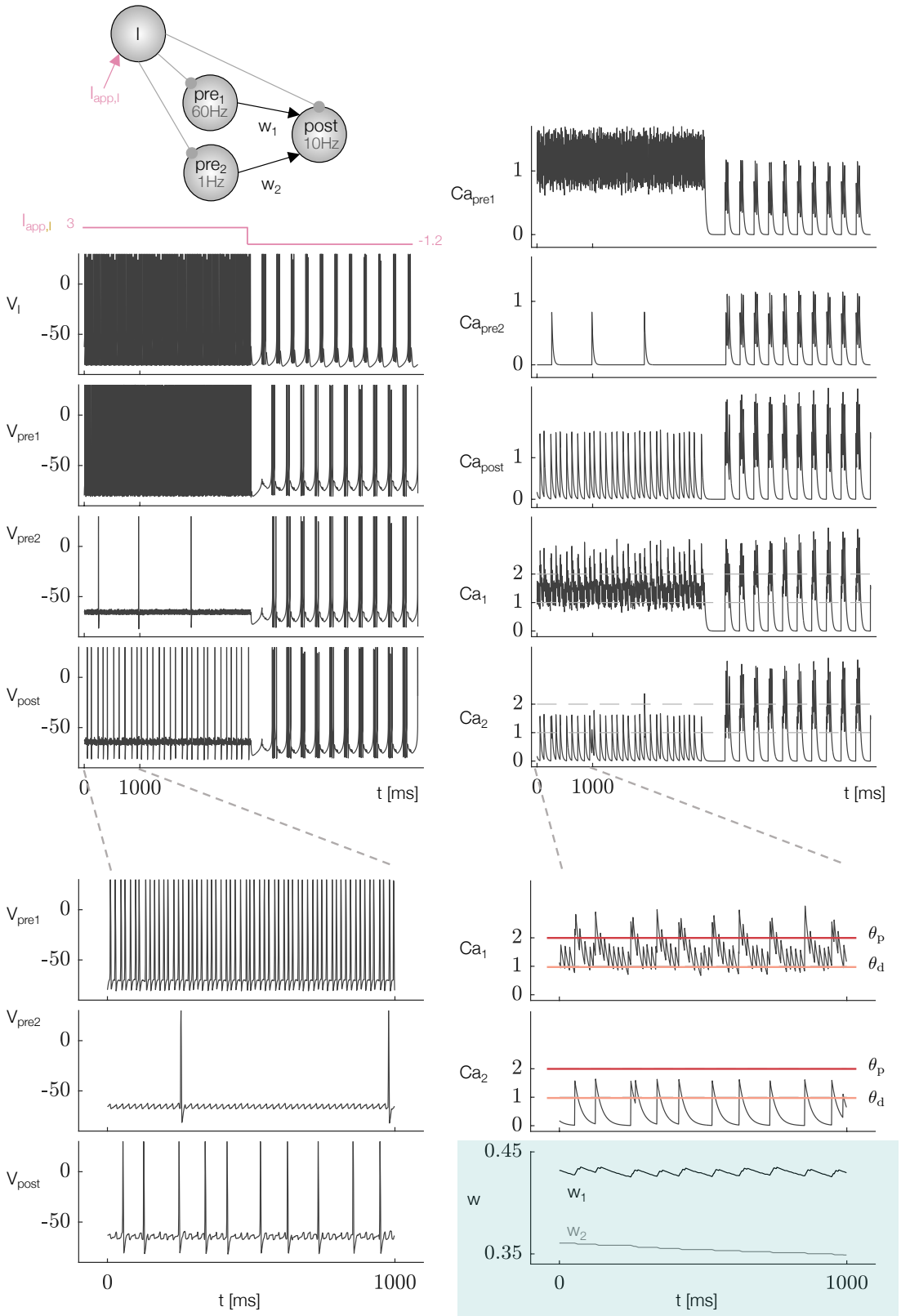

Figure 3.10: A small circuit exhibiting a switch from tonic firing to bursting, with synaptic weights driven by a calcium-based rule (Graupner et al., 2016). (left) Time-evolution of the membrane voltage of the different neurons. Their tonic firing frequencies are given in the circuit schematic (top-left). The time-evolution of the calcium traces are shown on the left.

3.5.5 Structural synaptic plasticity

The distinction between E-LTP and L-LTP has been clarified in Section 2.4.2. The first category relies on changes in postsynaptic receptor efficacy and the insertion of new receptors via exocytosis. The previous section has presented the different models often used in literature to describe this early phase of plasticity. Conversely, the Late Long Term Potentiation (L-LTP) is a bit less popular in computational neuroscience compared to the enormous quantities of articles describing STDP for example. In this section, we aim to classify diverse models of structural plasticity and derive the main modeling strategies.

Strategies encountered in literature to model structural plasticity

Structural plasticity models can be broadly classified into three main strategies (Figure 3.11: (A) mathematical, (B) biophysical, and (C) phenomenological

(A) The first strategy utilizes mathematical variables and statistics to drive structural changes based on pre- and postsynaptic activities (Helias, 2008; Van Ooyen et al., 1995) and avoid adding biophysical details. "The goal of the present work is to demonstrate the potential of local correlation detection at the spine while making minimal assumptions about the involved biophysical processes." (Deger et al., 2012). In this model, a correlation trace follows stochastic dynamics based on the causality between spike timings and noise, driving structural plasticity (Figure 3.11A). Another model simplifies structural plasticity by randomly adding new synaptic connections between unconnected excitatory cells, without considering biophysical information (Zheng et al., 2013).

(B) The second strategy describes structural plasticity through the signaling cascade, incorporating multiple variables to detail the intermediate steps from calcium influx to morphological changes. These models involve equations with kinetic rates (k_1 and k_2) for a variable x: $\dot{x} = k_1(1 - x) - k_2 x$ (Smolen et al., 2006). While this approach provides a better understanding of the involved steps and actors, computational time can be significant, making implementation in larger networks more challenging (Figure 3.11B).

For instance, (Smolen et al., 2006) describe a detailed chain of molecular reactions involving CaMKII, cAMP, PKA, and others, during the expression and maintenance of plasticity. It relies on the Synaptic Tagging and Capture (STC) hypothesis (as described in Section 2.4.3). In (Smolen, 2007), the cascade is simplified, considering a tagging variable and a variable representing the potential plasticity related products (PRP). The product of these two variables drives the change in synaptic strength. Such models facilitate the identification of the role of potential tags or PRPs, such as PKA or PKMζ (Smolen et al., 2020).

An alternative approach to investigate structural plasticity involves the utilization of biophysical measures such as the spine head volume, which directly correlates with morphological alterations(Amano et al., 2022).

(C) The third strategy for modeling the late phase of plasticity combines mathematical and biophysical approaches, simulating the biophysics of the signaling cascade without explicitly detailing all reactions. Two subcategories of structural phenomenological models exist (Figure 3.11C): those based on the Synaptic Tagging and Capture (STC) hypothesis using a tag variable, and those modeling structural synaptic plasticity with a variable linked to traditional synaptic plasticity.

In the former approach, studies such as (Lehr et al., 2022; Luboeinski and Tetzlaff, 2021; Li et al., 2016) utilize an early-phase weight governed by a calcium-based model and a late-phase weight influenced by synaptic tagging and the plasticity related products (PRP) (Figure 3.11C, left). The different steps explaining the STC hypothesis are presented: (i) potentiation triggers E-LTP, (ii) the synapse must be tagged, (iii) the number of PRP must be large enough, (iv) the PRP are captured and (v) finally the overall synapse increased. (Ziegler et al., 2015) derive an STC rule from the Tag-trig model by (Clopath et al., 2008).

Other approaches employ diverse methods for modeling structural plasticity without using the STC formalism but focusing on the conceptual difference between E-LTP and L-LTP (Butz and van Ooyen, 2013; Zenke et al., 2015; Bourjaily and Miller, 2011; Fauth and Van Rossum, 2019; Benuskova and Abraham, 2007).

(Bourjaily and Miller, 2011) replace synapses based on pre- and postsynaptic spiking, resembling Spike-Time Dependent Plasticity (STDP) but on a different timescale. (Benuskova and Abraham, 2007) employ a pair-based model with a potentiation parameter divided by a variable proportional to postsynaptic activity and a slower timescale function related to CREB. (Butz and van Ooyen, 2013) investigate axonal bouton and dendritic spine formation and removal, focusing on homeostatic mechanisms. (Fauth and Van Rossum, 2019) use a phenomenological synaptic rule based on pre- and postsynaptic firing rates, modifying synapse number through a deletion probability linked to synaptic weight. (Kirchner and Gjorgjieva, 2021) incorporate BDNF dynamics in driving synaptic weight changes and synapse replacement. (Gallinaro and Rotter, 2018) regulate structural plasticity based on the neuronal firing rate and homeostatic set point. Interestingly, (Zenke et al., 2015) combine various synaptic rules and a consolidation rule, leading to convergence of synaptic weight to a reference weight. This reference weight also changed according to the synaptic weight itself to observe consolidation. This model is inspired from (Clopath et al., 2008) without using explicitly tag and protein thresholds.

Overall, these models share a slow timescale governing the structural rule, distinguishing early and late phases of plasticity. Additionally, they can incorporate more complex mechanisms such as neuromodulators and exhibit Hebbian or

homeostatic characteristics. For a comprehensive review comparing different experimental and theoretical papers, refer to (Fauth and Tetzlaff, 2016).

Applications of structural plasticity rules

Modeling structural synaptic plasticity rules serves as a crucial tool for unraveling the intricate processes involved in synaptic growth and retraction, with diverse goals and applications.

One application of such modeling is to comprehend the brain's regenerative capabilities following injuries or diseases, enabling synapse regrowth (Butz and van Ooyen, 2013). By developing structural plasticity models, researchers gain insights into the underlying mechanisms and can explore therapeutic interventions for facilitating recovery. Additionally, modeling structural plasticity aids in studying brain and circuit development, as these processes involve significant structural changes critical for proper functioning (Poirazi and Mel, 2001). Biophysical models also provide valuable insights into the role of various molecules in conjunction with experimental neuroscience investigations (Smolen et al., 2006, 2020).

In computational models and machine learning applications, structural plasticity is often linked to memory storage and capacity (Fauth and Tetzlaff, 2016). Recent advancements incorporate more complex processes beyond traditional E-LTP, integrating short-term depression and structural plasticity to better understand learning and memory (Zenke et al., 2015; Fauth and Van Rossum, 2019).

Furthermore, structural plasticity serves as a homeostatic mechanism to maintain a balance between plasticity and stability (Miehl et al., 2022; Gallinaro et al., 2022). Hebbian and homeostatic structural rules are extensively discussed in (Fauth and Tetzlaff, 2016).

In summary, modeling structural plasticity rules provides a powerful approach to comprehend the intricate mechanisms underlying synaptic growth and retraction. This modeling enables insights into brain function and behavior, facilitates the development of recovery therapies, and enhances our understanding of memory storage and retrieval (Fauth and Tetzlaff, 2016).

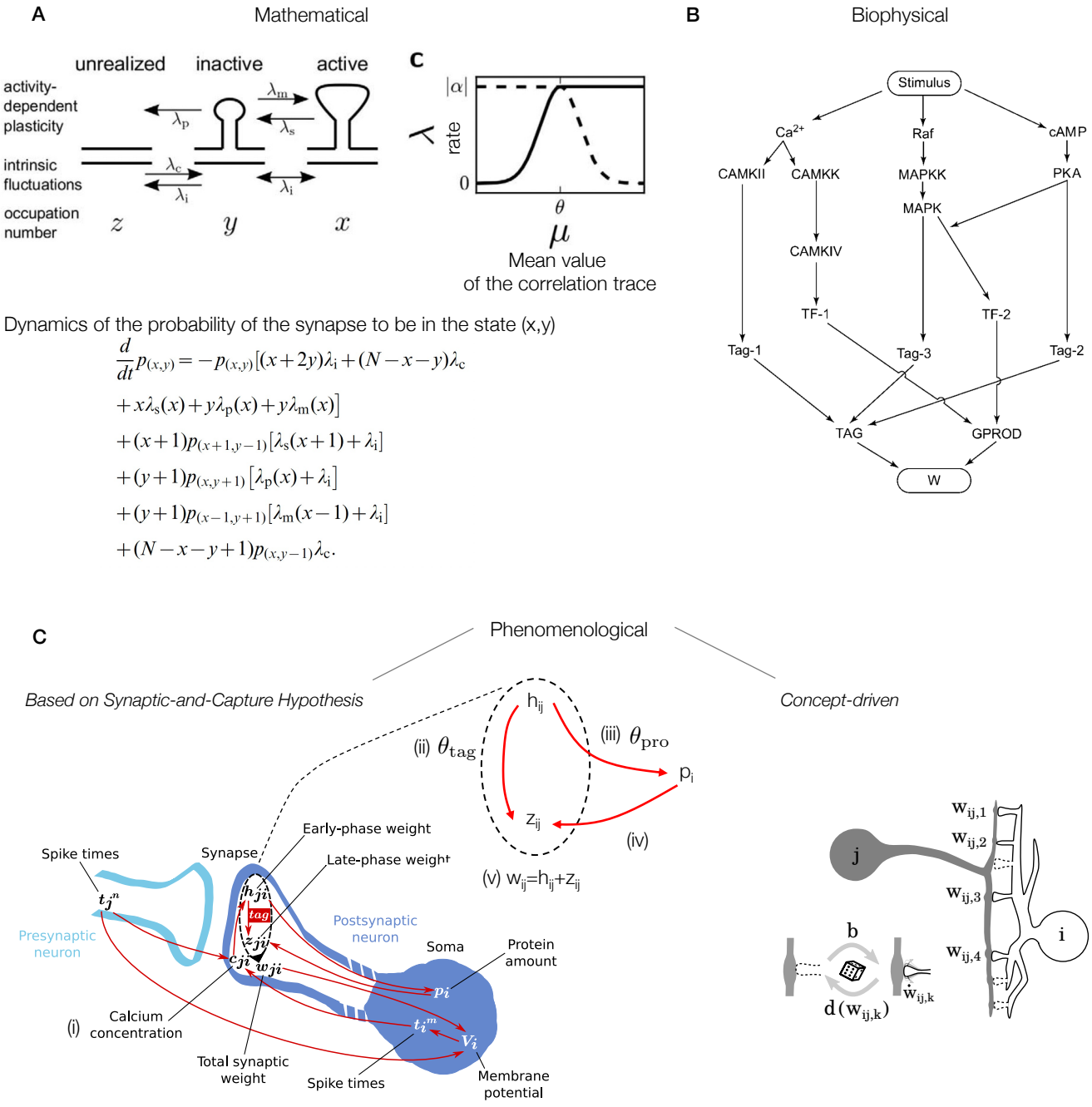

$$\frac{d}{dt}p_{(x,y)} = -p_{(x,y)}[(x+2y)\lambda_i + (N-x-y)\lambda_c + x\lambda_s(x) + y\lambda_p(x) + y\lambda_m(x)] + (x+1)p_{(x+1,y-1)}[\lambda_s(x+1)+\lambda_i] + (y+1)p_{(x,y+1)}[\lambda_p(x)+\lambda_i] + (y+1)p_{(x-1,y+1)}[\lambda_m(x-1)+\lambda_i] + (N-x-y+1)p_{(x,y-1)}\lambda_c.$$

Figure 3.11: Strategies to model structural plasticity A. Mathematical description of synapse formation based on the pre- and postsynaptic neuron activity correlation. Image from (Deger et al., 2012) **B.** Detailed description of the biophysical actors involved in structural plasticity. Image from (Smolen et al., 2006) **C.** (left) Using the Synaptic Tagging and Capture (STC) hypothesis to simulated structural plasticity Calcium concentration drives E-LTP. If the potentiation is greater than the threshold θ_{tag} (i), the synapse is tagged (ii). If the protein level is greater than the threshold θ_{pro} (iii), the PRPs are captured (iv). The total weight (w_{ij}) is the sum between the E-LTP (h_{ij}) and the L-LTP (z_{ij}). Adapted from (Luboeinski and Tetzlaff, 2021). (right) The depletion probability depends on the weight associated with the E-LTP. Image from (Fauth and Van Rossum, 2019)

CHAPTER 4

Robust switches in neuronal activity: a challenge in computational neuroscience

This thesis focuses on switches in brain states, accompanied by neuronal switches from tonic firing to bursting. This property relies on the interplay between different ion channels, which has been extensively investigated in experimental neuroscience for many years. However, translating this property to computational neuroscience is a challenging task that requires finding a compromise between including enough biological details while maintaining computational efficiency. In this research, we aim to use a neuron model that could switch and remain robust to neuromodulation, cellular variability and network heterogeneity. With the motivation to understand the impact on this switch on memory formation and consolidation, we must ensure that the chosen model is robust to synaptic plasticity as well.

To achieve this objective, we compared various conductance-based models that are capable of switching between the two firing patterns under consideration. It was observed that the most common approach in the literature to achieve this property is to use T-type calcium channels. However, two primary computational strategies were identified, where the activation of this channel is modeled either by a slow variable depending on the membrane voltage or by an instantaneous variable.

In order to use a reliable neuron model, we performed robustness tests at the cellular, circuit, and network levels. Through this analysis, we demonstrated that the T-type calcium channel must activate slower than the fast sodium channel but faster than the ultraslow inactivation of T-Type calcium channels. we used phase plane analysis to show this timescale separation must be maintained in reduced neuron models.

The results of our research have been published in an article (Jacquerie and Drion, 2021). I also had the opportunity to present this research at the COSYNE conference in 2019 held in Lisbon and the Annual Meeting of SfN in 2020 held in Chicago.

Adapted from: Kathleen Jacquerie[1] and Guillaume Drion[1].
Robust switches in thalamic network activity require a timescale separation between sodium and T-type calcium channel activations.
PLoS Computional Biology. 2021 May 18;17(5):e1008997.
doi: 10.1371/journal.pcbi.1008997.
PMID: 34003841;
PMCID: PMC8162675.
[1] University of Liege, Department of Electrical Engineering and Computer Science.

4.1 Introduction

Each day of our lives is characterized by different states, such as sleeping, waking up, walking, and reacting rapidly to our environment. We are also capable of thinking, learning, and remembering. These brain-states are recognizable by spatiotemporal signatures of the mean-field activity of large neuronal populations. Switches between these brain states can be fast and localized, such as for example those observed in different brain areas prior to movement initiation (Kühn et al., 2004), or global and long-lasting, such as those observed during the wake-sleep transition (McCormick and Salkoff, 2015; McGinley et al., 2015). These transitions also occurs during wakefulness from a state of active learning during *active waking* to a state of reduced consciousness during *quiet waking*. The change is remarkable, the mean-field activity rapidly switches from an fast active state to a slow oscillatory state.

These transitions from active state to slow oscillatory state are controlled by neuroactive chemicals, labelled *neuromodulators*, such as serotonin, norepinephrine, dopamine and acetylcholine, which undergo massive modifications (Zagha and McCormick, 2014; McCormick and Bal, 1997; Murray Sherman, 2001; McGinley et al., 2015; Ding et al., 2016). The transitions between these states are reflected in the switching of neuronal activities from *tonic firing* to *bursting*. As a reminder from chapter 2.2.2, bursting is defined as a succession of action potentials at high frequency interleaved by periods of silence (McGinley et al., 2015; Zagha, 2014; Bradley et al., 2022; Contreras and Steriade, 1995). These neuron dynamics are determined by a specific balance of ion currents (Yu et al., 2005). These ion currents are controlled by neuromodulators.

The mechanisms governing rhythm and neuronal fluctuations are poorly understood. This research problem is difficult to solve since it involves phenomena occurring at different scales; from population level, with interconnected neuron to molecular level, with neuronal proprety able to fastly change (Wang, 2010).

In parallel with these rhythm fluctuations, learning and memory are attributed to the ability of neurons to modify their connections with other cells based on experience, a property called *synaptic plasticity* (Citri and Malenka, 2008; Abbott and Nelson, 2000). Synaptic plasticity mechanisms often exploit the level of correlation in the activity of connected neurons (for example in spike-time dependent plasticity), and can therefore be affected by abrupt changes in neuronal excitability. Strong constraints are exerted on models of plasticity because neural circuits are adaptable to help animals to modify their behavior. At the same time, these circuits must be stable in spite of these changes. There is a balance between adaptability and stability (Abbott, 2003; Turrigiano et al., 1994).

The coexistence of these mechanisms raises challenging questions: how can switches in brain states remain reliable despite constant rewiring of neuron connectivity? how are these switches robust in heterogenous neuron population? How is synaptic plasticity affected by switches in brain states? Indeed, little is known about how shifts in network rhythms influence synaptic plasticity, hence learning, which is the core question of this thesis. One reason for this puzzle is that state-of-the-art computational models of switches in brain states have often focused on the role of connectivity changes in network rhythm modulation (Bevan, 2002; Destexhe et al., 1998; Esser et al., 2009; Krishnan et al., 2016). Such models are not appropriate to study the impact of transient network oscillations on synaptic plasticity and learning, since the rhythmic switch itself relies on a disruption of the connectivity established through learning.

Recent evidence suggests that control of rhythmic activity can happen *at the cellular level*. No matter how fast or long-lasting are the transitions, they are controlled without affecting neither synaptic strength nor the circuit interconnection topology (Marder and Bucher, 2007). Such mechanisms have been studied in small circuits, prominent examples being the crustacean stomatogastric system (Destexhe and Marder, 2004; Prinz et al., 2004; Schulz et al., 2006; Marder et al., 2014) , and the leech heart (Olypher and Calabrese, 2007; Roffman et al., 2012). These circuits are ideal supports to better understand how alteration in excitability regulates behavioral states. These works demonstrate that neuromodulation generates highly stable outputs. It has also been extensively shown that several combinations of ionic channels on the membrane or synaptic connections lead to the desired outcome (Marder et al., 1996; Schulz et al., 2006). It enhances the idea that rhythms cannot rely on a precise synaptic weight configuration or precise tuning of intrinsic parameters.

In this line of work; we aim at highlighting a *cellular property* that is critical for the generation of switches in brain states compatible with neuromodulation, cellular heterogeneity, synaptic plasticity and independent from network topology. This cellular property relies on a timescale separation between sodium and T-type calcium channel activations, providing a source of both fast and slow positive feedback loops at the cellular level. Slow positive feedback is accessible to all neurons that embed a sufficient amount of slowly activating voltage-gated calcium channels or slowly inactivating potassium channels in their membrane: the positive feedback comes from the fact that a calcium channel activation (resp. potassium channel inactivation) further amplifies the depolarization that gave rise to it, and slow means that calcium channel activation (resp. potassium channel inactivation) is at least one timescale slower than sodium channel activation. But the ultraslow inactivation of T-type calcium channels makes the slow positive feedback tunable: its gain depends on neuron polarization level. The presence of a slow positive feedback at the cellular level endows the neuron with an excitability switch, especially for the transition between tonic mode to bursting mode (Franci et al., 2013).

This present work studies the role played by the timescale separation between sodium and T-type calcium channel

activations on the robustness of six published thalamic neuron models. The thalamic neurons raise interest due to their varying firing patterns and contribution to brain states. Two models among the analyzed in this paper neglect this timescale separation by designing T-type calcium channel activation as an instantaneous event, a simplification often encounters in neuronal modeling. Here, we show through several computational experiments that the compatibility between neuromodulation, synaptic plasticity and switches in brain states correlates with the presence of the *slow* T-type calcium channel activation. As soon as intrinsic parameters and synaptic weights are affected respectively by neuromodulation and synaptic plasticity, the two models that speed up the calcium activation kinetics experience a drastic drop in their switching capabilities. However, restoring the slow activation of T-type calcium channels in these two models improves the robustness of their rhythmic activity.

To further quantify the importance of a timescale separation between sodium and T-type calcium channel activations, we vary T-type calcium channel activation kinetics in all models, ranging from the fast timescale of sodium channel activation to the ultraslow timescale of T-type calcium channel inactivation, and we test its robustness at the circuit level and at the population level. Our computational experiments confirm that the robustness of rhythmic activity is achieved when T-type calcium channel activation is an order of magnitude slower than sodium channel activation. This was observed in all models despite their quantitative differences.

We also analyze this timescale separation from a dynamical system approach. We reduce the high-dimensional conductance-based models into models with three variables; fast (V), slow (V_s) and ultraslow (V_u). Each variable of the original model is decomposed into its contribution in V, V_s and V_u using the logarithmic distance proposed in (Drion et al., 2015), which permits to track the effect of changes in gating time-constants. The slow-fast phase portrait of models with slow T-type calcium channel activation are all qualitatively equivalent: the robust switch to bursting is generated by the appearance of a lower branch in the V-nullcline (Franci et al., 2013, 2014, 2018; Van Pottelbergh et al., 2018). Speeding-up the activation of T-type calcium channels disrupts the appearance of this lower branch, which in turn disrupts the ability to switch to bursting.

Our results thus highlight the importance of respecting the physiological timescale separation between sodium and T-type calcium channel activations to guarantee compatibility between neuromodulation, synaptic plasticity, cellular heterogeneity, adaptable connectivity and switches in neuronal rhythms.

4.2 Results

4.2.1 Robust vs. fragile firing pattern transition at the single-cell level

Throughout this paper, we compared six well-established conductance-based models of thalamic neurons (Drion et al., 2018) (**model 1**), (Destexhe et al., 1996) (**model 2**), (Destexhe et al., 1998) (**model 3**), (McCormick and Huguenard, 1992) (Huguenard and McCormick, 1992) (**model 4**), (Wang, 1994) (**model 5**) and (Rush and Rinzel, 1994) (**model 6**). All these models include at least a sodium current, I_{Na}, a potassium current, I_K, T-type calcium, I_{CaT} and a leak current, I_{leak}. Each of these models is conceived to reproduce the different firing patterns observed in a thalamic neuron (a depolarized tonic mode, a hyperpolarized bursting mode, rebound bursting, etc.) and the switch between them (Guillery and Sherman, 2002; McCormick and Bal, 1997; Murray Sherman, 2001; Castro-Alamancos, 2004). The firing mode is controlled by the external current. A depolarizing current drives the neuron model in tonic mode. If it is followed by a hyperpolarizing current, it switches the neuron model from a regular spiking mode to a bursting mode; a transition called hyperpolarized-induced bursting (HIB) (see Figure 4.1A) (McCormick and Bal, 1997).

Experimental and computational studies have shown that a similar behavior or a similar firing pattern can emerge from neurons or circuits having very distinct intrinsic parameters (Alonso and Marder, 2019; Goldman et al., 2000; Marder and Prinz, 2002). Figure 4.1B illustrates the membrane voltage time-course of a thalamic neuron model for two different sets of maximal intrinsic conductances under the control of an external hyperpolarizing current (see black curves). The firing pattern is similar in both parameter sets and shows the typical switch occurring in thalamic neurons. However, the corresponding currentscapes reveal a variability in the contributions of the different ionic currents (Alonso and Marder, 2019). A H-current (orange curve) is involved in the first neuron (top currentscape) while it is almost absent in the second neuron (bottom currentscape). It shows that different combinations of ionic currents can lead to same firing pattern. This simple experiment motivated the rest of this work; a computational model must be able to reproduce a desired outcome for a broad range of intrinsic parameters as it happens in biology.

Here, we studied the robustness of conductance-based models to parameter variations with a special focus on the dynamics of the voltage-gated T-type calcium channel activation. The first four models (models 1 to 4) incorporate a *slow* activation of the T-type calcium (CaT) channels while the last two models (models 5 and 6) fix the activation as an instantaneous event. This simplification is often encountered in neuronal modeling (Wang, 1994; Rush and Rinzel, 1994; Pospischil et al., 2008; Kubota and Rubin, 2011; Rubin and Terman, 2004; Smith et al., 2000; Amarillo et al., 2015; Golomb et al., 1994). Indeed, it removes one differential equation, which decreases the simulation time - a computation intake that is non-negligible as soon as one moves toward network simulations.

First, we investigated the impact of the CaT channel activation *dynamics* in the model robustness at the single cell

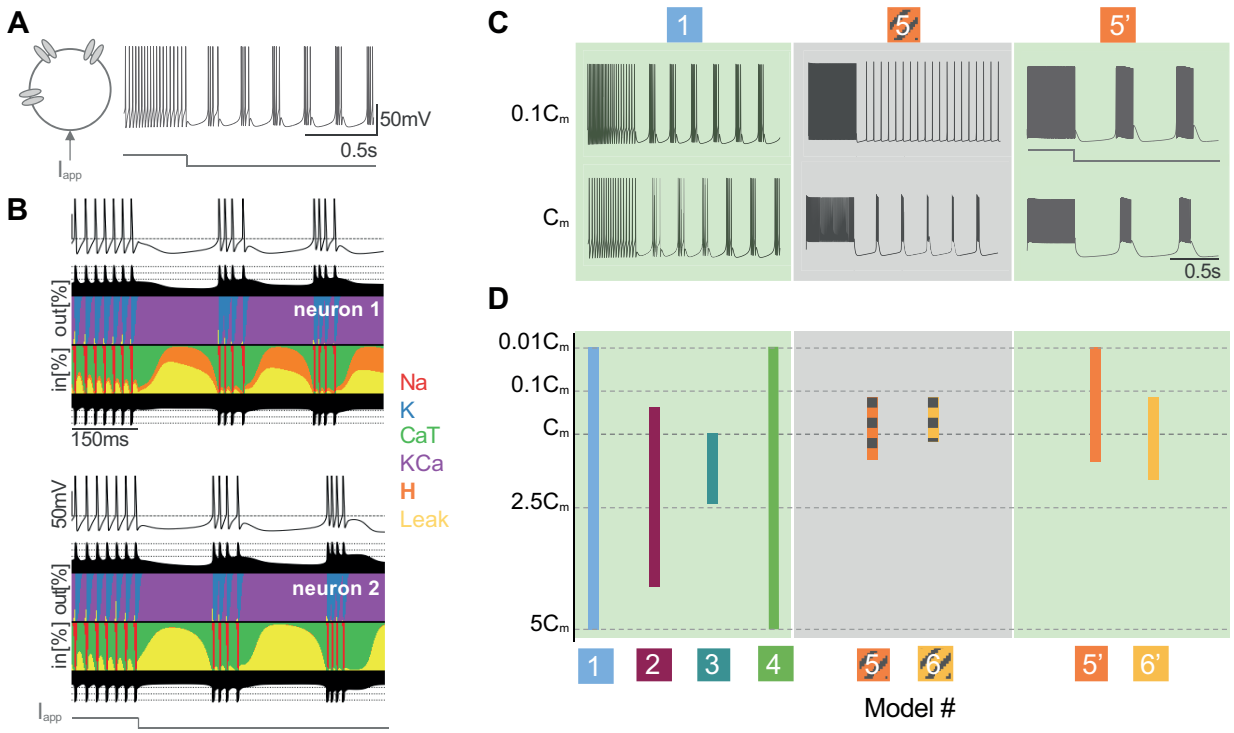

Figure 4.1: Slow T-type calcium channel activation ensures model robustness against neuron variability at single-cell level. **A:** The cell switches from a regular tonic mode to a bursting mode when a hyperpolarizing current is applied, a typical response called hyperpolarized-induced bursting (HIB). **B:** Currentscape for a neuron model with two different sets of maximal intrinsic conductances. After 150ms, the two neurons are hyperpolarized, leading to a HIB. Under the membrane-time curve, the black surface shows respectively on the top and bottom total inward outward currents on a logarithmic scale (see (Alonso and Marder, 2019)). Between the black surfaces, each color curve reveals the contribution of one particular ionic current as the percentage of the total current during the simulation. Both neurons display the same firing pattern but this outcome is achieved by different combinations of ion channels densities. **C:** Models 1, 2, 3, 4, 5' and 6' are robust to a uniform scaling of all the maximal conductances, modeled by a change in membrane capacitance (C_m)(left panel). Models 5 and 6 are fragile to this parameter alteration. They lose the ability to switch (center panel). Restoring the slow CaT channel activation is enough to recover the robustness (right panel). **D:** Quantitative analysis of neuron model robustness to change in membrane capacitance. Each model is launched for a capacitance value varying from a hundredth to five times its nominal value. Models 1, 2, 3, 4, 5' and 6' cover larger parameter range. By contrast, models lacking of slow CaT channel activation are fragile to membrane capacitance deviation. Replacing the instantaneous CaT channel activation by a slow activation turns these fragile models into more robust models. Hence, models 5' and 6' support larger variation of C_m.

level. To do so, we simply tested the ability to reproduce the switch from tonic to burst by changing a single parameter in the model, namely, the capacitance membrane C_m. An alteration in this parameter substitutes a change in cell size or a uniform scaling of all maximal ionic conductances (O'Leary et al., 2014; Franci et al., 2018) . Figure 4.1C reveals the striking consequence for the model robustness when the capacitance is scaled by a factor 1/10. Models 1 to 4 (left panel) including the slow activation of T-type calcium channel are able to reproduce the hyperpolarized-induced bursting while models that assume this activation is instantaneous are fragile. Indeed, models 5 and 6 (center panel) loose the ability to switch from tonic to burst. To make the comparison as fair as possible, we have restored the slow dynamics of the CaT channel activation in models 5 and 6. We reconstructed a differential equation for the activation variable whose time constant is voltage-dependent. **Models 5' and 6'** are their respective modified versions. The T-type calcium current previously described by $I_{CaT} = g_{CaT} \boldsymbol{m}^{a}_{\boldsymbol{CaT},\infty} h_{CaT}(V_m - V_{Ca})$ is replaced by $I_{CaT} = g_{CaT} \boldsymbol{m}^{a}_{\boldsymbol{CaT}}(\boldsymbol{V_m}) h_{CaT}(V_m - V_{Ca})$ where $dm_{CaT}/dt = (m_{CaT,\infty} - m_{CaT})/\tau_{m_{CaT}}(V_m)$ (see Supplementary Material in (Jacquerie and Drion, 2021) for details). This only modification is sufficient to recover the desired firing activity, *ie.* the switch from tonic to burst even for a division of the capacitance membrane by a factor of 10 (Figure 4.1C, right panel).

This computational experiment has been reproduced for membrane capacitance values scaled from a hundredth to five times its nominal value (see section Methods 4.4 for details). Figure 4.1D reveals that models 1 to 4 are able to switch for a large range of capacitance values (see left panel). Models 5 and 6 are fragile and cover a tiny range around the nominal value (C_m) (center panel). Reinstating the slow dynamics of this channel bounces back the robustness as shown by the increase of the orange and yellow bars (right panel). Models 5' and 6' are able to generate the firing pattern switch typical in thalamic cells given capacitance values for which models 5 and 6 are not able.

4.2.2 Slow T-type calcium channel activation makes an isolated excitatory-inhibitory circuit robust to neuromodulation and synaptic plasticity

To extend our results obtained at the single-cell level, we moved to the circuit level. We built an isolated excitatory-inhibitory circuit of two neurons. These neurons are connected through AMPA, $GABA_A$ and $GABA_B$ connections to model the asymmetric coupling between a subpopulation of excitatory (E) cells and a subpopulation of inhibitory (I) cells (Guillery and Sherman, 2002; McCormick and Salkoff, 2015). This topology is a typical configuration in the thalamus (McCormick and Bal, 1997; Sherman and Guillery, 1996). The E-I circuit and its expected rhythmic network activity are illustrated in Figure 4.2A (left and center panels). It is controlled by an external current injected on the inhibitory cell. Initially depolarized, the I-cell exhibits a tonic mode. The E-cell remains silent. As soon as the external current hyperpolarizes the I-cell; it deinactivates the T-type calcium channels, leading to a bursting mode. Then, thanks to the reciprocal connections, the circuit switches to a synchronous burst called the oscillatory mode.

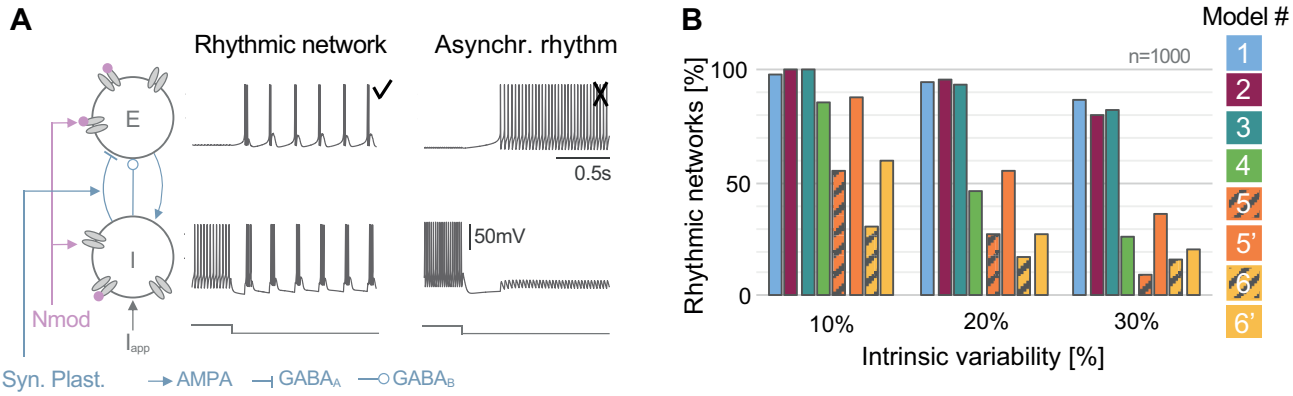

Figure 4.2: Slow T-type calcium channel activation ensures model compatibility with neuromodulation and synaptic plasticity at the circuit level.
A: (left) Two interconnected neurons (one excitatory neuron E and one inhibitory neuron I) under the control of an external current (I_{app}), affected by neuromodulation (Nmod, pink spheres) and synaptic plasticity (Syn. Plast., in grayish blue). (center) The external current initially depolarizes the inhibitory cell then hyperpolarizes it leading to a switch in the circuit rhythm into a synchronous bursting. (right) Voltage traces illustrating an asynchronous rhythm, undesired behavior in the circuit. **B:** Percentage of rhythmic networks observed in different neuron models as intrinsic variability increases. For each model, one thousand 2-cell circuits are generated with random ionic conductances varying from 10, 20 and 30% from their nominal values -mimicking the effect of neuromodulation, and synaptic conductances, randomly picked in a uniform distribution - mimicking the effect of synaptic plasticity. Models 1 to 3 embedding a slow activation of T-type calcium channels are robust to parameter variability. Model 4 is robust at low variability than its performance is decreased due to its high number of ionic channels. Models 5 and 6 that assume an instantaneous T-type calcium channel activation are fragile: parameter variations disrupt the nominal rhythm. Replacing the instantaneous activation into a slow activation restores the robustness as shown by models 5' and 6' (dashed orange and yellow bars).

With a simple computational experiment, we studied the robustness of these network switches to changes in neuron intrinsic properties, mimicking the effect of neuromodulation (modeled by maximal conductances), and changes in synaptic weights, mimicking the effect of synaptic plasticity (modeled by the synaptic conductances). For each model, we started from an E-I circuit capable of generating a switch. Then, one thousand 2-cell circuits were simulated for different parameter sets of maximal intrinsic conductances and synaptic weights. The maximal conductances varied within an interval of 10, 20 and 30% around their nominal values and the synaptic weights varied in a fixed range (see section Methods 4.4 for details). The percentage among the thousand 2-cell circuits that have performed the rhythmic transition was evaluated for the three intervals of variability in each conductance-based model. A rhythmic network is defined according to the firing pattern evolution shown in Figure 4.2A (center) representing a switch from silent-tonic to synchronous bursting while other activities are classified as an asynchronous rhythm, for example the pattern in Figure 4.2A (right). Quantification of the firing pattern properties *i.e.* frequencies in tonic and burst is available in Supplementary Material in (Jacquerie and Drion, 2021).

For a small intrinsic variability (10%), Figure 4.2B shows that models 1 to 4 are robust to neuromodulation and synaptic plasticity. More than 800 sets of parameters allow the circuit to switch. The absence of slow positive feedback in models 5 and 6 has a dramatic consequence on the model robustness. One every two parameter sets in model 5 cannot reproduce the typical thalamic activity transition. Model 6 is even more fragile. However, restoring the dynamical cellular property significantly improves the robustness as shown in models 5' and 6'.

For larger intrinsic variability (20% and 30%), models 1 to 3 maintain their capabilities to switch for a broad range of intrinsic and synaptic parameter ranges. Model 4 can be considered apart. It is shrinking as the variability increases. This decrease in performance is likely related to its high number of conductances (about twice as much as the other models). Indeed, we are exploring a 14-dimension space since this model has 11 intrinsic conductances and 3 synaptic

conductances. The parameter exploration for the other models occurs in a 7 to 9 dimension space reducing the model complexity. Models 5 and 6 have a similar number of intrinsic conductances as models 1 to 3 but they are extremely fragile to parameter changes. They are almost unable to perform rhythmic transition. The rhythm in an E-I circuit requires a precise tuning of intrinsic and synaptic parameters for models lacking of the slow kinetics of CaT channel activation. This computational choice makes the model incompatible with neuromodulation and synaptic plasticity. Once again, their modified versions embedding the slow positive feedback (correlated to the slow activation of T-type calcium channels) have a better response to parameter perturbations.

4.2.3 A timescale separation between sodium and T-type calcium channel activations ensures compatibility between circuit switch, neuromodulation and synaptic plasticity

So far, we have shown that modeling the T-type calcium channel activation with a slow kinetics drastically enhances the robustness of rhythmic switches at the cellular, and circuit levels. But one question remains: what does *slow* mean, and how tuned does the activation kinetics need to be to achieve robustness? Indeed, there exists different subtypes of T-type calcium channels whose activation kinetics can greatly differ (Hille, 2001; Perez-Reyes, 2003). To answer this question, we explored the impact of incrementally varying T-type calcium channel activation kinetics in a similar computational experiment as done in Figure 4.2. We focused on models 1, 2, 3, 4, 5' and 6' that describe the opening of the T-type calcium channel with a first order differential equation $dm_{CaT}(V_m)/dt = (m_{CaT,\infty} - m_{CaT})/\tau_{m_{CaT}}(V_m)$. The variable $\tau_{m_{CaT}}$ is the voltage-dependent activation time constant and characterizes the dynamics of channel opening. We started from an isolated 2-cell E-I circuit connected via AMPA, $GABA_A$ and $GABA_B$ synapses. The circuit is able to switch from tonic to burst at the nominal parameter values. Then, we added neuromodulatory effect - by varying intrinsic parameters, and synaptic plasticity - by changing extrinsic parameters. We built four hundred 2-cell circuits whose maximal ionic conductances and synaptic conductances were randomly picked in an interval of 20% around their basal values. Here, the novelty was to play with the time constant of CaT channel activation $\tau_{m_{CaT}}$ of the two neurons (see Figure 4.3A).

Figure 4.3B is a comparative table between time constants associated to sodium channel activation $\tau_{m_{Na}}$, T-type calcium channel activation $\tau_{m_{CaT}}$ and inactivation $\tau_{h_{CaT}}$ evaluated at their threshold voltage (see section Methods 4.4 for details). It points out the quantitative differences between models. Here, we were investigating the choice made for $\tau_{m_{CaT}}$ with respect to $\tau_{m_{Na}}$ and $\tau_{h_{CaT}}$. To do so, the time constant $\tau_{m_{CaT}}$ was scaled by several multiplicative factors from 0.01 to 100 times its nominal value. The smallest the coefficient, the fastest the CaT channel activation. For each scaled CaT time constant, we tested the model capability to switch from tonic to burst when the I-cell is hyperpolarized. Among the 400 tested circuits, the percentage of rhythmic circuits is placed on the y-axis (see Figure 4.3C). The x-axis is on a logarithmic graduation.

When the multiplicative factor is equal to one (marked by the gray circle), it indicates the CaT channel activation time constant initially designed for each model. The sodium channel activation time constant $\tau_{m_{Na}}$ and the CaT channel inactivation time constant $\tau_{h_{CaT}}$ are also drawn for each model in dashed lines (respectively $\tau_{m_{Na}}$ on the left and $\tau_{h_{CaT}}$ on the right). They are evaluated at their threshold voltage (see section Methods 4.4 for details). They respectively indicate the *fast* and the *ultraslow* timescale. For models 5' and 6', the sodium current activation is instantaneous. For model 6', the CaT channel inactivation does not appear on the graph since it is greater than 100 times its activation (see Table in Figure 4.3B).

The outcome of this computational experiment is compelling. Figure 4.3C reveals that models are robust to neuromodulation and synaptic plasticity when the timescale of the CaT channel is situated in a slow range. The meaning of slow stands by itself; it is bounded between the fast kinetics of the sodium channel activation and the ultraslow kinetics of CaT channel inactivation. For each model, the peak of robustness lies between these two timescales. The bump-shaped surface shows a relatively large width. It points out that the activation kinetics do not need to be perfectly equal to one specific value between the fast and ultraslow regions. But these kinetics just need to be included within the slow timescale range. However, as soon as the kinetics moves too far from this interval, the robustness loss is abrupt.

To go further in the analysis, the six models were superposed on each other by normalizing the logarithmic x-axis on Figure 4.3D. The left (resp. right) boundary is the time constant of the sodium channel activation (resp. CaT channel inactivation); namely, the fast and the ultraslow timescales. The number of rhythmic circuits is enhanced when the CaT activation occurs at a timescale slower than the sodium activation and faster than the CaT inactivation as highlighted by the bump-shaped surface. Modeling the CaT channel opening at a slow timescale guarantees the compatibility between neuromodulation, synaptic plasticity and switches in brain states. Indeed, the compatibility relies on the presence of a *slow positive feedback* at the cellular level, as mentioned above.

Model 4 maintains a steady robustness even if the CaT channel activation is accelerated. This can be explained by the presence of another source of slow positive feedback such as a slowly activating L-type calcium channels (see Supplementary Material in (Jacquerie and Drion, 2021) for more details about model 4). Models 5' and 6' display a modest robustness for a fast opening of the CaT channel. These models were initially designed to operate for an instantaneous activation. However, the favorable operating point is preferably at a slow timescale.

If the kinetics of the CaT channel opening slows down too much (meaning we are moving to the right on the x-axis), it reaches the same timescale as its inactivation. In other words, the activation gate opens while the inactivation gate closes

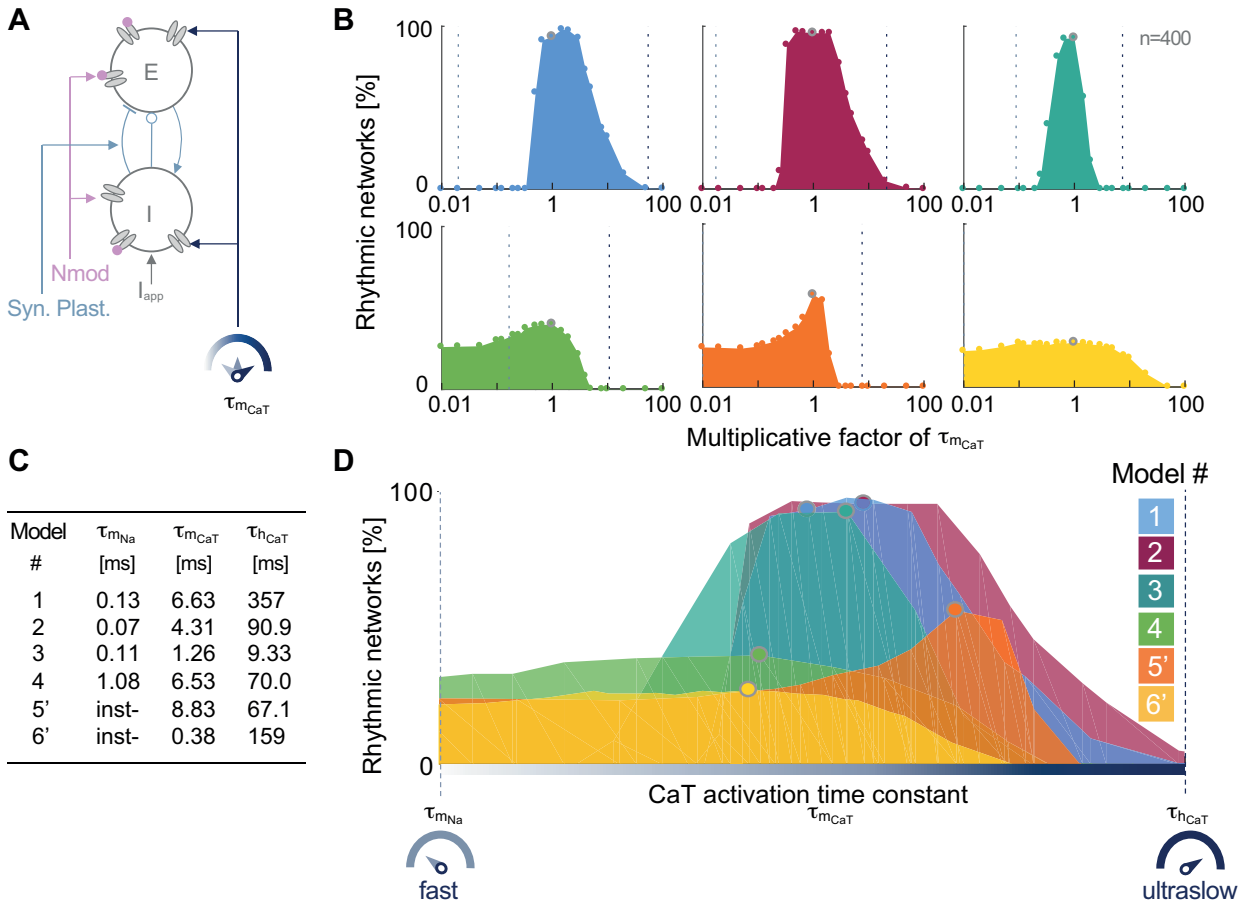

Figure 4.3: The physiological *slow* timescale of T-type calcium channel activation guarantees compatibility between circuit switch, neuromodulation and synaptic plasticity.
A: For each model, 400 E-I 2-cell circuits are built from scaled intrinsic and synaptic conductances picked in a uniform range of ± 20 % around their nominal values to mimic neuromodulation and synaptic plasticity. These same 400 circuits are then simulated for a varying CaT channel activation time constant ($\tau_{m_{CaT}}$). **B:** Comparison table between the time constants associated with sodium channel activation ($\tau_{m_{Na}}$), CaT channel activation and CaT channel inactivation ($\tau_{h_{CaT}}$). **C:** Effect of a varying CaT channel activation time constant on the switching capability in a 2-cell circuit for models 1, 2, 3, 4, 5' and 6'. The y-axis quantifies the percent of rhythmic networks among the 400 simulated random circuits under different values of $\tau_{m_{CaT}}$, scaled by a multiplicative factor varying from 0.01 to 100. The performance associated with the nominal (resp. scaled) CaT channel activation is depicted with a gray circle (resp full circle). The sodium channel activation (resp. CaT channel inactivation) time constant is marked with the left (resp. right) dashed vertical line. **D:** Each model is superposed between a window bounded on the left (resp. right) by the sodium channel activation (resp. CaT channel inactivation) time constant. The CaT activation time constant must remain confined in the *slow* timescale in order to guarantee model robustness to neuromodulation and synaptic plasticity.

leading to a zero flux of calcium ions. The kinetics of CaT channel activation must be slow but not too slow.

4.2.4 A timescale separation between sodium and T-type calcium channel activations promotes robustness of network states in large heterogeneous populations

From an isolated E-I circuit of two neurons, we built a larger network whose topology is emblematic of the thalamus, illustrating the interaction between relay neurons and the reticular nucleus. This population interaction is involved in state regulation such as the transition from wakefulness to sleep (McCormick and Bal, 1997; Murray Sherman, 2001). We replicated the two previous computational experiments performed at the circuit level, now on a neuronal population. To do so, we started with a 200-cell network where the population of 100 excitatory neurons is identical to the population of 100 inhibitory neurons. We neglected intra-population interaction, and we assumed all-to-all connectivity between the two populations. The E-cells projected AMPA synapses to all the I-cells and conversely, the I-cells were connected to the E-cells via $GABA_A$ and $GABA_B$ synapses. All the synaptic weights linking the neurons together were identical. An external current was exerted on the inhibitory cells (see Figure 4.4A). Hyperpolarizing this current caused a cellular switch and drives the neurons in a synchronous bursting mode as previously shown with the isolated E-I circuit in Figs 4.2A and 4.4B (voltage traces, two top curves) (Drion et al., 2018). This change in cellular firing pattern is translated by an oscillatory behavior at the network level. This oscillatory state can be visualized by computing the local field potential (LFP) of

the neuron population. LFP is measured as the sum of synaptic activity in a neuronal population (see Figure 4.4B, third curve). When the current hyperpolarizes the I-cells, the synaptic current is remarkably modified and reveals a stronger activity. The spectrogram of the LFP shows that the hyperpolarizing current turns on the mean-field rhythmic activity marked by a strong power LFP frequency band (see Figure 4.4B, frequency-time image at the bottom). For each model, the homogeneous network is able to switch from an active state to an oscillatory state.

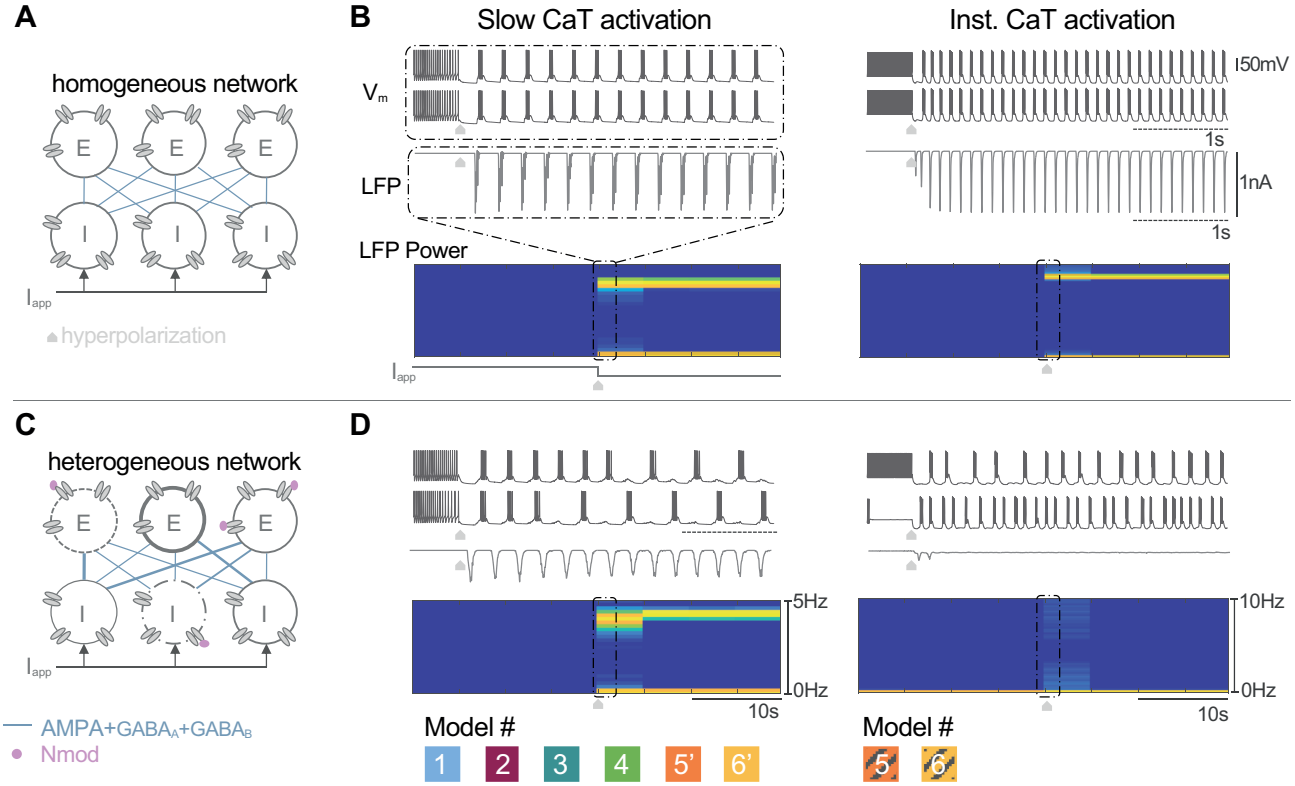

Figure 4.4: Slow T-type calcium channel activation guarantees robust network switch independent on the population heterogeneity.
A: A 200-cell network is built with the same neuron model; 100 excitatory cells connected via the AMPA synapses to 100 inhibitory cells projecting back $GABA_A$ and $GABA_B$ synapses. The network is homogeneous. All neurons have the same channel densities and the same synaptic weights. **B:** Voltage traces of two inhibitory cells (two top curves), time-course (third curve) and frequency-time graph (bottom spectrogram) of the local field potentials (LFPs) of the inhibitory neuron population for the homogeneous network. Hyperpolarization of the inhibitory neurons turns on the mean-field rhythm activity of the population depicted by a synchronous bursting at the cellular level, a oscillating synaptic activity shown on the LFP time course whose frequency is shown by the high power LFP frequency band on the spectrogram. **C:** A heterogeneous 200-cell network is built to take into account neuromodulation, cell variability, more representative topology and synaptic plasticity. Each ionic and synaptic conductance is randomly picked in a given range around its nominal value (see section Methods 4.4 for details). **D:** (left panel) Only models 1,2,3,4 5' and 6' display the switch in the mean field rhythm of the population marked with an oscillatory LFP time-course (third curve) and a significant power band in the spectrogram (bottom). (right panel) Models 5 and 6 that lack slow CaT channel activation are fragile to the network topology and the heterogeneity. Switch in population rhythm is recovered when the slow regenerativity is restored (models 5' and 6').

However, a perfect network with identical neurons and identical synaptic weights is not consistent with reality. Each neuron differs from its neighbor with different intrinsic parameters such as the cell size or the densities of ionic channels. In addition, connections between neurons are neither identical nor static. Therefore, we explored the model ability to maintain switch in brain states in presence of cellular heterogeneity and its independence on network topology (Drion et al., 2018, 2019). To do so, we built a 200-cell network where each neuron is different and the connectivity is uneven (see Figure 4.4C). The intrinsic and synaptic parameters were randomly picked in a given interval (see section Methods 4.4 for details). Figure 4.4D shows the astonishing contrast between the stability of models including the slow CaT channel activation (see left panel) and the fragility of models lacking of this property (see right panel). Models 1 to 4, 5' and 6' are still able to generate a switch into a synchronous burst as shown in Figure 4.4D (left). Due to intrinsic and synaptic variabilities, the voltage recordings from two I-cells are more realistic (two top traces). Even if each cell is not perfectly bursting at each cycle, the summation of the synaptic activity shown by the LFP curve is oscillating(third curve). The frequency of this oscillation is quantified in the spectrogram (bottom frequency-time graph). Models 5 and 6 are able to switch from an active state to an oscillatory when the network is homogeneous and the connectivity is perfectly balanced. However, as soon as the network is changed into a more realistic configuration, these models cannot preserve switches in brain states as shown by the asynchronous voltage-traces and the flat LFP curve translated by the absence of a marked

power band in the spectrogram (see Figure 4.4D right panels).

Models 1 to 3 show a marked power band in their spectrogram when intrinsic parameters vary in an interval of 20% around their nominal values. Once again, model 4 is less robust, certainly due to its high number of conductances. It continues to switch for an intrinsic variability of 10%. Model 5 (resp. model 6) does not tolerate a variability of 20% (resp. 5%). When the slow activation of T-type calcium channels is reestablished, models 5' and 6' switch from an active state to an oscillatory state at the same level of variability that the initial model was fragile. This modeling modification leads to a neuron model robust to cell variability and that does not rely on the network topology.

To go further, we explored once again the relevance of respecting physiological timescale separation in ionic current modeling but this time at the population level. To do so, we built a 200-cell network with 100 excitatory cells connected to 100 inhibitory cells via AMPA, $GABA_A$ and $GABA_B$ synapses. Models 1,2, 3, 4, 5' and 6' were switching their network state under a hyperpolarizing current for a homogeneous and a heterogeneous configuration, as shown in Figure 4.4B and 4.4D (left panels). Here, we tested which kinetics provides robustness to network heterogeneity. The CaT activation time constant $\tau_{m_{CaT}}$ of the 200 neurons was scaled by several multiplicative factors ranging from an eighth to eight times its nominal value. In addition, cellular and synaptic variabilities were introduced by randomly picking the maximal intrinsic and extrinsic conductances of each neuron in a given interval around their nominal values following a uniform distribution (see Figure 4.5A). These heterogeneous networks were constructed with parameters varying in an interval whose width was ranging from 0 to 50% with a step of 5%. At each scaled $\tau_{m_{CaT}}$, we tested the maximal possible variability width at which the heterogeneous network is able to switch. For example, we built the 200-cell network whose maximal ionic and synaptic conductances were picked in a range of 20% around their initial values. Then, we simulated the network under the control of an hyperpolarizing current at different scaled $\tau_{m_{CaT}}$. We finally checked for each timescale if the given heterogeneous network was switching or not, by analyzing its LFP activity. The network was switching if the time course of neuron population LFP displayed an oscillatory behavior in the hyperpolarized state and if its spectrogram was marked by a strong power band (see Fig 5B). We continued to increase the variability interval to quantify the correlation between the timescale and its robustness to cellular heterogeneity and uneven topology.

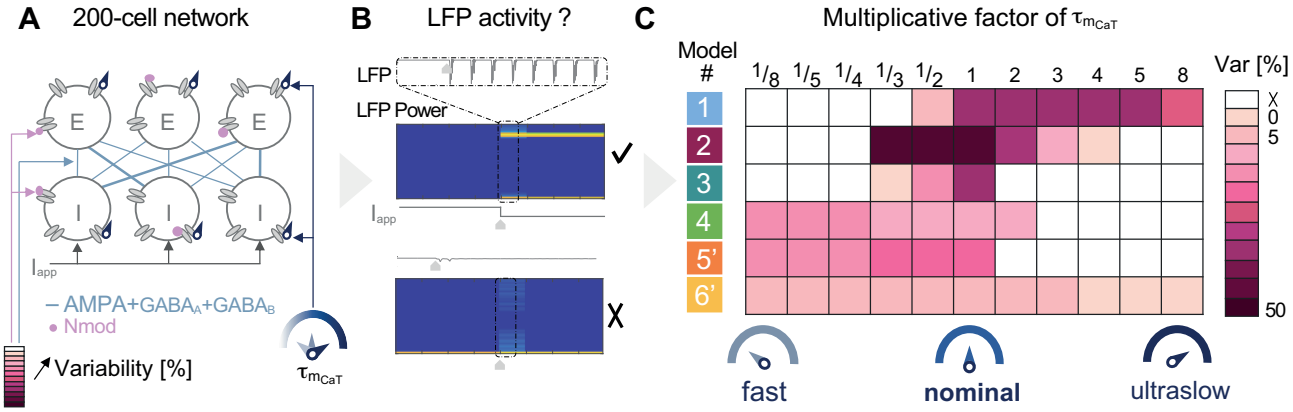

Figure 4.5: Comparison between fast, slow or ultraslow T-type calcium channel activation in generating robust mean-field activity transition.
A: A 200-cell network with 100 excitatory neurons and 100 inhibitory neurons connected via AMPA, $GABA_A$ and $GABA_B$ synapses under the control of an hyperpolarizing current. The intrinsic and extrinsic parameters are respectively affected by neuromodulation and synaptic plasticity; their values are randomly picked in a given interval (namely variability). The CaT channel activation time constant $\tau_{m_{CaT}}$ of each neuron is scaled by a multiplicative factor. **B:** At each scaled time constant, we check if the heterogeneous network is switching by analyzing the LFP activity. If the LFP timecourse presents a strong activity and its spectrogram shows a marked power band, the network displays an oscillatory state during the hyperpolarization state. **C:** The table summarizes the largest variability width at which the network presents a switch in its mean-field activity for several scaled time constants. Respecting the slow timescale of the CaT channel activation guarantees the switch in network rhythm compatible with variability in channel densities and synaptic weights. Driving the CaT channel activation to a fast or ultraslow timescale makes models more fragile to network topology and heterogeneity.

Figure 4.5C summarizes the model robustness at each scaled CaT time constant. It confirms our previous result; accelerating or decelerating the CaT channel opening makes the six models fragile to heterogeneity. In models 1 to 3, the best operating point to set the CaT time constant is confined between the fast timescale and the ultraslow timescale as shown by the darker zone. It enhances the model capability to switch in presence of cellular heterogeneity and synaptic plasticity. Model 4 is not really robust due to its high number of ionic currents. It is also assumed to embed another source of slow regenerativity helping it to operate at a faster timescale. As exhibited in Figure 4.3C for an isolated 2-cell circuit, models 5' and 6' also maintain a certain ability to switch even at a faster timescale because they were initially designed to operate at an instantaneous opening of CaT channels. As adapted versions of models designed to switch with an instantaneous T-type calcium activation, their robustness is lower than models 1 to 3 in all parameter ranges.

Overall, Figs 4.3 and 4.5 reveal the importance of considering the physiological kinetics range of ion channel gating in computational models and especially the timescale separation between the different ionic currents. Getting rid of the slow dynamics of the T-type calcium channel activation disrupts the timescale separation with sodium channel activation. It removes an important biological property of this neuron type and thus, disturb its ability to change its firing pattern under a hyperpolarization in presence of neuromodulation and synaptic plasticity. This deficiency is transposed at the population level as shown by the inability to turn on the mean-field activity as soon as the cellular heterogeneity and unbalanced connectivity are increased.

4.2.5 Slow T-type calcium channel shapes a robust phase portrait

How does the kinetics of T-type calcium channel shapes the phase portrait? To answer this question, we reduced the different high-dimensional models following the protocol presented in (Drion et al., 2015). The protocol is based on the decomposition of each variable into their role in a fast, slow and ultraslow timescale using a logarithmic distance (Drion et al., 2015). It allows us to reduce the different conductance-based models in a systematic and rigorous manner in order to obtain three dimensional models with three variables: the membrane voltage of the reduced model V, the slow variable V_s and the ultraslow variable V_u. The contribution of the activation or inactivation channel variables ($m_i(V)$ or $h_i(V)$ contracted as $X(V)$ to ease the reading) is projected on these three variables. The voltage-dependent gating variable is transformed into a weighted sum of three terms associated with the three timescales where the weights are voltage-dependent. The weighted sum is written as: $X(V) = w^X_{fs}(V)X_\infty(V) + (w^X_{su}(V) - w^X_{fs}(V))X_\infty(V_s) + (1 - w^X_{su}(V))X_\infty(V_u)$ where $w^X_{fs}(V)$ is the contribution of the gating variable on the fast time-scale, $(w^X_{su}(V) - w^X_{fs}(V))$ is the contribution on the slow time-scale and $(1-w^X_{su}(V))$ is the contribution on the ultraslow time-scale. Therefore, the 3D reduced model is described by the following differential equations: $C_m dV/dt = -\sum I_{ion} + \mathrm{I_{app}}$, $dV_s/dt = (V - V_s)/\tau_{m_K}(V)$ and $dV_u/dt = (V - V_u)/\tau_{h_{CaT}}(V)$. The time-constant of the sodium activation $\tau_{m_{Na}}(V)$ paces the fast time-scale, the time-constant of the potassium activation $\tau_{m_K}(V)$ paces the slow time-scale and the inactivation of the T-type calcium channel $\tau_{h_{CaT}}(V)$ paces the ultraslow time-scale.

In this work, we focus on the timescale attributed to the activation to the T-type calcium channel. We investigated the distortion of the phase portrait geometry when this time constant is increased or decreased. Figure 4.6 shows the analysis of a conductance-based model reduced under three different conditions applied on T-type calcium channel activation, when it is considered as fast,($\tau_{m_{CaT}}(V)/50$ - left column), slow (nominal $\tau_{m_{CaT}}(V)$ - center column) and ultraslow ($50\tau_{m_{CaT}}(V)$ - right column). Figure 4.6A shows the voltage time-courses when a hyperpolarizing current is applied to reproduce a hyperpolarized-induced bursting. Figure 4.6B exhibits the fast-slow phase portrait drawn at a given time (indicated by (1) in the voltage trace) in order to compare the tonic mode under the three conditions. Figure 4.6C is also the fast-slow phase portrait drawn this time at the saddle node bifurcation (indicated by 2 in the voltage trace, see section Methods 4.4 for details). Videos of the membrane voltage time course, the associated phase portrait including the evolution of the nullclines and the trajectory for the different kinetics are available in Supplementary Material in (Jacquerie and Drion, 2021). In Supplementary Material in (Jacquerie and Drion, 2021), simulations of the reduced models 2, 5', 6 and 6' are available.

First, the timescale chosen for CaT channel activation has no influence on the tonic mode. The reduced model is similarly spiking under the three conditions. The phase plane associated to the discharge mode is not affected. It shows the classical limit cycle extensively studied in spiking models. The trajectory is trapped in the limit cycle around the unstable fixed point present on the expected N-shaped V-nullcline. Second, considering the T-type calcium channel activation as slow as its inactivation removes the ability of the model to switch from tonic to burst (third column). The V-nullcline has a hourglass shape showing the influence of the inactivation of the T-type calcium channel (as shown in (Drion et al., 2012)). The trajectory is attracted by the stable fixed point at the hyperpolarized state. This highlights a lack of depolarizing current, which is due to the simultaneous activation and inactivation of T-type calcium channels.

Finally, the most interesting result is the comparison of the phase portraits during burst mode in the case of the fast activation (Figure 4.6C-left) versus the slow activation of T-type calcium channel (Figure 4.6C-center). We drawn both reduced models at the saddle node (SN) bifurcation (see section Methods 4.4 for details). The main difference comes from the V-nullcline: for the fast activation of CaT channel, the phase portrait is qualitatively similar to the one in spiking mode. For the nominal activation timescale, the phase portrait qualitatively changes by the appearance of a lower branch in the V-nullcline, which permits to robustly separate the silent region (which sits on the lower branch) and the spiking region of bursting (which sits on the upper branch).

Therefore, speeding up the activation of the T-type calcium activation disrupts the ability of T-type calcium channel deinactivation to qualitatively change the phase portrait structure from robust spiking to robust bursting in response to hyperpolarization (Drion et al., 2012; Franci et al., 2013, 2014). The same behavior is observed in all models regardless of their quantitative differences. This remarkable distortion of the phase portrait when $\tau_{m_{CaT}}$ is scaled from the fast timescale to the ultraslow is shown on video in Supplementary Material in (Jacquerie and Drion, 2021).

The consequence on robustness and tunability of this qualitative change is illustrated in Figure 4.7. This figure compares the phase portrait of the reduced version of model 1(embedding a slow T-type calcium channel activation) and the

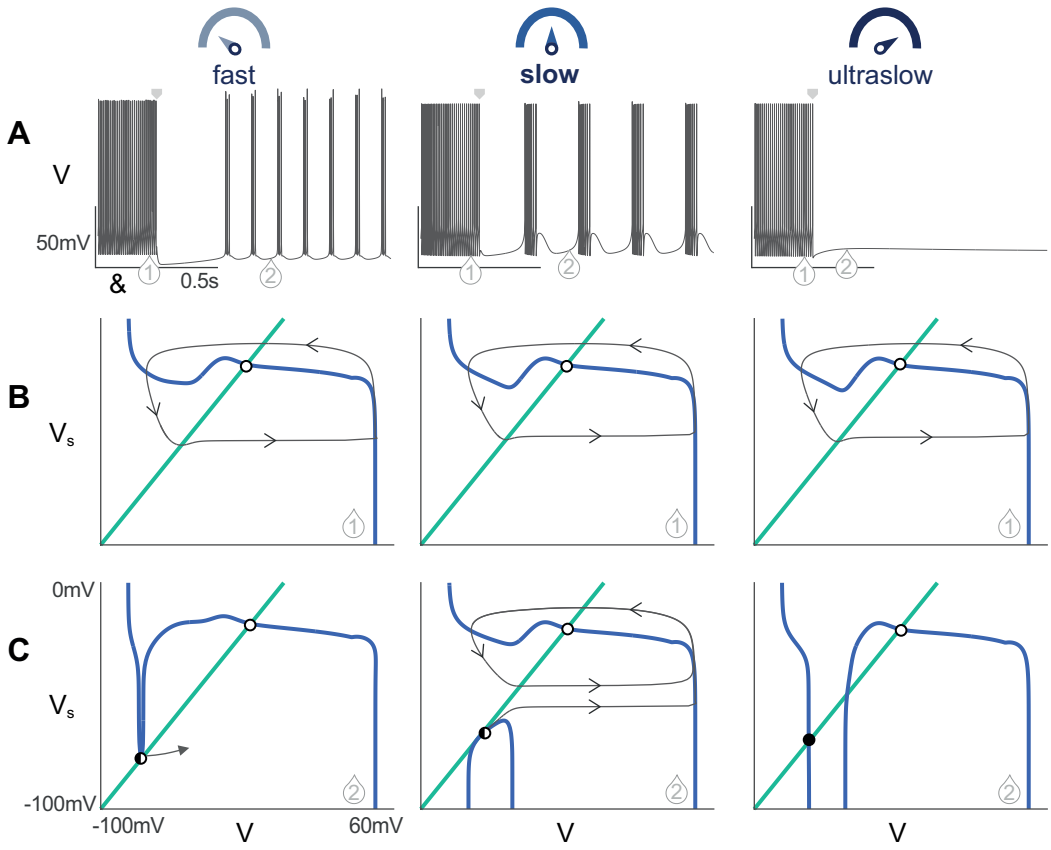

Figure 4.6: Distortion of the phase portrait when the T-type calcium channel activation is considered as fast, slow or ultraslow. **A:** Voltage traces of a reduced model under the three conditions during a hyperpolarized-induced bursting. The square arrow indicates the hyperpolarizing current step. When the CaT activation is ultraslow, the model is not able to switch from tonic to burst. **B:** Comparison of the portrait geometry during tonic mode (arrow 1) under the three timescales. V-(resp. Vs-) nullcline is sketched in blue (resp. green). The unstable fixed point is marked in open circle. The limit cycle followed by the trajectory is sketched in gray. The timescale chosen for the CaT channel activation is not affecting the tonic mode. **C:** Comparison of the portrait geometry during burst mode (at the saddle node bifurcation, arrow 2) under the three timescales. The stable fixed point is marked as a filled black circle and the saddle point meeting the stable fixed point is indicated by the black half-circle. At the ultraslow timescale (right), there is no saddle-node bifurcation,the V-nullcline is distorted into its hourglass shape trapping the trajectory into its stable fixed point. (left) For the *fast* CaT activation channel, the V-nullcline presents only the upper branch where the saddle node bifurcation occurs (center) For the *slow* activation, the V-nullcline exhibits a lower branch. This branch robustly separates the silent region and the spiking region of bursting. Videos of the simulations under the three conditions are available in Supplementary Material in (Jacquerie and Drion, 2021)

reduced version of model 5 (embedding an instantaneous T-type calcium channel activation) when the capacitance membrane is divided by three. We have chosen the membrane capacitance for two reasons. First, as done in Figure 4.1 it is a suitable parameter to test the model robustness to a uniform scaling of maximal conductances or mimicking a change in cell size. Then, from a dynamical viewpoint, the membrane capacitance sets the timescale of the voltage equation. Reducing its value does not affect the nullcline shape nor the fixed point locations but solely affects the vector field.

Both models are able to switch from tonic to burst at the nominal value C_m, but they do so through two different mechanisms. Model 1 uses the appearance of a lower branch in the V-nullcline (see Figure 4.7A,left), whereas model 5 relies on the presence of a region where the timescale separation between the fast and slow timescales is inverted, *i.e.* the slow timescale becomes faster, which is illustrated by vertical trajectories and vector field away from the nullclines (see Figure 4.7B,left). Both mechanisms permit to generate bursting. However, the second mechanism relying on such a dynamical property, it is very fragile to changes in membrane parameters: a reduction of the membrane capacitance removes this region of inverted time-scale separation, hence disrupts the ability to burst (Figure 4.7B,right). The mechanism based on the lower branch of the V-nullcline is structural, hence robust to changes in dynamics created by changes in membrane properties (Figure 4.7A,right). Videos of the simulations are available in Supplementary Material in (Jacquerie and Drion, 2021).

The reader is referred to (Drion et al., 2012; Franci et al., 2012, 2013) for a detailed explanation of the origin and the effect of the lower branch present in the V-nullcline in model with the slow CaT calcium channel activation. More explanations about the robustness and tunability provided by the presence of the lower branch in the V-nullcline versus the classical N-shape are presented in (Franci et al., 2018).

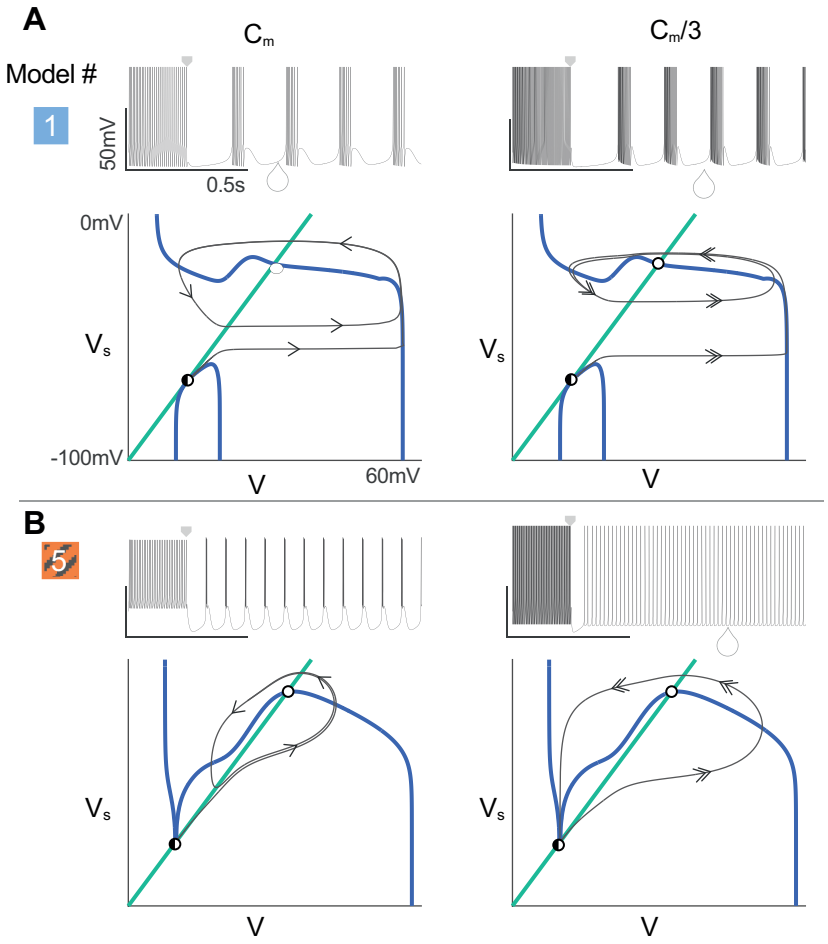

Figure 4.7: The slow activation of T-type calcium channel reveals the appearance of a lower branch in the V-nullcline providing robustness to parameter variation.
A-B: (top) Recording of the membrane voltage during a hyperpolarized-induced bursting (bottom). Phase portrait at the saddle node bifurcation. V-(resp. Vs-) nullcline is sketched in blue (resp. green). The square arrow indicates the hyperpolarizing current step. The unstable fixed point is marked by an open circle and the saddle point meeting the stable fixed point is indicated by the black half-circle. The trajectory is sketched in gray and the arrow indicates the speed along the x-axis. (left to right) the membrane capacitance is divided by 3. The velocity along the x-axis is increased. **A:** The V-nullcline exhibits a lower branch making the phase portrait robust to membrane capacitance variation due to the sharp separation between the limit cycle and the hyperpolarized state. **B:** When the membrane capacitance is divided by three, the reduced model 5 is no more able to switch from tonic to burst. Small deviations destroy the rest-spike bistability. Videos of the different simulations are available in Supplementary Material in (Jacquerie and Drion, 2021)

4.3 Discussion

4.3.1 The physiological timescale separation between sodium and T-type calcium channel activations.

A quotation from Bertil Hille's book (Hille, 2001), " The time course of rapid activation and inactivation of T-type I_{Ca} has been described by an m^3h model like that for I_{Na} (Coulter et al.1989) (Coulter et al., 1989) ; (Herrington and Lingle 1992) (Herrington and Lingle, 1992), but the derived time constants τ_m and τ_h are 20 to 50 times longer than those for I_{Na} of an axon at the same temperature.", highlights a physiological timescale separation between sodium and T-type calcium channel gating kinetics. T-type calcium channel presents of portfolio of activation kinetics depending on their isotype (i.e. $Ca_V3.1$, $Ca_V3.2$ or $Ca_V3.3$), but all isotypes share the property of activating a timescale slower than sodium channels: the activation time constant ranges between 1ms and 50ms (Klöckner et al., 1999; Cain and Snutch, 2010; Chemin et al., 2002; Clapham and Garbers, 2005; Perez-Reyes, 2003; Frazier et al., 2001; Choi et al., 2015). By contrast, the activation time constant of sodium channel is lower than 1ms (Hodgkin and Huxley, 1952; Gilly et al., 1997; Reckziegel et al., 1998; Hille, 2001). As explicitly shown with these numbers, there is one order of magnitude between these two gating time constants.

T-type calcium channels play a major role in oscillations generated, sustained or propagated by the thalamic circuit such as in sleep or in epilepsy. They are known to be modulated by several signaling cascades or also targets of several

experimental and clinical drugs (Perez-Reyes, 2003; Zamponi et al., 2015; Chen et al., 2014; Blesneac et al., 2015; Lambert et al., 2008; Huc et al., 2009; Traboulsie et al., 2007). These modulations can change the kinetics of this channel activation. Our computational experiments are physiologically relevant since modifying the activation kinetics can lead to undesired behavior.

4.3.2 Modeling T-type calcium channel activation in conductance-based models

In a conductance-based model, the opening of an ion channel is represented by a voltage-dependent gating variable. This variable is described with a first order differential equation whose time constant is also voltage-dependent. In this paper, we investigated the kinetics chosen for the T-type calcium channel activation with respect to sodium channel activation. In other words, we compared these time constants with respect to each other.

There is a growing trend to design T-type calcium channel activation as the equivalent of a sodium channel activation. It often based on the fact that these two channels activate on a faster timescale than their own inactivation. For example in the published paper associated to model 5, it is said that "the activation variable [of T-type calcium channel] s is relatively fast and is replaced by its equilibrium function. (...) The activation kinetics [of the sodium current] being fast, the variable m is replaced by its equilibrium function (...) " (Wang, 1994). However, in the original version published three years before, the activation of T-type calcium channel was not at the same timescale as the sodium channel activation (Wang et al., 1991). In the same way for model 6, it is written "We employ a simplified version of the quantitative model originally formulated by Wang et al. (1991). Activation s is rapid, and inactivation h is relatively slow, (...) activation is assumed to be instantaneous. " (Rush and Rinzel, 1994). The similar simplification occurs for model 3 published in 1998: ten years later, the author mentioned "Note that the activation variable s is considered here at steady-state, because the activation in fast compared to inactivation. This T-current model was also used with an independent activation variable ((Destexhe et al., 1998)), but produced very similar results as the model with activation at steady-state" (Pospischil et al., 2008).

Modeling the T-type calcium channel activation on the same timescale as the sodium channel activiation is a modeling simplification that does not only appears in models of thalamic neurons. For example in basal ganglia, subthalamic neurons are excitatory neurons projecting to inhibitory globus pallidus neurons. These neurons present a switch in firing activity that leads to different brain states, particularly relevant in movement generation and in Parkinson's disease (Uhlhaas and Singer, 2006; Bevan, 2002; Gatev et al., 2006; Kühn et al., 2004; Brown and Williams, 2005; Swann et al., 2011). Subthalamic neurons also embed T-type calcium channels. Once again, it is common to see that the activation of sodium and T-type calcium channels are modeled on the same timescale or even considered as instantaneous (Kubota and Rubin, 2011; Terman et al., 2002; Rubin and Terman, 2004). In both situations, these models are operational. It means that differentiating the sodium and T-type calcium channel activations is *not indispensable to reproduce* discharge modes. Those models are able to fire in tonic and burst. This timescale separation between the activation of these two different channels is neglected because it seems to be a computational detail. Figs 4.3, 4.5 and 4.7 confirm that models initially considering a fast activation of T-type calcium channel can perform the desired activity. However, our results stress the crucial importance of this timescale separation for the *robustness* in network switches. The optimum operating timescale for T-type calcium channel activation is located between the fast activation of sodium channels and the ultraslow inactivation of T-type calcium channels.

As mentioned earlier, both channels have different electrophysiological properties. Assuming the T-type calcium channel activation as fast as sodium channel activation means that it is just a current summation. This has for consequence to drastically reduce the ability of generating a robust network activity as shown in our computational experiments.

4.3.3 Compatibility between switches in brain states, synaptic plasticity and neuromodulation

Neuronal oscillations, synaptic plasticity and neuromodulation are hot topics in neuroscience since they are building blocks for information processing, learning, memory or adaptability. Studying the interaction between them requires computational models that generate *robust* activity even if the synaptic connectivity and the endogenous parameters are altered.

Altogether, this paper reveals that the *robustness* in the brain state switches in presence of cellular variability, heterogeneity at the network level is *correlated with the timescale separation* between sodium and T-type calcium channel activations. Despite the quantitative differences between the models, this timescale separation makes the rhythmic transition compatible with temporal variability and spatial heterogeneity induced by regulatory functions like neuromodulation, synaptic plasticity and homeostasis. In particular, triggering oscillations without any modification of synaptic connectivity makes the models well suited to study how a change in network activity can affect learning.

The mechanism highlighted in this paper can be exploited in other models than thalamic neuron models. It is can be extended to neurons that embeds slow-activating voltage-gated calcium channels or slow-inactivating potassium channels (Franci et al., 2013). The term slow confirms that the model should conserve the timescale distinction between the fast activation of sodium channels and the slow operating timescale of these two specified channels. This physiological timescale separation is imposed by ion channel dynamics. In conductance-based models, this corresponds to the time

constant of the differential equation associated to the channel gating variable. It means that the time constant associated to sodium channel activation is an order of magnitude smaller than the time constant associated to the T-calcium channel activation.

Talking in terms of positive feedback sources can be another approach to support the importance of differentiating ion channel kinetics. On one hand, sodium channel activation acts as a *source of fast positive feedback* because depolarizing the cell drives sodium ions in, making the cell even more depolarized and allowing more and more sodium ions to enter and so on. And the other hand, calcium channel activation operates in a similar way; it is also a source of positive feedback. However, there is a crucial dynamical difference between these two sources: they operates on two different timescales. If the two sources are acting on the same timescale, it is simply a sum of positive feedbacks. As shown by our experiments, it significantly decreases the robustness in presence of neuromodulation and synaptic plasticity. Each type of channel activation or inactivation that is a source of slow positive feedback, for example slow-activating voltage-gated calcium channels or slow-inactivating potassium channels, must be modeled an order of magnitude slower than the sodium channel activation.

Beyond the argument based on the time constant or the source of positive feedback, this time scale separation can be brought to light by dynamical analyses (see Figs 4.6 and 4.7). The slow activation of T-type calcium channels unfolds a lower branch in the V-nullcline during the bursting mode. This shape is required for a robust and tunable firing activity as shown by computational experiments (Drion et al., 2012; Franci et al., 2013, 2014, 2018; Van Pottelbergh et al., 2018). Accelerating this channel activation distorts the V-nullcline and makes disappear this lower branch. The switch to bursting becomes fragile and rigid.

4.4 Methods

All simulations were performed using the Julia programming language citation for Julia (Bezanson et al., 2017). Analysis were performed either in Matlab and Excel. Code files are freely available at `http://www.montefiore.ulg.ac.be/~guilldrion/Files/Jacquerie2021_codes.zip` and `https://osf.io/sth4d/`.

4.4.1 Conductance-based modeling

In this chapter, a neuron is described using single-compartment Hodgkin-Huxley models as described in the chapter dedicated to modeling techniques (section 3.1.1). Different conductance-based models are compared. Their differences are explaiend in the following 'Results' section. The function and parameter values are listed in Supplementary Material D.

4.4.2 Computational experiment at single-cell

Figure 4.1A shows a switch from tonic firing to bursting due to a hyperpolarizing current as introduced in section 3.4.1. This model is labelled model 1 in this chapter. The external current, which hyperpolarizes the cell after 0.5s, switches the firing activity from tonic mode to bursting mode.

Figure 4.1B shows the currentscape of the neuron in model 1 during a switch. A currentscape is a technique constructed elaborated in (Alonso and Marder, 2019). The currentscape helps to visualize the contribution of each ionic current as the percentage of the total current.

Figure 4.1C displays time-evolution of the membrane voltage of models 1, 5 and 5' simulated for two values of the membrane capacitance: the nominal value C_m and when it is divided by 10 ($C_m/10$). The current protocol is depolarizing during 0.5s and then hyperpolarizing during 1.5s.

Figure 4.1D is a quantitative representation of the model capability to switch from tonic to burst for several values of the membrane capacitance C_m. A depolarizing current is applied during 1.5s followed by a hyperpolarizing current during 5.5s. We automatically check the rhythmic pattern; we wait for 0.5s to take into account transient effects, then we record spike times. A spike is considered when the voltage value is greater than -10mV and we save the time at which the event occurs. From spike times, we can deduce the firing pattern. A cell that has no recorded spike time is defined as *silent*. The distinction between tonic mode and bursting mode is based on the comparison of the maximal and minimal interspike-interval (ISI). A neuron is *bursting* when the maximal value of ISI is three times greater than the smallest ISI (max[ISI] > 3 min[ISI]). It ensures the cell to have clusters of action potentials separated from each other by silent intervals . If this criterion is not respected, the cell is classified as a *tonically firing* cell with regular action potential generations (Drion et al., 2018; Goldman et al., 2000). For the nominal parameter set, the value of I_{app} is known to generate tonic mode. Afterwards, the membrane capacitance C_m is altered with a multiplicative factor varying from 0.01 to 0.1 with a step of 0.01 ([0.01:0.01:0.1]C_m), then from 0.1 to 5 with a step of 0.1 ([0.1:0.1:5] C_m). In addition, at each tested value of C_m, we scan several values I_{app} in order to find the largest range of capacitance values leading to a switch from tonic to burst. The step time is also adapted for small values of the membrane capacitance to guarantee stability when solving the ode with Euler's method (for numerical values see Supplementary Information directly on (Jacquerie and Drion, 2021)).

4.4.3 Computational experiment on a 2-cell circuit

Connecting neurons with each other follow the explanations in in the chapter dedicated to modeling techniques (section 3.2).

Synaptic weights ($\bar{g}_{syn}$ referring to $\bar{g}_{\text{AMPA}}$, $\bar{g}_{\text{GABA}_\text{A}}$ and $\bar{g}_{\text{GABA}_\text{B}}$) are initially chosen for each model in a way that the 2-cell circuit performs a rhythmic transition when the inhibitory cell is hyperpolarized. Figure 4.2A, center panel illustrates traces of the desired outcome (recording from model 1 with two identical cells). By contrast, Figure 4.2A, right panel exhibits an arrhythmic state (recording from model 1 when $\bar{g}_{KCa}$ is divided by 10 and $\bar{g}_{CaT}$ is divided by 5).

Figure 4.2B is a quantitative comparison of model capability to switch for an increasing intrinsic variability. The intrinsic feature refers to maximal ionic conductances ($\bar{g}_i$). Each maximal conductance is randomly picked with respect to a uniform distribution in a fixed interval around its nominal value. The interval width defines the variability level, as a percentage around this nominal value. For instance, for an intrinsic variability of 10%, each ionic conductance is selected in the range: $[\bar{g}_i - 0.1\bar{g}_i, \bar{g}_i + 0.1\bar{g}_i]$. Regarding synaptic connections, each synaptic weight ($\bar{g}_{syn}$) is taken randomly with respect to uniform distribution around its nominal value in this interval $[\bar{g}_{syn} - \bar{g}_{syn}/8, \bar{g}_{syn} + \bar{g}_{syn}/8]$. For each model, one thousand sets of parameters are generated in order to build one thousand 2-cell circuits.

Each circuit is simulated during 82s. The external current depolarizes the inhibitory cell during 41s and then hyperpolarizes it during 41s. After 1s of transient period in each state, we record the spike time, *i.e.* a spike is considered when the membrane voltage is greater than -20mV. Then we identify the firing pattern of each cell based on its spike times. A cell is silent when it has not fired. A cell is bursting when the maximal interspike interval is four times greater than the minimum interspike interval, otherwise, the cell is in tonic mode. Then, we identify if the circuit is performing a rhythmic transition. During the depolarized state, the excitatory cell is silent and the inhibitory cell is spiking. During the hyperpolarized state, both cells are synchronously bursting.

4.4.4 Computational experiment on a 2-cell circuit with a varying T-type calcium activation time constant

Figure 4.3A shows the excitatory-inhibitory 2-cell circuit affected by neuromodulation, synaptic plasticity and a tunable time constant for the T-type calcium channel activation ($\tau_{m_{CaT}}$). For each model, we generate 400 different 2-cell circuits. For each circuit, maximal intrinsic conductances and synaptic conductances are randomly picked with respect to a uniform distribution in an interval of 20% around their nominal value ($[\bar{g}_i - 20\%\bar{g}_i; \bar{g}_i + 20\%\bar{g}_i]$). These 400 circuits associated with 400 sets of conductances are simulated for varying CaT channel activation time constant; $\tau_{m_{CaT}}$ is scaled with the following multiplicative factors; [1/100, 1/50, 1/20, 1/10, 1/8, 1/5, 1/4, 1/3, 1/2, 1/1.5, 1, 1.5, 2, 3, 4, 5, 8, 10, 20, 50, 100]. For each model, we check automatically, at every scaled $\tau_{m_{CaT}}$, how many circuits among the 400 simulated have performed a rhythmic transition according the same procedure as described above.

Figure 4.3B summarizes the numerical values of $\tau_{m_{Na}}(V_m = V_{th})$, $\tau_{m_{CaT}}(V_m = V_{th})$ and $\tau_{h_{CaT}}(V_m = V_{th})$. Since the time constants are voltage-dependent, to compare them we fix V_m equal to a threshold voltage, V_{th}. The threshold voltage for calcium channel activation is chosen at the beginning of the spike upstroke.The threshold voltage for sodium channel activation is chosen at the spike initiation depending on each model. The threshold voltage for calcium channel inactivation is fixed at the beginning of the calcium spike (see Supplementary Material in (Jacquerie and Drion, 2021) for numerical values).

On Figure 4.3C, the x-axis represents the *scaled* CaT activation time constant *i.e.* the multiplicative factor of $\tau_{m_{CaT}}(V_{th})$ displayed on a logarithmic scale. In order to graduate the axis with a numerical value, the expression is evaluated at the threshold voltage $V_m = V_{th}$. The y-axis represents the percentage of rhythmic circuits. The time constants of the Na channel activation, $\tau_{m_{Na}}(V_m)$ and inactivation $\tau_{h_{CaT}}(V_m)$ are also marked on the graph with dashed vertical lines. They are evaluated at the threshold voltage $V_m = V_{th}$. The results are robust to the choice of the threshold voltage. Models 5' and 6' have an instantaneous sodium activation channel, therefore the right boundary is replaced by $\tau_{m_{CaT}}/100$.

Figure 4.3D combines the individual model robustness analysis on one graph. Since channel activation or inactivation time constants have not the same order of magnitude between each model, the x-axis is a *normalized* logarithmic scale. It is normalized such as the left (resp. right) boundary is the time constant of the Na channel activation (resp. CaT channel inactivation) evaluated at its threshold voltage. We scale the axis with a logarithmic scale such as $\frac{\log(\tau_{m_{CaT}}(V_{th})) - \log(\tau_{m_{Na}}(V_{th}))}{\log(\tau_{h_{CaT}}(V_{th})) - \log(\tau_{m_{Na}}(V_{th}))}$ where $\tau_{m_{CaT}}(V_{th})$ is affected by the multiplicative factor. The idea was to superpose every model between their respective fast timescale (associated with $\tau_{m_{Na}}$) and ultraslow timescale (associated with $\tau_{h_{CaT}}$). It corresponds to scale each individual plot from Figure 4.3C in the window bounded by $\tau_{m_{Na}}(V_{th})$ and $\tau_{h_{CaT}}(V_{th})$.

4.4.5 Computational experiment on a 200-cell network

Figure 4.4A (resp. C) displays the network configuration and the connectivity between the excitatory and inhibitory neuron populations for a homogeneous (resp. heterogeneous) network. E-cells are connected to I-cells via AMPA synapses and I-cells are connected to E-cells via GABA_A and GABA_B. A homogeneous network is built with 200 identical neurons,

and the synaptic weights are the same between each neuron. By contrast, a heterogeneous network is built with neuron models whose maximal ionic conductances are randomly picked in an interval whose width is model-dependent. The interval width is equal to 20% around their nominal values for models 1,2,3,5', 10% for models 4 and 6' and 5% for model 5. Synaptic weights are taken randomly with respect to uniform distribution around its nominal value in this interval $[\bar{g}_{syn} - \bar{g}_{syn}/8, \bar{g}_{syn} + \bar{g}_{syn}/8]$.

Figs 4.4B and 4.4D display a zoom of the the voltage-traces from two I-cells of the population during 4s, starting 500ms before the switch(recording from model 1 - left column, and model 5 -right column). Analyzing activity in a large neuron population is performed through the computation of the local field potential (LFP). It is the mean field measure of the average behavior of interacting neurons (Buzsáki, 2009; Lee and Dan, 2012; Destexhe, 1998). Figs 4.4B and D (third curves) reflect the collective synaptic activity of the neuronal population. It is modeled by the normalized sum of the post-synaptic currents: LFP $= \frac{1}{M}\sum_{j=1}^{M} I_{syn,j}$ where M is the number of post-synaptic neurons in the population. The post-synaptic current from neuron i to neuron j is

$$I_{syn,ij} = -g_{k,i}(V_m - V_k)$$

where k is the receptor type (AMPA, $GABA_A$ and $GABA_B$). The entire post synaptic current of the neuron j is the sum of the post-synaptic current for all the neighboring pre-synaptic neurons. The sum over the N neuron is computed:

$$I_{syn,j} = \frac{1}{N}\sum_{i=1}^{N} I_{syn,ij}$$

where N is the number of pre-synaptic neurons to the neuron j. Finally, to compute the local field potential, the sum of all the post-synaptic current of all the neurons are given by:

$$LFP = \frac{1}{M}\sum_{j=1}^{M} I_{syn,j}$$

where M is the number of post-synaptic neurons in the population.

The time-course of LFP traces shows a oscillating pattern when neurons switch in synchronous bursting. This comes from the large synaptic currents during a burst times the number of neurons in the large population of 200 cells compared to the single input during a spike. To analyse the frequency content of this oscillating trace, LFPs are low-pass filtered at 100Hz via a fourth order Butterworth filter reflecting the use of macro-electrodes in LFP acquisition. The time-frequency plot shows the evolution of the frequency content along time. It results from a logarithmic representation of the spectrogram LFP obtained via a short-time Fourier transform (Drion et al., 2018). Spectrograms are obtained via Matlab function `spectrogram` and the input parameters such as the sampling frequency, the time window, the overlap period, the signal-noise-ration (SNR) are adapted for each model (see Supplementary Material in (Jacquerie and Drion, 2021) for numerical values).

Figs 4.4B and 4.4D illustrate the spectrogram of the LFP of the inhibitory neuron population for model 1 (resp. model 5) on the left (resp. right) panel. The homogeneous and the heterogeneous network are respectively on top and bottom. The simulation is performed during 42s split into 21s of depolarized state followed by 21s of hyperpolarized state. When the network is in oscillatory state, the spectrogram is marked by a high power LFP frequency band (yellow band) characterizing that the mean-field rhythmic activity is turned on.

4.4.6 Computational experiment on a 200-cell network with a varying T-type calcium activation time constant

Figure 4.5 reproduces the 200-cell network of the Figure 4.4 with the same current protocol. The 200-cell network is built by randomly picked intrinsic and synaptic conductances in a given interval around their nominal values. The width of the interval is successively increased with steps of 5% around the nominal values (from 0% to 50%). At each variability order, the heterogeneous network sees the CaT activation time constant $\tau_{m_{CaT}}(V_m)$ of every neuron scaled by a multiplicative factor equal to [1/8, 1/5, 1/4, 1/3, 1/2, 1, 2, 3, 4, 5, 8]. The LFP activity of the neuron population is plotted similarly as in Figure 4.4. At each scaled time constant, we detect if the mean-field activity is turned on by analyzing the time course and the spectrogram of the LFP. If the time-course shows a transition in active state to an oscillatory state and if the spectrogram is marked by a high power band during the hyperpolarized state, the network is considered to switch. We summarize the computational experiment in a table showing vertically the different multiplicative factor and the color shows the largest width of the variability interval at which the network switches.

4.4.7 Construction of the reduced models and phase portrait analysis

We reduce high-dimensional conductance-based models into a minimal model built with three variables: the membrane voltage V, the slow variable V_s and the ultraslow variable V_u. We chose on purpose to write V_m for the membrane voltage

in conductance based models and V for the membrane voltage variable in reduced models to insist on the modeling difference. The dimensionality reduction is performed in a rigorous and systematic manner.

The reduced model is described by three differential equations:

$$\begin{aligned} C_m dV/dt &= -\sum I_i + \mathrm{I_{app}} \\ dV_s/dt &= (V - V_s)/\tau_s(V) \\ dV_u/dt &= (V - V_u)/\tau_u(V) \end{aligned}$$

The slow (resp. ultraslow) variable is a filtered version of the membrane voltage whose time constant is voltage dependent defined as $\tau_s(V)$ (resp.$\tau_u(V)$). The activation of potassium channel (resp. inactivation of T-type calcium channel) paces the slow (resp. ultraslow) timescale *ie.* $\tau_s(V) = \tau_{m_K}(V)$ and $\tau_u(V) = \tau_{h_{CaT}}(V)$. The fast timescale is governed by the activation of sodium channel ($\tau_f(V) = \tau_{m_{Na}}(V)$). Model 5,5',6 and 6' have considered the activation this channel as instantaneous, therefore there is no differential equation and no timeconstant for this activation. In those models, the fast timescale is governed by the activation of potassium channel divided by 10 $\tau_f(V) = \tau_{m_K}(V)/10$. Increasing the division factor does not change our results.

Each ionic current is expressed in terms of activation and inactivation variables (resp. m_i and h_i). By contrast with the conductance-based models, these variables are no more computed through differential equations. The idea is to decompose the contribution of each ionic current into the three timescales (Drion et al., 2015). In model reduction, it is common to assume that an activation or an inactivation variable is globally evolving on a given timescale. Here, we perform an evaluation of the activation and inactivation kinetics at each membrane voltage.

$$I_i = \bar{g}_i m_i^{p_i}(V, V_s, V_u) h_i^{q_i}(V, V_s, V_u)(V - E_i)$$

These activation and inactivation variables are decomposed into a weighted sum of three terms to account for their contribution in each timescale (m_i and h_i are contracted into X to ease the reading):

$$\begin{array}{rcll} X(V, V_s, V_u) & = & w^X_{fs}(V) & X_\infty(V) \quad \text{fast} \\ & + & (w^X_{su}(V) - w^X_{fs}(V)) & X_\infty(V_s) \quad \text{slow} \\ & + & (1 - w^X_{su}(V)) & X_\infty(V_u) \quad \text{ultraslow} \end{array}$$

The two voltage-dependent weighting factors $w^X_{fs}(V)$ $w^X_{su}(V)$ of the activation or inactivation variable are obtained by comparing its associated time constant defined in the conductance-based model ($\tau_X(V)$) at a given membrane voltage with respect to the three timescales pacing each timescale ($\tau_f(V)$, $\tau_s(V)$ and $\tau_u(V)$).

$$\begin{array}{l} \text{if } \tau_X(V) \le \tau_f(V) \\ \quad w^X_{fs}(V) = 1 \\ \quad w^X_{su}(V) = 1 \\ \text{else if } \tau_f(V) < \tau_X(V) \le \tau_s(V) \\ \quad w^X_{fs}(V) = \dfrac{\log(\tau_s(V)) - \log(\tau_X(V))}{\log(\tau_s(V)) - \log(\tau_f(V))} \\ \quad w^X_{su}(V) = 1 \\ \text{else if } \tau_s(V) < \tau_X(V) \le \tau_u(V) \\ \quad w^X_{fs}(V) = 0 \\ \quad w^X_{su}(V) = \dfrac{\log(\tau_u(V)) - \log(\tau_X(V))}{\log(\tau_u(V)) - \log(\tau_s(V))} \\ \text{else if } \tau_X(V) > \tau_u(V) \\ \quad w^X_{fs}(V) = 0 \\ \quad w^X_{su}(V) = 0 \end{array}$$

The weights are either 0,1 or equal to the logarithmic distance between the referential time constants (for more explanations about the algorithm see (Drion et al., 2015)).

Figure 4.6 shows the voltage trace of the reduced model 1 and its associated phase portrait at two given instants indicated by 1 and 2. Each column corresponds to a reduction under three conditions imposed on the time constant of the T-type calcium channel activation $\tau_{m_{CaT}}(V)$; $\tau_{m_{CaT}}(V)/50$ (left), $\tau_{m_{CaT}}(V)$ (center) and $50\tau_{m_{CaT}}(V)$ (right). This modification has an effect on the weighted sum association to the $m_{CaT}(V, V_s, V_u)$ since the contribution of this channel into the three timescales is affected by the multiplicative factor.

The phase plane analysis is performed on Matlab. The V-nullcline is defined by $dV/dt = 0$ giving

$$0 = (1/C_m)(-\sum m_i^{p_i}(V, V_s, V_u) h_i^{q_i}(V, V_s, V_u)(V - E_i) + \mathrm{I}_{app})$$

. The Vs-nullcline is equal to $0 = (V - V_s)/\tau_s(V)$ leading to $V_s = V$ (as shown by the straight line in the different phase portraits). In the tonic mode, the V-nullcline is computed at a given time during the depolarized state. In the bursting

mode, the V-nullcline is changing its shape throughout the burst generation. It mimics the physiological activation and inactivation of the T-type calcium current and in the reduced model it corresponds to oscillation of the ultraslow variable (see (Drion et al., 2012) for more explanations). Therefore, to compare the different phase portrait between the different models and the different CaT time constant, we chose to draw the phase portrait at the saddle node bifurcation. By definition, at the saddle node bifurcation, the two nullclines are intersecting each other and the determinant of the jacobian must be equal to zero. To obtain the value of V_u at the saddle node bifurcation, the system to solve is equal to:

$$\begin{aligned} 0 &= -\sum_i I_i + \mathrm{I_{app}} \\ 0 &= (V - V_s)/\tau_s(V) \\ 0 &= \begin{vmatrix} \frac{\partial(dV/dt)}{\partial V} & \frac{\partial(dV/dt)}{\partial V_s} \\ \frac{\partial(dV_s/dt)}{\partial V} & \frac{\partial(dV_s/dt)}{\partial V_s} \end{vmatrix} \end{aligned}$$

When there is no saddle-node bifurcation, the phase portrait is drawn at the fixed point computed by: $dV/dt = 0, dV_s/dt = 0, dV_u/dt = 0$. The membrane voltage is indeed attracted by a hyperpolarized stable fixed point and remains silent.

Figure 4.7 is obtained in a similar manner as Figure 4.6 except that the membrane capacitance C_m is scaled by a factor of 1/3 (right column). The phase portraits are drawn at the saddle-node bifurcation. The algorithm to compute the V-nullcline is the same. The trajectory is added on the phase plane to illustrate the first action potential from the hyerpolarized state towards the limit cycle. As shown in Video in Supplementary Material in (Jacquerie and Drion, 2021) the V-nullcline is changing its shape. The scaling factor only affects the first equation $dV/dt = (3/C_m)(-\sum I_i + I_{app})$. The velocity in the horizontal axis is increased by 3. It is clearly shown by the trajectory profile that is stronger attracted along the x-axis.

More information concerning the model reduction is available on Julia and Matlab codes. The numerical values for each reduced model are given in Supplementary Material S1 in (Jacquerie and Drion, 2021).

4.5 Acknowledgments

The authors gratefully acknowledge Leandro M. Alonso, from Volen Center and Department of Biology in Brandeis University, for his python codes used for the currentscape generation.

CHAPTER 5

Questioning the robustness of synaptic plasticity rules to neuromodulation, cellular and network perturbations

The primary objective of this thesis is to investigate the role of brain-state in memory consolidation, focusing on the transition from active waking to quiet waking. Rather than approaching this research question at the level of the entire brain, we have chosen to study it at the neuronal level, building a computational framework that examines the switches in brain-states alongside changes in neuronal firing activities and synaptic plasticity.

In the preceding chapter, we established the foundation for this thesis by exploring computational neuron models capable of switching between tonic firing and bursting. We highlighted the importance of a timescale separation between sodium and T-type calcium channel activations for generating robust switches.

The next critical step involves integrating memory into the network of biophysical neuron models. This necessitates the inclusion of synaptic plasticity between neurons. We presented various models of synaptic plasticity, including phenomenological and calcium-based approaches, which account for early changes in synaptic strength in section 3.5. The taxonomy developed in this chapter encompasses a wide range of computational models, considering factors such as neuron model type, network size, and the definition of synaptic strength.

Determining which synaptic plasticity rules to employ in our computational framework is a crucial question. To address this, we utilize the taxonomy to discuss the main trends and limitations associated with implementing traditional synaptic rules.

Finally, we conduct two fundamental computational experiments to evaluate the performance of the triplet rule from the phenomenological category and the two-threshold rule from the calcium-based category. These experiments show the difference in response of the rules to switches from tonic firing to bursting and examine the effects of small intrinsic perturbations on their output.

This chapter prompts reflection and discussion among experimental and theoretical neuroscientists, exploring the reasons behind the existence of various synaptic plasticity rules and their differential behavior in the presence of small perturbations.

Furthermore, it is worth noting that this research was presented as an oral presentation at the Annual Meeting of the Belgian Society for Neuroscience in 2022, held in Brussels, and will be included in a review.

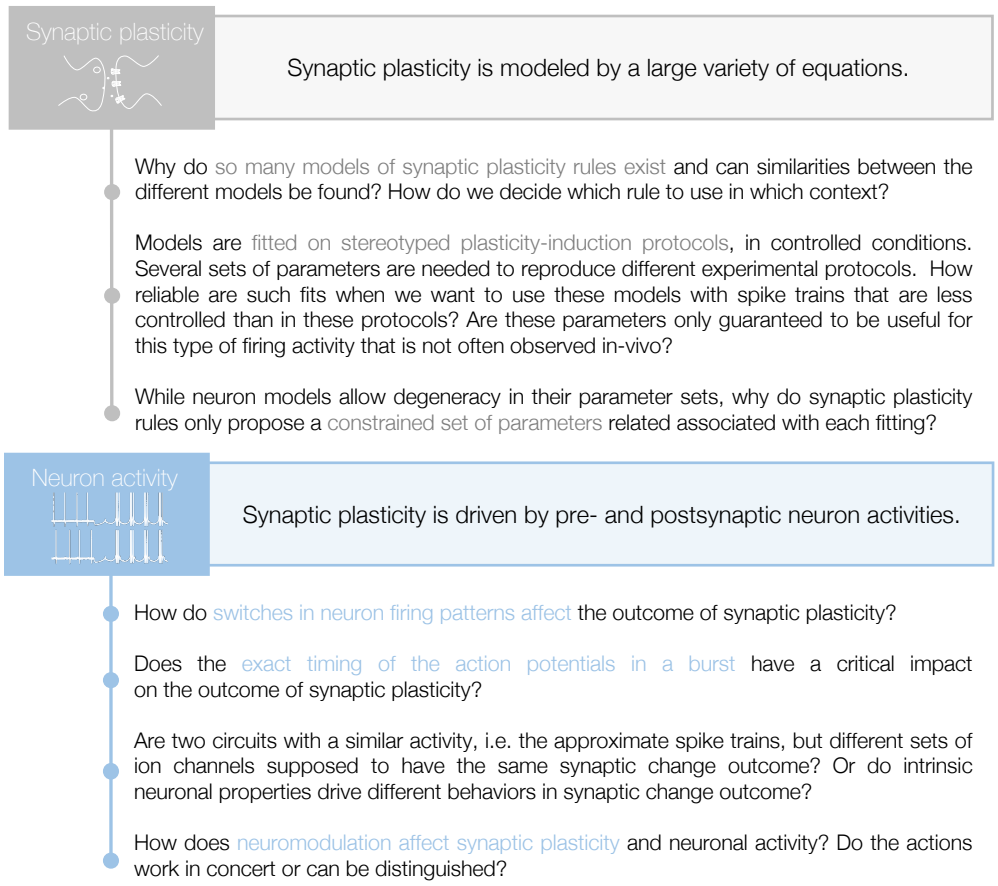

Figure 5.1: The current models of synaptic plasticity are questioned due to the large amount of equations and the lack of unified framework, the stereotyped protocols used to obtain the parameters which make them rigid. The interplay between switches in neuronal activities, variability in intrinsic neuronal properties, neuromodulation and synaptic plasticity is underinvestigated.

5.1 Introduction

Synaptic plasticity is a crucial property of our brain, allowing the wiring between neurons to change. It relies on the ability of neurons to improve or depress synaptic transmission between each other, enabling the brain to adapt, learn, and form memory.

Zooming at the synapse level, the presynaptic neuron communicates with the postsynaptic neuron by releasing neurotransmitters that bind to the postsynaptic receptors, allowing calcium influx in the postsynaptic neuron that triggers a signalling cascade. It is well accepted that 'two neurons that fire together, wire together' as postulated by (Hebb, 1949). Therefore, the activity of the pre- and postsynaptic neurons critically affects their connections.

For many years, researchers in computational neuroscience have developed models and equations to describe synaptic plasticity, leading to an abundance of papers on the subject (Gerstner, 2011; Citri and Malenka, 2008). Strategies for modeling synaptic plasticity encompass a wide range, from phenomenological to biophysical models, with variations in implementing neuron dynamics (such as conductance-based models, IF models, rate-based models, or more biophysical descriptions), defining synaptic strength, and constructing network architectures using synaptic rules. In Section 3.5, we explained these *model features* along with the most frequently encountered synaptic plasticity models, proposing a taxonomy to classify existing papers (section 3.5.3).

In this work, our primary goal is to critically examine the current state-of-the-art in modeling synaptic plasticity. Firstly, we transversely analyze this taxonomy to derive common modeling strategies presented in the literature. For example, we investigate whether specific model features are more commonly used for certain applications or if no specific strategy prevails. *This raises several questions, such as why there are numerous models of synaptic plasticity rules, whether similarities exist between different models, and how we determine the appropriate rule for a given context.*

Furthermore, within this vast array of synaptic plasticity rules, researchers have demonstrated relationships between them and even the fact that they produce similar results (Graupner et al., 2016; Babadi and Abbott, 2016). We expand upon this work by highlighting similarities between the two main calcium-based rules, particularly the two-threshold calcium rule (Graupner et al., 2016) and the rule utilizing the continuous function of calcium (Shouval et al., 2002). Their equations driving the change in synaptic weight can be written with an common equation.

Additionally, we delve into the interaction between plasticity and neuronal activity. Our brain has the ability to transition between different states, often associated with distinct behaviors, such as the switch from small-amplitude, high-frequency population activity (recorded through LFP or EEG) to large-amplitude, low-frequency activity, characterizing the transition from active waking to quiet waking (McGinley et al., 2015). This transition reflects the shift from tonic firing to bursting.

However, neuronal activity influences synaptic plasticity, necessitating an examination of how switches in neuron firing patterns affect the outcome of synaptic plasticity. Surprisingly, this question remains largely unexplored in the literature. One potential explanation is that plasticity rules were initially designed to replicate plasticity-induced protocols achieved under highly controlled conditions where pre- and postsynaptic activities are precisely regulated (Sjöström et al., 2001; Bi and Poo, 1998). *This raises the question of how commonly used synaptic plasticity rules would function when neurons exhibit less controlled spiking patterns and switch their firing patterns*.

Moreover, these switches in neuronal or circuit activity are often regulated by neuromodulators, which also play a crucial role in synaptic plasticity at multiple levels (see section 2.1.6). This complexity poses significant challenges in designing new plasticity models or selecting existing ones, as it requires considering numerous factors and making numerous assumptions.

To illustrate this perplexing state-of-the-art, we compare two frequently used synaptic rules: the triplet model proposed by (Pfister and Gerstner, 2006) in the phenomenological category, and the two-threshold model introduced by (Graupner et al., 2016) in the calcium-based category, under two different scenarios. First, we employ a small circuit capable of transitioning from tonic firing to bursting, comparing the outcomes of these two rules when the bursting activity is slightly altered, exhibiting modifications that are barely visible but likely to occur in in-vivo recordings. Second, we examine the outcomes of these two rules when neurons experience minor fluctuations in intrinsic properties that do not affect the spiking regime. In both experiments, the results differ between the two models, confirming the lack of flexibility in current models found in the literature.

In conclusion, the modeling of synaptic plasticity is a complex and challenging task, and the literature is filled with different models and equations. In this paper, we discussed the taxonomy to classify the different models and their features, and used it to question the current state-of-the-art in the field. We highlighted the lack of understanding of the interaction between plasticity and neuronal activity linked to neuromodulators. Furthermore, we compared two commonly used synaptic rules and demonstrated their lack of malleability in different scenarios.

5.2 Modeling synaptic plasticity is puzzling

5.2.1 Trends in modeling synaptic plasticity

The taxonomy presented in Section 3.5.3 reveals that the state-of-the-art in synaptic plasticity rule models is dispersed. First, we present the primary observation for the choice of the neuron model and the synaptic plasticity model.

As a reminder, phenomenological models use the activity of the pre- and postsynaptic neurons to drive changes in the synaptic weight. The rate-based plasticity model is governed by the presynaptic and postsynaptic spiking frequencies. It often uses a neuron directly described by a rate-based neuron model. The pair-based and the triplet models are governed by the spiking times (Song et al., 2000; Pfister and Gerstner, 2006). Therefore, the neuron can be modeled either by an IF or a conductance-based framework, but it requires an intermediate step that converts the membrane voltage evolution into a spike train by extracting the timing when the neuron reaches its spiking threshold. To avoid this step, an event-based neuron model is often used directly. It means that a distribution process such as a Poisson distribution will directly provide the spike train. For the voltage-based model (Clopath and Gerstner, 2010), the postsynaptic neuron must at least have a basic description of its subthreshold dynamics.

Calcium-based models translate the calcium fluctuations into synaptic weight change. One practice is to derive calcium dynamics from calcium currents. These currents can either be modeled by a full description of the NMDA receptors or voltage-dependent calcium channels with either complex processes or more simply, using decaying exponential translating directly the effect of a pre- and postsynaptic spike on calcium increase. In both cases, the neuron dynamics can follow a conductance-based model, an IF model, or can be simplified by its event-based implementation. A full description of the membrane voltage dynamics using conductance-based models allows for a more faithful description of the current. Refer to Table D.3 for the different ways to implement calcium.

At this stage, no consensus or clear match between the model features and the synaptic rule itself has been highlighted. Using a conductance-based model helps to describe more biophysical properties of the neuron dynamics, such as the refractory period. Using spike trains gets rid of such behaviors. Nevertheless, some common practices appear, such as conductance-based models, are mainly used in calcium-based modeling with a focus on the postsynaptic cell. This combination provides a more reliable framework to explore the biophysical mechanisms underlying synaptic plasticity. Conversely, phenomenological rules are mostly used with IF neuron models or event-based neurons in large networks. Therefore, these rules are employed as a tool to study memory formation or consolidation. This association permits saving computation time especially in computational experiments relying on large networks. By contrast, the

association of conductance-based models with calcium-based rules requires more differential equations, implying longer time-computing.

The current trend in the field of synaptic plasticity is to expand and enhance phenomenological and calcium-based rules (section 3.5.2). These rules are being extended to meet specific application requirements or modified to achieve desired results. This trend raises concerns about the limitations of existing synaptic rules and suggests the possibility of returning to more fundamental and reliable implementations of synaptic rules.

To draw a parallel, when studying a new type of neuron or a novel firing pattern, it is common practice to begin constructing its model by experimentally identifying the various ionic currents that drive the neuronal dynamics. Based on the Hodgkin-Huxley paradigm, a conductance-based model can then be derived, incorporating the appropriate ion channels. The parameters of the Hodgkin-Huxley model can be adjusted to better represent the neuron itself. A similar methodology has been applied to fit synaptic plasticity rules to different protocols induced by plasticity in various regions. For example, the triplet model (Pfister and Gerstner, 2006) has one parameter set to reproduce the STDP protocol observed in the hippocampus (Bi and Poo, 1998), and another parameter set to replicate the frequency protocol observed in the cortex (Sjöström et al., 2001). Similarly, the calcium-based model (Graupner et al., 2016) also includes parameters that depend on the specific plasticity-induced protocol being modeled. However, this raises a pertinent question regarding the reliability of such fits when using these models with spike trains that are less controlled than those observed in these two protocols. *Do these parameters only ensure the efficacy of these rules for firing activity types that are not frequently observed in-vivo?*

Additionally, for neuron models, the different conductances can have a range of values that still produce the desired activity, ensuring *degeneracy* (Golowasch et al., 2002). Indeed, different neurons in the same region can show a large range of values that must be observed also in computational models (Marder and Taylor, 2011). For plasticity rules, Artola and Singer also raised the flag about degeneracy in synaptic plasticity variability. (Artola and Singer, 1993) postulated that "the mechanisms for the manifestation of LTP and LTD are not expressed to the same extent in all cells." This notion is supported by the different parameter sets. They also mentioned that "Thus, different cells or even different synapses on the same cell are likely to differ with respect to the probability with which a particular increase in [Ca] triggers LTP or LTD" (Artola and Singer, 1993). However, synaptic plasticity rules in networks tend to be uniform across cells, despite the fact that cells have different intrinsic properties. It raises the question *why there is a lack of variation in synaptic plasticity parameters between cells and why homogeneous rules are commonly observed instead.*

5.2.2 Relationships and discrepancies in synaptic plasticity rules

Synaptic plasticity rules aim at providing equations for synaptic weight change (Magee and Grienberger, 2020). Over the years, numerous synaptic rules have been derived, and theoreticians have attempted to establish relationships or discrepancies between the different rules (Graupner et al., 2016).

For phenomenological models of plasticity, despite their distinct implementations, relationships have been discovered. The triplet model is an improvement on the classical pair-based model, and it can match a wider range of experimental protocols (Pfister and Gerstner, 2006). It has been demonstrated that it can also be mapped to rate-based learning rule as the BCM (Gjorgjieva et al., 2011). The sliding threshold of Bienenstock's theory is also derived by introducing metaplasticity and other time-scales in the model (El Boustani et al., 2012). The voltage-based model is an extension of the triplet model (Clopath et al., 2010). Heterosynaptic plasticity is achieved by using a STDP rule combined with metaplasticity (Benuskova and Abraham, 2007).

The distinction between soft-bounds and hard-bounds weight dependency is often discussed, but this can also be encapsulated in one variable, μ. As a reminder, the concept of soft-bound weight dependencies aims to model the fact that synaptic plasticity itself can depend on the synaptic weight (Van Rossum and Shippi, 2013; Gütig et al., 2003). Stronger weights are more easily depressed and less easily potentiated, and vice versa for weaker weights. The potentiation and depression parameters are weight-dependent. Conversely, for hard-bounds, the weight increases and decreases with a fixed amount, and so upper and lower bounds are fixed. (Gütig et al., 2003) showed that the same set of equations can describe both weight-dependencies by controlling the value of μ. Further details are provided in 5.6.2.

Similar mappings are demonstrated in calcium-based rules. As mentioned in section 3.5, calcium-based rules are either described by a two-thresholds calcium function (Graupner and Brunel, 2012) or a continuous calcium-dependent sigmoid function (Shouval et al., 2002). Here we show that the two formulations are identical and can be expressed by a generic model: $\tau([Ca])\dot{w} = \Omega([Ca]) - \mu w$ where $\tau([Ca])$ is the calcium-dependent time constant, $\Omega([Ca])$ is the calcium-dependent steady-state value and μ indicates soft-bounds ($\mu = 1$) or hard-bounds ($\mu = 0$). The analytical demonstration and coefficient identification is done in Methods 5.6.

Phenomenological and biophysical models are often compared, as demonstrated in (Yeung et al., 2003; Graupner and Brunel, 2012; Graupner et al., 2016; Babadi and Abbott, 2016).

5.3 The interplay between switches in neuronal activity and synaptic plasticity is underinvestigated

Hebbian learning has been extensively described in the literature. When two neurons exhibit correlated activity, their connections are strengthened (Figure 5.2, left) (Heidelberger et al., 2014). Conversely, connections between neurons with uncorrelated activity either remain stable or can weaken. This phenomenon is well captured by many traditional synaptic plasticity models. However, neurons are capable of generating complex firing patterns such as pacemaking, bursting, or plateau potentials (see section 2.2.2, Figure 2.8). Moreover, they can transition between these patterns. In this study, we specifically focus on switches from tonic firing to bursting, as they have been observed in various neuronal populations located in different brain regions (Figure 2.11).

This raises the question of *how switches from tonic firing to bursting interact with synaptic plasticity*. While tonic firing has been extensively studied, bursting activity has received comparatively less attention in the literature. Bursting has been shown to play a crucial role in various behaviors and learning processes (Dias et al., 2021). However, it remains unclear whether the mechanisms of synaptic plasticity during bursting are similar to those observed during tonic firing.

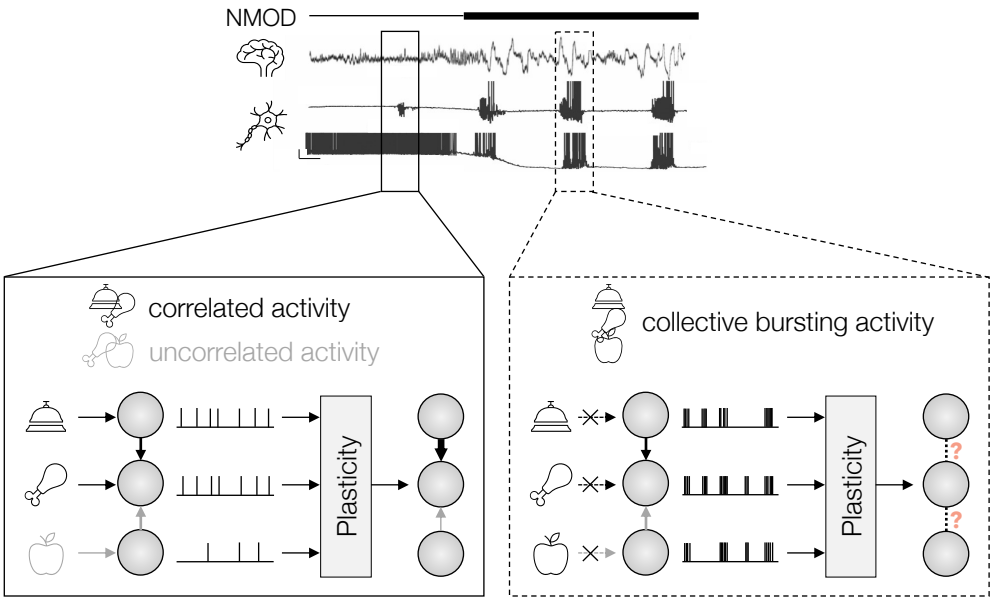

Figure 5.2: The impact of switches in brain states, neuronal activity onto synaptic plasticity remains unclear. (Top) Switches in brain states (recorded by EEG signal) reflecting switches in neuronal firing activity are orchestrated by neuromodulators (adapted from Zagha and McCormick (2014)). (Bottom-left) During tonic firing associated to an active state, correlated neurons (bell-chicken) increase their synaptic weights while uncorrelated neurons (chicken-appel) decrease the weights. (Bottom-right) During synchronized bursting associated to a quiet state, external inputs are disconnected, neurons are bursting; synaptic change is not yet elucidated.

At the moment, we note several models that tends to explain plasticity during burst. For example, the impact of successive action potentials has been demonstrated to play a role in short-term plasticity, as it affects the availability of resources at the presynaptic neurons (Castro-Alamancos and Connors, 1997; Heidelberger et al., 2014). Other models of synaptic plasticity during bursts have been proposed, considering bursts as single units, and the synaptic weight changes based on the time latency, also known as the interburst interval, between pre- and postsynaptic bursts (Gjorgjieva et al., 2009; Tupikov and Jin, 2021; Zhou et al., 2019; Paludo Silveira et al., 2021; Butts et al., 2007; Delattre et al., 2015). Burst-dependent plasticity models have been developed using eligibility traces to detect bursts (Payeur et al., 2020; Fuchsberger et al., 2022).

5.4 Testing the robustness of the triplet model and the calcium-based model

5.4.1 Unveiling the impact of bursting activity on synaptic plasticity: insights from a computational study

Synaptic plasticity has been commonly studied using highly stereotyped spiking protocols (as discussed in Section 3.5.2, Figure 2.16). For instance, pair-based or triplet models rely on precise spike timing between a presynaptic neuron and a postsynaptic neuron, resulting in either potentiation or depression (Bi and Poo, 1998). These plasticity rules are fitted to such protocols and can replicate experimentally observed synaptic changes during controlled spiking activity induced

by current-clamp (Figure 5.3, tonic activity). However, neurons in vivo do not exhibit such controlled spiking patterns under normal conditions. In this study, we examine the behavior of these plasticity rules in the context of bursting activity, where the focus is not solely on spike timing but rather on the synchronicity of the entire rhythmic activity.

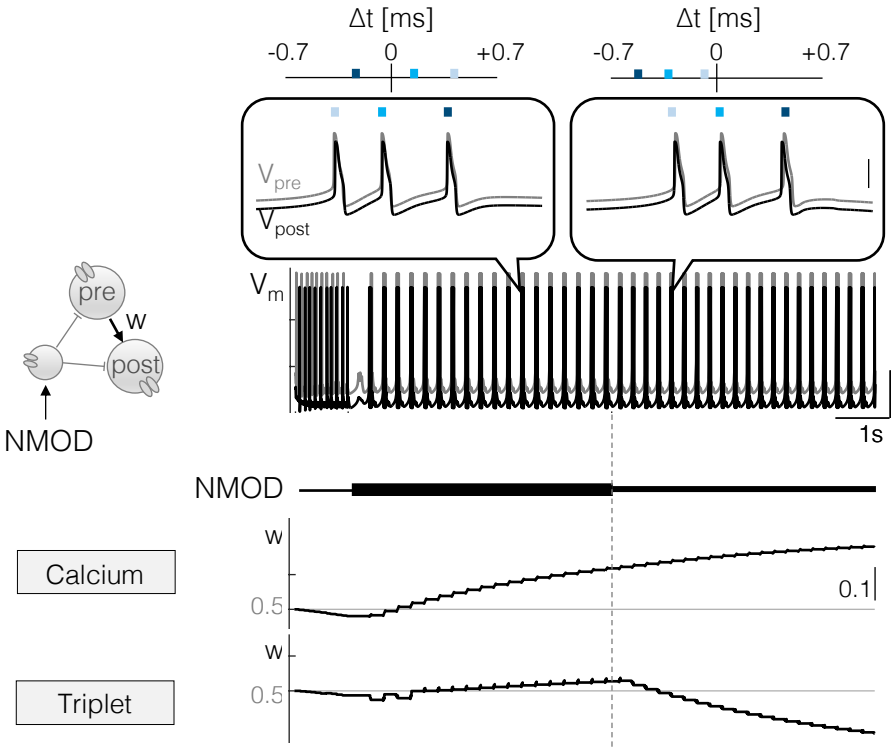

Figure 5.3: Phenomenological rules are sensitive to the relative spike times within an endogenous burst rhythm. A 3-cell circuit composed of an inhibitory neuron connected to two excitatory neurons that have a plastic connection. Each neuron is a conductance-based model.Two seemingly similar patterns driven by slightly different neuromodulator levels (change in black bar size) lead to a slight difference on the pre-post pairing (blue squares on Δt). It results in an opposite synaptic weight change for phenomenological models (phenom.). On the contrary, calcium-based model is blind to the change in neuromodulator level. (yscale-zoom: 50mV, time window-zoom: 90ms, voltage y-scale: 50mV, gray and black voltage traces are respectively the pre and postsynaptic neuron activity).

To explore this, we conduct a simple computational experiment using a neuron circuit capable of switching between asynchronous spiking and rhythmic bursting states (Jacquerie and Drion, 2021). Employing a conductance-based modeling paradigm, the circuit reproduces activities observed in cortical networks during state transitions in the brain, such as sleep-wake cycles (McCormick and Bal, 1997; Zagha and McCormick, 2014; Chrol-Cannon and Jin, 2014), among others. In this circuit, an inhibitory neuron projects GABA currents onto two excitatory neurons connected by an AMPA current (Figure 5.3, left). The synaptic strength between these two neurons is modulated by synaptic plasticity, which can be modeled using either a biophysical rule (based on two-threshold calcium levels established by (Graupner et al., 2016)) or a phenomenological rule (triplet rule from (Pfister and Gerstner, 2006)). The circuit is capable of transitioning from tonic firing to bursting, driven by neuromodulators that can change the circuit's state (Marder et al., 2014). These neuromodulators are dynamically regulated, meaning their quantity fluctuates over time. Even within a given brain state, small variations in their concentration are observed. In our model, we simulate neuromodulators by applying a hyperpolarizing current to the inhibitory cell (mimicking changes in acetylcholine levels, for example). During bursting, this current is altered by 5% (Figure 5.3, right). Here, we emphasize that the bursting activity is an endogenous response of the circuit and not a controlled generation of successive action potentials that response to a current input. It corresponds to an intrinsic burst generation (for reminder see Figure 2.9). Although bursting activity remains similar, with consistent intraburst frequency, duty cycle, and number of spikes per burst, the evolution of synaptic weight computed by the two models leads to distinct responses. The phenomenological model proves to be highly sensitive to this small change in neuromodulator level, which is barely discernible to the naked eye (see Figure 5.3, bottom trace). The spike times are slightly shifted from a mainly pre-post pattern, inducing potentiation, to a post-pre pattern, inducing depression (zoom in Figure 5.3), significantly impacting the temporal evolution of the synaptic weight. In contrast, biophysical models are insensitive to this perturbation, as the calcium dynamics are driven by the burst itself rather than the relative spike timing within the burst.

Overall, these observations raise questions about how synaptic plasticity is influenced by transitions from tonic firing to bursting and how to effectively study this interaction using computational models. Should we transition from triplet-based rules to burst-time-dependent plasticity? Is it plausible to consider that the rhythm itself disrupts synaptic plasticity?

Could this be mediated by neuromodulators that orchestrate the neuronal shift? Burst-time-dependent plasticity rules, as developed in (Gjorgjieva et al., 2009), offer an avenue for exploration. These rules often treat bursts as single units and compute synaptic changes based on the interburst latency between pre- and postsynaptic bursts. This raises questions about *the neuron's ability to switch from spike detection to burst detection and also the role of the burst itself if it is considered as a single unit* (which implies that the burst's duration, number of spikes per burst, and intraburst frequency are negligible).

This straightforward computational experiment highlights the lack of investigation into the intertwined relationship between synaptic plasticity and switches in neuronal activity.

5.4.2 Exploring the compatibility between synaptic plasticity rules and intrinsic neuronal variability

Neurons are highly variable in types, shapes, and even within the same category of neurons, intrinsic parameters are vastly different (Marder and Taylor, 2011). Similar circuit activities can result from a large set of intrinsic conductances. These conductances are also ongoing turnover or they are under the control of neuromodulators (see section 2.3). Here, we challenge the compatibility between synaptic plasticity rules and intrinsic variability. We use the same circuit in asynchronous spiking activity. Two intrinsic conductances are modified by 25% to 50%. The activity is not perturbed but the evolution of the synaptic weight is different between the biophysical and the phenomenological rules (Figure 5.4). This difference in robustness comes from the driving mechanisms of the synaptic rule. For phenomenological models, the spike time is blind to change in intrinsic parameters. By contrast, the biophysical models are translating the calcium fluctuations into synaptic weight change. The intrinsic variability affects the calcium ion channels resulting in a change of intracellular calcium concentration, drastically impacting the evolution of the synaptic weight. It raises the question that *two circuits with a similar activity but different sets of ion channels are supposed to have the same synaptic change (as seen in phenomenological rules) or these intrinsic differences drive different behavior in the synaptic connection* (Artola and Singer, 1993).

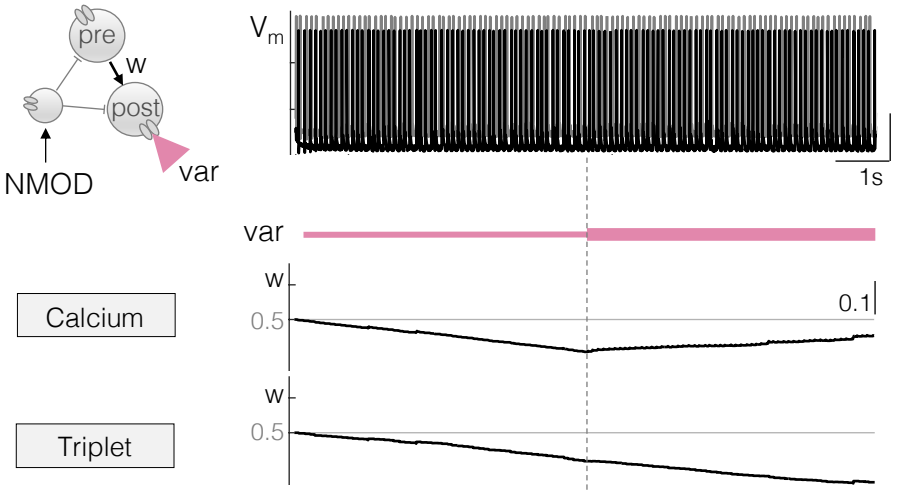

Figure 5.4: Change in intrinsic parameters affects the outcome of the biophysical models. A 3-cell circuit composed of an inhibitory neuron projecting to two excitatory neurons whom synaptic strength is plastic. Each neuron is a conductance-based model. The circuit is in asynchronous spiking regime. As soon as the postsynaptic neuron conductance is affected by variability (var) mimicking the effect of neuromodulator, the outcome of the biophysical rule is affected. The phenomenological rule (Phenom.) is blind since the spiking activity is not modified. (Voltage scale: 50mV, gray and black voltage traces are respectively the pre and postynaptic neuron activity)

5.5 Discussion

This chapter aims to shed light on the gap between existing synaptic plasticity rules, neuromodulation, as well as their robustness against cellular and network perturbations.

Modeling synaptic plasticity is a complex task that involves constructing neuron models, selecting the appropriate equations (ranging from biophysical to mathematical), and calibrating the parameters using controlled experimental data. The sheer number of available rules can be overwhelming. Despite finding some similarities among them, we have demonstrated through two small computational experiments that their outputs under similar conditions can vary significantly. These experiments were designed to investigate how different rules behave in the presence of changes in neuronal

activity and perturbations. Notably, the results obtained from different rules diverged considerably.

In overall, a myriad of questions remain unsolved. It highlights the need for further research to improve the understanding and modeling of synaptic plasticity, particularly in relation to switches in neuronal activity and neuromodulation.

5.6 Methods

Simulations were performed using the Julia programming language Bezanson et al. (2017). Data processing were performed either in Matlab. Code files are freely available at `https://github.com/KJacquerie/Review`.

5.6.1 Neuron model and synaptic plasticity rules

A 3-cell circuit was modeled using a conductance-based model. The neuronal model is the same presented in section 3.2. The inhibitory cell controls the rhythm of the circuit. An hyperpolarizing current applied to the inhibitory neuron switches the whole circuit in rhythmic bursting mode. This hyperpolarizing current models the effect of a neuromodulator signal (NMOD) (Zagha and McCormick, 2014).

Regarding the plasticity between the pre- and postsynaptic cells, we used the triplet model defined in (Pfister and Gerstner, 2006) for the phenomenological rule and the calcium-based model is defined in (Graupner et al., 2016). More information is available in Section 3.5.4.

5.6.2 Equivalence between calcium-based plasticity rules

One pioneered calcium-based plasticity rule was developed by Shouval et al. in 2002 in which the synaptic weight evolves as sigmoid continuous function of the calcium level defined by $\Omega([\mathrm{Ca}])$

$$\tau_w([\mathrm{Ca}])\dot{w} = \Omega([\mathrm{Ca}])$$

where the time constant is also calcium-dependent (Shouval et al., 2002).

To avoid the configuration where the variable w increases linearly with time to infinity, Shouval et al. proposed to add hard-bounds by constraining w between 0 and $w_{\max}$. Another solution that he proposed is using a calcium-dependent weight decay term using the following formula:

$$\tau_w([\mathrm{Ca}])\dot{w} = \Omega([\mathrm{Ca}]) - w$$

which is basically a first-order differential equation whom steady state value is Ω and is calcium-dependent. For low calcium level, the time constant is large and Ω is intermediate. It means that w is extermely slowly converging to an initial value around 0.5. For intermediate calcium level, w is relatively slowly decreasing towards to small values of Ω (depression). For high calcium level, w is fastly converging towards to high value of Ω (potentiation).

Then, Graupner and Brunel proposed a simplified calcium-based rule named two-calcium thresholds (Graupner and Brunel, 2012; Graupner et al., 2016) written as:

$$\tau_w\dot{w} = \gamma_{\mathrm{p}}(1-w)\Theta([\mathrm{Ca}]-\theta_{\mathrm{p}}) - \gamma_{\mathrm{d}}w\Theta([\mathrm{Ca}]-\theta_{\mathrm{d}})$$

The potentiation rate γ_{p} and the depression rate γ_d are weight-dependent. Therefore, this model is using soft-bounds. Stronger weights are less potentiating than weak weights.

To remove the weight-dependency meaning to replace soft-bounds by hard-bounds, we proposed to adapt these two terms $(1-w)$ and w balancing the rate of change by considering w equal to 0.5. The model becomes:

$$\tau_w\dot{w} = 0.5\gamma_p\Theta([\mathrm{Ca}]-\theta_p) - 0.5\gamma_d w\Theta([\mathrm{Ca}]-\theta_d)$$

Table 5.1 compares the equations between calcium-continuous function or two-calcium thresholds in hard- and soft-bound.

Bounds	Calcium-continuous function		Two-calcium thresholds
Hard bound	$\tau_w([\text{Ca}])\dot{w} = \Omega([\text{Ca}])$	$0 < [\text{Ca}] < \theta_\text{d}$	$\tau_w\dot{w} = 0$
		$\theta_\text{d} < [\text{Ca}] < \theta_\text{p}$	$\tau_w\dot{w} = -0.5\gamma_\text{d}$
		$[\text{Ca}] > \theta_p$	$\tau_w\dot{w} = 0.5(\gamma_\text{p} - \gamma_\text{d})$
Soft bound	$\tau_w([\text{Ca}])\dot{w} = \Omega([\text{Ca}]) - w$	$[\text{Ca}] < \theta_\text{d}$	$\tau_w\dot{w} = 0$
		$\theta_\text{d} < [\text{Ca}] < \theta_\text{p}$	$\tau_w\dot{w} = -\gamma_d w$
		$[\text{Ca}] > \theta_\text{p}$	$\tau_w\dot{w} = \gamma_\text{p}(1 - w) - \gamma_d w$

Table 5.1: Comparative table between the different calcium-based model equations. Continuous calcium-dependent sigmoid function as proposed by Shouval et al. (2002) or when potentiation and depression are activated above given thresholds Graupner and Brunel (2012).

The two different rules present different equations and can be adapted for hard-bound and soft-bounds. Here, we aim to demonstrate that they can be written with the standard form of first-order differential equation:

$$\tau_w([\text{Ca}])\dot{w} = \Omega([Ca]) - \mu w$$

where μ equals 1 for soft bound and 0 for hard bounds. In (Shouval et al., 2002) proposed a continuous steady-state and time constant that are both function of calcium. We replaced the equations in (Graupner et al., 2016) by a similar idea except that there are only three possible values for the steady-states and the time constants depending on the three calcium regions.

$$\begin{aligned}
&0 < [\text{Ca}] < \theta_\text{d} && \tau_w^0\dot{w} = \Omega^0 - \mu w \\
&\theta_\text{d} < [\text{Ca}] < \theta_\text{p} && \tau_w^\text{d}\dot{w} = \Omega^\text{d} - \mu w \\
&[\text{Ca}] > \theta_\text{p} && \tau_w^\text{p}\dot{w} = \Omega^\text{p} - \mu w
\end{aligned}$$

These three possible values for the steady-state and the time constants are simply obtained by coefficient identification as done in Table 5.2.

Writing synaptic plasticity with the standard form of a first-order differential equation helps to predict the converging of the weight in case of soft-bounds and the constant change rate in case of hard-bounds. It proposes an unified form to merge the different synaptic plasticity rules.

Bounds	Steady-state value		Time constant	
Hard bound	Ω^0	0	τ_w^0	0
	Ω^d	$-0.5\gamma_\text{d}$	τ_w^d	τ_w
	Ω^p	$0.5(\gamma_\text{p} - \gamma_\text{d})$	τ_w^p	τ_w
Soft bound	Ω^0	undefined ($\diamond$)	τ_w^0	0
	Ω^d	0	τ_w^d	$\frac{\tau_w}{\gamma_\text{d}}$
	Ω^p	$\frac{\gamma_\text{p}}{\gamma_\text{p} + \gamma_\text{d}}$	τ_w^d	$\frac{\tau_w}{\gamma_\text{p} + \gamma_\text{d}}$

Table 5.2: Parameter identification between two calcium-based models from (Shouval et al., 2002) and (Graupner et al., 2016) to match the standard form proposed in this review. ($\diamond$) Since the time constant is null, the steady state value at low calcium level does not need to be defined.

5.6.3 Computational experiments

Figure 5.3 shows a neuronal switch from tonic to burst induced by neuromodulation with variable neuromodulator drive. Tonic activity is simulated by inducing spikes in the pre and postsynaptic cells with a strong current $I_\text{app} = 50\text{nA/cm}^2$ for a short duration of 3ms at a frequency of 10 Hz for 1s. The interspike intervals follow an independent Normal Distribution $\mathcal{N}(\frac{1}{f_0}, (\frac{0.1}{f_0})^2)$, $f_0 = 10\text{Hz}$. Then, A current $I_\text{app,I} = -1.2\text{nA/cm}^2$ is then applied to the inhibitory cell to mimic the impact of neuromodulators and induce bursting. After 6s, the applied current is changed to $I_\text{app,I} = -1.\text{nA/cm}^2$.

Plasticity is implemented between the pre- and postsynaptic neurons using the triplet and the calcium-based model mentioned above. The synaptic weight (w) evolution shows that both plasticity rules evolve the same in tonic mode according to the pairing protocol (Sjöström et al., 2001). However, the switch to burst induce divergent results between the two types of rules.

Figure 5.4 shows a tonic firing pattern with differences in the g_{CaT}, $g_{\mathrm{K,Ca}}$ conductances and affecting the postsynaptic calcium influx (more specially the parameter C_{post} in the calcium-based model (Graupner et al., 2016)). Spikes are generated by applying a strong current $I_{\mathrm{app}} = 50\mathrm{nA/cm}^2$ for a short duration of 3ms. The interspike intervals following independent Normal distributions $\mathcal{N}(\frac{1}{f_0}, (\frac{0.1}{f_0})^2)$, $f_0 = 10\mathrm{Hz}$. From 0 to 5.5s, conductances values are $g_{\mathrm{CaT}} = 0.55$, $g_{\mathrm{K,Ca}} = 4$, $C_{\mathrm{Post}} = 1.62138$. Then, $g_{\mathrm{CaT}} = 0.55 \cdot 1.5$, $g_{\mathrm{K,Ca}} = 4 \cdot 0.75$, $C_{\mathrm{Post}} = 1.62138 \cdot 1.5$.

CHAPTER 6

Switches to slow rhythmic neuronal activity lead to a plasticity-induced reset in synaptic weights

As outlined in the initial stages of my thesis, our goal is to investigate the role of brain-states, more specifically, switches between active and quiet waking on memory. To do so, we have zoomed at the neuronal level, by modeling the switches from tonic firing to bursting for the transition between the brain states and synaptic plasticity for memory. The preceding chapters have laid the groundwork for this thesis, with the first piece providing a circuit consisting of biophysical neurons capable of generating robust switches (Chapter 4). The second piece involved an extensive exploration of the literature, surveying the vast array of synaptic plasticity rules with their numerous variations. In this previous chapter (Chapter 5), we delved into the compatibility between switches in neuronal activities and these diverse synaptic plasticity rules, highlighting the unexplored nature of this research context.

Here, in this chapter, we delve into the heart of the project and assemble the different pieces of the puzzle. On one hand, we have the biophysical neuronal network able to switch from tonic firing to bursting. On the other hand, the synaptic weights between these neurons are affected by traditional synaptic plasticity rules (such as pair-based, triplet, or calcium-based rules), modeling early stage of Long Term Potentiation. We perform computational experiments to track the evolution of the synaptic weights during these switches in neuronal activities.

The results uncover a serendipitous phenomenon. During active waking, neurons normally encode inputs demonstrating the network ability to learn information. Then, surprisingly, switching to quiet waking, associated with a collective bursting activity within the network, triggers a *homeostatic reset* of all synaptic weights. Strong weights undergo depression while weak weights undergo potentiation. This occurs regardless of the specific traditional rule employed, as it utilizes soft bounds.

Therefore, the homeostatic reset adds another crucial element to the puzzle, offering both benefits and drawbacks. On one hand, it facilitates the formation of new memories by enabling the integration of fresh information. On the other hand, it poses a detriment by erasing any previous learning or acquired knowledge.

The results of my research have been published in an article (Jacquerie et al., 2022). Additionally, I had the opportunity to present this research at several conferences for poster presentations, including the FENS conference in July 2020 (virtual), the Annual Meeting of SfN in November 2021 (virtual), the COSYNE conference in March 2022 (held in Portugal), ENCODS and FENS in July 2022 (held in Paris), and the Bernstein Conference in September 2022 (held in Berlin).

Adapted from: Kathleen Jacquerie[1], Caroline Minne[1], Juliette Ponnet[1], Nora Benghalem[1], Pierre Sacré[1], and Guillaume Drion[1].
Switches to slow rhythmic neuronal activity lead to a plasticity-induced reset in synaptic weights.
BiorXiv. 2022 July 16.
doi: 10.1101/2022.07.15.500198
[1] University of Liege, Department of Electrical Engineering and Computer Science.
Keywords: *synaptic plasticity*, *STDP*, *calcium-dependent plasticity*, *brain states*, *neuromodulation*, *homeostasis*, *excitability*, *memory consolidation*

6.1 Introduction

We investigate how network switches from asynchronous tonic spiking to synchronized collective bursting, as those observed when transitioning from active to quiet waking, affect the outcome of several synaptic plasticity rules. To this end, we construct a neuronal circuit capable of rapidly switching between these two firing patterns under the action of neuromodulators. This circuit is made of conductance-based model neurons and comprises an inhibitory neuron that projects onto excitatory neurons. Its robustness analysis is performed in Chapter 4. The synaptic connections between the excitatory neurons are governed by a synaptic plasticity rule. We compare 20 different rule variations, ranging from spike-time dependent plasticity rules (such as pair-based and triplet (Song et al., 2000; Van Rossum et al., 2000; Pfister and Gerstner, 2006)) to calcium-dependent rules (Shouval et al., 2002; Graupner et al., 2016; Deperrois and Graupner, 2020). All rules are parameterized to fit experimental data obtained either on a spike-timing protocol (Bi and Poo, 1998) or on a frequency-pairing protocol (Sjöström et al., 2001). We then compare how strong and weak synaptic weights acquired during tonic spiking, associated with active waking, evolve as the network switches into rhythmic bursting mode, associated with quiet waking.

A switch to rhythmic bursting mode results in a reset of synaptic weights: whatever the strength established during active waking, the network resets its connectivity to a single steady-state value during quiet waking, regardless of the implemented plasticity rule. We refer to this process as a *homeostatic reset* of synaptic weights, as it fully relies on endogenous network properties and promotes the synaptic weight restoration during quiet wakefulness. The homeostatic reset is shown to be robust to the level of neuromodulation, and to both variability and heterogeneity in circuit parameters. Further analytical investigations show that the mechanisms underlying the reset are rooted in the interactions between the endogenous dynamics of network rhythmic bursting activity and the plasticity rules themselves, both being largely independent of initial synaptic weights.

6.2 Results

6.2.1 Switches to a rhythmic bursting reminiscent of quiet waking lead to a homeostatic reset of synaptic weights

We first investigated how switches in brain states, neuromodulation of activity, and synaptic plasticity interact by implementing a triplet rule from (Pfister and Gerstner, 2006) in a neuron circuit capable of switching between asynchronous tonic spiking and rhythmic bursting states (Drion et al., 2018; Jacquerie and Drion, 2021). The neuron circuit follows a conductance-based modeling paradigm and reproduces the activities observed in cortical networks during switches in brain states (McCormick and Bal, 1997; Zagha and McCormick, 2014; Chrol-Cannon and Jin, 2014), among others. The circuit comprises an inhibitory neuron that projects GABAergic currents onto two excitatory neurons, which are connected by an AMPAergic current (Figure 6.1A, left). This 3-cell circuit provides an appropriate support to study the transition between several firing patterns and its functional consequence on the evolution of synaptic weight. Indeed, this topology is often encountered in different brain regions; such as the thalamus between reticular and relay cells (Steriade et al., 2001; Sherman and Guillery, 1996), the cortex between pyramidal and inhibitory cells (Bazhenov et al., 2002; Hill and Tononi, 2005), or even between different organs like striatum and basal ganglia (Humphries, 2012; Kühn et al., 2004). Applying a hyperpolarizing current to the inhibitory cell, which models the effect of neuromodulators (NMOD, Figure 6.1A), switches the whole circuit from tonic firing to synchronous bursting (Figure 6.1A, right).

The LFP is computed in a network of 6 excitatory neurons connected to 6 postsynaptic neurons. It measures the average synaptic activity in the network. The transition from tonic to burst at the cellular level is translated by the marked transition from the low amplitude, high frequency activity to a large, low-frequency rhythmic activity. It mimics e.g. the type of switches observed during transitions from active to quiet waking (Reimer et al., 2014; McGinley et al., 2015; Zagha, 2014; Dastgheib et al., 2022).

We then implemented a synaptic plasticity rule between the two excitatory neurons in the circuit. The connection strength between the neurons, or synaptic weight, is characterized by a variable w (Figure 6.1A). Synaptic plasticity is modeled by a synaptic rule describing the evolution of the synaptic weight throughout time (Figure 6.1A, right). We used a classical triplet model as the synaptic plasticity rule in this neuronal model due to its prevalence in the literature (Pfister and Gerstner, 2006). The rule parameters was fitted on the well-established experimental data obtained through a frequency pairing protocol (Sjöström et al., 2001).

To investigate how fast switches in firing patterns affect synaptic connections in the presence of the triplet model, we subjected six circuit models to two transitions from active to quiet waking and back (ie. from tonic spiking to bursting), while letting the plasticity rule run its course (Figure 6.1B). Among thse six circuits, three were designed to exhibit a correlated activity between the excitatory neurons with the presynaptic neuron firing slightly before the postsynaptic neuron, mimicking the activity of neurons receiving functionally related inputs (curves in Figure 6.1B). The three others were designed to exhibit an uncorrelated, random activity, mimicking the activity of neurons receiving unrelated inputs

(gray curves in Figure 6.1B). We then compared the evolution of the synaptic weight in these six circuits along the two transitions from tonic firing to burst firing (see middle panel of Figure 6.1B).

During active waking, neurons are in tonic firing mode and the synaptic weights evolve according to the level of correlation between the presynaptic and postsynaptic neurons, consistent with the triplet rule. The connection strengths between neurons exhibiting correlated activities increase(Figure 6.1B, top left), whereas the connection strengths between neurons exhibiting uncorrelated activities decrease (Figure 6.1B, bottom left).

As the circuit switches to quiet waking, the neurons switch to a rhythmic, low-frequency bursting mode. This change in activity radically affects the time evolution of the synaptic weights under the triplet rule: connections that were potentiated during the previous active tonic firing phase start to depress (Figure 6.1B, top right), whereas connections that were depressed start to potentiate (Figure 6.1B, bottom right), and all connection strengths eventually converge to a single, stable point. This convergence point is fully independent of what happened during learning. We call this phenomenon a *homeostatic reset* of synaptic weights, as it relies on a switch to an endogenous, rhythmic bursting activity of the network and his independent from external inputs and learning history.

The potential functional consequences of the homeostatic reset are twofold. On the one hand, it promotes the restoration of synaptic weights during periods of quiet waking, which in turn restores the ability to learn new information. On the other hand, it disrupts any learning that may have occurred during the previous active waking, if one solely relies on the evolution of w under the triplet rule.

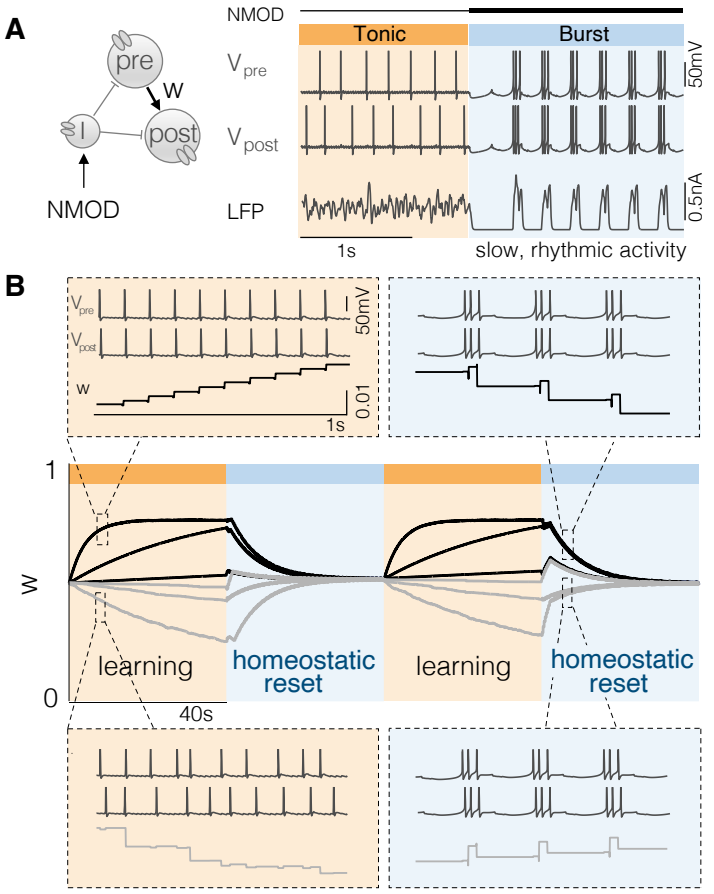

Figure 6.1: A homeostatic reset of synaptic weights is observed during rhythmic bursting mode whatever the neuronal activity correlation in tonic spiking

A. (Left) scheme of the three-cell circuit. The circuit is composed of an inhibitory cell (I) that projects GABA current onto excitatory pre- and postsynaptic neurons (resp. pre and post), which are connected by AMPA currents. The synaptic strength between pre-post w is governed by a triplet rule. (Right,top) Applying neuromodulators (NMOD) onto the I-cell induces the transition from tonic to burst in the circuit. (middle) Membrane potential of the pre- and postsynaptic neurons. on tonic mode (yellow background), and rhythmic bursting mode (blue background). (bottom) Local Field Potential (LFP) recordings in a network of 6 postsynaptic neurons. Transition to neuronal bursting activity appears as high amplitude and low frequency rhythmic LFP.

B. Evolution of the synaptic weight in 6 circuits during two brain state transitions. During tonic firing (yellow background), 3 circuits have a strong, resp. weak, correlated activity between pre- and post-synaptic neurons resulting in a synaptic weight increase, resp. decrease, shown in dark, resp. gray. During burst firing (blue background), all the synaptic weights are reset to the same value — a phenomenon that we called the *homeostatic reset*. Top and bottom panels provide zooms on the voltage traces and the associated synaptic weight evolution during spiking mode (learning) and bursting mode (homeostatic reset).

6.2.2 The homeostatic reset occurs in both phenomenological and biophysical models of synaptic plasticity

So far, we have seen that a classical triplet rule leads to a homeostatic reset in synaptic weights during a switch in network state from active waking to quiet waking referring to a cellular switch from tonic to burst. We further investigated the generality of the homeostatic reset by testing 20 variations of 7 published synaptic plasticity models. These synaptic plasticity models can be split into two categories (Figure 6.2A). The first category comprises phenomenological models, which use spike timing of presynaptic and postsynaptic neurons as the main input that drives changes in synaptic weights. Prominent examples of such models are the pair-based rule using the pre- and post-spiking times (Song et al., 2000; Van Rossum et al., 2000) and the triplet rule using pre-post-pre- or post-pre-post-spiking activity to change the synaptic weight (Pfister and Gerstner, 2006; Graupner et al., 2016) (Figure 6.2A, left gray box). The second category comprises biophysical models, which use intracellular calcium concentration as the key signal that drives synaptic change (Graupner et al., 2016; Graupner and Brunel, 2012; Shouval et al., 2002; Deperrois and Graupner, 2020) (Figure 6.2A, right gray box). The two representations into the gray boxes are simplified to provide a comprehensive overview of the rules. Then, we compare two different *weight-dependency plasticity* for each category of model by implementing either hard bounds or soft bounds (van Rossum et al., 2012; Gütig et al., 2003).

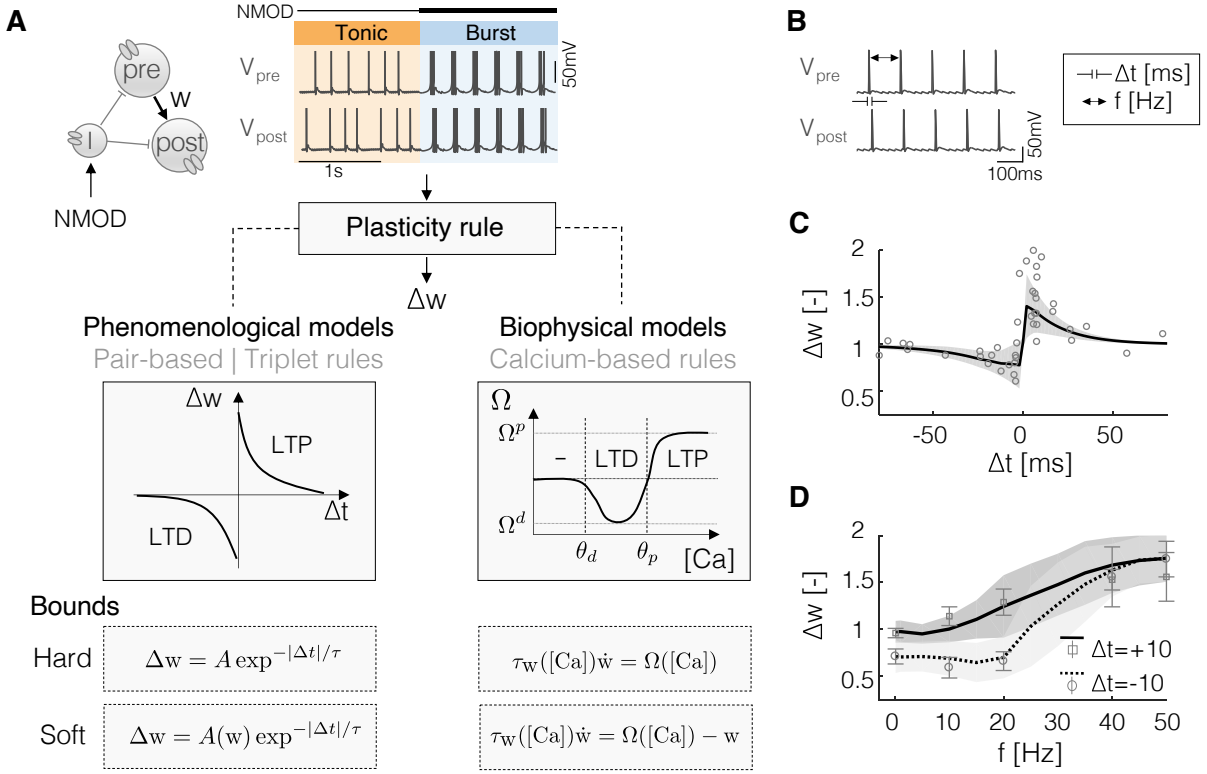

Figure 6.2: Two categories of synaptic plasticity rules reproduce experimental data from plasticity-induced protocol.
A. The three-cell circuit able to switch from tonic to burst. The synaptic weight w between pre- and postsynaptic neurons is affected by plasticity. Two categories of plasticity rules are tested. (Left) *Phenomenological models* focusing on the spike timing such as the pair-based and triplet models (Abbott and Nelson, 2000; Pfister and Gerstner, 2006; Graupner et al., 2016) such as $w \rightarrow w + \Delta w$ and $\Delta t = t_{\text{post}} - t_{\text{pre}}$ provoking Long-Term Depression (LTD) or Long-Term Potentiation (TOP). The weight-dependency is affecting the potentiation/depression parameter A. (Right) *Biophysical models* use the intracellular calcium to drive synaptic change such as $\tau_w([\text{Ca}])\dot{w} = F(w, [\text{Ca}])$. Intermediate (resp. high) calcium level leads to slow (resp. fast) depression (resp. potentiation). Either the plasticity rule is a continuous function of calcium (as in (Shouval et al., 2002)) or use depression and potentiation levels (Ω^{d} and Ω^{p}) associated to two calcium thresholds (depression or potentiation θ_{d} or θ_{p}), as in (Graupner et al., 2016)). The weight-dependency modifies the synaptic plasticity equation.
B. Plasticity induced protocols focus on maintaining either the simulation frequency and varying the pre- and post-spike time $\Delta t = t_{\text{post}} - t_{\text{pre}}$ (Bi and Poo, 1998) or maintaining a constant time lag and varying the spike frequency f (Sjöström et al., 2001).
C. The change of synaptic strength (Δw) is shown as a function of the pre-post pairings (Δt) for a frequency of 1 Hz, reproducing (Bi and Poo, 1998) experimental data (circles). The fit obtained in all models for hippocampus data is averaged. The mean (black line) and the standard deviation (gray shadow) are shown.
D. The change of the synaptic strength is shown as a function of frequency pairings for regular pre-post pairs ($\Delta t = 10$ ms (full line) and $\Delta t = -10$ ms (dotted line) reproducing (Sjöström et al., 2001) experimental data obtained in cortex (circles, squares, mean + std). The fit obtained in all models is averaged. The mean and standard deviation are shown by the black line and the gray shadow, respectively.

Altogether, 2 classes of phenomenological rules (see Table 6.1) and 5 classes of calcium-dependent plasticity rules (see Table 6.2) are studied in this paper. For each class, the parameter set is related to a region, a pairing protocol, a type of bound listed in Tables 6.1 and 6.2. This raised the issue that fitting plasticity rule is a complex problem. The paper aiming at comparing the general behavior of plasticity rules during switches from tonic to burst firing, we first fitted all 20 model variations based on two well-established experimental plasticity induction protocols (Figure 6.2B). In the first induction protocol, the time lag between pre- and postsynaptic spikes is tested for a given frequency after several pairs. This protocol reproduces the experiment done in (Bi and Poo, 1998). Figure 6.2C shows the average (black curve) and standard deviation (gray shadow) of the behavior of the different models after parameterization, together with the experimental data of (Bi and Poo, 1998) (circles). In the second induction protocol, a fixed time lag is maintained while the impact of the stimulation frequency is varied. Similarly, Figure 6.2D shows the average (black curve) and standard deviation (gray shadow) of the behavior of the different models after parameterization for the second protocol, together with the experimental data (Sjöström et al., 2001) (circles). For each model, a specific datasheet provides the parameter values as well as the validation on experimental data and the evolution of the synaptic weight during burst mode (see *SI Appendix* in (Jacquerie et al., 2022)).

Name	**Region**	**Bounds**	**Reference**	ID
Pair-based	H	Soft	(Van Rossum et al., 2000)	1
	H	Hard	(Song et al., 2000)	2
Triplet	H	Soft	adapted from (Pfister and Gerstner, 2006)	3
	H	Hard	(Pfister and Gerstner, 2006)	4
	C	Soft	(Graupner et al., 2016)	5
	C	Hard	(Pfister and Gerstner, 2006)	6

Table 6.1: Phenomenological models covered in this paper. Region is linked to the parameter choice depending on the brain area where the rule is fitted: (C) cortex, (H) hippocampus. The weight-dependency is either modeled by (Soft) soft bounds or (Hard) hard bounds.

Model	**Formalism**	**Region**	**Bounds**	**Ca^{2+}-coupling**	**STD**	**Reference**	**ID**
Graupner 2016	Th*	C	Soft	No	No	(Graupner et al., 2016)	1
	Th	C	Soft	No	No	adapted from (Graupner et al., 2016)	2
	Th	H	Soft	No	No	adapted from (Graupner et al., 2016)	3
	Th	C	Hard	No	No	adapted from (Graupner et al., 2016)	9
Graupner 2012	Th	C	Soft	No	No	(Graupner and Brunel, 2012)	4
	Th	H	Soft	No	No	(Graupner and Brunel, 2012)	5
Shouval 2002	Cont	C	Soft	No	No	adapted from (Shouval et al., 2002)	6
	Cont	C	Hard	No	No	adapted from (Shouval et al., 2002)	10
Deperrois 2020	Th	C	Soft	Yes	No	(Deperrois and Graupner, 2020)	7
	Th	C	Hard	Yes	No	adapted from (Deperrois and Graupner, 2020)	11
	Cont	C	Hard	Yes	No	adapted from (Deperrois and Graupner, 2020)	12
Deperrois 2020	Th	C	Soft	Yes	Yes	(Deperrois and Graupner, 2020)	8
	Th	C	Hard	Yes	Yes	adapted from (Deperrois and Graupner, 2020)	13
	Cont	C	Hard	Yes	Yes	adapted from (Deperrois and Graupner, 2020)	14

Table 6.2: Biophysical models investigated in this paper. (Th*) stands for calcium thresholds such as two opposing calcium-triggered pathways leading increases or decreases of synaptic strength (Graupner et al., 2016; Graupner and Brunel, 2012; Deperrois and Graupner, 2020). (Th) uses calcium-dependent steady state value and time-constant. (Cont) stands for the continuous function of the calcium dependency (Shouval et al., 2002). Region is linked to the parameter choice depending on the brain area where the rule is fitted: (C) cortex, (H) hippocampus. The weight-dependency is either modeled by soft bounds (Soft) or hard bounds (Hard). (Ca^{2+}-coupling) The presynaptic calcium influx is coupled with the synaptic weight (Yes/No). The models include an equation considering the depression of presynaptic vesicles labeled short-term depression (STD) (Yes/No). The parameters come from an original paper or are adapted to reproduce the frequency dependency in a pairing protocol (for cortex as in (Sjöström et al., 2001)) or a STDP protocol (for hippocampus as in (Bi and Poo, 1998)).

We generalized the computational experiment performed in Figure 6.1B to all 20 synaptic model variations (see *SI Appendix* for a simulation trace of each individual simulation). In all model configurations, implementing a soft bound, a network switch from tonic spiking to bursting generated a homeostatic reset of synaptic weights, very reminiscent of what is shown in 6.1B. In all model configurations implementing a hard bound, a network switch from tonic spiking to bursting generated a convergence of the synaptic weights towards the extreme value with a constant velocity whatever its initial weight. Such saturation phenomenon of all synaptic weights was previously shown in other applications (Chen et al., 2013). Although the convergence dynamics are different between the two cases, the outcome is the same: a switch to bursting restores synaptic weights, potentially disrupting any learning that might have occurred during the active waking period (characterized by tonic spiking). This shows that such homeostatic reset of synaptic weights observed during switches in brain states is a robust phenomenon that does not depend on the specifics of any synaptic plasticity model.

6.2.3 The homeostatic reset is robust to variability and heterogeneity in circuit parameters

We next tested the robustness of the homeostatic reset to changes in the parameters of the neuronal circuits. We introduced variability in three parameters: (i) the level of neuromodulator concentration, which is modeled by a variable inhibitory drive onto the circuit inhibitory neuron (Figure 6.3A), (ii) variability in neuron intrinsic parameters such as maximal conductance values (Figure 6.3B), and (iii) network size, with the introduction of heterogeneity in neuron parameters within the network (Figure 6.3C).

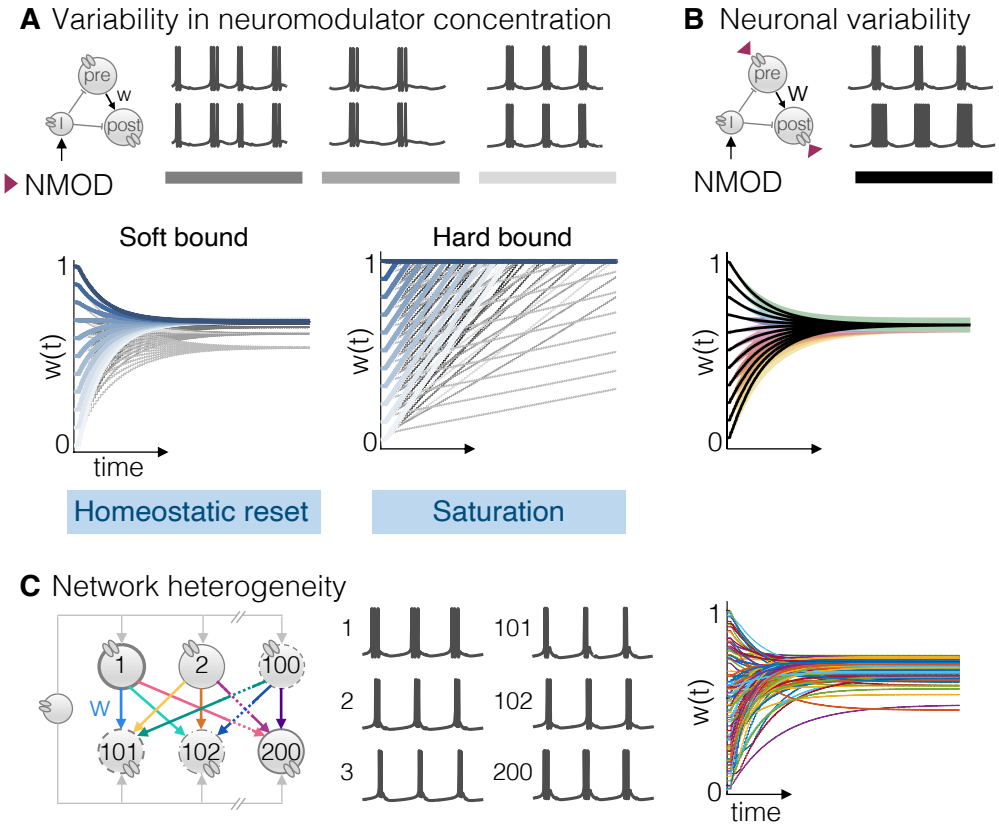

Figure 6.3: The homeostatic reset occurs for the different category of synaptic plasticity rules and is robust to intrinsic variability and network heterogeneity.
A. Pre- and postsynaptic neurons burst under neuromodulatory input. Different neuromodulator concentrations lead to different bursting patterns (gray line - top traces). The time evolution of the synaptic weight is computed in all synaptic plasticity models considering two weight-dependencies. (Left) Soft bounds lead to a *homeostatic reset* (each blue line is associated to one initial value). The value of the reset is altered by bursting patterns (see gray lines). (Right) For hard bounds, all synaptic weights saturate to the extreme values at different rates depending on the burst profile. (Time window: 40 s.)
B. 10 circuits are generated with variability in their intrinsic parameters affecting the bursting rhythm. Each circuit shows the homeostatic reset. (Averaged weight in black line and its standard deviation in color shadow, time duration: 40 s.).
C. A fully connected feedforward network of 100 pre to 100 postsynaptic neurons is built with heterogeneous intrinsic variability. All initial weights are initialized at random values between 0 and 1. Despite heterogeneity in the network, all synaptic weights present the homeostatic reset and converge towards the same range of values. Each voltage trace lasts 0.9 s - *y*-scale: 140 mV, 100 weight traces among the 10 000 are shown for model Ca 1, during 50 s.

The results of variability in neuromodulator concentration are shown in Figure 6.3A. At the circuit level, different concentrations of neuromodulator leads to diverse bursting patterns. These bursting patterns vary in terms of the number of spikes per burst, the intraburst frequency, the interburst frequency and the duty cycle (Jacquerie and Drion, 2021; Drion et al., 2018), which can potentially affect the behavior of the plasticity rules. However, a homeostatic reset of synaptic weights is observed each time the circuit enters a rhythmic mode, and this reset is robust to the specific properties of the pattern itself. A change in the rhythmic pattern solely affects the convergence rate and reset value in the case of soft bounds, and the slope of the linear convergence rate in the case of hard bounds (see Figure 6.3A, bottom panels, where the different shades of gray represent one circuit simulated with one neuromodulator level). The results show that the homeostatic reset is a robust phenomenon relying on network rhythmic state, but whose reset value is tunable through neuromodulation level.

We then added some variability in order to grow closer to what is observed in biological systems (Jacquerie and Drion, 2021; Marder and Taylor, 2011; Gjorgjieva et al., 2016a; Schulz et al., 2006; Marder et al., 1996). To this end,

ten circuits varying in their parameter sets of maximal intrinsic conductances and applied currents were simulated. The maximal conductances varied within an interval of 10 %. Each circuit is first verified to switch from tonic to bursting mode. Similarly to neuromodulation level, introducing variability affects the bursting pattern, but also breaks the pattern symmetry between the presynaptic and postsynaptic neurons: each neuron exhibits differences in its neuronal rhythm (Figure 6.3B, top). This breaking of symmetry does not affect the outcome. In all 10 circuits, whatever the initial weight acquired in tonic mode, the synaptic weights reset in bursting mode. The exact value of the reset is slightly different in different circuits, as shown in Figure 6.3B, bottom (the mean evolution of the weights in the 10 circuits is shown in black, whereas the colored shadows depict the standard deviation for each initial condition). The mean reset value is equal to 0.6347 and the standard deviation is equal to 0.0108 for the biophysical model 2. For phenomenological models, the standard deviation is higher due to the sensitivity of the exact spike time inside the intraburst (for the pair-based model: mean = 0.6002, std = 0.0714).

Finally, we increased the network size to account for the impact of heterogeneity between neurons of the same network. We built a heterogeneous network composed of 2 layers of 100 excitatory neurons each fully connected in a feedforward configuration. Each neuron has different intrinsic properties. The inhibitory neuron drives the transition from tonic to burst thanks to the neuromodulatory input (see Figure 6.3C, left).The network is initialized with random connectivity, mimicking a situation after a learning period (a similar procedure is done in (González-Rueda et al., 2018; Fauth and Van Rossum, 2019). The neurons show different burst rhythms with various intraburst frequencies and different number of spikes per burst (see Figure 6.3, center). The evolution of the synaptic weights are displayed in Figure 6.3C, right. Network heterogeneity induces heterogeneity in reset values within the network. This heterogeneity is related to the variability in pre- and postsynaptic burst properties, it is not dependent on the initial synaptic weight.

Altogether, these different computational experiments convincingly show that the mechanisms underlying the homeostatic reset of synaptic weights are robust to synaptic model type, the fitted region, the presence of short-term depression, the neuromodulation level, the neuronal circuit variability and the network heterogeneity. In all cases, strong weights decrease and weak weights grow toward a reset value. This exact value is moderately influenced by rhythm properties, hence tunable by neuromodulator level. Turning soft-bound into hard bound simply drives all the weights toward saturation.

6.2.4 The endogenous nature of rhythmic bursting leads to homeostatic reset

In order to gain more insights into the mechanisms underlying the homeostatic reset, and particularly understand why this phenomenon specifically occurs during bursting activity observed in quiet waking state, we analyzed how phenomenological and biophysical plasticity models interact with circuit activity. In particular, we took advantage of previous analytical work linking the time evolution and convergence of synaptic weights to either spike time statistics (for phenomenological models) or calcium dynamics (for biophysical models) (Billings and van Rossum, 2009; Jedrzejewska-Szmek et al., 2017; Babadi and Abbott, 2016; Rubin et al., 2001; Park et al., 2017).

In phenomenological models, the time evolution of a synaptic weight and its convergence occurs on a time interval much larger than typical interspike intervals. Therefore, following the work of (Gütig et al., 2003; Legenstein and Maass, 2005), we can average the dynamics of the synaptic weight (see (6.3) in Section 5.6) over a time interval T and get

$$\dot{w} = -A^- w^\mu \int_{-\infty}^{0} e^{s/\tau^-} C(s;t) ds + A^+ (1-w)^\mu \int_{0}^{\infty} e^{-s/\tau^+} C(s;t) ds,$$

where A^+ and A^- are the potentiation and depression parameters, μ stands for the weight-dependency, $e^{-|s|/\tau^\pm}$ stands for the STDP kernel in potentiation or depression with τ^+ and τ^- being the time-constants given in the pair-based model, and $C(s;t)$ is the (temporally averaged) correlation function between the pre and post spike trains, respectively noted $S_{\text{pre}}(t) = \sum_k \delta(t - t_{\text{pre},k})$ and $S_{\text{post}}(t) = \sum_k \delta(t - t_{\text{post},k})$, that is,

$$C(s;t) = \frac{1}{T} \int_{t}^{t+T} S_{\text{pre}}(\tau) S_{\text{post}}(\tau + s) d\tau.$$

Assuming the stationarity of both spike trains, the correlation function is time-invariant, *i.e.*, $C(s;t) = C(s)$, and the time evolution of the synaptic weight can be computed as (Legenstein and Maass, 2005):

$$\dot{w} = A^+ (1-w)^\mu C^+ - A^- w^\mu C^-,$$

where $C^+ = \int_0^\infty e^{-s/\tau^+} C(s) ds$ and $C^- = \int_{-\infty}^0 e^{s/\tau^-} C(s) ds$.

A qualitative analysis of this equation helps to understand why synaptic weights converge towards a single steady-state for any stationary value of $C(s)$, considering soft-bound dependency *i.e.* $\mu = 1$. The term $A^+(1-w)C^+$ computes the weight increase due to all postsynaptic spikes following presynaptic spikes considering the associated time lag. The term $A^- w C^-$ computes the weight decrease due to all postsynaptic spikes preceding presynaptic spikes. When modeling soft bounds, both terms are weight-dependent, which deforms the plasticity kernel (Figure 6.4A). When the synaptic weight is weak, the term $A^+(1-w)C^+$ dominates, and potentiation overcomes depression (Figure 6.4A, left). When the synaptic

weight is strong, the term $A^- w C^-$ dominates, and depression overcomes potentiation (Figure 6.4A, center). The drift eventually stabilizes at the synaptic weight value for which depression balances potentiation, *i.e.*, $A^+(1-w)C^+ = A^- w C^-$ (Figure 6.4A, right). This convergence value can be computed analytically by solving this balance equation.The reset value w_{HR} is obtained analytically by

$$w_{\mathrm{HR}} = \frac{\frac{A^+C^+}{A^-C^-}}{1+\frac{A^+C^+}{A^-C^-}}. \tag{6.1}$$

This equation states that the reset value depends on a ratio between the potentiation parameter weighted by the correlation between pre-post spikes and the depression parameter weighted by the correlation between post-pre spikes.

We applied this methodology to compare the convergence of the synaptic weights in tonic spiking and bursting. To this end, we used the previously built heterogeneous network composed of 2 layers of 100 excitatory neurons fully connected in a feedforward configuration (Figure 6.4B). The network is initialized with random connectivities. In tonic mode, excitatory neurons receive external stimulation at random frequencies, ranging from 0.01 Hz up to 50 Hz, which mimics the effect of sensory drive, among others (Figure 6.4B, top). In bursting mode, a neuromodulatory drive to the inhibitory cell switches the network to rhythmic mode (Figure 6.4B, bottom).

First, we computed the correlation ratio C^+/C^- between the pre and post (binary) spike trains for all 10 000 synaptically coupled pairs, both in tonic and burst modes. The results are reported in a correlation matrix for each mode (Figure 6.4C, left). These correlation matrices show that correlation values are highly heterogeneous in tonic mode, whereas they are highly homogeneous in burst mode. This is due to the fact that spike trains are variable during active waking, whereas the network switches to a global, rhythmic activity during quiet waking mode (Figure 6.4C, center). As a consequence, synaptic weights are predicted to converge towards many different values during tonic mode, but towards very similar values in bursting mode, which partially explains why the homeostatic reset is only observed during the latter.

Secondly, we compared the synaptic weight values obtained from model simulations with the prediction values w_{HR}. Prediction values were computed on the complete time period T, as well as on two transient time periods T_1 and T_2, and results are provided on a raster plot for each time period in both modes (Figure 6.4C, right, mean prediction error ± standard deviation over 8 different neuromodulator drives: mean = 0.0031, std = 0.0027, see *SI Appendix* for details). The figures show that, although there is an almost perfect match between simulated and predicted reset values in bursting mode, simulated synaptic weights do not converge towards their predicted values during tonic mode for any time window. This is explained by the assumption that the correlation function between the spike trains is stationary over the time windows, *i.e.*, $C(s;t) \approx C(s)$, is only true in bursting mode, due to the endogenous nature of the rhythmic bursting activity. As a result, a reset of synaptic weights is only really observed during quiet waking.

In biophysical models, a similar analytical approach can be derived based on calcium dynamics by comparing the time spent in depression and potentiation (Graupner and Brunel, 2012). Again the time evolution of a synaptic weight and its convergence occur on a time interval much larger than typical calcium oscillations. Therefore, we can average the dynamics of the synaptic weight (see (6.4) in Methods) over a time interval T and get

$$\dot{w} = \frac{1}{T}\int_t^{t+T} \frac{1}{\tau_w([\mathrm{Ca}](s))}\left[\Omega([\mathrm{Ca}](s)) - \mu\, w\right] ds,$$

where $\Omega([\mathrm{Ca}])$ and $\tau_w([\mathrm{Ca}])$ are functions that map intracellular calcium concentration to potentiation (Ω^{p}) and depression (Ω^{d}) levels and potentiation (τ_{p}) and depression (τ_{d}) time-constants, as in (Graupner et al., 2016) (see *SI Appendix*). We note the effective time spent in each region α^{d} and α^{p} as the time spent balanced by the time-constant of potentiation/depression in the corresponding region, that is,

$$\alpha^{\mathrm{d}} = \frac{1}{\tau_{\mathrm{d}}}\frac{1}{T}\int_t^{t+T} I(\theta_{\mathrm{d}} < [\mathrm{Ca}](s) < \theta_{\mathrm{p}}) ds,$$
$$\alpha^{\mathrm{p}} = \frac{1}{\tau_{\mathrm{p}}}\frac{1}{T}\int_t^{t+T} I([\mathrm{Ca}](s) > \theta_{\mathrm{p}}) ds,$$

where $I(x)$ is the indicator function equals 1 when x is true and 0 when x is false. The synaptic weights reach a stable state once the potentiation level Ω^{p} and the depression level Ω^{d} weighted by their effective time spent in the corresponding regions are balanced. It gives

$$w_{\mathrm{HR}} = \frac{\Omega^{\mathrm{d}}\alpha^{\mathrm{d}} + \Omega^{\mathrm{p}}\alpha^{\mathrm{p}}}{\alpha^{\mathrm{d}} + \alpha^{\mathrm{p}}}. \tag{6.2}$$

The comparison between the value of the homeostatic reset obtained via computational simulations and the analytic approach is provided in *SI Appendix, Tab.S7*. Again, w_{HR} is only predictive if the effective time spent in each region α^{d} and α^{p} can be considered stable over time, which is only true in bursting mode, as attested by the good match between predicted and simulated reset values (mean prediction error ± standard deviation over 8 different neuromodulatory drives: mean error = 0.0016, std = 0.0019)).

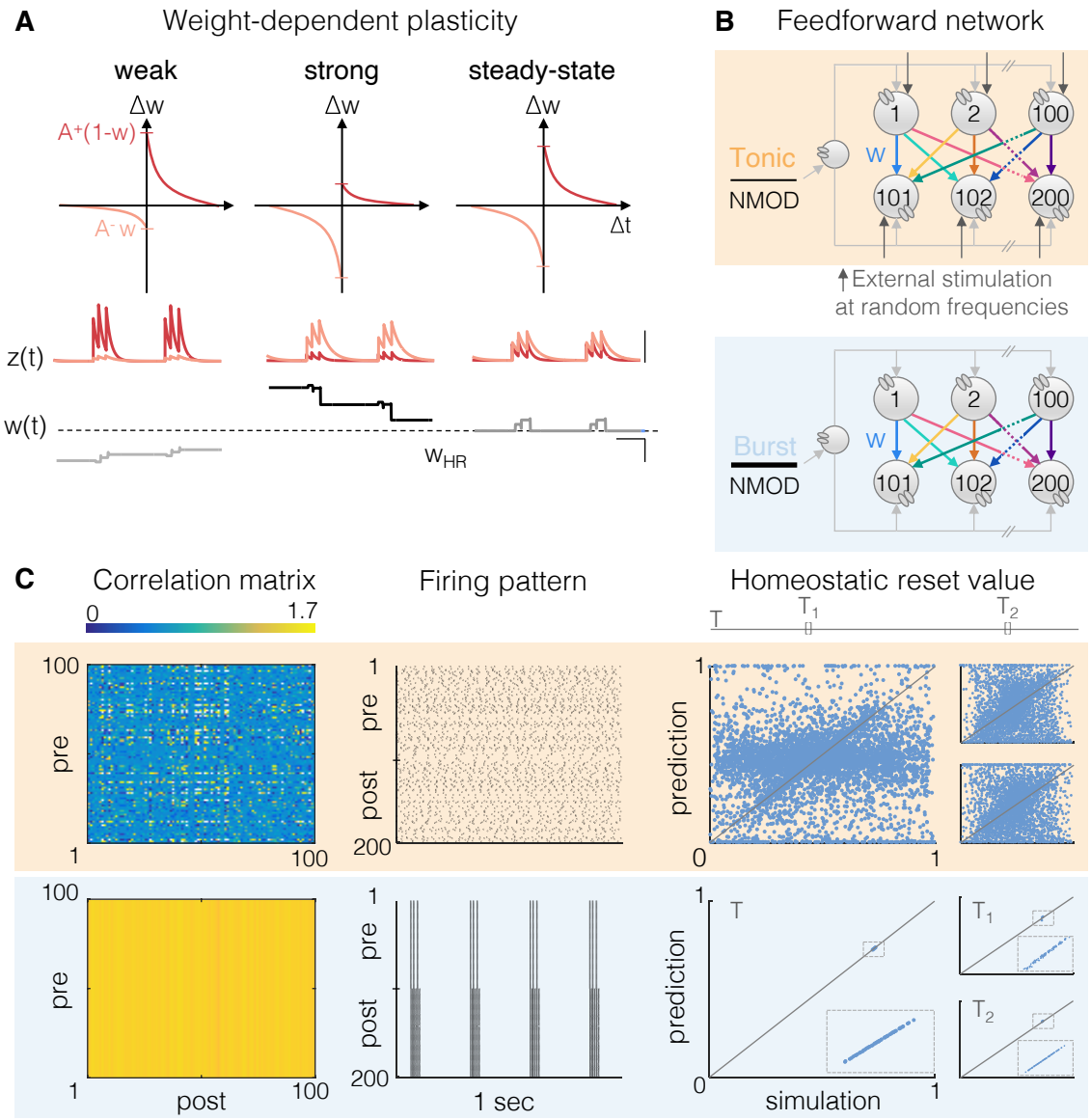

Figure 6.4: The homeostatic reset relies on the endogenous nature of rhythmic bursting.
A. Weight-dependent plasticity modulates the potentiation and depression parameters with respect to the synaptic weights. The spike-time dependent plasticity kernel is weight-dependent. The potentiation and depression traces (z(t)) are shown respectively in red and orange with the associated synaptic weight evolution (w(t)) considering two successions of endogenous burst (x-scale: 0.6 s, y-scale for z: 0.06 %, y-scale for w: 2.5 %.)
B. A 2-layer feedforward network with the same 100 neurons fully connected to the same 100 postsynaptic neurons. All the synaptic weights (resp. AMPA connections) are randomly initialized between 0 to 1 (resp. 0.01 to 4). In tonic spiking (top, yellow background), neurons are excited by external stimulation at random frequencies between 0.01 to 50 Hz. In bursting mode (bottom, blue background), the neuromodulation (NMOD) level drives the neurons in burst mode.
C. (Left) The correlation between presynaptic spike trains and postsynaptic spike trains are computed. We show the ratio between the positive correlation (C^+ associates to the potentiation correlation when a postsynaptic neuron spikes after a presynaptic neuron) and the negative correlation (C^- for a pre spikes after a post spikes) in tonic spiking and bursting (resp. yellow background and bottom blue background). (Center, top) In tonic mode, neurons are in exogenous spiking mode. (Center, bottom) In bursting mode, neurons are in endogenous burst mode. (Right) The spike trains correlation is computed for the entire simulation T and compared with the correlation at two given times T_1 and T_2 (equal to 10 s and 40 s). Scatter plots between the reset value obtained via simulation (converging point) and the predicted value obtained analytically.

Finally, both analytical analyses can be extended to the case of hard bounds. In this case, all synaptic weights converge towards saturation in quiet waking mode due to burst mode, and the saturation speed λ, or slope, depends on the neuromodulatory drive. In phenomenological models, this saturation slope can be predicted by the equation

$$\lambda = A^+C^+ - A^-C^-,$$

where T is the time-window considered to compute the correlation. In biophysical models, the saturation slope cor-

responds to the sum of the depression rate and potentiation rate, each weighted by the fraction of time spent in their corresponding regions α^{d} and α^{p}, which writes

$$\lambda = \alpha^{\mathrm{p}}\Omega^{\mathrm{p}} + \alpha^{\mathrm{d}}\Omega^{\mathrm{d}}.$$

The values of the saturation slope obtained via computational simulations match the analytic predictions for both model types (*SI Appendix, Tab. S7* - calcium model: mean error = 0.049, std = 0.039, pair-based model: mean error = 0.027, std = 0.033 over 8 neuromodulatory drives). Complementary explanations about the origin of the homeostatic reset are available in *SI Appendix.*

In summary, analytical analyses of the mechanisms underlying time evolution of synaptic weights showed that a homeostatic reset solely occurs during quiet waking mode due to the endogenous, global nature of the network rhythmic bursting activity in this mode, both in phenomenological models and biophysical models of synaptic plasticity.

6.2.5 The homeostatic reset is robust to neuromodulation of synaptic plasticity rules

Recent evidence shows that synaptic plasticity rules are also under the control of neuromodulators for example, acetylcholine, dopamine, noradrenaline, serotonin, and histamine (Brzosko et al., 2019; Zannone et al., 2018; Foncelle et al., 2018; Salgado et al., 2012; Nadim and Bucher, 2014; Lisman et al., 2011; Pawlak, 2010; Kirkwood, 2007; Shine et al., 2021; Gerstner et al., 2018; Izhikevich, 2007). Neuromodulators are affecting synaptic plasticity at different stages as explained in (Seol et al., 2007; Bazzari and Parri, 2019; Nadim and Bucher, 2014; Pawlak, 2010). Several computational models were developed in the last years in different fields of neuroscience implementing this notion of neuromodulated synaptic plasticity rules (Butson, 2012; Frémaux and Gerstner, 2015). For example, in the context of sleep-dependent memory consolidation (González-Rueda et al., 2018), the classical depression-potentiation kernel in wakefulness is deformed into a depression kernel in sleep to show weight downselection. A similar modeling approach is done in (Brzosko et al., 2017; Pedrosa and Clopath, 2017). The STDP kernel is sequentially shifted due to dopamine and acetylcholine for reward-based navigation or to explore receptive field plasticity. There exist other computational techniques to incorporate neuromodulation in synaptic plasticity rules such as the introduction of an eligibility trace or a third factor (Gerstner et al., 2018; Izhikevich, 2007; Foncelle et al., 2018).

Inspired by this line of work, we introduced neuromodulation of synaptic plasticity rules to test its effect during rhythmic bursting activity and on the homeostatic reset. In phenomenological plasticity rules, it is simply translated by modifications of the rule parameters (Figure 6.5A, top-left). Based on (6.1), modifying the potentiation or depression parameters (A^+ and A^-) has a direct effect on the homeostatic reset value. To confirm our analytical predictions, we simulated the circuit during bursting activity with different initial synaptic weights (as done in Figure 6.3A) and compared the reset value with and without neuromodulation on the synaptic plasticity rule (as shown respectively by pink and blue curves, Figure 6.5B, top-right). The homeostatic reset is robust and neuromodulation only affects its set point. For calcium-based plasticity rules, neuromodulators can similarly target several parameters such the potential and depression levels (Ω^{p} and Ω^{d}) (see in Figure 6.5A, bottom-left). As given in the analytical expression of the homeostatic reset value in (6.2), modifying those parameters changes the value whatever the initial weight. Figure 6.5A (bottom-right) confirms the prediction through the computational experiment. For both rule categories, other parameters can be modulated and the results are provided in *SI appendix*. Overall, neuromodulating the synaptic plasticity rule does not disrupt the homeostatic reset.

However, now that we have presented a mechanism to tune the value of the reset, it can be leveraged to obtain a bimodal behavior in the evolution of the synaptic weights during the rhythmic bursting regime, hence permitting memory consolidation. In such bimodal behavior, strong weights would converge to a high reset value while weak values are downscaled to a low reset value. This idea is perfectly in line with the synaptic-and-capture hypothesis (STC) (Seibt and Frank, 2019; Okuda et al., 2021). To implement this hypothesis in the different synaptic rules, the parameters are required to be dependent on the weight acquired during the learning phase. The strong weights formed during the correlated learning activity create the potential for consolidation by setting a *TAG*. A connection is tagged when the weight acquired during learning is higher than a threshold value (Frey and Morris, 1997; Redondo and Morris, 2011; Seibt and Frank, 2019). For tagged connections, the potentiation parameter has a higher value compared to weak weights leading to a higher reset point. It was shown in phenomenological and calcium-based rules in Figure 6.5B (respectively top and bottom). As soon as the neurons switch in rhythmic bursting mode, synaptic weights are converging towards their reset values but this time dictated by the presence of the TAG (see Figure 6.5B, right).

Figures 6.5C and D repeat the experiment done in Figure 6.1B expect that during the last bursting state, the synaptic plasticity rule is neuromodulated (Figure 6.5C) or neuromodulated and tag-dependent (Figure 6.5D). It confirms that the burst-induced homeostatic reset is robust to alteration in the synaptic plasticity rules. At the last bursting stage, the weights converge to a low reset point altogether in Figure 6.5C. The only way to exploit it is to build a TAG-dependent rule as done in Figure 6.5D where weights that are strong enough are maintained. It suggests a potential function for the role of burst and its associated homeostatic reset for consolidation of strong weights acquired during learning.

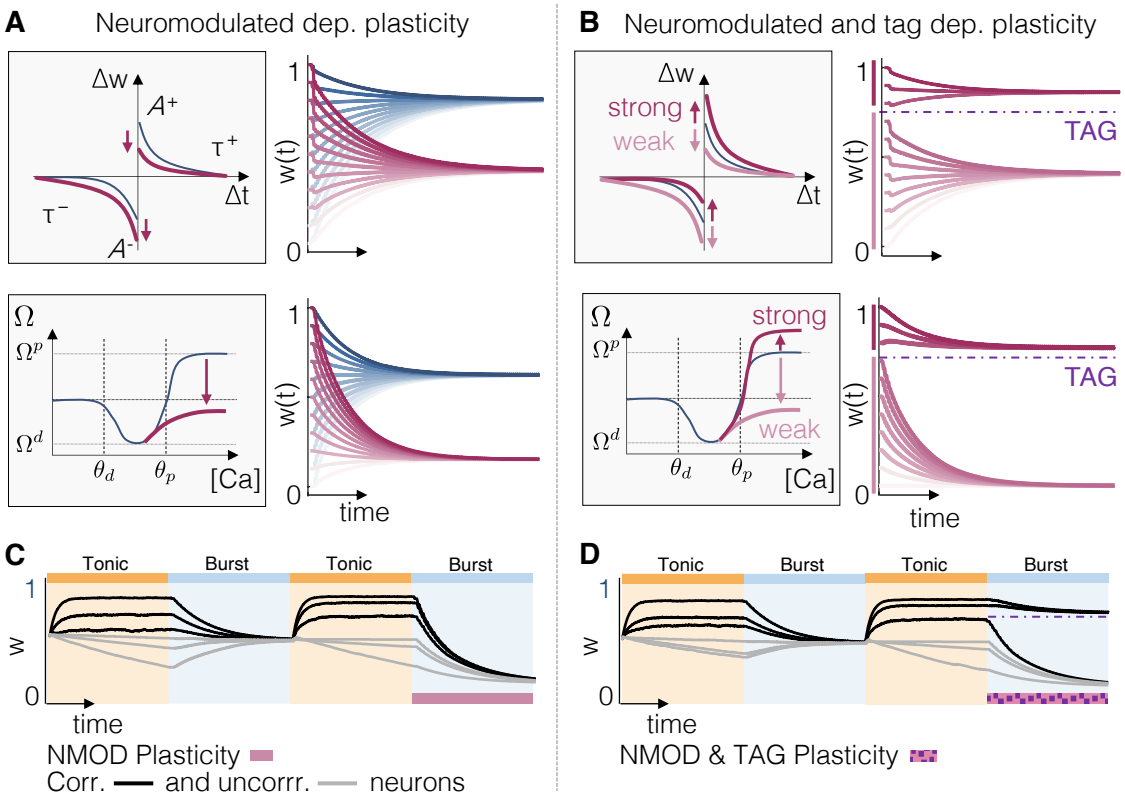

Figure 6.5: Neuromodulated and tag-dependent synaptic plasticity rules exploit the burst-induced homeostatic reset for memory consolidation.
A. Phenomenological (top, right) and calcium-based (bottom, right) plasticity rules are neuromodulated by changing the potentiation and depression paramters (respectively A^+, A^- and Ω^p). Time-evolution of the synaptic weights when the synaptic rule is neuromodulated (pink curves) or not (blue curves - similar as shown in Figure 6.3). The homeostatic reset is moved. **B.** (left) Parameters are neuromodulated according to the weight acquired during learning (here the initial weights). Strong weights ($w >$ TAG, indicated by the purple line) follow the plasticity rule drawn in dark pink while weak weights follow the rule drawn in light pink. (right) Time-evolution of the synaptic weights when the synaptic rule is neuromodulated and tag-dependent. Strong weights are preserved while weak weights are depressed as shown by two resets at high and low values in a phenomenological (top) and calcium-based (bottom) rule. (x-scale: 10 s, simulation duration: 40 s). **C and D.** Evolution of the synaptic weights in 6 circuits during two tonic-burst transitions (as done in Figure 6.1B, yellow background for tonic firing and blue background for bursting) except that the last stage is either under a neuromodulated plasticity rule (C, indicated by the yellow bar) or neuromodulated and tag-dependent plasticity rule (D, indicated by the pink and purple bars). Half of the circuits have correlated activity (dark lines) and the rest have uncorrelated activity (gray lines). The homeostatic reset is robust to neuromodulation but can be exploited to provide a bimodal convergence thanks to a tagging mechanism (30 s by state, total simulation 120 s).

6.3 Discussion

A key step in understanding how switches in brain states affect memory encoding is finding ways to study the interactions between synaptic plasticity rules and neuromodulation of brain activity. It represents a challenge, as plasticity rules and neuromodulation target neurons at the molecular and cellular levels, whereas brain states and memory emerge at the population level. In this work, we leverage the power of computational modeling to study how network connections formed via any of 20 variations of 7 well-established plasticity rules are affected by a switch from asynchronous tonic spiking to rhythmic bursting, mimicking transitions between active and quiet waking states. We showed that transitions to quiet waking induce a homeostatic reset of all synaptic weights towards a specific value for all tested synaptic plasticity rules.

For a newly described phenomenon in a computational modeling work to be of physiological relevance, it has to be shown that it does not arise from an artifact of the choice of models and parameters used in the study. We therefore thoroughly tested the robustness of the homeostatic reset to variability in models and parameters. First, we showed that the homeostatic reset arises from both phenomenological models and biophysical models of synaptic plasticity, which ruled out the possibility of an artifact of the chosen model type. Second, the homeostatic reset was shown to be robust to changes in neuromodulator drive, variability in neuron and circuit parameters, and heterogeneity in larger neuronal populations. Changes in neuromodulator drive however affected the reset value, which suggests that the homeostatic reset is both a robust and tunable phenomenon. Finally, using mathematical analyses that directly link firing activity or calcium

dynamics to changes in synaptic weights, we showed that the homeostatic reset is limited to the quiet waking period due to the highly endogenous, rhythmic activity globally shared by the network during that period.

The main effect of the homeostatic reset is that it restores synaptic weights during quiet waking regardless of their evolution during learning. The consequences of this restoration are twofold. On the one hand, it provides a mechanism by which synaptic weight returns to a homeostatic set point between two learning periods, restoring the ability of the network to learn new information. Such a mechanism could play a central role in memory homeostasis. On the other hand, the homeostatic reset disrupts any learning that occurred during the previous period, which could lead to catastrophic forgetting (González et al., 2020). This forgetting may be overcome via mechanisms that transfer learning encoded in synaptic weight into long-lasting, structural changes in synaptic connections, such as the number of receptors at each synapse, the number and size of synapses, etc (Zenke and Gerstner, 2017; Luboeinski and Tetzlaff, 2021). Another possibility would be to exploit the homeostatic reset itself through neuromodulator-induced changes in synaptic rules (Pedrosa and Clopath, 2017; González-Rueda et al., 2018; Foncelle et al., 2018; Brzosko et al., 2017). We have however shown that such a mechanism would need to take into account the history of weight evolution to permit a bimodal behavior of synaptic weights, which is a quite strong requirement. This could however be potentially achieved following the synaptic tagging hypothesis.

6.4 Methods

6.4.1 Conductance-based modeling

All neurons are modeled using a single-compartment Hodgkin and Huxley formalism. This computational technique is described in Section 3.4.1. The membrane voltage V_m evolves as follows (Drion et al., 2018; Jacquerie and Drion, 2021):

$$C_\mathrm{m}\dot{V}_\mathrm{m} = -\sum_i I_{\mathrm{ion},i} + I_\mathrm{app}$$

where C_m is the membrane capacitance, $I_{\mathrm{ion},i}$ is the ith current carried by ionic channels ion, and I_app is an external applied current.

The neuron circuit is composed of three neurons (see Figure 6.1). The two excitatory neurons are connected through a feedforward AMPA synapse where the afferent neuron is referred to as the presynaptic (pre) neuron, and the efferent neuron as the postsynaptic (post) neuron. An inhibitory neuron (I) is connected to two excitatory neurons through $\mathrm{GABA_A}$ and $\mathrm{GABA_B}$ connections. The synaptic currents are described in Section 3.2.

The inhibitory cell controls the state of the circuit. A tonic firing in the inhibitory neuron puts the two excitatory cells in a resting state. If the pre- or postsynaptic cell receives a external depolarizing pulse, it generates an action potential. A hyperpolarizing current applied to the inhibitory neuron switches the whole circuit into rhythmic bursting mode. This hyperpolarizing current models the effect of a neuromodulator signal (NMOD) (Zagha and McCormick, 2014).

6.4.2 Synaptic plasticity

The synaptic AMPA connection between the presynaptic neuron and the postsynaptic neuron is subjected to plasticity. The time evolution of this connection is studied during both tonic and bursting modes. This AMPA synapse is modeled by $g_\mathrm{AMPA}(t) = w(t)\ \bar{g}_\mathrm{AMPA}$ where $w(t)$ the synaptic weight, and $\bar{g}_\mathrm{AMPA}$ is the constant maximal conductance. A very small initial connectivity $\bar{g}_\mathrm{AMPA}$ equal to $0.01\ \mathrm{mS/cm^2}$ is taken such as the induced Excitatory Post-Synaptic Potential (EPSP) at the postsynaptic site does not initiate a spike. The variable $w(t)$ is weighing the synaptic current and is driven by a synaptic plasticity rule.

Two main categories of synaptic plasticity rules are explored in this paper: phenomenological rules and calcium-based rules (Gerstner, 2011; Gerstner and Kistler, 2002). The first category uses the pre- and postsynaptic spike times to drive the synaptic change while the second category uses the calcium signal.

Phenomenological models

The pair-based model considers the pre- and postsynaptic spike time (resp. t_pre and t_post) with a time difference $\Delta t = t_\mathrm{post} - t_\mathrm{pre}$ to induce the change in synaptic weight. To reproduce the classical STDP window, a pair-based model was implemented (Abbott and Nelson, 2000; Song et al., 2000; Morrison et al., 2008; Rubin et al., 2001; Van Rossum et al., 2000):

$$w \to \begin{cases} w + A^+(1-w)^\mu e^{-\Delta t/\tau^+}, & \text{at } t_\mathrm{post} \text{ if } t_\mathrm{pre} < t_\mathrm{post}, \\ w - A^- w^\mu e^{\Delta t/\tau^-}, & \text{at } t_\mathrm{pre} \text{ if } t_\mathrm{pre} > t_\mathrm{post}, \end{cases}$$

where $A^+ > 0$, $A^- > 0$ (Morrison et al., 2008; Song et al., 2000). The weight dynamics can be constrained in two manners; either by using *hard bounds* or *soft bounds*. Hard bounds permits to stop the weight increase or decrease by

adding upper or lower limits. Soft bounds decelerates the evolution if the weight reaches a bound. It is modeled by the weight-dependency parameter μ: μ is equal to 0 for hard-bounds and to 1 for soft-bounds) (Gerstner and Kistler, 2002).

The functions $e^{-|\Delta t|/\tau^{\pm}}$ are the temporal kernel of potentiation and depression. If we introduce $S_{\text{pre}}(t) = \sum_k \delta(t - t_{\text{pre},k})$ and $S_{\text{post}}(t) = \sum_k \delta(t - t_{\text{post},k})$ for the spike trains of pre- and postsynaptic neurons, the evolution of the synaptic weight can be written as follows:

$$\dot{w} = -A^- w^\mu \left[\int_{-\infty}^{0} e^{s/\tau^-} S_{\text{post}}(t-s) ds \right] S_{\text{pre}}(t) + A^+ (1-w)^\mu \left[\int_{0}^{\infty} e^{-s/\tau^+} S_{\text{pre}}(t-s) ds \right] S_{\text{post}}(t). \tag{6.3}$$

The triplet-based model extends the pair-based model to account for three spikes patterns, such as pre-post-pre and post-pre-post (Pfister and Gerstner, 2006). We implemented both pair and triplet using trace variables following (Pfister and Gerstner, 2006).

Biophysical models

We modeled calcium dynamics by following (Graupner and Brunel, 2012; Graupner et al., 2016). The global equation for the calcium-dependent plasticity rule is written as

$$\tau_w([\text{Ca}])\dot{w} = \Omega([\text{Ca}]) - \mu\, w, \tag{6.4}$$

where μ modulates the weight-dependency: $\mu = 0$ (resp. $\mu = 1$) refers to hard (resp. soft) bounds. In total, we have investigated five major calcium-based dependent models in this paper. Some rules were adapted to fit either *frequency-dependent protocol* (cortical experimental data (Sjöström et al., 2001)) or a *STDP* protocol (hippocampus experimental data (Bi and Poo, 1998)). Different *weight-dependencies* (soft bounds or hard bounds) are compared. The impact of the *coupling* between the presynaptic calcium influx and the synaptic weight or the presence of *short-term depression* are also tested (Deperrois and Graupner, 2020). Calcium-based rules are either implemented using two-triggered calcium thresholds for potentiation and depression, or using a continuous function for calcium dependency.

6.4.3 Computational experiments

Figure 6.1A shows the local field potential (LFP) in a circuit composed 6 excitatory neurons connected to 6 other excitatory neurons. They all receive an inhibitory current from the inhibitory cell. The local field potential measures the average behavior of interacting neurons (Jacquerie and Drion, 2021; Mazzoni et al., 2015; Telenczuk et al., 2020). It reflects the collective excitatory synaptic activity received by the postsynaptic neuron population. The postsynaptic current from neuron i to neuron j is $I_{\text{syn,j}}(t) = -\bar{g}_{\text{AMPA}} w_{ij}(t) s_{\text{AMPA}}(V_m - 0)$. The overall synaptic activity is measured by the mean of the individual synaptic current $\text{LFP}(t) = 1/6 \sum_{j=1}^{6} I_{\text{syn,j}}(t)$.

Figure 6.1B simulates two switches from tonic activity followed by bursting activity of 40 s each for 6 neuronal circuits. Among these 6 circuits, three of them have a correlated tonic firing while the three other circuits have uncorrelated tonic firing. For correlated circuits, the two excitatory neurons are tonically spiking at high frequencies with close pre-post pairs of spike. This activity correlation induces an increase in synaptic weight. For uncorrelated circuits, pre and post cells fire independently at the same nominal frequency f_0. Spike timings are generated with interspike intervals following independent Normal distributions $\mathcal{N}(\frac{1}{f_0}, (\frac{0.3}{f_0})^2)$. During burst firing, the level of neuromodulators is modeled by a hyperpolarizing current applied to the inhibitory neuron. The synaptic plasticity rule is the triplet rule (Pfister and Gerstner, 2006).

In Figure 6.3A, the variability in neuromodulator concentrations (shades of gray) is obtained by varying the hyperpolarizing current value applied to the inhibitory cell, ranging from -1 to $-1.7\,\text{nA/cm}^2$ resulting in different bursting patterns (see all traces in *SI Appendix, Fig.S5*). Figure 6.3B depicts the mean of the synaptic weight time evolution for 10 circuits in which variability in the ionic conductances is added. Each circuit is initialized with maximal conductances that are randomly picked from a Uniform distribution on an interval of 10 % around its nominal value $\bar{g}_0$, such as $[\bar{g}_0 - 0.1\bar{g}_0, \bar{g}_0 + 0.1\bar{g}_0]$. The plasticity rule used is the calcium model from (Graupner et al., 2016). Figure 6.3C considers a network of 2 layers with 100 presynaptic neurons fully connected to 100 postsynaptic neurons in a feedforward configuration. The connections (colors) are initialized randomly between 0 and 1. Intrinsic parameters of all cells are randomized by adding variability in the ionic conductances $g_{\text{K,Ca}}$ and $g_{\text{Ca,T}}$ in the same way as in the Figure 6.3B, with 20 % variability. The plasticity rule used is the calcium model from (Graupner et al., 2016).

Synaptic weight equilibrium value can be found by analytical demonstration (see in *SI Appendix* for details).

Figure 6.4A shows the kernel of pair-based plasticity rule considering the synaptic weight-dependency. It unravels the effective value of the potentiation and depression increment respectively labeled $A^+(1-w)$ and $A^- w$. Figure 6.4C (left) gives the ratio between the positive and negative correlation. The positive correlation describes the correlation for a presynaptic spike followed by a postsynaptic spike. The negative correlation describes the inverse relation for a postsynaptic spike followed by a presynaptic spike. Figure 6.4C (right), the simulated value is equal to the converging value in the time evolution of the synaptic weight. The predicted value is computed from the analytical formula provided w_{HR}.

Figure 6.5A shows the kernel of the pair-based plasticity rule (top, left) and calcium-based rule (bottom, left) with potentiation and depression parameters that are affected by neuromodulators. The evolution of the synaptic weights during bursting activity is shown in Figure 6.5A when the initial weight is tested between 0 and 1 (right). Blue curves are obtained using the traditional synaptic rule and pink curves are obtained using the neuromodulated synaptic plasticity rule. Figure 6.5B shows the same experiment but the parameters are dependent on the initial synaptic weights to mimic tag-dependency. We consider a strong weight when at the end of the learning phase the weight is greater than 0.75 setting the threshold tag value. Figure 6.5C reproduces the computational experiment presented in Figure 6.1. Six neuronal circuits are tested during 2 cycles of tonic-burst activity (each state lasts 30 s). For correlated circuits (dark), each neuron fires independently at a frequency higher than 30Hz. For uncorrelated circuits (gray), each neuron fires at a low value. During burst, the inhibitory neuron is hyperpolarized. At the second burst phase, the plasticity rule is neuromodulated (Figure 6.5C) or neuromodulated and tag-dependent (Figure 6.5D).

More details on all computational experiments can be found in *SI Appendix*. Simulations were performed using the Julia programming language (Bezanson et al., 2017). Analyses were performed either in Matlab. Code files are freely available at `https://github.com/KJacquerie/HomeostaticReset`.

CHAPTER 7

Switches from tonic firing to bursting support structural plasticity for memory consolidation

The previous chapter has revealed a serendipitous phenomenon: switching from tonic firing, associated with active learning, to collective synchronized bursting, associated with quiet waking, results in a homeostatic reset of synaptic weights when using a traditional synaptic plasticity rule with soft bounds. This finding was counterintuitive, as strong weights decrease while weak weights potentiate, ultimately leading to a steady-state configuration.

In this chapter, we continue to solve our puzzle by questioning whether this homeostatic reset during quiet waking is a beneficial or detrimental feature for memory consolidation. We explore methods to either remove this reset or, conversely, leverage the burst-induced reset to drive consolidation. To prevent the homeostatic reset, we employ two strategies: either we block bursting activity in the network or we replace the soft bounds with hard bounds. Conversely, to exploit the reset, we combine a traditional synaptic rule that models early synaptic changes (as previously done) with an additional structural synaptic plasticity that models late synaptic changes. This structural plasticity allows for the transfer of information acquired via the traditional plasticity during active waking and provides an innovative and elegant computational model for investigating the role of the reset in memory consolidation.

Switching to bursting enables neurons to consolidate synapses by creating new proteins and promoting synapse growth, while simultaneously restoring the efficacy of postsynaptic receptors for new learning. The novel plasticity rule is validated by comparing it with traditional synaptic rules in various memory tasks during the succession of brain states. The results demonstrate that switches from tonic firing to bursting combined with the novel structural plasticity enhance learning and memory consolidation.

This work has been presented at the Annual Meeting of SfN in 2022 held in San Diego (poster), ENCODS held in Faro (poster and talk), and later at the annual conference of OCNS held in Leipzig (poster). I also had the opportunity to present it during seminars at Larry Abbott's Lab at Columbia University in New York and Claudia Clopath's Lab at Imperial College in London.

7.1 Introduction

This raises the question of how switching from tonic firing to bursting affects the outcome of synaptic plasticity and whether it can support memory consolidation.

In the previous chapter, we showed for a variety of synaptic plasticity models (Pfister and Gerstner, 2006; Song et al., 2000; Graupner et al., 2016; Shouval et al., 2002; Deperrois and Graupner, 2020) that *switching* a network of neurons *collectively into burst* leads to a *homeostatic reset*, in which synaptic weights return to a fixed intermediate baseline value irrespective of the starting point (Jacquerie et al., 2022). This homeostatic reset causes the network to forget any learned information. This mechanism is independent of neuronal properties such as variability in ion channel conductances, properties of the burst (the number of spikes per burst or the intra- and interburst frequency), and the size of the network. It occurs with traditional synaptic plasticity models such as pair-based, triplet, and calcium-based models that use *soft-bounds* - where a stronger weight is more easily depressed and less easily potentiated. Intuitively, a circuit composed of collective bursting neurons displays a low-frequency oscillation that is stationary and, combined with the soft-bound property, causes a perfect balance between potentiation and depression, where strong weights depress and weak weights potentiate until they both reach a set-up. Replacing soft-bounds with hard-bounds causes a fixed increase or decrease of

the weight caused by the collective bursting activity no matter the value of the weight towards saturation at the upper or lower bounds (Jacquerie et al., 2022).

Interestingly, the homeostatic reset proposes an unexplored mechanism to restore the weights within the network by switching neurons to bursting. It allows the formation of new memory but causes the forgetting of previous learning (Jacquerie et al., 2022).

To address this issue, we propose to combine a traditional synaptic plasticity rule that models Early Long Term Potentiation (E-LTP) with an additional structural synaptic plasticity rule that models Late Long Term Potentiation (L-LTP). E-LTP refers to changes in postsynaptic receptor efficacy and the insertion of new receptors via exocytosis from available resources in a pool (Poirazi and Mel, 2001; Lamprecht and LeDoux, 2004). Traditional synaptic plasticity models are well-suited for describing these phenomena and are fitted on plasticity-induced protocols such as those described by (Bi and Poo, 1998; Sjöström et al., 2001). However, as experimental studies have shown, the maintenance and long-lasting synaptic changes are achieved by Late Long Term Potentiation (L-LTP), which relies on de novo protein synthesis and morphological changes (Lamprecht and LeDoux, 2004; Luboeinski and Tetzlaff, 2021). Refer to Section 2.4 for further explanations related to the biophysics of E-LTP and L-LTP.

We differentiate the synaptic weight as the *product of two terms*: the *early-phase synaptic weight (early-weight)* and the *late-phase synaptic weight (late-weight)*, inspired by (Luboeinski and Tetzlaff, 2021; Clopath et al., 2008). The early-weight is governed by traditional synaptic plasticity models (Song et al., 2000; Pfister and Gerstner, 2006; Graupner et al., 2016; Deperrois and Graupner, 2020), while the late-weight is driven by our novel structural plasticity rule during bursts. During bursting, the early-weights undergo homeostatic reset, while the late-weights consolidate previous learning. Specifically, a strong early-weight acquired after correlated tonic firing is decreased during bursting, but simultaneously leads to an increase in the corresponding late-weight. Conversely, a weak early-weight that increases during bursting results in a decrease in the corresponding late-weight.

We showcase the effectiveness of this mechanism in a network of neurons using a conductance-based model capable of transitioning between various neuronal activities. Additionally, we employ a traditional calcium-based synaptic rule to drive changes in the early-weight (Graupner et al., 2016). Our investigation delves into the intricate interplay between switches in neuronal activity and the diverse plasticity mechanisms at play.

To explore this, we establish different switches from tonic firing to bursting or tonic firing to inactive states. We then compare these switches under two conditions: employing solely traditional synaptic plasticity rules (using soft-bounds and hard-bounds) or incorporating the novel structural plasticity rule proposed in this study. We evaluate these distinct configurations across three memory tasks. The first task is inspired by (González-Rueda et al., 2018), while the second task involves pattern recognition and draws inspiration from (Zenke et al., 2015; Gurunathan and Iyer, 2020). Lastly, we tackle a simplified MNIST recognition task (Garg et al., 2022).

Our research sheds light on the understudied role of switches in neuronal firing patterns for synaptic plasticity. Traditional plasticity rules that utilize soft-bound mechanisms lead to a burst-induced homeostatic reset of early-weights, which is incompatible with memory consolidation. While using hard-bounds prevents the reset, it causes an increase of the early-weight independent of the acquired learning. However, our burst-driven structural plasticity offers a promising solution by bridging the gap between switches in tonic firing and bursting, ultimately facilitating memory consolidation.

7.2 Results

7.2.1 Interaction between switches in neuronal activities and synaptic plasticity rules

In this study, our objective is to investigate the effects of switches in firing activity and synaptic plasticity within computational modeling. We first described a circuit that can switch between tonic firing, inactivity, and collective bursting. Subsequently, we clarified the mechanisms of synaptic plasticity and differentiate between traditional synaptic plasticity and structural plasticity. Finally, we examined how different synaptic rules behave during switches in neuronal activity.

To begin, we considered a simple testbed consisting of biophysical conductance-based model neurons. The circuit consists of two layers, with two presynaptic neurons (pre) connected to two postsynaptic neurons (post) in a feedforward configuration and one inhibitory neuron connected to all the excitatory neurons. By applying a hyperpolarizing current to the inhibitory neuron, we simulate the effects of neuromodulators and switch the network state from tonic firing to bursting (Drion et al., 2018; Jacquerie and Drion, 2021).

Within the circuit, the ”post” neuron receives current from the ”pre” neuron in proportion to the *synaptic weight*. This weight quantifies the synaptic response of the presynaptic neuron to the postsynaptic neuron (Luboeinski and Tetzlaff, 2021). The response is mediated by postsynaptic receptors primarily located in the postsynaptic density (PSD) of the spine (Lamprecht and LeDoux, 2004). As a brief reminder, calcium influx resulting from correlated activity between pre- and postsynaptic neurons triggers an increase in postsynaptic receptor efficacy and the insertion of new receptors via fast trafficking known as Early Long Term Potentiation (E-LTP) or the induction of long-term plasticity (Lamprecht and LeDoux, 2004). Additionally, Late Long Term Potentiation (L-LTP), which is synonymous with maintenance in long-term plasticity, and *structural plasticity* involve morphological changes in the spine. This includes new protein synthesis

activated by transcription factors, leading to the insertion of newly generated receptors at the PSD and an increase in spine volume.

Mathematically, we considered the synaptic weight as the product of the early-phase synaptic weight (early-weight) w and the late-phase synaptic weight (late-weight) l (Figure 7.1A). This distinction arises from the different mechanisms that modify the synaptic weight. Traditional plasticity rules such as pair-based, triplet, and calcium-based rules (Song et al., 2000; Graupner et al., 2016; Pfister and Gerstner, 2006; Deperrois and Graupner, 2020) propose plasticity dynamics $\dot{w}$ to update the early-weight w. These rules have been previously validated in this model using experimental data (Sjöström et al., 2001; Bi and Poo, 1998). They accurately explain changes that are independent of de novo protein synthesis (Abraham et al., 2019; Lamprecht and LeDoux, 2004). In these models, the late-weight l is either not considered or remains constant. Therefore, the total synaptic weight $w \cdot l$ exhibits the same dynamics as the early-weight w.

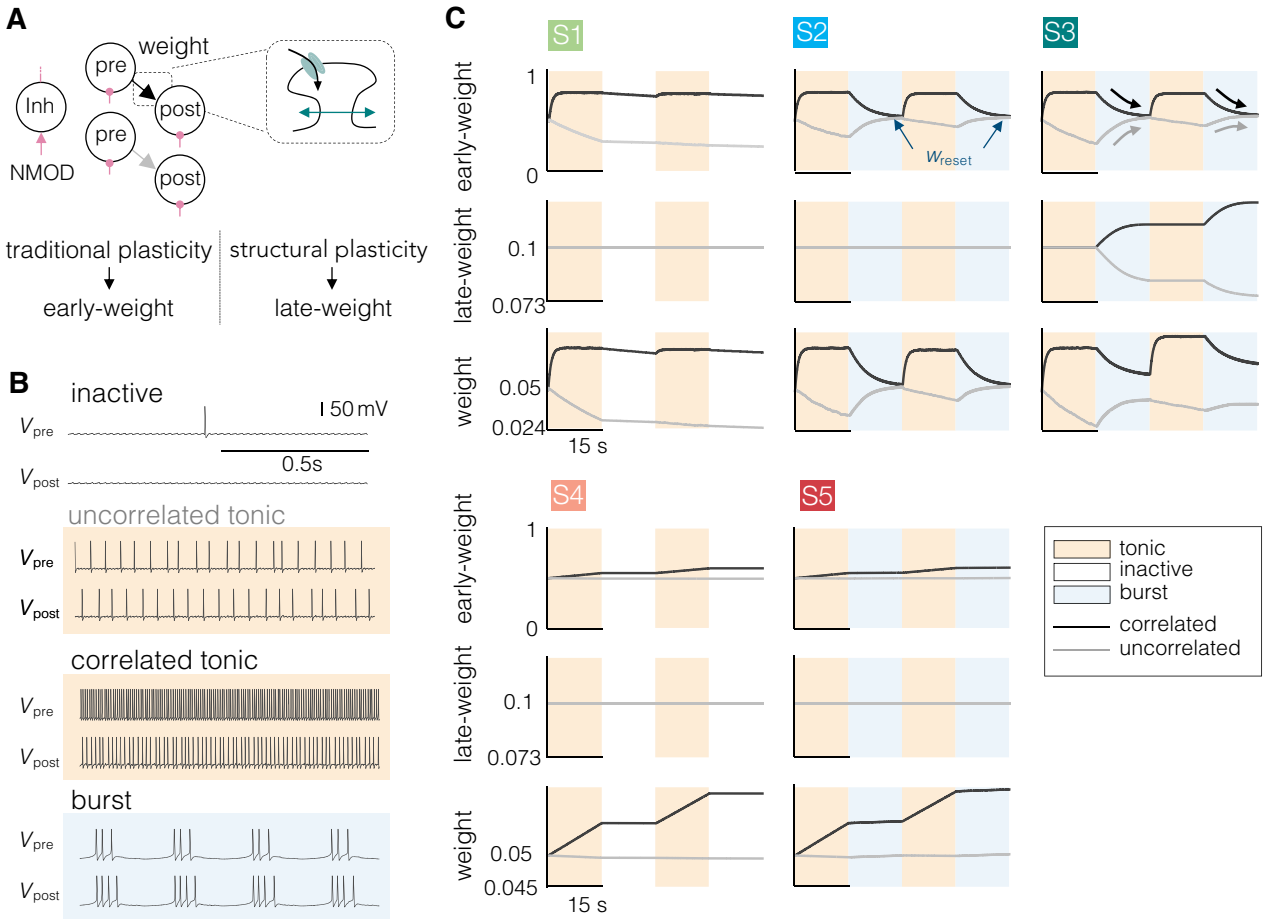

Figure 7.1: Interplay of Firing Pattern Switches and Synaptic Plasticity Rules in a biophysical neuronal circuit. A. The synaptic weight quantifies the proportion of synaptic current received by the postsynaptic neuron. It is determined by the product of the early-phase synaptic weight (early-weight), modified by the traditional plasticity rule, and the late-phase synaptic weight (late-weight), modified by structural plasticity. The inhibitory neuron (Inh) synapses onto all the excitatory neurons (rounded arrows), and neuromodulators (NMOD) are modeled by a hyperpolarizing current acting on Inh.**B.** Neurons can exhibit different firing regimes: inactive (no input current), uncorrelated or correlated tonic firing, and bursting.**C.** Comparative analysis of different combinations of neuronal activity switches and synaptic rules in two-layer feedforward circuits consisting of two presynaptic and two postsynaptic neurons. One inhibitory neuron is synapsing GABA currents with the other four neurons. One pair of presynaptic and postsynaptic neurons exhibits correlated tonic firing (black line), while the other pair demonstrates uncorrelated tonic firing (gray line). Scenario S1 illustrates the transition from tonic firing to inactivity using a traditional calcium-based rule with soft bounds. Scenario S2 replaces the inactive state with bursting, leading to a homeostatic reset of synaptic weights. Scenario S3 incorporates structural plasticity along with the bursting activity. Scenarios S4 and S5 replicate S1 and S2, respectively, but employ hard bounds instead of soft bounds.

In our exploration, we investigated the interaction between synaptic plasticity and global brain states by defining three neuronal firing patterns: inactive, tonic firing (correlated or uncorrelated between pre- and postsynaptic neurons to simulate learning or non-learning), and bursting (Figure 7.1B). Here, we considered an exclusive connection between one neuron pre and one neuron post. The first pair of neurons are driven by correlated high-frequency stimulus (represented by a black arrow in Figure 7.1A and black line in B). The second pair of neurons exhibits uncorrelated low-frequency tonic (represented by a gray line). Initially, we simulate the circuit in a tonic firing state with calcium-based plasticity driving changes in the early-weight w (Graupner et al., 2016). This state mimics learning by providing the excitatory neurons with

either correlated or uncorrelated inputs (Figure 7.1C, yellow panels). As expected, strongly correlated neurons exhibit an increase in their early-weight (black curve), while weakly correlated ones show no change or a decrease in early-weight (Figure 7.1C, gray curves).

Next, we investigated how learning is affected when tonic firing is followed by another firing pattern. In Scenario S1, when neurons transition from tonic firing to an inactive state where they barely any spike, the synaptic weight remains unchanged. This situation represents a blocking of bursting, such as in the absence of external stimuli or with the presence of neuromodulator blockers (Figure 7.1C, S1). During a subsequent learning state, the early-weight undergoes a slight increase, indicating limited consolidation of memory while utilizing a traditional calcium-based rule with soft bounds.

As previously demonstrated, the transition from tonic firing to bursting triggers (Scenario S2) a phenomenon known as *homeostatic reset*. The synaptic weights revert to their baseline values, regardless of the previously learned information (Figure 7.1C, S2). This reset mechanism occurs when the brain state shifts into a regime associated with low-frequency oscillations, characterized by collective bursting activity (McGinley et al., 2015; Polack et al., 2013; Zagha, 2014). This reset is robust against intrinsic neuronal variabilities, network heterogeneity, and neuromodulation (Jacquerie et al., 2022). This homeostatic reset is caused by soft bounds implemented in the traditional synaptic rule (here calcium-based rule from (Graupner et al., 2016) is used). Bursting leads to a stationary regime between the pre- and postsynaptic activities, resulting in a balance between potentiation and depression. Postsynaptic receptors with strong early-weights depress, and conversely, receptors with weak early-weights potentiate. The stationary bursting state drives the early-weights to a set point. Since there is no change in morphology, the synaptic weight (consisting of fixed morphology modeled by l and the early-weights w) resets. This phenomenon has also been observed in pair-based (Song et al., 2000) and triplet (Pfister and Gerstner, 2006) traditional synaptic rules (Jacquerie et al., 2022).

While the homeostatic reset mechanism erases previously stored information, it also presents an attractive opportunity for the network to learn new memories. To explore alternatives, we consider two options. First, we replace soft bounds with hard bounds in Scenarios S4 and S5. In S4, the circuit is similar to S1, where neurons switch from tonic firing to an inactive state, and the synaptic weight remains unchanged (since there is barely no spike). S5 is similar to S2, but the hard-bound leads to a small constant increase in the synaptic weight toward its upper limits (Jacquerie et al., 2022) (Figure 7.1, S4-S5). By replacing soft bounds with hard bounds, the homeostatic reset of synaptic weight is prevented, but the synaptic weight changes occur regardless of the initial values. It causes a *upscale* of all the weights caused by the collective bursting. Table 7.1 summarizes the evolution of the early-weight for the different combinations of neuronal activities and traditional synaptic rule using hard bounds or soft bounds. Eventually, S1, S2, S4, and S5 do not provide mechanisms for memory consolidation.

→ neuronal activity ↓ plasticity rule bounds	**tonic**	**inactive**	**burst**
hard-bounds	learn	no change	increase with a fixed slope $\forall\ w_0$
soft-bounds	learn	no change	reset

Table 7.1: Summary of the outcome in early-phase synaptic weight (early-weight) for different combination of neuronal activity and traditional synaptic rule. Learn means that two pairs of neurons with correlated activity results in a increase in w.

Finally, we proposed a mechanism of structural plasticity driven by the homeostatic reset, specifically through dynamics in the late-phase synaptic weight (late-weight) $\dot{l}$, referred to as L-LTP (Scenario S3). While the early-weight w undergoes the homeostatic reset as before, the late-weight l consolidates the learned information. If the w is higher than its reset value, the late-weight l increases through spine growth or the insertion of newly synthesized receptors (Figure 7.1C, S3-black arrows). Conversely, if w is lower than its reset value, l decreases through down-selection (Figure 7.1C, S3-gray arrows). The structural plasticity on l is driven by the traditional plasticity rule on w. The change in postsynaptic receptor efficacy acquired during learning needs to be maintained as a long-lasting and persistent change in the spine's morphology. Bursting associated with quiet waking helps restore efficacy and drive this structural plasticity (Poirazi and Mel, 2001).

In summary, this investigation focuses on the effect of switches in firing activity and synaptic plasticity. We first describe a circuit that can switch between tonic firing, inactivity, and collective bursting. We then clarify the mechanism of synaptic plasticity, distinguishing between traditional synaptic plasticity and structural plasticity. Finally, we explore the behavior of different synaptic rules during switches in neuronal activity. A summary is provided in Table 7.2. The homeostatic reset phenomenon, observed during the transition from tonic firing to bursting caused by soft-bound, erases previously acquired learning but also provides an opportunity for the network to learn new memories. The replacement of soft bounds with hard bounds or the utilization of structural plasticity driven by the homeostatic reset offers potential alternatives for memory consolidation. By taking advantage of the homeostatic reset phenomenon, burst-associated structural plasticity allows for the long-term storage of information by generating new postsynaptic receptors, even as their efficacy reset.

Model	Bounds	early-weight	late-weight	Switch	Outcome
S1	soft	$\tau_w([\text{Ca}])\dot{w} = \Omega([\text{Ca}]) - w$	fixed	tonic-inactive	learn-no change
S2	soft	$\tau_w([\text{Ca}])\dot{w} = \Omega([\text{Ca}]) - w$	fixed	tonic-burst	learn-reset
S3	soft	$\tau_w([\text{Ca}])\dot{w} = \Omega([\text{Ca}]) - w$	$\tau_l\dot{l} = \Delta l$	tonic-burst	learn-structural plasticity
S4	hard	$\tau_w([\text{Ca}])\dot{w} = \Omega([\text{Ca}])$	fixed	tonic-inactive	learn-no change
S5	hard	$\tau_w([\text{Ca}])\dot{w} = \Omega([\text{Ca}])$	fixed	tonic-burst	learn-constant increase

Table 7.2: Overview of the different combinations of switches and synaptic plasticity. The early-weight w is modeled by a traditional calcium-based synaptic rule (Graupner et al., 2016) either using soft or hard bounds. The late-weight l is modified only in S3. Neurons can be in different firing modes; tonic firing, inactive, or bursting.

7.2.2 Switches from tonic firing to bursting with structural plasticity has the potential to improve the SNR

To assess the effectiveness of our novel burst-driven homeostatic reset-dependent structural plasticity, we conduct a memory task similar to the one proposed by (González-Rueda et al., 2018). Our objective was to investigate memory formation and consolidation during switches in firing patterns within a small network.

We paired five out of 100 presynaptic neurons with a single postsynaptic neuron, stimulating them with correlated inputs in a tonic firing learning state characterized by high-frequency spiking. The remaining presynaptic neurons were uncorrelated and exhibited very low-frequency spiking. We compared our five previous scenarios, where the tonic state was interleaved with either inactive states (S1, S4) or bursting states (S2, S3, S5) using traditional synaptic plasticity with soft-bounds (S1,S2,S3) or hard-bounds (S4,S5). Our findings revealed that only burst-driven homeostatic reset combined with structural plasticity (S3) resulted in an increasing Signal-to-Noise Ratio (SNR) in the synaptic weights across multiple states.

When considering only the traditional synaptic plasticity rule with soft-bounds (Graupner et al., 2016), we observed either saturation of the SNR (S1) or homeostatic reset (S2). In scenario S1, the network failed to consolidate its memory due to the soft bounds, which made it challenging for strong weights to undergo further potentiation. During inactive states, the weights remained largely unchanged since the neurons exhibited minimal spiking activity. On the other hand, replacing soft bounds with hard bounds (S4, S5) prevented SNR saturation. In scenarios S4 and S5, the SNR at the end of the learning state and the inactive state remained approximately the same. The network only learned during the tonic state, leading to an increase in SNR. In S4, during the inactive state, the synaptic efficacy remained relatively stable, resulting in minimal change to the SNR. In S5, regardless of the synaptic weight change acquired during learning, bursting similarly increased the weight. This behavior stemmed from the collective bursting activity observed throughout the network, which is inherent to the properties of the neurons. The slope of change in the black and gray curves was found to be identical, as previously computed analytically (Jacquerie et al., 2022).

In conclusion, our results demonstrate that combining a traditional soft-bound plasticity rule with structural plasticity increases the SNR during switches between tonic firing and bursting. During tonic firing, the SNR improves due to the synaptic weight changes driven by correlated activity, as dictated by the traditional plasticity rule. During bursting, the structural plasticity rule aids in consolidating the weights potentiated during tonic firing and down-scaling the weights depressed during bursting.

7.2.3 Pattern recognition task and network robustness to interference

We designed a second memory task involving a pattern recognition task. In this task, the network learns to identify two patterns consisting of 4 active pixels arranged in a 3x3 grid (Figure 7.3A). These two patterns are defined without overlapping (without overlap) pixels or with one shared pixel (with overlap). We drew inspiration from similar computational experiments conducted by (Fauth and Van Rossum, 2019; Gjorgjieva et al., 2011; Zenke et al., 2015; Gurunathan and Iyer, 2020). Our feedforward network consists of 9 input neurons and two output neurons. Each pixel in the grid corresponds to an input neuron (Gurunathan and Iyer, 2020). To introduce pattern diversity, the input neurons associated with pixels belonging to the pattern fire tonically at a rate on average of 55Hz, while the other pixels fire on average at 1Hz. During the tonic firing learning state, each pattern is paired with a corresponding output neuron by simultaneously activating it on average at 40Hz. The learning states are interleaved with either inactive states (S1, S4) or bursting states (S2, S3, S5), similar to the first task. We compared the effects of soft bounds (S1, S2, S3) and hard bounds (S4, S5). To assess the network's robustness to interference, a noisy state is introduced in which all input neurons fire tonically at around 15Hz. During testing, we presented either one pattern or the other, and the corresponding output neuron should be the only one to fire. We created 50 variations of each pattern.

The accuracy is computed after each state switch and represents the percentage of recognized patterns out of the 100 presented patterns, along with the associated certainty (see Figure 7.3B). We observed that S3 performs exceptionally well, with accuracy and certainty quickly reaching their maximum. S3 also exhibits robustness to noise compared to the

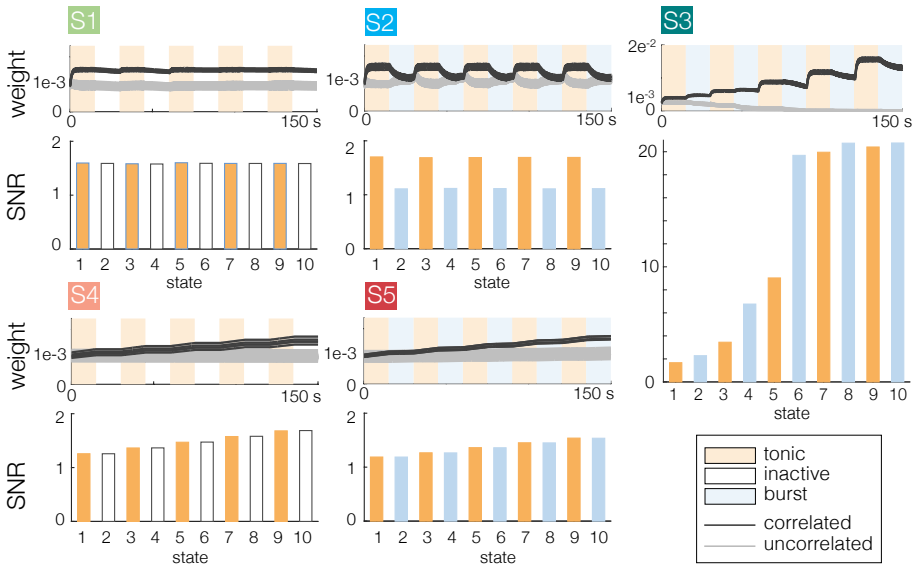

Figure 7.2: SNR is improved with switches from tonic firing to bursting and structural plasticity.
Time-evolution of the synaptic weights is shown for the different scenarios and the associated SNR. Five presynaptic neurons among 100 are paired with an output neuron (black lines). The 95 uncorrelated neurons are shown in gray. The interplay between tonic learning state and inactivity does not affect the SNR (S1,S4). Traditional synaptic plasticity rule results in a reset of the SNR during bursting (S2). Using hard-bound does not improve SNR since all the weights evolve in the same way (S5). Using burst-driven structural plasticity leads to an increase in the SNR (S3).

other cases (S1, S2), where the ability to predict the pattern is lost. In S1 (purple curve), the network, which demonstrates the interplay between tonic firing and inactivity, with the traditional soft-bound synaptic plasticity rule alone, completely forgets any learning as soon as noisy patterns are presented. In S2 (blue curve), we again observe that each bursting state resets the learning, resulting in a performance of 0% during each bursting state (even state).

Using hard bounds (S4, S5, represented by the orange and red curves, respectively) appears to make the network less sensitive to noise but also leads to a lower certainty. While S5 shows an increasing accuracy, its certainty decreases. Once again, this is due to the constant increase in weights during bursting, *i.e. all* synaptic weights grow with the same slope, making it more difficult for the network to differentiate between different patterns and resulting in lower certainty. These results confirm the findings of the previous experiment, where the SNR did not improve before and after bursting in S5.

7.2.4 Weakness of calcium-based synaptic plasticity rules for learning overlapping patterns

The pattern recognition task depicted in Figure 7.3 is replicated using two patterns that have an overlapping pixel. The results for accuracy and certainty are reduced to those obtained with non-overlapping patterns (Figure 7.3B).

To delve into the analysis, we examined the evolution of the receptive fields at the end of each state for the two experiments, considering patterns without or with an overlapping pixel (see Supplementary Figures, Figures 7.8 and 7.9). Receptive fields provide the weight matrix associated with each output neuron. After learning, spatially structured features are expected to appear in the receptive fields, causing the output neuron to respond to the learned pattern (Zenke et al., 2015). In the case of non-overlapping patterns, the receptive fields clearly exhibit both patterns in S3. Conversely, for the other scenarios, the receptive fields show less contrast. An active pixel strengthens its early-weight with the associated output neuron, as indicated by the purple line in Figure 7.3D, illustrating the evolution of the upper-centered pixel associated to the first output neuron. The late-weight further consolidates this learning. The same active pixel

Figure 7.3: (Next page) **Pattern recognition task in a circuit with successive switches of neuronal activities and different synaptic plasticity rules. A.** Implementation of a 3x3 grid pattern recognition task in a biophysical network. Each pixel corresponds to an input neuron whose activity depends on the pattern. The output neurons learn to recognize the two patterns. The network is tested on 100 variations of the patterns. Prediction is based on the output neuron with the highest firing rate (above a threshold of f_{th}), and the associated certainty is computed. Accuracy represents the percentage of correctly identified patterns, and mean certainty is calculated. **B.** Evolution of accuracy and certainty during different switches in firing activities compared across different scenarios (S1 to S5). **C.** Same as B, but for the dataset with overlapping patterns. **D.** Time-evolution of the early-weights, late-weights, and total weights during switches between different states in S3. (bottom) The receptive fields (receptive field (RF)) of the two output neurons exhibit structures that match the learned patterns. **E.** Same as D, but with two overlapping patterns that share a pixel. The star highlights the decrease in weight between the input neuron coding for the shared pixel and the first output neuron when the second pattern is presented.

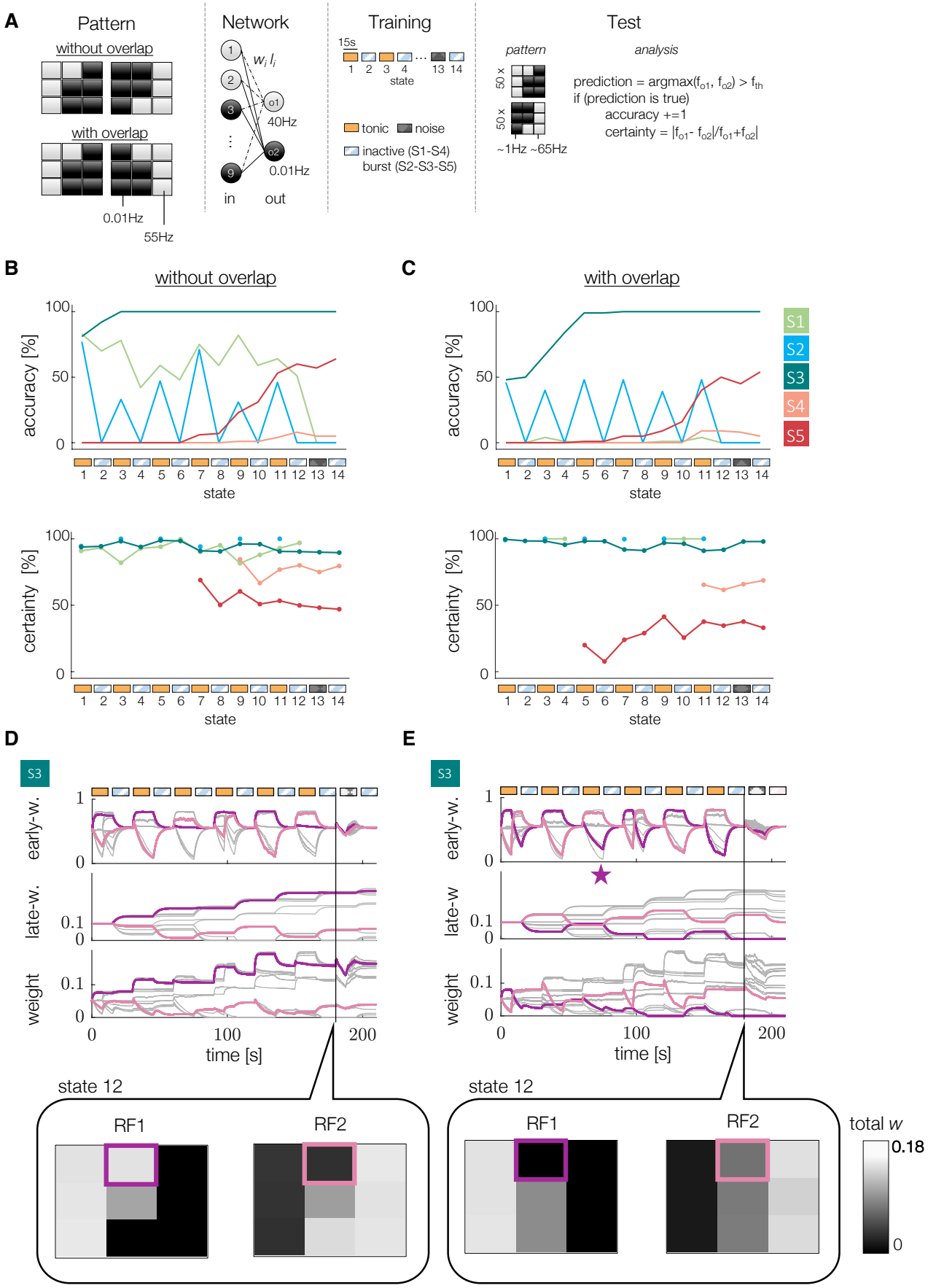

Figure 7.3: (Caption previous page.)

weakens its early-weight with the other neuron, as a consequence of the calcium rule itself. When a presynaptic neuron spikes alone on average around 50Hz with a silent output neuron, the calcium level is at an intermediate level, causing a decrease in the early-weight. This is shown by the red line in Figure 7.3D. When the first pattern is presented, this pixel is reinforced for the first output neuron and decreased for the second output neuron. This was previously confirmed by the increased SNR in Figure 7.1.

However, for overlapping patterns that share a common pixel, it results in forgetting this pixel. If the common pixel is active, it increases the early-weight for one output neuron and decreases it for the other output neuron, thereby erasing any previous learning (Figure 7.3E, star). The receptive fields lack the shared pixel.

This forgetting of the pixel reflects the behavior of the traditional calcium-based rule using soft bounds. The same observation is made in S1 and S2 (Supplementary Figures, Figure 7.9). It is further amplified by the structural plasticity rule (S3). Replacing soft bounds with hard bounds prevents this forgetting of the pixel (Supplementary Figures, Figure 7.10). Since all the weights grow during bursts, the receptive fields exhibit less contrast, resulting in moderate certainty.

The overall accuracy and certainty decrease compared to the non-overlapping training because the receptive fields lack a crucial strong weight that enables synaptic transmission during the testing phase.

7.2.5 Traditional synaptic plasticity rules using soft-bounds require precise tuning of the initial network connectivity.

The previous computational experiment reveals a hidden fragility in the traditional synaptic plasticity rule with soft bounds. The fixed value of the late-weight (l_0) must be finely adjusted to enable synaptic transmission during the testing phase. Since the early-weight (w) is bounded between 0 and 1, the total synaptic weight ($w \cdot l$) is also bounded between 0 and l_0. If the fixed value of l_0 is too low, the postsynaptic neuron does not receive a strong enough synaptic current to trigger a response, resulting in a lack of network prediction. Fine-tuning is also playing a role in scenarios S4 and S5, where w can increase until it reaches the upper limits and l is fixed. Initially, the early-weight is not sufficient for information transmission, as indicated by the accuracy of zero. However, after several states, the circuit begins to transmit spikes to the output neurons.

To quantify the lack of robustness in the network's initial wiring, we replicated the previous computational experiment (shown in Figure 7.3,B without overlapping patterns) while initializing the network at three other values of l_0. The evolution of accuracy during firing pattern switches and the corresponding certainty are shown in Figure 7.4. Darker inner and outer circles indicate higher accuracy and certainty, respectively. For a low initial l_0, scenarios S1 and S2 are unable to recognize any pattern because even though w increases during learning, the synaptic weight remains bounded between 0 and l_0, preventing synaptic responses. In the case of S4 and S5, synaptic activation is possible, but it requires a significant number of switches. Conversely, S3 initially struggles to recognize all patterns, but after several switches, its accuracy and certainty improve.

As l_0 increases (top to bottom), the models using soft bounds without structural plasticity (S1, S2) operate within the fine-tuned range, enabling synaptic transmission. Models using hard bounds (S4, S5) can recognize some patterns because synaptic weight increases during learning. S5 demonstrates pattern recognition several switches earlier than S4 due to the additional increase in weight during bursting prevented in S4.

This parameter analysis reaffirms that soft bounds necessitate precise tuning of the initial connectome. In these cases, maintaining bursting leads to similar accuracy as the previous learning state, while bursting alone triggers a reset, rendering pattern classification impossible. It is shown by the alternation of black and white circles (S2). With hard bounds (S4,S5), an increase in synaptic weight during bursting adversely affects the network's ability to classify patterns shown by light gray inner circles. In contrast, S3 is less sensitive to the initial connectome because structural plasticity increases the late-weight and allows synaptic transmission after several switches. The downselection between strong and weak early-weight, as demonstrated in Figures 7.1 and 7.2, empowers the network with high certainty.

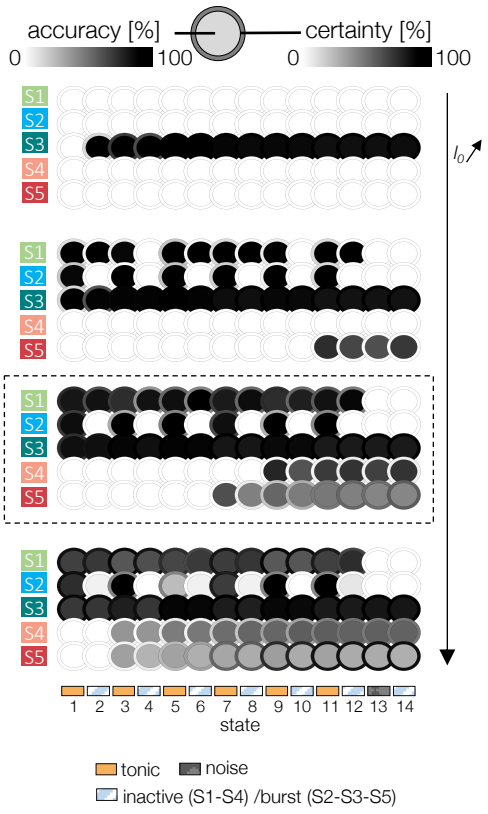

Figure 7.4: Analysis of the initial value of the late-weight l_0 on the circuit's accuracy and certainty.

To comprehend the biological mechanisms underlying the observed computational experiment, let us delve into the biophysics of synaptic plasticity. Synaptic transmission relies on the efficacy and quantity of postsynaptic receptors. In

the case of using only the traditional synaptic rule with soft bounds (S1,S2), it exclusively permits Early Long Term Potentiation (E-LTP), which encompasses an increase in receptor efficacy and receptor numbers originating from pools with limited resources. This limited form of plasticity imposes constraints on synaptic transmission. Consequently, when the number of receptors is insufficient (small I_0), the synaptic transmission lacks the strength necessary to elicit a response in the output neurons, which results in no or poor accuracy or certainty. However, Late Long Term Potentiation (L-LTP) facilitates an increase in receptor numbers through the generation of new proteins. Consequently, we observe that even with a low initial number of receptors, scenario S3 eventually exhibits synaptic transmission and effectively reads the activity of the output neuron. Intriguingly, our model suggests that bursting may serve as a set-up for the neuron to restore postsynaptic receptor efficacy and enhance protein generation.

7.2.6 Bursting and structural synaptic enhances selective memory consolidation

We compare learning and memory consolidation in a MNIST recognition task with different combinations of switches in neuronal activity and synaptic rules.

To implement this complex pattern recognition task, we utilized a reduced and cropped MNIST dataset on a 10x10 pixel grid (Garg et al., 2022), including only the first three digits: 0, 1, and 2. We constructed a feedforward network consisting of 100 input neurons, each associated with a pixel, and 3 output neurons (Figure 7.5). Each output neuron is intended to be associated with one of the three digits. The network comprises a total of 300 synaptic weights. During the tonic state, M samples of either the same digit (Figure 7.5, unique) or a random digit (Figure 7.5, random) are presented. The tonic state is then alternated with either an inactive state (S1, S4) or a bursting state (S2, S3, S5). The second-to-last state corresponds to a noisy state.

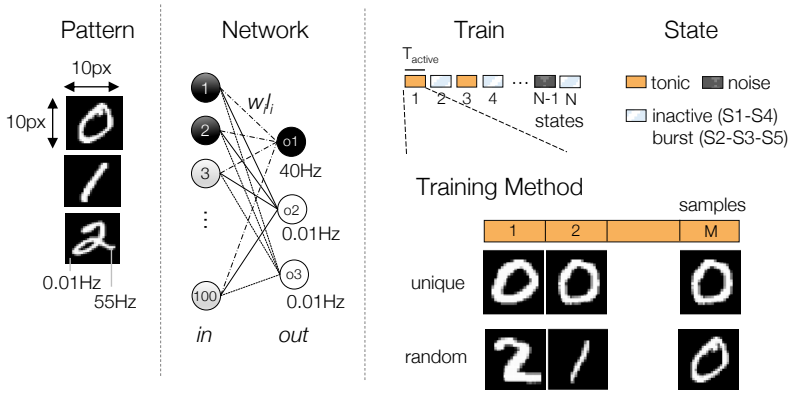

Figure 7.5: Schematic of the reduced MNIST memory task. The network learns 3 digits (0,1,2) in a reduced MNIST dataset (image of 10x10pixels). The network is composed of 100 input neurons to 3 output neurons. An active (inactive) pixel makes fire its associated neuron at approximately 55Hz (0.1Hz). The network learns during N states where tonic learning is interleaved with a bursting or an inactive state. During each tonic learning state, M digits are presented. Either the same digit is shown per state with different samples (unique) or M samples of digits randomly selected are presented.

We tested the network's ability to learn the three digits using three different training methods, and we studied the receptive fields associated with the three output neurons during the succession of states. The three training methods are as follows: (i) training the network only on digit 0 and presenting digit 1 during one tonic state (Figure 7.6), (ii) training the network on a randomly selected digit at each state and using different samples of the same digit for training (Supplementary Figure 7.11), and (iii) training the network on random samples of digits (Supplementary Figure 7.12).

In each training method, S1 and S2 exhibit sensitivity to noise and promptly forget any previously acquired learning. S2 consistently demonstrates a reset and forgets at each switch. In S1, the network quickly forgets any previous learning as soon as it is trained on a new digit during the tonic state. When different samples are presented within the same tonic state, the last digit is retained while the previous samples are nearly forgotten (Supplementary Figure 7.12). Conversely, in S4 and S5, the network successfully learns, as indicated by the receptive fields displaying distinct digits. During bursting in S5, the patterns experience further *non-selective consolidation*, meaning that all the weights increased in the same manner. In S3, more pronounced receptive fields are observed showing a selective memory consolidation through burst-drive structural plasticity. However, when digits share overlapping pixels, these pixels vanish from each receptive field. This was explained on simple patterns in the previous task with one overlapping pixel. Figure 7.6 shows that the network recovers the missing pixels in S3 when digit 1 is shown only once but on the other training methods, S3 still shows this weakness. Notably, in S5, digit 1 undergoes additional consolidation despite being presented only once.

Among the different training methods, presenting random samples of different digits at each state (Figure 7.6) seems to facilitate faster learning and prevents the immediate disappearance of overlapping pixels.

In conclusion, using a traditional synaptic rule with soft bounds leads to forgetting as soon as the network switches to

collective bursting. Exploiting this reset to drive a structural plasticity rule promotes consolidation of acquired learning, but it lacks robustness when dealing with more complex patterns with overlapping pixels. Using a traditional synaptic plasticity rule (such as the calcium-based rule) with hard bounds supports non-selective memory consolidation during collective bursting.

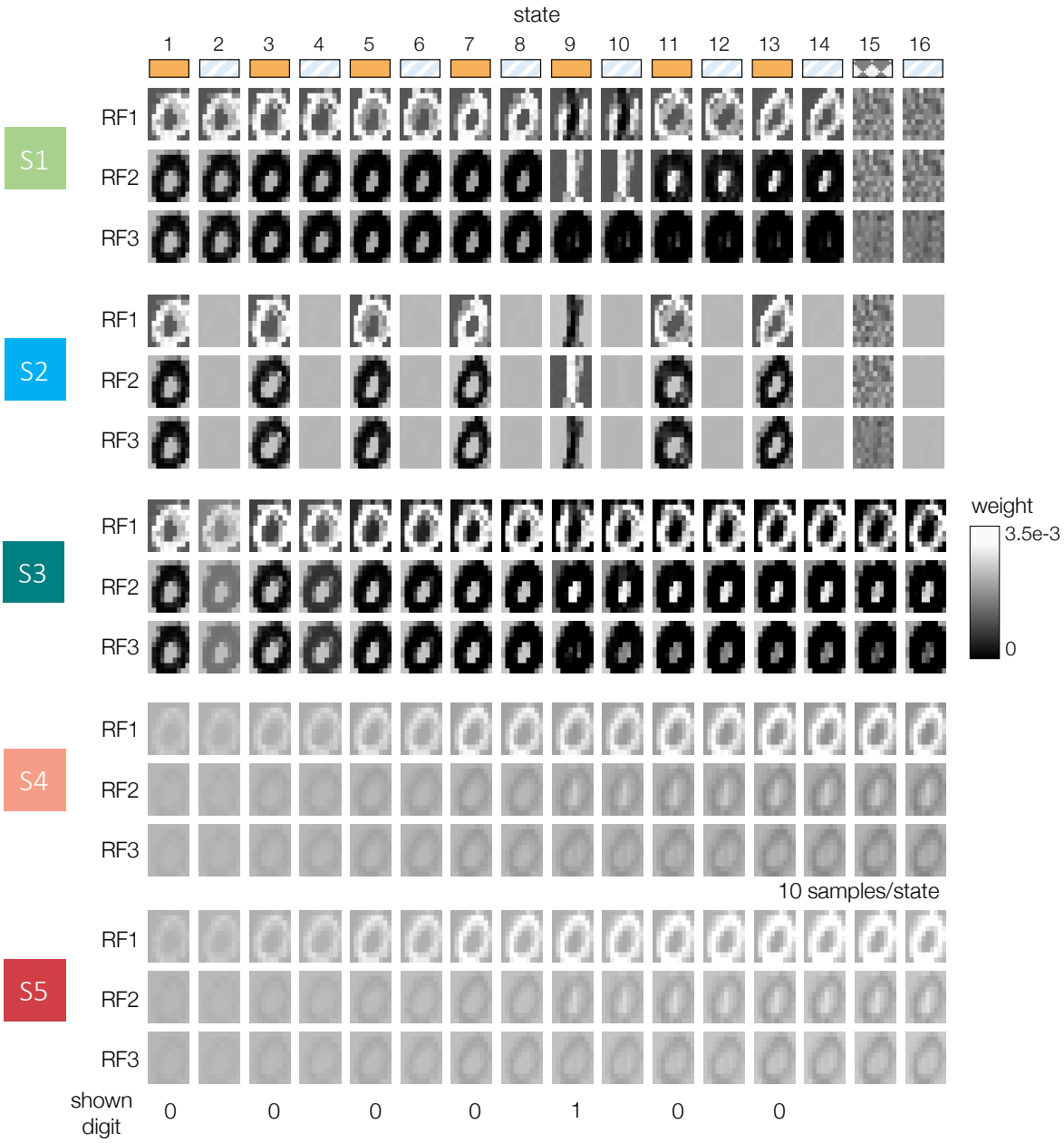

Figure 7.6: Evolution of receptive fields (RF) during successive switches of neuronal activities with the presentation of an unexpected digit. S1 and S2 are sensitive to noise. S2 resets the three RF during bursting, while S3 consolidates memory by showing a structured and contrasted RF representing the shown digit. The RFs in S4 and S5 display gradual growth but with less contrast compared to S3. Due to the overlapping nature of the digit 1 with 0, its RF is not prominently visible in S3 but undergoes non-selective consolidation in S4 and S5.

7.3 Discussion

Switches in neuronal activity, such as tonic firing to bursting, play a critical role in memory consolidation. Combining the burst-driven homeostatic reset caused by the traditional synaptic plasticity rule using soft-bound and structural plasticity provides a potential for memory consolidation.

To demonstrate the validity of our proposed mechanism, we investigated the role of homeostatic reset and question whether it is a detrimental and beneficial feature for memory consolidation. We considered both perspectives. Firstly, we

tested the hypothesis that the reset is a disadvantageous feature because it leads to forgetting. Therefore, we investigated strategies to eliminate it, namely replacing soft-bounds with hard-bounds or blocking bursting (replacing bursting by inactivity).

Conversely, the reset can be seen as a beneficial feature that restores the efficacy of postsynaptic receptors and enables the formation of new memories. In this case, the previous learning needs to be encoded in another variable. To address this, we developed a structural plasticity mechanism that takes advantage of the burst-induced reset. This novel approach distinguishes between traditional synaptic plasticity rules, which model Early Long Term Potentiation (E-LTP), and structural plasticity rules, which model Late Long Term Potentiation (L-LTP). We proposed that the early-weights and the late-weights can be treated separately, providing a simple mathematical framework for the consolidation of previous learning even during bursts. The definition of the structural plasticity rule is independent of the choice of the traditional plasticity rule as long as soft-bounds are used. The early-weights can be governed by calcium-based rules or any phenomenological rule that employs soft-bounds. [1]. As the early-weights reset during bursts, the late-weights evolve to encode the learning acquired during tonic.

7.3.1 Traditional synaptic plasticity rules using hard-bounds causes a non-selective memory consolidation

The first strategy to remove the reset is to replace soft-bounds with hard-bounds. This approach causes an independent change in synaptic weights regardless of the acquired learning during tonic firing. All the synaptic weights are affected in the same manner; there is no downselection of weak weights nor upscaling of strong weights acquired during learning. Our results show that this approach leads to a slight improvement in the SNR, moderate performance with moderate certainty, and low-contrasted consolidation of receptive fields.

This approach raises questions about the role of bursting in a network that uses hard-bounds. When neuromodulators switch the network from active waking to quiet waking, bursting serves as a neuronal activity that allows for a global increase in weight. In an extreme case where the bursting state is prolonged for an extended period, all weights reach the upper and lower bounds imposed by the traditional rule. This leads to a pathological situation of extreme learning during bursting, which seems implausible. Furthermore, Figure 7.6 demonstrates that learning obtained from a one-shot learning digit is consolidated over several subsequent states. While this can be an advantageous strategy for novel memory consolidation, it can be detrimental in cases of misleading or errors in the pairing. Lastly, the choice of traditional plasticity rules using hard-bounds, such as calcium-based or phenomenological rules, can have a drastic effect on the direction of change, as explained in Chapter 5.

7.3.2 Blocking Bursting: eliminating the homeostatic reset but preventing memory consolidation

Blocking bursting activity can be achieved by using ion channel blockers or neuromodulator blockers. When the network no longer receives any driving input, the neurons become inactive, resulting in unchanged synaptic weights. Blocking bursting prevents memory consolidation.

Combining this strategy with hard bounds leads to a situation where the network only increases its synaptic efficacy during the learning phase (S4). This approach provides moderate SNR and low accuracy. Conversely, when using soft bounds, which constrain the efficacy between 0 and 1, the network is unable to consolidate its memory (S1). As soon as the network is exposed to a new pattern or noise, it forgets what it had previously learned.

Recent experimental work has shown that blocking bursting activity inhibits memory consolidation (Dias et al., 2021). These experiments were performed on in vitro models of cortical cultures using multi-electrode arrays (MEA). The activities of these cultures are controlled by cholinergic concentration, where low concentration is associated with spontaneous network bursts, while high concentration is linked to reduced network excitability and fewer network bursts. It was demonstrated that increasing cholinergic tone hinders memory trace formation and consolidation (Dias et al., 2021).

Our computational results reinforce these findings. Neuromodulators play a crucial role in our brain, orchestrating switches in neuronal activity that manifest as different brain states. We demonstrate that blocking bursting by inhibiting network hyperpolarization (mimicking sustained high acetylcholine levels) is associated with reduced memory consolidation.

7.3.3 A structural plasticity governed by burst-induced reset: comparison with existing structural plasticity models

In this project, we have developed an innovative structural plasticity rule that relies on burst-induced reset in the early-phase synaptic weights (early-weights). In the literature, various structural plasticity rules exist, ranging from highly detailed biophysical implementations that model different protein kinetics (Smolen et al., 2006), to more mathematical

[1] These computational experiments are done by Justine Magis and Emmy Kellens during their master thesis

approaches (Deger et al., 2012) that utilize activity correlations to promote synapse removal (see SECTION 3.5.5). The first category is valuable for gaining a better understanding of the biological mechanisms involved in structural plasticity. However, it requires a larger number of equations, leading to increased computational time, especially as the network size grows. The second category provides a useful framework for deriving analytical predictions but lacks biological interpretation. These approaches may be too mathematically oriented and oversimplified to effectively study the effects of neuronal activity switches and capture the complex nature of bursting.

More recently, phenomenological rules have been proposed for structural plasticity, such as those presented in (Zenke et al., 2015; Fauth and Van Rossum, 2019; Luboeinski and Tetzlaff, 2021), which also combine E-LTP and L-LTP. However, these rules are not compatible with the burst-driven homeostatic reset.

In (Zenke et al., 2015), the synaptic weight is influenced by a combination of traditional synaptic rules, including triplet LTP, pair-based LTD, and others.

$$\begin{aligned}\frac{dw_{ij}}{dt} &= \text{triplet LTP} \\ &\quad + \text{pair-based LTD} \\ &\quad + \text{transmitter induced} \\ &\quad + \beta(\tilde{w} - w_{ij})z^{-}(t-\epsilon)^3 S_i(t)\end{aligned}$$

where $\tilde{w}$ represents the reference weight, β is set to 0.05, and z and S track presynaptic activities. According to this equation, the reference weight acts as a steady state value for the weight. Simultaneously, this reference weight has a slow dynamics, governed by a "negative gradient of a double well potential" (Zenke et al., 2015). Depending on the value of w_{ij}, $\tilde{w}$ gradually evolves towards specific fixed points. Using this algorithm during bursting will not drive memory consolidation. As burst leads to a reset in all the synaptic weight w, which in turn affects the value of $\tilde{w}$. In turn, it resets the consolidation term. Our approach introduces a degree of freedom by decomposing early and late long-term plasticity into the product of early- and late-weight. This decomposition allows bursting to reset the value of w while the late-weight can respond differently.

In (Fauth and Van Rossum, 2019), the probability of synapse removal depends on w. Once again, during learning associated with tonic activity, w increases, resulting in a low probability of removal. However, during bursting, a strong early-weight of recently acquired w decreases, thereby increasing the probability of removal. Overall, models that rely on the value of w itself to implement the late phase of plasticity (or maintenance and structural plasticity) are not compatible with burst-induced reset in w.

An alternative solution for memory consolidation is proposed by modeling the Synaptic Tagging and Capture (STC) hypothesis(Seibt and Frank, 2019). As a reminder, a potentiated synapse generates a local tag that activates and synthesizes plasticity related products (PRP) (Smolen et al., 2020). The maintenance of potentiation is achieved through the capture of PRP. However, implementing this hypothesis can be achieved by either describing the kinetics of different components, leading to a set of equations that becomes too complex for network use, or as an alternative, the synaptic weight is the sum of the early and late phase weights (Luboeinski and Tetzlaff, 2021; Clopath et al., 2008). The early-phase weight follows traditional plasticity rules, while the late-phase weight changes if the early-phase weight surpasses a certain threshold. This mechanism is particularly effective in learning associated with tonic activity, where the early-phase weight increases between correlated neurons, and the late-phase weight further consolidates. However, considering this rule during bursting activity results in a reset of all the early-phase weight affecting once again dragging the late-phase weight in the same direction.

Finally, one could suggest using burst-time dependent plasticity as the neuron switches to bursting. However, this approach considers the burst, which is the succession of action potentials, as a single unit. While it shows potential in certain applications (Gjorgjieva et al., 2009; Payeur et al., 2020; Fuchsberger et al., 2022), it raises the question of how neurons switch from spike-time dependent plasticity to burst-time dependent plasticity, by sensing first the timing of the action potentials then the timing of bursting.

Conversely, our proposed mechanism allows bursting to restore postsynaptic receptor efficacy and drive simultaneous morphological changes. It is governed by the neuron's state itself. During bursting, neurons are disconnected from external stimuli, providing a period of time for protein synthesis and synapse growth. However, this structural plasticity rule has some limitations. First, the rule lacks of robustness for overlapping patterns due to the behavior of the traditional synaptic rule itself. Further investigation on the training methods might help to overcome this issue [2]. Currently, it only operates during bursting activity. We assume that the rule is activated by the same neuromodulators that induce the switch in neuronal activity (Brzosko et al., 2019). As explained earlier, these neuromodulators enable a transition from learning with tonic firing to bursting. They are also likely to affect the signaling cascade that triggers protein synthesis, responsible for the morphological changes in the synapse (Shine et al., 2021; Foncelle et al., 2018). Additionally, the

[2]Master thesis done by Emmy Kellens in 2022-2023.

current structural plasticity rule relies on estimating the reset value itself. This limitation can be overcome by developing a structural plasticity mechanism that directly depends on the slope of early-weight change during bursting [3].

7.3.4 Switching neuronal activities in learning and memory consolidation is underinvestigated

This work opens the way to further research in understanding the interplay between fluctuations in brain states and learning. A neuronal population is able to switch between different states to account for different behaviors. These switches likely have an impact on learning. Here we proposed to explore this in a simple biophysical circuit using neurons modeled with conductance-based paradigm. It shows that bursting enhances memory consolidation and more generally it reinforces previous observations that "short period of quiet rest can facilitate memory consolidation processes" (Brokaw et al., 2016).

We aim to provide a computational support to drive further research in experimental neuroscience exploring switches in neuronal activities and synaptic plasticity. For the moment, plasticity is often studied by inducing stereotyped controlled plasticity protocol. Here, we aim to suggest experiments done with more in-vivo neuronal activity.

Eventually, this work can be extended to improve learning performance in artificial intelligence, using machine learning algorithms. For the moment, learning relies on rate-based model or spiking-neural network that is trained by mimicking the learning state. Here, we aim to suggest to interplay learning state with quiet waking allowing the network to restore its connectivity and consolidate its memory. To bridge the gap between this work and machine learning, research on bursting artificial neural networks must be investigated as well as adding neuromodulators as initiated in (Vecoven et al., 2020).

7.4 Methods and Computational experiments

7.4.1 Conductance-based modeling

Neurons are modeled using a single-compartment Hodgkin and Huxley formalism. The membrane voltage follows the general method (see section 3.2) derived from (Drion et al., 2018; Jacquerie and Drion, 2021; Jacquerie et al., 2022). The circuit consists of one inhibitory neuron (Inh) projecting on all the excitatory neurons through a $GABA_A$ and $GABA_B$ connections. The number of excitatory neurons varies depending on the computational experiments. In a general manner, the presynaptic neuron (pre) is connected to the postsynaptic neuron (post) via an AMPA synapse. The excitatory synaptic current perceived by the postsynaptic neuron is described by:

$$I_{\text{AMPA}} = w \cdot l \;\; s_{\text{AMPA}}(V_{\text{pre}})(V_{\text{post}} - E_{\text{AMPA}})$$

where w is the early-phase synaptic weight (early-weight), l is the late-phase synaptic weight (late-weight), their product $w \cdot l$ is defined as the synaptic weight, s_{AMPA} is the gating variable of the AMPA postsynaptic receptor driven by the presynaptic membrane voltage and E_{AMPA} is the reversal potential of AMPAr. Previously in (Jacquerie and Drion, 2021; Jacquerie et al., 2022), the term $\bar{g}_{\text{AMPA}}$ was denoted as the maximal conductance of the AMPA receptors. This notation has to be updated to take into account E-LTP and L-LTP.

7.4.2 Synaptic plasticity

Definition of the synaptic early-weight, the synaptic late-weight, the synaptic weight, and the associated plasticity rules

The early-phase synaptic weight (early-weight) w is driven by the traditional synaptic plasticity rule, namely the calcium-based plasticity rule (Graupner et al., 2016). Change in the early-weight is associated to Early Long Term Potentiation (E-LTP), modeling change in synaptic receptor efficacy and fast trafficking of AMPA receptors.

The late-phase synaptic weight (late-weight) l is considered as a constant in traditional synaptic plasticity rules. It sets the connectome. Here, we developed a structural plasticity rule to consider the morphological change in the spine depending on the creation of de-novo protein referring to Late Long Term Potentiation (L-LTP).

Traditional synaptic plasticity rule: the calcium-based model

The change in early-weights w is governed by the calcium-based model of (Graupner et al., 2016):

$$\tau_w \dot{w} = \gamma_{\text{p}}(1 - w)I([\text{Ca}] - \theta_{\text{p}}) - \gamma_{\text{d}} w I([\text{Ca}] - \theta_{\text{d}})$$

[3] Master thesis done by Justine Magis in 2022-2023.

where τ_w is the timeconstant, γ_p is the potentiation rate, γ_d is the depression rate, θ_p is the potentiation threshold and θ_d is the depression threshold. $I(\cdot)$ is the Heaviside function means that $I([Ca] - \theta_p)$=1 if [Ca] is greater than θ_p.

Briefly, pre- and postsynaptic activity results in fluctuations in calcium concentration. Calcium level below the depression threshold does not affect w. Calcium between the depression and potentiation thresholds decreases w. Calcium above the potentiation threshold increases w. This calcium level is the sum of two terms: calcium due to presynaptic activity and calcium due to postsynaptic activity. A pre- or postsynaptic spike is translated in a calcium exponential decay. More explanations are provided in section 3.5.4.

Soft-bounds vs Hard-bounds

The calcium-based rule defined by (Graupner et al., 2016) implements soft-bound as the potentiation rate γ_p is balanced by $(1 - w)$. For strong w, the perceived potentiation rate is smaller compared to weak w. The same reasoning can be derived for the depression rate γ_d

In chapter 5, the model was modified to implement hard bound. The dependency on w is removed from the main equation such as

$$\tau_w \dot{w} = \gamma_p I([Ca] - \theta_p) - \gamma_d I([Ca] - \theta_d)$$

For easier understanding, the initial model can be formulated by its first-order differential equation:

$$\tau_w([Ca]\dot{w} = \Omega([Ca]) - w$$

It means that w is converging towards Ω that depends on the calcium oscillation. To remove the steady-state configuration and use hard-bound, the equation becomes

$$\tau_w([Ca]) = \Omega([Ca])$$

More details are provided in chapter 5.

Structural plasticity: plasticity on the late-phase synaptic weight

The Late Long Term Potentiation (L-LTP) relies on the generation of de novo proteins and morphological changes (Poirazi and Mel, 2001; Lamprecht and LeDoux, 2004). These changes are encapsulated in a variable l, for simplicity called the late-phase synaptic weight (late-weight). The rule governing the change in this variable refers to structural plasticity.

We developed a simple equation driven by the *homeostatic reset* (Figure 7.7), which is the result of the traditional plasticity rule using soft-bound acting on w during burst (Jacquerie et al., 2022). Structural plasticity is governed by a simple equation:

$$\tau_l \dot{l} = \Delta l$$

where Δl is comprised between -1 and 1 and decides if the late-weight increases (positive value of Δl) or decreases (negative value of Δl). The term τ_l scales the speed of change in order of magnitude of 1 to 10 seconds.

During bursting activity only, the variable Δl has the following dynamics:

$$\tau_\Delta \dot{\Delta l} = f(w) - \Delta l$$

where τ_Δ is the time constant associated with the change in Δl and $f(w)$ is a sigmoidal function between -1 and 1 written as:

$$f(w) = -1 + 2\left(\frac{e^{S(w - w_{HR})}}{1 + e^{S(w - w_{HR})}}\right)$$

where S defines the steepness of the sigmoid (the largest the value, the steepest the transition from -1 to 1). The term w_{HR} is the homeostatic reset estimated each second during the bursting activity.

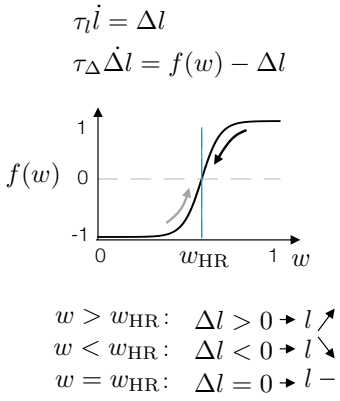

Figure 7.7: Overview of the structural plasticity rule. The dynamics of the late-phase synaptic weight (late-weight) (l) are governed by Δl, which reaches a steady-state value depending on the early-phase synaptic weight (early-weight) (w). Once w reaches the reset point, the value of l remains constant.

For the calcium-based rule, the estimated reset value is computed by

$$w_{HR} = \frac{\Omega^d \alpha^d + \Omega^p \alpha^p}{\alpha^d + \alpha^p}.$$

where Ω^d and Ω^p are respectively the depression and potentiation levels (a combined expression with γ_p and γ_d and the effective time spent in each region α^d and α^p are defined as the time spent balanced by the time-constant of potentiation/depression in the corresponding region (as demonstrated in (Jacquerie et al., 2022)).

The bursting rhythm governs the magnitude of the homeostatic reset. As this rhythm can be modulated during the state, for instance, through the influence of neuromodulators or increased connectivity, the estimated value of the reset is calculated every second. This frequency of computation aligns with the realistic interburst frequency, which is approximately 100Hz.

If the neuron is not bursting, $\tau_\Delta \dot{\Delta l} = -\Delta l$. This value is converging towards 0. It guarantees the late-weights to remain unchanged during the other states - an assumption made in this project.

The parameters of the structural plasticity rules are adapted depending on the computational experiments. Table 7.3 provides an overview of the different parameters.

Parameters	S	τ_l	τ_Δ	Ω^p	l_0
Figure 7.1	20	5e5	100	0.75	0.1
Figure 7.2	15	1e6	100	0.7	$\mathcal{N}$(0.01 , 0.01. 0.05)
Figure 7.4B	20	1e5	100	0.6	0.1
Figure 7.4C	20	1e5	100	0.6	[0.3:0.05:0.45]/4
Figure MNIST	20	5e6	100	0.6	5e-3

Table 7.3: Parameters associated with structural plasticity are adapted for the different computational experiments.

Computational experiments

Computational experiment 1: Circuit configuration and input stimulation for neuronal activity patterns

We use a circuit composed of 5 cells: one inhibitory cell is connected via $GABA_A$ and $GABA_B$ currents to four excitatory cells which are connected in a two-layer feedforward configuration with two input neurons and two output neurons (Figure 7.1). Two input presynaptic cells are connected to two output postsynaptic cells in a one-to-one configuration. One pair of neurons has an correlated activity, while the second pair has a uncorrelated activity. These neurons are driven by an externally applied current to make them spike at a mean fixed frequency f_0 (given in Table 7.4). The current is shaped as a square pulse when each pulse lasts 3ms and has an amplitude of 50nA/cm^2. Spike timings are generated with interspike intervals following independent Normal distributions $\mathcal{N}(\frac{1}{f_0}, (\frac{0.1}{f_0})^2)$.

input neuron	**tonic 1**	**tonic 2**	**output neuron**	**tonic 1**	**tonic 2**
1	70Hz	65Hz	1	35Hz	35Hz
2	10Hz	8Hz	2	8Hz	3Hz

Table 7.4: Firing frequencies of the four excitatory neurons during two tonic states for the experiment shown in Figure 7.1

In the same circuit configuration, we investigate the impact of switching neuronal activities. Each state has a duration of 15 s. The tonic firing state is generated as described earlier and the inhibitory neuron receives a constant depolarizing current of 3nA/cm^2, resulting in a sustained spiking mode (refer to section 3.5.4 for more details). The transition to bursting activity is achieved by hyperpolarizing the inhibitory neuron to -1.2nA/cm^2 and blocking all external currents applied to the excitatory neurons. This hyperpolarizing current triggers bursting behavior in the inhibitory neuron, subsequently leading to bursting activity in all the excitatory neurons. It is important to emphasize that the intrinsic bursting observed in the circuit is a direct outcome of the inherent properties of the neurons, manifested by a sequence of action potentials followed by a period of silence. The inactive state, on the other hand, is similar to tonic firing, with the exception that all the excitatory neurons are stimulated externally to fire at frequencies of 0.1, 0.5, or 1 Hz.

(Figure 7.1) compares five different combinations of switches and synaptic plasticity rules, as summarized in Table 7.2. Scenario S1 corresponds to a circuit that transitions from tonic firing to an inactive state using the traditional calcium-based rule with soft-bound and constant late-weights. Scenario S2 represents a circuit that switches from tonic firing to bursting using the same traditional calcium-based rule with soft-bound and constant late-weights. Scenario S3 is similar to S2, but the late-weights are regulated by the structural plasticity rule. Scenarios S4 and S5 are equivalent to S1 and S2, respectively, except that soft-bound is replaced with hard-bound.

Computational experiment 2: Pairing neurons and comparison of SNR

Network

We reproduce a similar computational experiment as in (González-Rueda et al., 2018). We build a 2-layer network with 100 input neurons connected to one output neuron. An inhibitory neuron is connected via $GABA_A$ and $GABA_B$ currents

to all the excitatory neurons without inhibitory plasticity((Figure 7.2).

To mimic biophysical variability, the intrinsic conductances are randomly picked in an interval of ± 5% around their nominal values. Each connection is initialized as follows $l_0 = abs(rand(\mathcal{N}(0.01, 0.01 * 0.05)), 100)$ and $w_0 = abs(rand(\mathrm{N}(0.5, 0.5 * 0.05)), 100)$.

States
The network has three possible states: tonic firing, bursting, and inactive.

- During the tonic-firing learning state, we pair 5 of the 100 presynaptic neurons with the postsynaptic neuron by driving them with correlated inputs. The active input neuron receives a depolarizing current of 50 nA/cm^2 during 3ms at a frequency of $f_0 = 60$ Hz. The output neuron receives a similar input at $f_0 = 40$ Hz (Gurunathan and Iyer, 2020). This input is sufficient to generate an action potential in the conductance-based model. To build a more realistic simulation, the spike timings are generated with interspike intervals following independent Normal distributions $\mathcal{N}(\frac{1}{f_0}, (\frac{0.1}{f_0})^2)$. The 95 non-correlated input neurons are stimulated in the similar manner except that the frequency f_0 is chosen between the following values (0.1, 0.25, 0.5, 0.75, 1, 1.25, 1.5, 2) Hz from a uniform distribution. The output neuron is stimulated with a pulse train at 40Hz whose interspike intervals follow independent Normal distribution $\mathcal{N}(\frac{1}{f_0}, (\frac{0.1}{f_0})^2)$.

- During bursting, the inhibitory cell is hyperpolarized with an external applied current equal to -1.2 nA/cm^2. The potentiation level Ω^{p} in the traditional calcium-based synaptic plasticity rule is modified to 0.7. It controls the position of the reset around $w_{\mathrm{HR}} = 0.5$. It was demonstrated and discussed in (Jacquerie et al., 2022). The value of the reset is evaluated each second.

- During inactive state, the neurons are driven with an applied current generating pulse at a frequency f_0 chosen in the range (0.1, 0.5, 1) Hz. The spike timings are generated in the same manner following independent Normal distributions $\mathcal{N}(\frac{1}{f_0}, (\frac{0.1}{f_0})^2)$.

Table 7.3 provides a table with the different value of the parameter used for the synaptic plasticity rules.

Protocols
We monitor the progression of the early-weights and late-weights during ten states, which alternate between a tonic firing learning state and either an intermittent bursting state or an inactive state without bursting. Each state has a duration of 15 seconds.

Analysis
To analyze the evolution of the total synaptic weight during the simulation, the Signal-to-Noise Ratio (SNR) is computed at the end of each state (Figure 7.2). The SNR is computed according to (González-Rueda et al., 2018):

$$\mathrm{SNR} = \max(wl)/\mathrm{mean}(wl).$$

Computational experiment 3: Pattern recognition

Network
In the pattern recognition task, we build a network of 9 presynaptic neurons connected to two postsynaptic neurons (Figure 7.3). The network learns to identify two patterns created in 3x3 pixel grid. Each pixel is associated with one neuron. An inhibitory neuron is connected via $\mathrm{GABA_A}$ and $\mathrm{GABA_B}$ currents to all the excitatory neurons without inhibitory plasticity.

States
The network can be in four different states:

- learning state: inputs neurons are driven with an external current according to the pattern. If the pixel is active, the associated input neuron receives an applied current as a pulse at a frequency f_0 chosen in a normal distribution $\mathcal{N}(55\mathrm{Hz}, 10)$. The amplitude of the pulse is equal to 50nA/cm^2 and the duration is equal to 3ms. To mimic less regular spiking trains, the interspike interval is obtained in $\mathcal{N}(\frac{1}{f_0}, (\frac{0.1}{f_0})^2)$. If the pixel is inactive, a similar stimulation is applied for a frequency f_0 chosen in a normal distribution $\mathcal{N}(1\mathrm{Hz}, 0.01)$. The output neuron associated with the presented pattern is stimulated with a pulse train at f_0 = 40Hz whose interspike intervals follow independent Normal distribution $\mathcal{N}(\frac{1}{f_0}, (\frac{0.1}{f_0})^2)$. The other neuron has a similar pulse train except that f_0 = 0.01Hz.

- bursting state: the inhibitory neuron is hyperpolarized by a current of -1.2nA/cm^2.

- inactive state: all excitatory neurons are inactive and receive a pulse train at a frequency f_0 chosen in a normal distribution $\mathcal{N}(1\text{Hz}, 0.1)$.
- noisy state: to mimic a noisy state, all neurons receive a pulse train at a frequency f_0 chosen in a normal distribution $\mathcal{N}(15\text{Hz}, 10)$.

Protocols
We have devised the following protocol to compare the different models with and without the structural plasticity rule and examine the effect of the bursting state. The network undergoes 14 consecutive states.

During the first 12 states, a learning state is alternated with a bursting state (S2, S3, S5). The thirteenth state is a noisy state followed by a bursting state (S2, S3, S5). In order to study the impact of bursts in the simulation, we replicate the same protocol by replacing all the bursting states with resting states (S1, S4).

During the learning phase, we choose to present either one sample of the first pattern (pattern 1) for half of the state duration, followed by one sample of the second pattern (pattern 2), or we show two samples of the same pattern. Each state lasts for 15 seconds. Table 7.5 provides more details.

state	1	3	5	7	9	11
pattern learnt	1-2	1-1	2-2	1-2	1-1	2-2

Table 7.5: Succession of patterns shown during learning state

Testing
The network has been simulated using the same protocol and samples for each scenario. In order to assess their ability to recognize the two patterns, we generated 50 samples of the first pattern and 50 samples of the second pattern. For each sample, active pixels corresponding to the pattern fired according to a pulse train at a frequency f_0, which was chosen from a normal distribution $\mathcal{N}(65Hz, 10)$. Similarly, inactive pixels were stimulated at a frequency f_0 drawn from $\mathcal{N}(1Hz, 0.5)$.

Each pattern was presented for 1 second, during which we recorded the number of spikes generated by the two output neurons. This provided us with the frequency of the output neurons. The output neuron itself was not stimulated, allowing us to accurately measure the number of spikes transmitted from the input neurons to the output neuron.

The network was initialized with a fixed connectivity $w \cdot l$ obtained at the end of each state during the training phase.

Analysis
For each sample, we count the number of spikes from both output neurons over a duration of one second, denoted as f_{o1} and f_{o2}. The neuron with the highest frequency above a threshold f_{th} of 10Hz is considered to predict the digit. If neuron 1 has the highest frequency and exceeds the threshold, the network predicts that the first pattern was presented. We introduce the threshold to mitigate the impact of noise, although the specific threshold value is not critical. If both neurons fire below the threshold, the network does not provide a prediction and it is considered as 'I don't know'.

In the case of a correct prediction, the network's performance is enhanced, and the certainty is calculated as the absolute difference between the two firing rates divided by their sum:

$$\frac{|f_{o1} - f_{o2}|}{f_{o1} + f_{o2}}.$$

This computation aims to implement the following logic: if the first neuron fires at 25Hz and the second neuron at 5Hz, the certainty for this prediction is 66%. Conversely, if the network is less certain when the first neuron fires at 30Hz and the second neuron at 29Hz, the certainty is 1/59. We display the network's accuracy for the 100 presented samples and the average certainty.

Computational experiment 4: Overlapping patterns

The pattern recognition experiment is reproduced in the exact same manner except that the second pattern is modified. He has one pixel in common with the pattern one. The accuracy and certainty are computed with the same formula (Figure 7.3).

Receptive fields To estimate the learning progression, we display the receptive field (RF) of each output neuron, as inspired by (Zenke et al., 2015; Gjorgjieva et al., 2009). The RF corresponds to the weight matrix associated with each output neuron or in other words, the weight of the 9 presynaptic neurons onto a given output neuron reshaped in a 3x3 grid matrix. The color of each pixel on the RF is proportional to the synaptic weight wl obtained at the end of each state.

The total weights are normalized between 0 and 1 for each scenario following this equation:

$$\bar{wl} = \frac{wl - wl_{\text{min}}}{wl_{\text{max}} - wl_{\text{min}}}$$

where wl_{min} is 0 and wl_{max} equals 0.18 for S3 and 0.07 for S5.

Computational experiment 5: Effect of the network connectivity

The initial connectivity of the network can impact the outcome of the memory task. We reproduce the same experiment as presented in the previous section with three other different values of l_0 as provided in Table 7.3. The initial value for w_0 is also equal to 0.5.

The parameter plot is providing the value of the accuracy and the certainty at each cycle obtained in the same manner as described in the previous section.

Computational experiment 6: MNIST

Network
We proposed a memory task based on pattern recognition from MNIST dataset (LeCun et al., 1998). The initial dataset of 128x128 pixels is reduced. Five columns and rows are removed from the top, bottom, left and right. We only considered the three first digits (0,1,2). The handwritten digit is binarized; either the pixel is active (white) or inactive (black). Each pixel is associated to an input neuron. Therefore, the network is composed of 100 input neurons connected to three output neurons. An inhibitory neuron is connected via $GABA_A$ and $GABA_B$ currents to all the excitatory neurons with fixed connectivity.

States
The network can be in four different states as done for the previous experiment:

- learning state: During each tonic learning state, M samples are shown during 3 seconds. The succession of patterns can depend on the experiment. Either the same digit is learnt during a tonic period with different samples (Figure 7.5, unique) or random samples of any digit can be shown during the same tonic period (Figure 7.5, random). Input neurons associated to active (inactive) pixels are firing around 55Hz (0.01Hz) following the same stimulation procedure as before. The output neuron associated to the shown digit is also stimulated around 40Hz while the two other output neurons are spiking around 0.01Hz.
- bursting state: the inhibitory neuron is hyperpolarized by a current of -1.2nA/cm^2. The other neurons do not receive any input current.
- inactive state: same as for the pattern recognition task.
- noisy state: same as for the pattern recognition task.

Protocols
A similar protocol as the previous one is implemented. Each tonic learning state is interleaved by either inactive (S1,S4) or bursting state (S2,S3,S5). At the second to last state, a blurry image is shown meaning that all the pixels are moderately active and make each input neuron fire around 15Hz. The last state is either inactive or bursting depending on the model. There are 16 states and 10 samples presented per state. Each sample is shown for 3 seconds.

In Figure 7.6, random samples of the digit 0 are shown at each tonic state except at state 9 where the digit 1 is taught. In Figure 7.11, 10 different samples of a single digit (randomly chosen) are sown during each tonic state. In Figure 7.12, 10 different random samples of any digit are shown during each tonic state. The samples are always randomly selected and might not be the same for different tonic states.

Analysis
To analyse the learning progression, the receptive fields are derived. The weights of the 100 presynaptic neurons onto a given output neuron reshaped in a 10x10 grid matrix. The color of each pixel on the RF is proportional to the synaptic weight wl obtained at the end of each state. The weights are scaled between 0 and 1 with the same equation as before with wl_{max} equal to 3.5e-3 for each scenario in order to compare properly the different evolutions.

7.5 Supplementary Figures

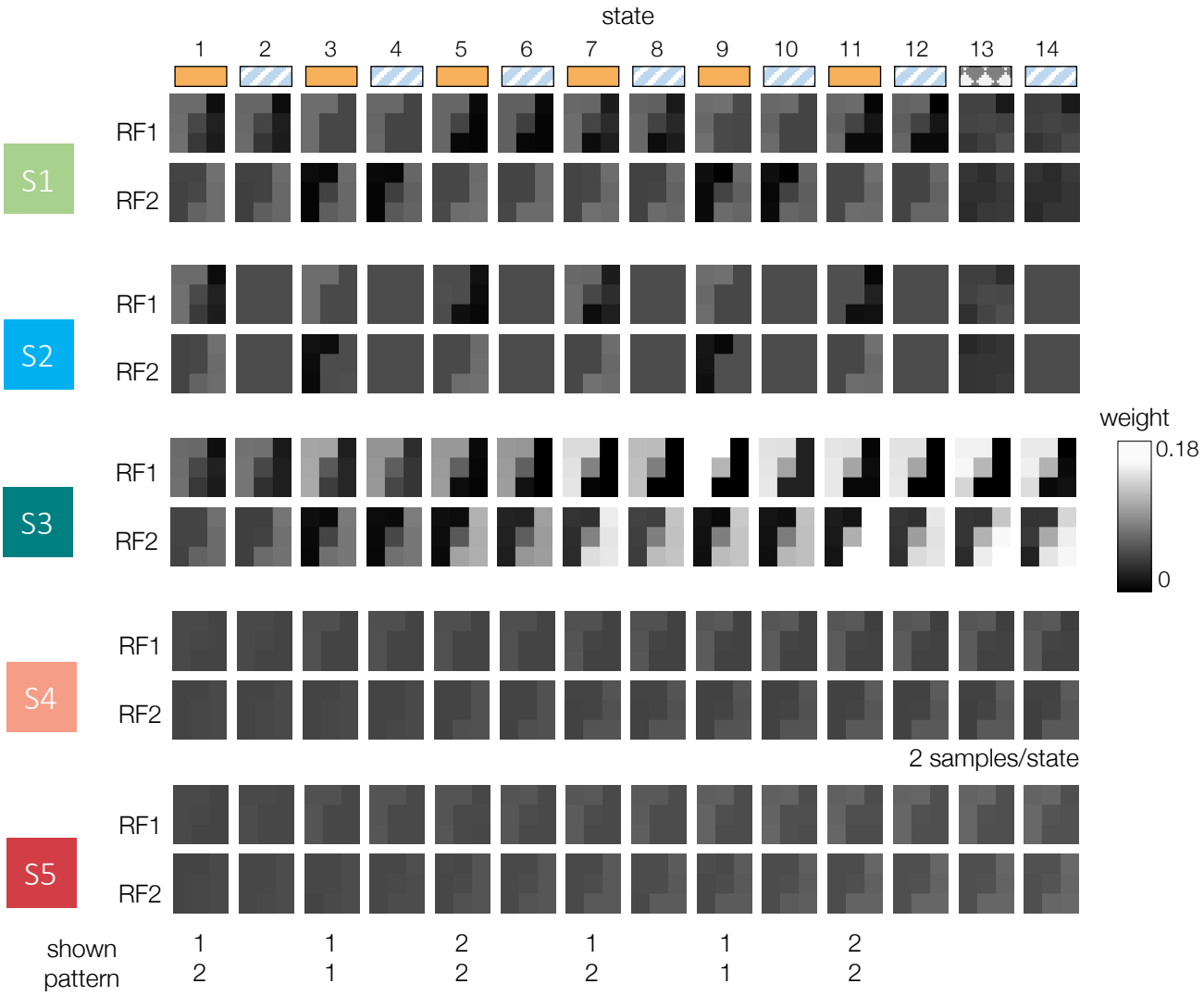

Figure 7.8: Evolution of receptive fields (RF) during successive switches of neuronal activities. Two samples are presented during each tonic state: either the same pattern twice or alternating between the first and second patterns. S1 and S2 are susceptible to noise and exhibit fragility. S2 undergoes RF reset during bursts. S3 demonstrates robust consolidation of the RF. S4 and S5 engage in learning during tonic states. S4 remains unchanged during inactivity, while S5 undergoes non-selective consolidation during bursts, with all weights growing similarly.

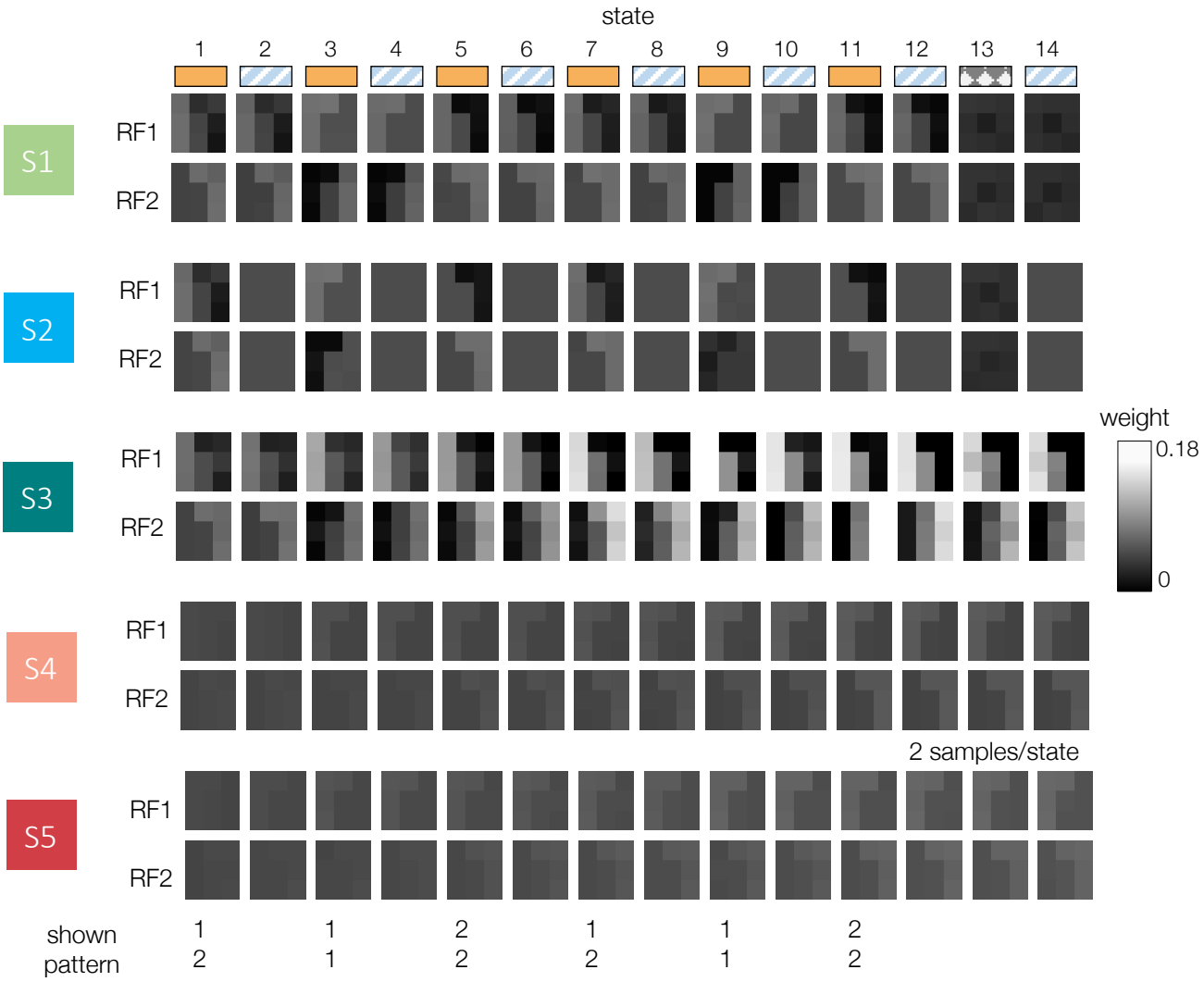

Figure 7.9: Evolution of receptive fields (RF) during successive switches of neuronal activities. Two samples are presented during each tonic state: either the same pattern twice or alternating between the first and second patterns. S1 and S2 are susceptible to noise and exhibit fragility. S2 undergoes RF reset during bursts. S3 demonstrates robust consolidation of the RF except for the overlapping pixel within the two patterns. This pixel gets erased on both RF. S4 and S5 engage in learning during tonic states. S4 remains unchanged during inactivity, while S5 undergoes non-selective consolidation during bursts, with all weights growing similarly.

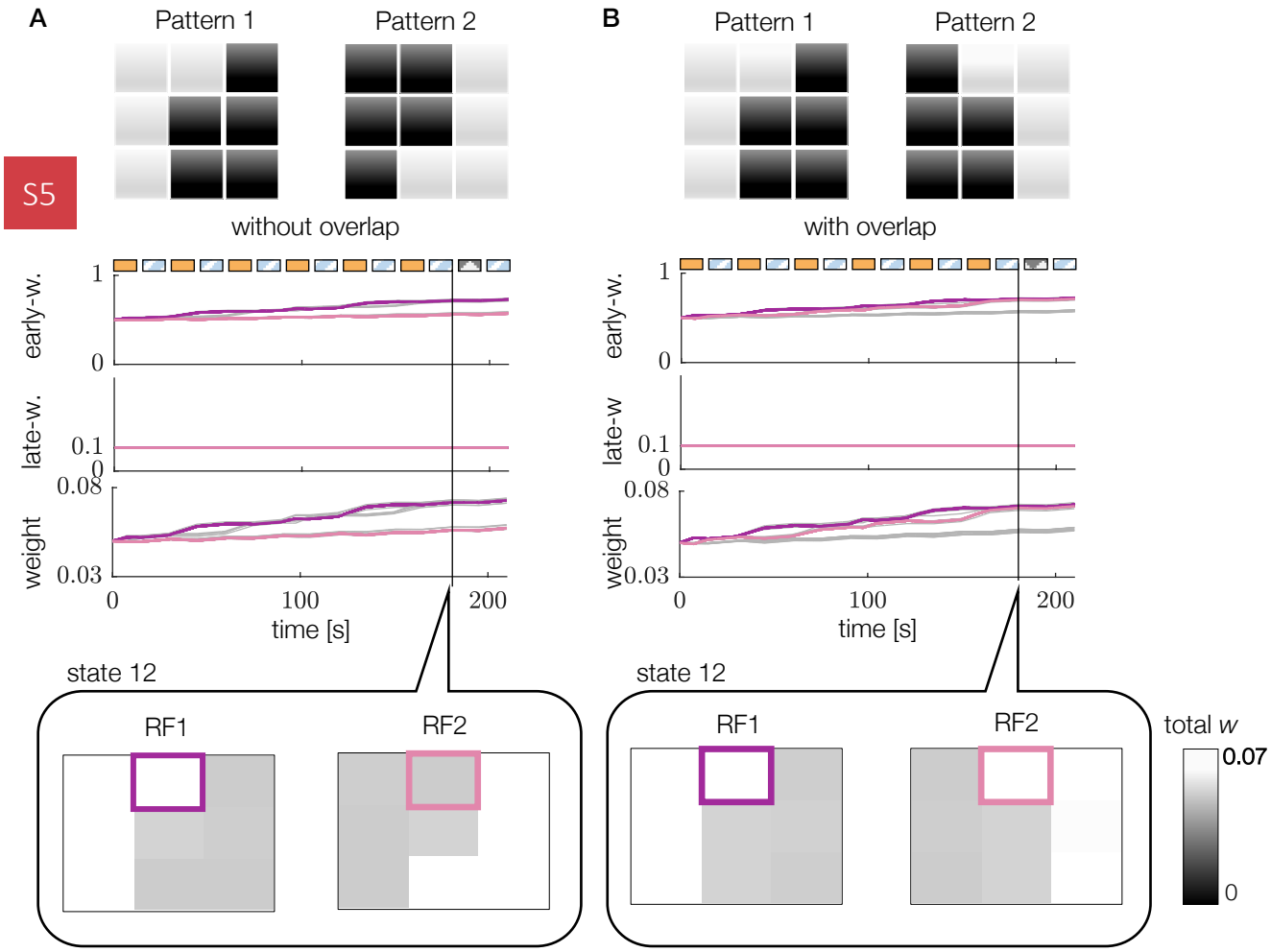

Figure 7.10: Time-evolution of the early-weights, late-weights, and total weights during switches between different states in S5. (bottom) The receptive fields (receptive field (RF)) of the two output neurons exhibit structures that match the learned patterns in both experiments (without or with overlapping patterns, shown in A and B respectively). The weights are growing during bursting showing a non-selective memory consolidation.

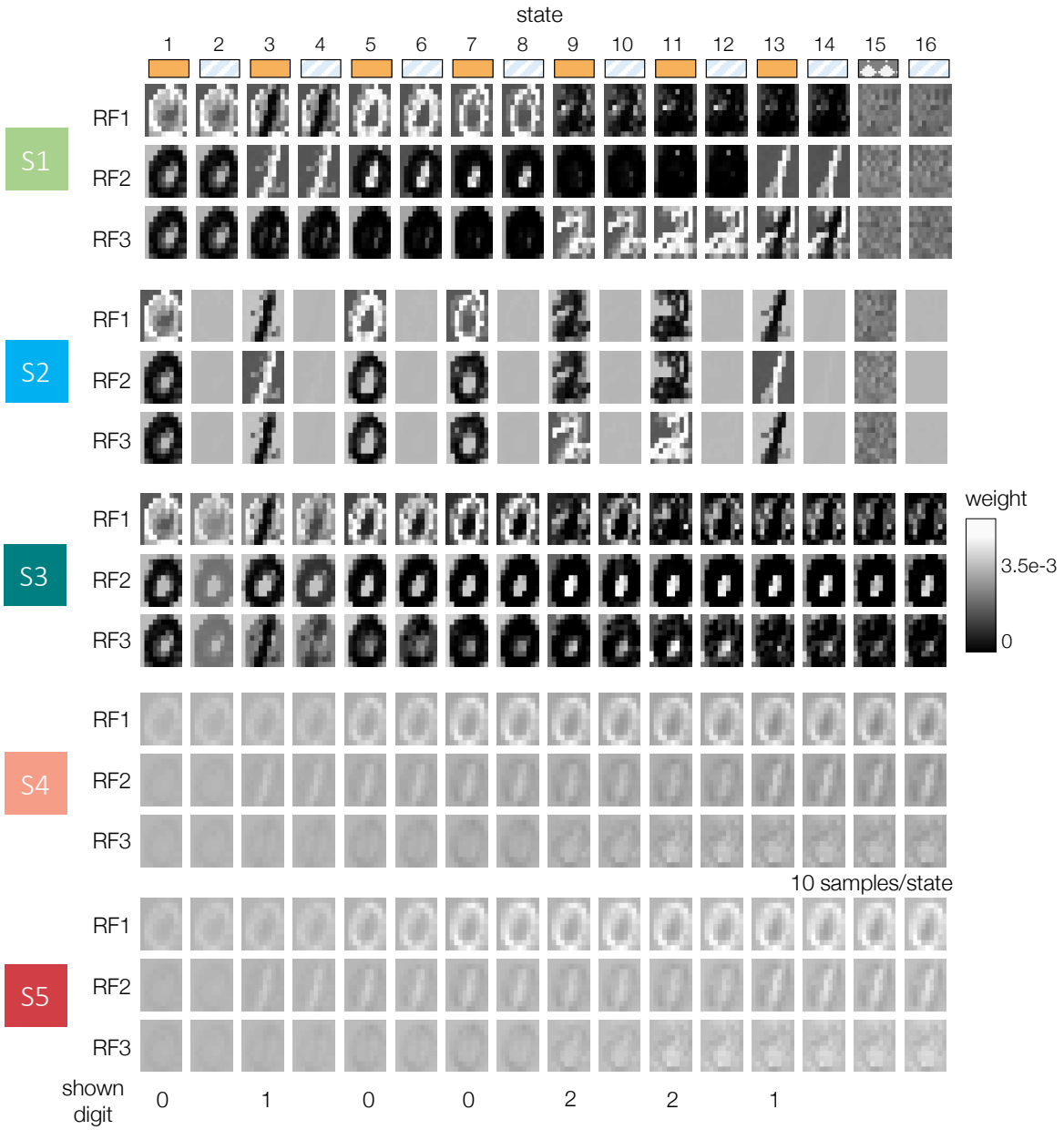

Figure 7.11: Evolution of receptive fields (RF) during successive switches of neuronal activities with the presentation of 10 different samples of a single digit per tonic state. S1 and S2 exhibit sensitivity to noise and tend to forget previously learned digits. S2 undergoes RF reset for all three neurons during bursting. Due to overlapping pixels between the digits, S3 erases shared pixels in each RF (as explained in Figure 7.3E). In contrast, S4 and S5 successfully learn the different digits and subsequently undergo non-selective consolidation, wherein all weights increase by the same amount.

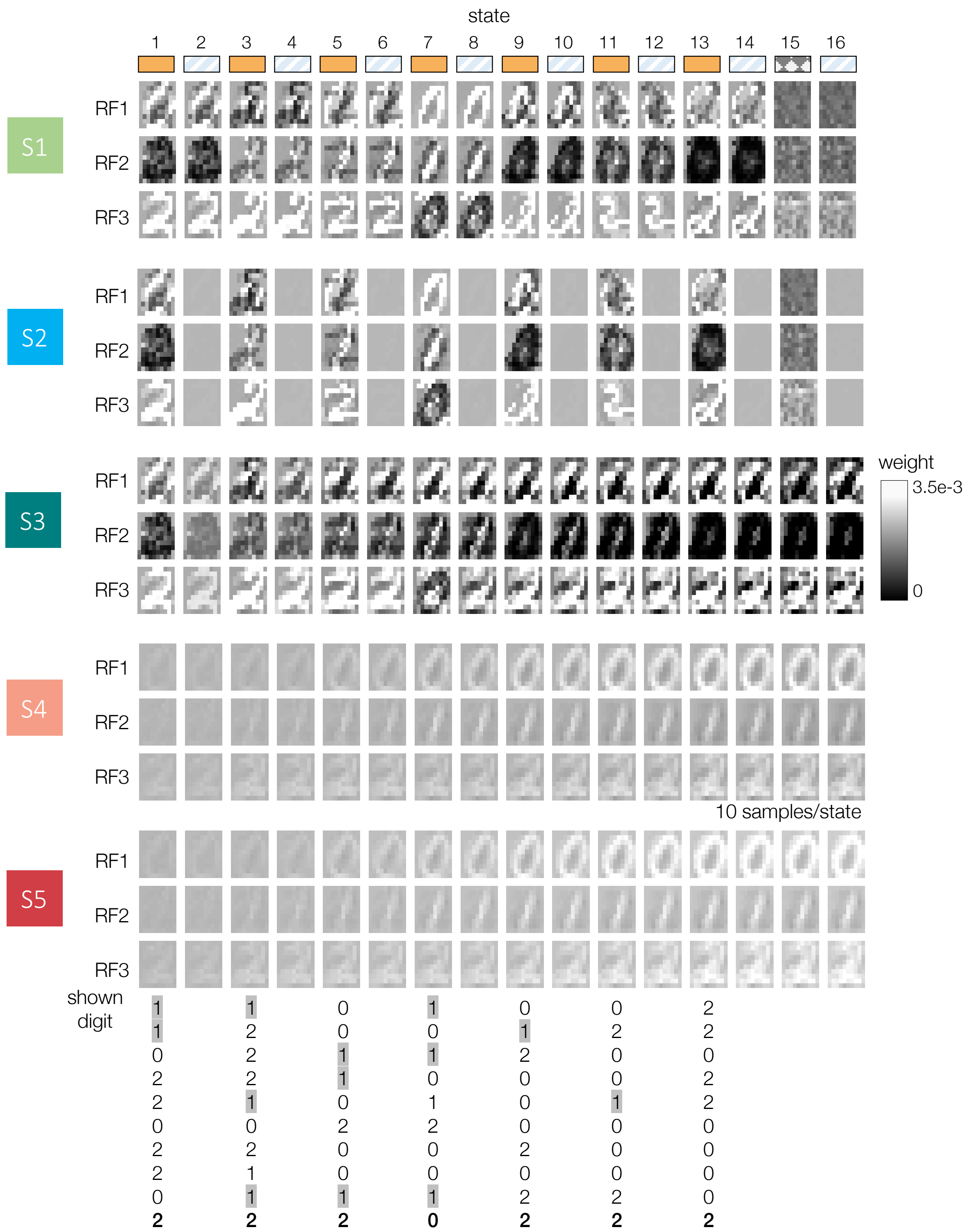

Figure 7.12: Evolution of receptive fields (RF) during successive switches of neuronal activities with the presentation of 10 different samples of any digit per tonic state. S1 and S2 exhibit sensitivity to noise and tend to remember only the last digit shown at the end of the tonic state. S2 undergoes RF reset for all three neurons during bursting. Due to overlapping pixels between the digits, S3 erases shared pixels in each RF (as explained in Figure 7.3E) but this succession of different samples during the same tonic state tends to balance this mechanism. The digit 1 is less shown than the others at the end and resulting in a dark RF. In contrast, S4 and S5 successfully learn the different digits and subsequently undergo non-selective consolidation, wherein all weights increase by the same amount.

CHAPTER 8

Synthesis and Perspectives

This thesis investigates brain-state dependent memory consolidation, specifically focusing on the transitions from active waking to quiet waking. At the neuronal level, it examines the intricate relationship between switches from tonic firing to bursting and synaptic plasticity. Through the utilization of computational models of biophysical neurons, the thesis demonstrates the potential of collective bursting to enhance memory consolidation through structural plasticity.

Overall, this thesis makes a significant contribution to the field of neuroscience. It presents a computational framework that enables the study of brain-state and memory by modeling neurons and their connectivity. This framework not only serves as a valuable tool for experimentalists to design and guide new experiments, but also for researchers in artificial intelligence by shedding light on the underexplored capacity of neurons to operate in different modes and their influence on learning and memory processes.

In this chapter, we synthesize the key results obtained throughout this thesis and provide a discussion on the limitations and future perspectives of this research.

Synthesis

Robust switches in neuronal activity rely on the slow activation of T-type calcium channels.
We discuss the implementation of biophysical neuron models that are compatible with switches in neuronal activity and synaptic plasticity. It emphasizes the importance of a timescale separation in the activation of sodium and T-type calcium channels to maintain robust switches in firing patterns against cellular and network heterogeneity. Computational experiments at the cellular, circuit, and network levels, along with phase-plane analyses performed on six published models, demonstrate that T-type calcium channel activation must occur between the fast activation of sodium channels and the ultraslow inactivation of T-type calcium channels (Chapter 4). The findings of this study not only confirm the results obtained through electrophysiological experiments but also emphasize the crucial importance of accurately representing the kinetics of different ion channels when transitioning from experimental data to computational modeling. It highlights the well-established trade-off between highly complex models with intricate equations and overly simplified models. Striking the right balance becomes essential for developing robust neuron models in computational studies.

Synaptic plasticity rules show limited resilience in the presence of neuronal activity switches or variabilities.
The robustness of current synaptic plasticity rules is examined in the face of neuronal and circuit perturbations, switches in neuronal activity, and neuromodulators. By analyzing a taxonomy of state-of-the-art rules, this chapter explores their similarities and discrepancies. It specifically focuses on qualitatively testing the response of two categories of synaptic plasticity rules, namely phenomenological and calcium-based rules, when subjected to small perturbations. Firstly, a slight change in the bursting pattern is introduced. While the calcium-based rule remains unaffected by this small perturbation, the phenomenological rule produces an opposite response. Secondly, a slight alteration is made to the calcium conductance, and conversely, the phenomenological model remains indifferent to this intrinsic perturbation while the calcium-based rule changes its response entirely. Overall, this chapter aims to question the current state of the art in modeling synaptic plasticity in the presence of small perturbations in firing activity or small changes in neuronal properties.

Furthermore, this part of the thesis raises numerous questions regarding the proliferation of synaptic plasticity rules and their diverse implementations, as well as the impact of fitting these rules to experimental protocols. These obser-

vations underscore the ongoing challenge in neuroscience to comprehensively understand and accurately model synaptic plasticity. The sheer abundance of existing rules and their variations emphasizes the complex nature of this phenomenon and highlights the need for further interactions between experimentalists and theoretical researchers. (Chapter 5).

Synaptic plasticity models using soft-bound during collective bursting activity lead to a homeostatic reset in synaptic weights.
Interactions between switches from asynchronuous tonic firing to collective synchronized bursting and synaptic plasticity models are investigated. We demonstrate that bursting activity leads to a homeostatic reset, causing synaptic weights to return to a fixed baseline value regardless of the initial state. Strong weights depress, and weak weights increase. Mathematical analysis reveals that this reset is rooted in the endogenous nature of synchronized bursting activity combined with soft-bounds synaptic plasticity. The chapter also proposes a potential mechanism for the Synaptic Tagging and Capture hypothesis by leveraging the homeostatic reset induced by neuromodulator-driven changes in synaptic rules (Chapter 6).

The homeostatic reset combined with structural plasticity enhances memory consolidation
We exploit the mechanism of homeostatic reset for memory consolidation by introducing a burst-driven structural plasticity model. While traditional synaptic plasticity rules primarily focus on dynamically regulating synaptic weights during Early Long-Term Potentiation (E-LTP), this chapter presents a novel structural plasticity model that takes into account changes in spine morphology and the synthesis of new proteins during bursting activity, thereby explaining Late Long-Term Potentiation (L-LTP). Active waking, characterized by asynchronous tonic firing activity, allows for learning and the formation of new memories through E-LTP, which is modeled by traditional synaptic plasticity rules. In contrast, quiet waking provides a state in which neurons do not receive external inputs, enabling them to enter a collective synchronized bursting mode that facilitates L-LTP. To demonstrate this, we develop a burst-driven structural plasticity rule that drives memory consolidation.

In summary, the intricate interplay between switches from tonic firing to bursting, combined with the integration of E-LTP (traditional rule) and L-LTP (structural rule), holds significant potential to enhance memory consolidation across various memory tasks (Chapter 7).

The illustration on the next page proposes a roadmap between the different contributions and results proposed through my PhD thesis

Brain-state

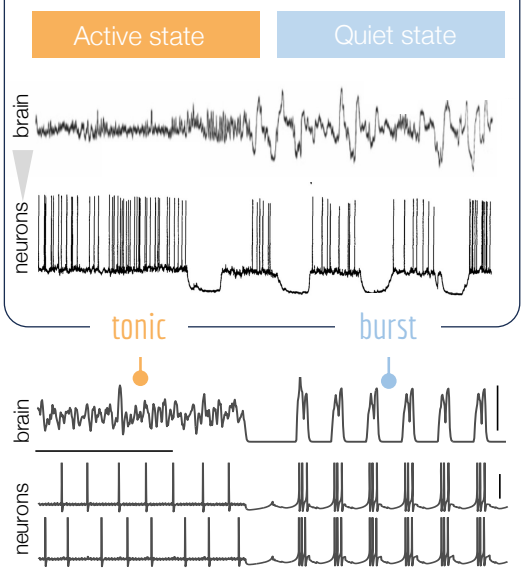

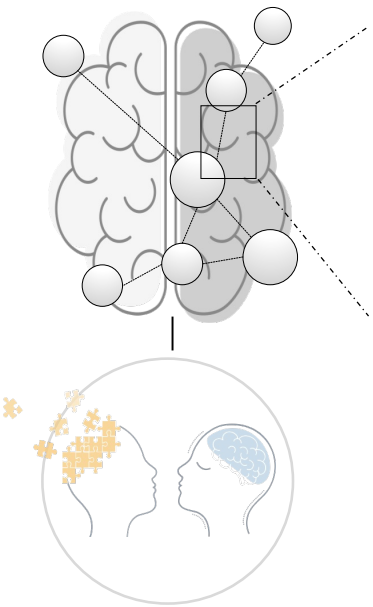

Memory

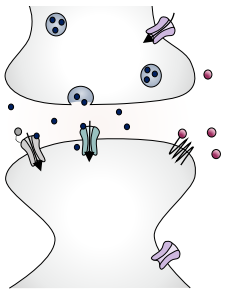

synaptic plasticity

Neuron activities → Black Box modeling → w

Chapter 4

How to guarantee robust switches in neuronal activities in the presence of plasticity and variability?

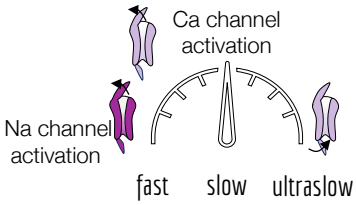

Timescale separation between ion channel activations

Chapter 5

Are existing synaptic plasticity rules compatible with neuronal variabilities and switches?

- Literature review
- Taxonomy of the different rules

- Minors neuronal variabilities lead to different outcomes depending on the synaptic rules
- Combined work between experimental and computational becomes crucial.

Interplay between switches from tonic firing to bursting & synaptic plasticity

Chapter 6

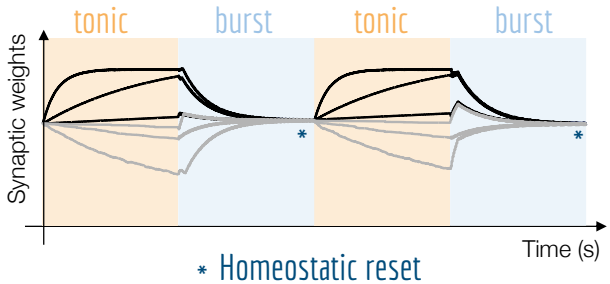

* Homeostatic reset

Observations

Strong weights depress and weak weights potentiate during bursting

Causes

- Collective bursting activity combined with
- any synaptic rule using *soft bounds*

Tests

- Robust to neuronal variabilities and network heterogeneity
- Mathematical analyses to predict the homeostatic reset
- Neuromodulation can upscale the reset for strong weights.

Chapter 7

Is the homeostatic reset a bad or a good feature for memory consolidation?

Bad feature

Learning acquired during active waking (tonic) is forgotten during quiet waking (burst).

Solution 1
Blocking Burst

X Memory is not consolidated

Solution 2
Replace soft-bounds by hard-bounds

? Non-selective memory consolidation and poor SNR

Good feature

Quiet waking helps to restore synaptic to learn new information, but memory must be stored.

Solution 3
A novel burst-driven structural plasticity rule that exploits the reset

✓ Quiet waking restores spine efficiency and changes spine morphology.

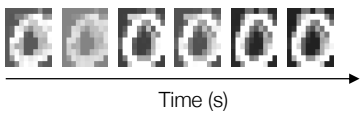

Perspectives

This thesis embarks on a challenging exploration of two fundamental domains in neuroscience: brain states and memory, employing a computational approach. Models, with their inherent flexibility and capacity to simulate scenarios based on experimental findings and unknowns, serve as a valuable tool, albeit constrained by computational resources (Poirazi and Papoutsi, 2020). While the modeling approach has enabled us to investigate brain states and memory, it is crucial to acknowledge that no model is perfect. Therefore, the main focus of future work in this thesis lies in further exploring and refining the assumptions underlying our models. By delving deeper into these assumptions, we can enhance our understanding and refine the models to better capture the intricacies of brain states and memory processes.

Incorporating a more detailed model of calcium dynamics

Selecting a synaptic plasticity rule for a specific application is not a straightforward process (Chapters 3 and 5). In this thesis, we opted to compare different rules to avoid drawing hasty conclusions that could indicate fragility in the synaptic rule models. Therefore, we employed both phenomenological rules (such as pair-based and triplet rules) and calcium-based rules. These rules yielded similar outcomes during switches from tonic firing to bursting, ensuring that our results are independent of the specific type of synaptic plasticity rules employed.

As outlined in Chapter 2, calcium dynamics play a crucial role in synaptic plasticity. In this thesis, we utilized a simplified calcium dynamics model based on the work by (Graupner et al., 2016). This model translates pre- and postsynaptic spikes into calcium spikes followed by decay. Although this current calcium dynamics model has shown success in simulating synaptic plasticity under tonic firing conditions and replicating experimental data, it remains somewhat phenomenological and fails to capture the full complexity of calcium signaling within neurons. Therefore, there is room for improvement by incorporating more realistic calcium fluctuations. To enhance the accuracy of synaptic plasticity models, future work could consider additional factors, such as calcium microdomains within dendritic spines (Poirazi and Kastellakis, 2017), and incorporate calcium from various sources, including voltage-dependent calcium channels and NMDA receptors. This avenue of research was initiated by Chloé Marchal, a graduate student in biomedical engineering, in her master's thesis.

Dendrites are the command center of synaptic changes

Chapter 2 introduced dendrites as key components in synaptic transmission. These intricate structures serve as the command center for both early and late changes in synaptic plasticity. Within dendrites, postsynaptic receptors play a critical role, exhibiting varying efficiency and size. Then, dendrites are also being capable of undergoing significant morphological changes. Although this thesis has primarily focused on modeling neurons as single units using the Hodgkin and Huxley formalism, the recent prominence of dendrites in both biological and modeling research (Kirchner and Gjorgjieva, 2022; Acharya et al., 2022; Poirazi and Papoutsi, 2020; Petousakis et al., 2022) makes their inclusion a compelling and coherent extension to our model. By incorporating dendrites, we can better characterize calcium dynamics and gain a more precise understanding of how bursting activity relates to structural plasticity. This expansion holds promise for refining and enriching our model's capacity to explore the complexities of synaptic plasticity and neuronal function.

Generalizing our results in a bigger architecture with recurrent connections

Brain-state and memory processes are intricately tied to the functioning of individual neurons. While some approaches focus on modeling global brain activity and memory, our thesis takes a closer look at the underlying neuronal mechanisms. To capture the dynamics of interconnected neurons, our model includes both inhibitory and excitatory neurons. The investigation of learning and memory predominantly revolves around the excitatory connections in a feedforward manner, as this configuration is often observed in associative memory tasks. In Chapter 7, we opted for the feedforward configuration to specifically address associative memory tasks.

Although our current model features a feedforward architecture, incorporating recurrent connections into the network would enhance its realism (Gjorgjieva et al., 2016b). In fact, in Chapter 4, we have already demonstrated the robust ability of a recurrent neural network configuration to switch between different states. Notably, the strengths of the recurrent connections did not hinder the switching ability.

For future work, expanding the model to include recurrent connections and scaling up the network size would be an intriguing extension of this project. Such enhancements are likely to reinforce the core message of the thesis without altering its overall significance.

Incorporating various forms of synaptic plasticity: intrinsic, inhibitory and homeostatic

Furthermore, to gain a comprehensive understanding of the role of switches from tonic firing to bursting and synaptic plasticity, it is necessary to explore the integration of other mechanisms, such as intrinsic plasticity, homeostatic plasticity, and inhibitory plasticity.

Firstly, intrinsic plasticity holds great potential for advancing this project and further exploring its implications. It has been established that neurons possess a remarkable ability to regulate their intrinsic parameters, such as ion channel conductances, to facilitate memory storage while maintaining a target activity level, known as intrinsic homeostatic plasticity. Various computational models have proposed dynamic adjustments of ionic conductance to ensure a consistent calcium level within the neuron (Liu et al., 1998; O'Leary et al., 2014). Additionally, neurons exhibit degeneracy, allowing them to operate effectively within a wide range of parameter values while still achieving the desired function (Prinz et al., 2004). These concepts are particularly relevant in our research context. Notably, we have observed distinct profiles in calcium dynamics during tonic firing and bursting activities (Figure 3.10). Furthermore, Figure 5.4 reveals that alterations in ion channel conductances have minimal impact on tonic firing due to the degeneracy and robustness of the neuron. However, these alterations can significantly affect the outcome of synaptic plasticity when using calcium-based models. It is worth noting that changes in calcium conductance may also influence calcium fluctuations during bursting, thereby potentially influencing the outcome of synaptic plasticity. Collectively, these findings raise questions about the intricate interplay among neuronal activities, synaptic plasticity, and intrinsic plasticity, highlighting their crucial role in ensuring the proper operation of neurons and circuits and supporting memory consolidation.

In this thesis, our focus was solely on excitatory synaptic plasticity, employing a Hebbian learning rule between excitatory neurons. However, Hebbian learning is known for its inherent instability. Neurons encode external stimuli and strengthen their connections, resulting in an amplification of firing rates within the network, commonly referred to as Hebbian runaway dynamics (Turrigiano and Nelson, 2004). This phenomenon is well-characterized in tonic firing (Turrigiano et al., 1994). In bursting, a presynaptic neuron spike within the burst triggers a postsynaptic neuron spike, it simply contributes to the population of spikes comprising the endogenous burst of the postsynaptic neuron. As mentioned in Chapter 5, the presence of the reset in synaptic weights is independent of the number of spikes per burst. A stronger connectivity within the network, resulting from strong Hebbian learning during tonic firing, simply shifts the reset value to a different magnitude for traditional plasticity rules that use soft-bounds or adjusts the slope of change for rules that use hard-bounds. This Hebbian runaway dynamics poses an inherent problem in tonic firing associated with learning.

To address this issue, homeostatic solutions are often employed, such as synaptic scaling or the imposition of maximal connectivity within the network to prevent excessive firing activity during learning. In Chapter 7 of this thesis, while learning the MNIST dataset, we configure our network in a subthreshold setup. This means that presynaptic neuron spikes only elicit subthreshold activity in the postsynaptic neuron (i.e., an EPSP response) without triggering an action potential. We ensure that the acquired learning maintains the network in this subthreshold configuration. In contrast, initializing the network with strong initial connectivity clearly demonstrates the Hebbian runaway dynamics during tonic firing. This parameterization was remarkably deepen by Emmy Kellens, a graduate student in biomedical engineering, in her master's thesis. She demonstrated the impact of Hebbian runaway dynamics during tonic learning and confirmed that it originates from the design of the traditional synaptic plasticity rule itself, which has been implemented for many years. In this thesis, we have to face this issue and to pay attention while designing our memory task as a side-problem.

An interesting avenue of research to address this issue more robustly is the incorporation of inhibitory plasticity (Miehl et al., 2022; Wu et al., 2022; Miehl and Gjorgjieva, 2022). Studies such as (Miehl and Gjorgjieva, 2022) have proposed mechanisms of inhibitory plasticity that can effectively counteract uncontrolled positive feedback in neural circuits. In our circuit, the inhibitory neuron has fixed connectivity with the excitatory neurons, and hyperpolarizing this neuron drives the collective bursting activity in the circuit. In our previous work (Jacquerie and Drion, 2021), we demonstrated the robustness of this circuit to changes in inhibitory connections. Therefore, our model can be expanded by incorporating switches in neuronal activities, excitatory plasticity, and inhibitory plasticity. This type of additional inhibitory plasticity is likely to help prevent runaway dynamics in the circuit's rhythm. It operates in the same direction as excitatory plasticity to counteract the runaway dynamics of excitatory weights and can effectively regulate the firing rates of the excitatory population. Furthermore, it enables flexible learning, as demonstrated in (Miehl and Gjorgjieva, 2022). Exploring the behavior of inhibitory plasticity during bursting and its interactions with the findings obtained in this thesis would be an interesting future project.

Combining multiple synaptic plasticity mechanisms is really trendy in computational neuroscience. Indeed, only using an hebbian traditional synaptic plasticity rule limits the understanding of learning and memory, as previously discussed. Several researchs interstingly combine differnt rules and deeper dig into understanding the interactions between all these rules (Zenke et al., 2015; Fauth and Van Rossum, 2019)

Switches between neuronal activities, reflecting transition in brain states have potential in many research fields
This thesis paves the way for future research in various fields, including neuroscience, machine learning, and neuromorphic engineering (Figure 8.1).

In experimental neuroscience, this work paves the way for new avenues of research; by driving experiments focused on switches in neuronal activities and plasticity, while also providing computational support for further many researches in neuroscience involving switches in brain-states, switches in neuronal activities, plasticity, and memory.

Current experimental protocols in plasticity research predominantly rely on controlled and standardized paradigms, as discussed in Chapters 3 and 5. However, the shifts between different brain states present captivating opportunities for open-ended exploration and in vivo recording of bursting plasticity. Moreover, this thesis encourages deeper investigations at the molecular level, aiming to delve into the underlying processes and potentially unravel the mechanisms behind the homeostatic reset phenomenon.

This thesis serves as a powerful computational tool that expands research possibilities. Notably, within the developing cerebral cortex, there is a prevalence of spontaneous and sensory-evoked spindle bursts (Yang et al., 2016), and this thesis can provide support for understanding the intricate interplay between bursting activity in newborns and plasticity. Additionally, the use of computational models becomes particularly relevant in exploring the increase in creativity observed during offline periods (Lacaux et al., 2019).

Ultimately, a close collaboration between computational and experimental neuroscientists is imperative to acquire a profound understanding of the biophysical mechanisms that govern brain-state switches and the complex dynamics of memory consolidation. By combining computational tools with experimental approaches, researchers can further unravel the mysteries of neuronal activities and their impact on plasticity, leading to significant advancements in our understanding of brain function and cognition.

Artificial intelligence shows increasing potential in our life. However, it still lacks of adaptability in changing environments as shown in the Hapless Boston Dynamics robot (video (URL, i)). Drawing inspiration from our brain helps to develop better algorithms. For example, neuromodulation was introduced in (Vecoven et al., 2020; Shine et al., 2021). Here, we claim that switches in neuronal activities also hold relevance in the context of artificial intelligence. Current algorithms in machine learning rely on active learning to train artificial neural networks. However, it is not how our brain operates. We alternative periods of active waking with learning and engaged consciousness, with periods of quiet waking with reduced consciousness. This work aims to catalyze further research in the field by emulating the dynamic nature of the brain and investigating the integration of switches in neuronal activities into artificial neural networks. By employing spiking neural networks capable of transitioning from spiking to bursting, we can develop more versatile machine learning algorithms that exhibit adaptability to changing environments.

Moreover, the impact of switches in neuronal activities extends to neuromorphic engineering, which strives to develop hardware systems that emulate the intricate functionalities of the brain. By exploiting the potential of silicon neurons and designing circuits that faithfully replicate the behavior of biological neurons (Dias et al., 2021), researchers can exploit the power of switches on brain states to create highly efficient and intelligent systems. In the current context of an electrical crisis, the development of energy-efficient technologies takes on heightened importance. These neuromorphic architectures possess the potential to revolutionize a range of fields, including robotics, sensor technology, and artificial intelligence. A deeper understanding of brain states and plasticity can lay the groundwork for future endeavors, such as chip-state dependent memory, further pushing the boundaries of neuromorphic engineering.

In summary, switches in neuronal activities offer rich avenues for research and innovation across biology, neuroscience, machine learning, and neuromorphic engineering. By exploring the interplay between switches in brain state and memory and their implications in various contexts, this thesis sets the stage for interdisciplinary collaboration, pushing the boundaries of scientific knowledge and technological innovation.

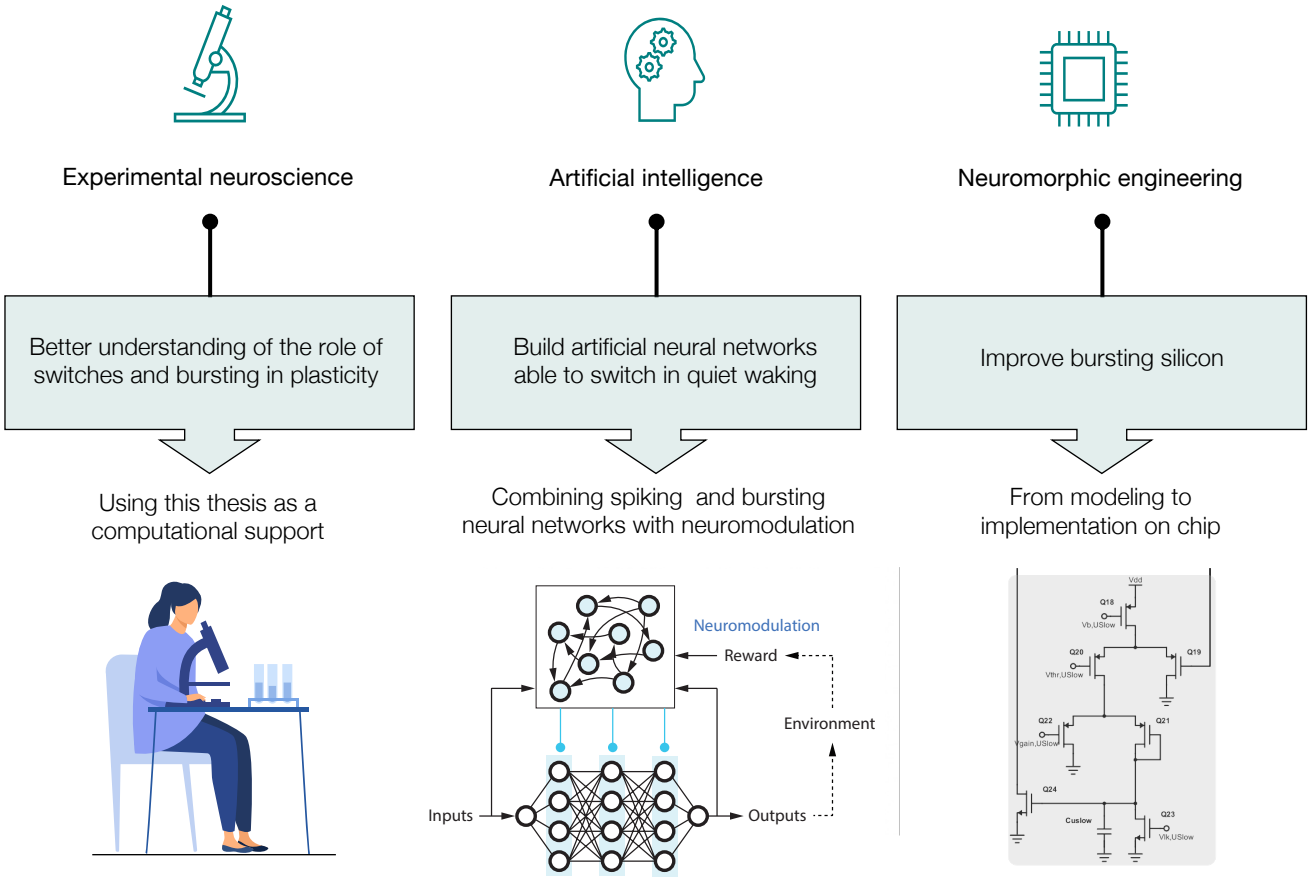

Figure 8.1: Investigation the role of switches in brain-states, switches in neuronal activities on memory has the potentiation in experimental neuroscience, artificial intelligence, and neuromorphic engineering. Artwork from pch.vector/freepik, (Vecoven et al., 2020) and LTSpice from Loris Mendolia.

Conclusions

Learning and memory are processes that occur continuously in our daily lives. They play a crucial role from retaining our childhood memories to shaping our critical thinking abilities. When memorizing new information, it is commonly assumed that the more effort and time we invest, the better our performance will be. However, it turns out that taking occasional breaks associated with a restful brain may be precisely what we require. This thesis, employing biophysical neuron models, illuminates the significance of these quiet periods in reinforcing the memories formed during active learning states.

APPENDIX A

Side projects

In addition to my PhD research, I actively engaged in three types of side projects: analyzing channelopathies, serving as a teaching assistant, and supervising master's students for their theses.

Under the guidance of Professor Seutin at GIGA Neuroscience, I entered the world of experimental neuroscience, initially focusing on data analysis and later conducting experimental recordings related to channelopathies. This experience expanded through collaboration with Professor Lory at the Institute of Functional Genomics.

Parallel to my research, I served as a teaching assistant for the course "Introduction to Signals and Systems" for five years. To enhance learning, I created a companion book with theoretical reviews and exercises accessed at `https://hdl.handle.net/2268/264163`.

Additionally, I had the opportunity to supervise nine talented young women pursuing biomedical engineering degrees for their master's theses, directly related to my PhD projects.

These side projects were invaluable, allowing me to develop skills in experimental neuroscience and teaching.

A.1 Analysis of channelopathies

A.1.1 Myotonia congenita

My first side project was related to the analysis of a ion channel mutation done in collaboration with Professor Vincent Seutin and Doctor Kevin Jehasse. This section is adapted from (Jehasse et al., 2021):
"Functional analysis of the F337C mutation in the CLCN1 gene associated with dominant myotonia congenita reveals an alteration of the macroscopic conductance and voltage dependence"

Kevin Jehasse[1], Kathleen Jacquerie [2], Alice de Froidmont[1], Camille Lemoine[1], and Thierry Grisar[3], Katrien Stouffs[4], Bernard Lakaye[3] and Vincent Seutin[1].

[1] Laboratory of Neurophysiology, GIGA Institute, Liege, Belgium; [2] Department of Electrical Engineering and Computer Science, Liège University, Liège, Belgium; [3] Laboratory of Molecular Regulation of Neurogenesis, GIGA Institute, Liège, Belgium; 4 Neurogenetics Research Group, Vrije Universiteit Brussel (VUB, Universitair Ziekenhuis Brussel (UZ Brussel), Reproduction and Genetics, Brussels, Belgium

Molecular Genetics and Genomic Medicine.
28 January 2021
doi: 10.1002/mgg3.1588

keywords: channel gating, CLCN1, microscopy, myotonia, patch clamp

Abstract
Background: Myotonia congenita (MC) is a common channelopathy affecting skeletal muscle and which is due to pathogenic variants within the CLCN1 gene. Various alterations in the function of the channel have been reported and we here illustrate a novel one.
Methods: A patient presenting the symptoms of myotonia congenita was shown to bear a new heterozygous missense variant in exon 9 of the CLCN1 gene (c.1010 T > G, p.(Phe337Cys)). Confocal imaging and patch clamp recordings of transiently transfected HEK293 cells were used to functionally analyze the effect of this variant on channel properties.
Results: Confocal imaging showed that the F337C mutant incorporated as well as the WT channel into the plasma membrane. However, in patch clamp, we observed a smaller conductance for F337C at -80mV. We also found a marked reduction of the fast gating component in the mutant channels, as well as an overall reduced voltage dependence.
Conclusion: To our knowledge, this is the first report of a mixed alteration in the biophysical properties of hClC-1 consisting of a reduced conductance at resting potential and an almost abolished voltage dependence.

Contributions
Myotonia Congenita is the most common genetic channelopathy affecting altering the skeletal muscle. As a reminder, a channelopathy is a disease defecting an ion channel caused by genetic or external factors. Here, "CLCN1 gene" (OMIM accession number 118425), which encodes the ClC-1 channel protein, a chloride ion channel. This channel mainly contributes to the resting conductance of skeletal muscle.

Kevin Jehasse performed patch clamp recordings on transfected HEK293 cells (human embryonic kidney, used as cultured cells) to investigate the effect of this variant on the channel properties. He compared the mutant channel with the wild-type (WT) and a mixed transfection of WT and mutant channels.

Based on the current traces current-voltage curves of the instantaneous and steady state currents, I performed two data analyses on MATLAB (Figure A.1):
(i) I computed the apparent open probability voltage curve (P_o). As a reminder, it measures of the likelihood that a single ion channel will be open at any given time. It is defined as the fraction of time that the channel spends in the open state. It helps to understand the voltage dependence of channel activation as a function of the pre-pulse voltage ranging from -200mV to 90mV. The fitting was done via:

$$P_o(V) = \text{Min} + \frac{1 - \text{Min}}{1 + \exp((V_{1/2} - V)/S}$$

where Min is the minimal value of P_o, $V_{1/2}$ is the half-maximal activation potential, and S is the slope factor (Figure A.1(d)).

(ii) I analyzed the time course of current deactivation. I fitted the decay of currents elicited between -200 and -60 mV with a sum of two exponential and a time-independent component. The following equation was used :

$$I(t) = A_{\text{fast}} \exp(-t/\tau_{\text{fast}}) + A_{\text{slow}} \exp(-t/\tau_{\text{slow}}) + C$$

where τ_{fast} and τ_{slow} are the time constants of the fast and slow components of current relaxation/deactivation, and A_{fast}, A_{slow}, are the weights of the fast and slow components, and C is the steady-state component of the current. Relative A_{fast}, A_{slow}, and C were defined as the ratio of the parameter on the sum of A_{fast}, A_{slow}, and C (Figure A.1(e)).

A.1.2 Paramyotonia congenita

My PhD project included a parenthesis in which I had the opportunity to work with Professor Vincent Seutin on the functional characterization of a Nav1.4 channel mutation responsible for paramyotonia congenita, using whole-cell patch-clamp recordings on HEK 293 cells. This project allowed me to explore a channelopathy related to sodium channels and gain valuable experience in the experimental side of neuroscience.

Professor Seutin taught me how to perform patch-clamp recordings, which would not have been possible without the guidance of Laura Robaye, who helped me with solution preparation, set up and the patch clamp recording, and Laura Vandries, who provided me with the transfected cells. I am grateful for their support, which opened me the doors of experimental neuroscience.

Working on this project showed me the fundamental importance of rigor in experimental manipulations. I learned to appreciate the variability in the data not as something to be avoided but as a robustness of the experimental approach. This variability should be reflected in the models we build, as it can provide insights into the mechanisms underlying the phenomena we study.

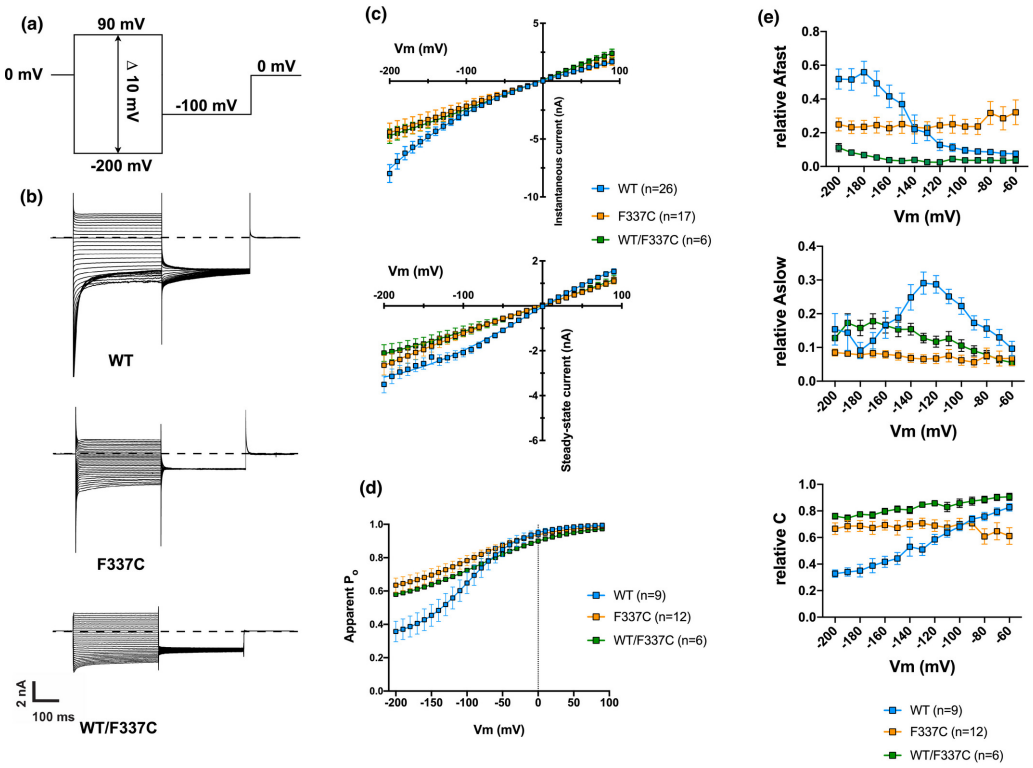

Figure A.1: Functional analysis of the control ion channel and its mutation. More detailed in (Jehasse et al., 2021)

A.1.3 Cerebellar atrophy cause by mutations on calcium channels

I was contacted by Prof. Philippe Lory from the Institute of Functional Genomics (IGF) in Montpellier. He is working in the department of Neurosciences focusing on ion channels in neuronal excitability and diseases. His research focuses of cerebellar atrophy. The gene CACNA1G encodes the Cav3.1 subunit of T-Type calcium channels expressing in Purkinje neurons and deep cerebellar nuclei. Mutations impaired the appropriate neuronal behavior by modifying the ion channel kinetics (Chemin et al., 2018). I am currently implementing their physiological data on the conductance-based model I developed in (Jacquerie and Drion, 2021) to gain a better insight into the disease mechanisms.

It is an incredible collaboration merging the IGF skills in electrophysiology recordings, their knowledge related to ion channel behaviors and my computational skills combined with my good understanding of conductance-based models. The mutant channel shows a pathological excitability which is completely coherent with the experimental observation. Further experimental and computational analyses are under progress with Clement Marchal and Amael Dakavan, PhD students at the IGF.

A.1.4 Framework to study channelopathy

In the future, my goal is to continue collaborating with Professors Vincent Seutin and Philippe Lory and further bridge the gap between experimental and computational neuroscience. Specifically, I plan to develop a comprehensive framework for incorporating various channel mutations into conductance-based models, aiming to gain a better understanding of how these mutations affect neuronal excitability. This framework will enable experimentalists to integrate their mutated channels into the models and directly compare their pharmacological findings with the model simulations. I have already begun working on this framework during the master thesis of Pauline Garcia Garcia, which involves reproducing pharmacological experiments on a conductance-based model of the dopaminergic neuron.

A.2 Master thesis supervision

Supervising master thesis was one of the most valuable part of my PhD. I had the opportunity to be in charge of nine brilliant master students in Biomedical Engineering.

In 2021-2022:

- Caroline Minne: "Interactions between synaptic plasticity and switches in brain states for memory consolidation: a modeling study" http://hdl.handle.net/2268.2/11471
- Chloé Marchal: "Modeling calcium-dependent synaptic plasticity and its role in sleep-dependent memory consolidation" http://hdl.handle.net/2268.2/11513
- Chloé Preud'homme: "Modeling of the interaction between neuronal populations involved in memory consolidation during the sleep-wake switch" http://hdl.handle.net/2268.2/11559

In 2022-2023:

- Juliette Ponnet: "Neuromodulation of calcium-based plasticity rules" http://hdl.handle.net/2268.2/14570. This project obtained the award of the Association des Ingénieurs de Montefiore (AIM) best master thesis.
- Nora Benghalem: "Neuromodulation of phenomenological plasticity rules" http://hdl.handle.net/2268.2/14373
- Nora Sautois: "Implementation of heterosynaptic plasticity in biological neuron models and application in the context of allodynia" http://hdl.handle.net/2268.2/14394
- Pauline Garcia-Garcia Modeling and dynamical analysis of dopaminergic neuron activity and its role in reward quantification http://hdl.handle.net/2268.2/14511

In 2022-2023:

- Emmy Kellens "Modeling memory tasks in a biophysical neuron network"
- Justine Magis "Modeling a burst-induced structural synaptic plasticity"

I participated in weekly progress meetings. In addition, I guided them during their literature review or with their codes to obtain meaningful results. Their projects were complementary to my PhD project. Most of these master theses were presented at different conferences or inserted in publications which revealed the good quality of their researches.

APPENDIX B

The brain and its main structures

Throughout the thesis, certain brain structures are mentioned without further elaboration. In this section, I provide a brief overview of their location and respective roles.

- *basal ganglia*: collection of structures located deep within the brain that are involved in the control of movement, particularly in the initiation and suppression of movements.
- the *striatum* is involved in the control of movement, it sends output to the motor cortex.
- *brainstem* is composed of the midbrain, pons and medulla, it connects the brain to the spinal cord the
- the *locus coeruleus*, inside the pons, is involved in the regulation of attention and arousal. It releases the neurotransmitter norepinephrine, which can modulate the activity of other brain regions.
- the *basal forebrain* involved in the regulation of attention, learning, and memory. It contains several different nuclei that release the neurotransmitter acetylcholine.
- the *nucleus basalis of Meynert* is a group of neurons located in the basal forebrain that release acetylcholine and play an important role in attention and memory.
- the *amygdala*, in the temporal lobe, is involved in the processing of emotions, particularly fear and anxiety.
- the *raphe nuclei* is a collection of nuclei located in the brainstem that release the neurotransmitter serotonin. They are involved in the regulation of mood, sleep, and appetite)
- the *substantia nigra* is a structure located in the midbrain that is involved in the control of movement. It releases the neurotransmitter dopamine, which is important for the initiation and control of voluntary movements.)
- the *ventral tegmental area* is a group of neurons located in the midbrain that release dopamine and play an important role in reward processing and motivation.
- the *hypothalamus* is a small structure located near the base of the brain that plays a crucial role in regulating many physiological processes, such as hunger or thirst.

APPENDIX C

Phase plane analysis: a powerful tool

In Chapter 4, I conducted a dynamic system analysis on a reduced neuron model, employing phase plane analysis to gain insights into the significance of T-type calcium channels (Jacquerie and Drion, 2021).

This section introduces the toolbox for comprehending nonlinear systems analysis, based on a booklet of the lecture 'Introduction to Signals and Systems' (fr: Introduction aux signaux et systèmes) `https://hdl.handle.net/2268/264163`.

Mathematical reminders

We start with a non-linear system of two variables x_1 and x_2 such as :

$$\begin{cases} \dot{x}_1 &= f_1(x_1, x_2) \\ \dot{x}_2 &= f_2(x_1, x_2) \end{cases}$$

Graphical analysis in the phase plane

Without solving complicated math, the phase plane allows to understand globally the dynamics of the systems. The phase portrait is a 2D plane and the horizontal axis is associated with the x_1 and the vertical axis is x_2.

We define the *nullclines* which are defined as the locus of points where one of the derivative is null:

$$\begin{cases} x_1\text{-nullcline} : \dot{x}_1 = 0 \rightarrow f_1(x_1, x_2) = 0 \\ x_2\text{-nullcline} : \dot{x}_2 = 0 \rightarrow f_2(x_1, x_2) = 0 \end{cases}$$

The intersections between the two nullclines where $\dot{x}_1 = 0$ and $\dot{x}_2 = 0$ simultaneously defines the *fixed points*: (x_1^*, x_2^*).

At each point on the plane, we can compute

$$\begin{cases} \dot{x}_1^* &= f_1(x_1^*, x_2^*) \\ \dot{x}_2^* &= f_2(x_1^*, x_2^*) \end{cases}$$

where $\dot{x}_1^*$ gives the horizontal velocity and $\dot{x}_2^*$ gives the vertical velocity. The resulting vector is the velocity at the given point in the plane. We can draw these vectors for plenty of points in the plane which brings out the *vector field*. By analogy, we imagine a piece of wood on a water, the vector field simply provides the direction of the current, the fixed points are locations where the piece of wood remains fixed.

To determine the stability of the fixed points, we watch the direction of the fields. When all the lines converge towards this point, it is a *stable* fixed point. By contrast, if all the line diverge, it is a *unstable* fixed point. We can also differenciate if the lines rotates towards the fixed points; it defines a stable spirale while if its direclty converges towards the point it is stable node. A similar reasoning permits to observe unstable spirale or unstable node. We can also define limit case such as center where the vector field is never converging and diverging from the node and saddle node where the vector field is attracted in one direction and repulse in the other direction.

As you can see, this analysis provides a good way to study non linear system without solving all the differential equations and without doing any computations.

Analytical analysis in the phase plane

We can also determine the stability of the phase plane via analytic computations. We introduce the Jacobian matrix:

$$A = \begin{pmatrix} \frac{\partial f_1}{\partial x_1} & \frac{\partial f_1}{\partial x_2} \\ \frac{\partial f_2}{\partial x_1} & \frac{\partial f_2}{\partial x_2} \end{pmatrix}$$

Then the eigenvalues of the Jacobian evaluated at the fixed points give the nature and stability of the fixed points. Here we consider a 2D system, the stability can be determined based on the determinant and the trace of the jacobian following Figure C.1.

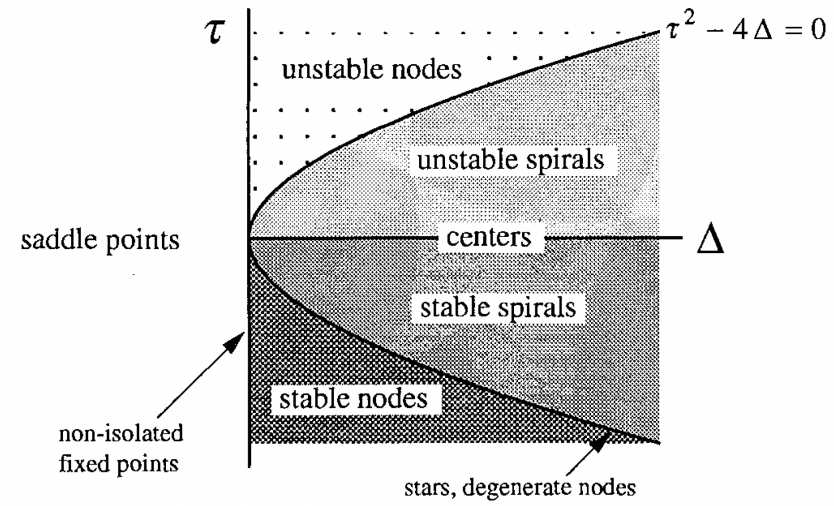

Figure C.1: The stability of the fixed points in a 2D system is defined by the values of the trace (τ) and the determinant (Δ) of the jacobian evaluated at the fixed points (Strogatz, 2015)

APPENDIX D

Conductance-based model used in the thesis

The conductance-based model used in the thesis is introduced in Section 3.1.2. Here, I added supplementary information and the parameter values.

In this conductance-based model, the calcium Ca^{2+} is entering through the T-type calcium channel. The dynamics of the calcium concentration is thus given by:

$$\frac{d[\mathrm{Ca^T}]}{dt} = -k_1 I_{\mathrm{Ca,T}} - k_2[\mathrm{Ca^T}],$$

where k_1 and k_2 are the rate variables. The calcium-activated potassium current considers this calcium entry to update its gating variable:

$$m_{\mathrm{K,Ca}}([\mathrm{Ca^T}]) = \left(\frac{[\mathrm{Ca^T}]}{[\mathrm{Ca^T}] + K_{\mathrm{D}}}\right)^2,$$

where K_{D} is a calcium-activation constant.

Model parameters			
C_{m}	1	g_{leak}	0.055
E_{Na}	50	g_{Na}	170
$E_{\mathrm{K,D}}$	−85	$g_{\mathrm{K,D}}$	40
E_{Ca}	120	g_{H}	0.01
E_{leak}	−55	$g_{\mathrm{K,Ca}}$	4
E_{H}	20	$g_{\mathrm{Ca,T}}$	0.55
K_{D}	170	k_1	0.1
		k_2	0.01

Table D.1: Conductance-based model parameters. (Left) Membrane capacitance (C_{m} [μF/cm^2]) and the reversal potential (E [mV]) of the different ion channels. (Right) Cell parameters, identical for each cell of the circuit. The ion channel conductances are expressed in [mS/cm^2].

Param.	$V_{X,\mathrm{half}}$	slope$_X$	Param.	A	B	$V_{\tau,\mathrm{half}}$	slope$_\tau$
$m_{\mathrm{Na},\infty}$	35.5	−5.29	$\tau_{m_{\mathrm{Na}}}$	1.32	1.26	120	−25
$h_{\mathrm{Na},\infty}$	48.9	5.18	$\tau_{h_{\mathrm{Na}}}$	$(0.67/(1+\exp((V+62.9)/-10.0))) \cdot (1.5 + 1/(1+\exp((V+34.9)/3.6)))$			
$m_{\mathrm{K,D},\infty}$	12.3	−11.8	$\tau_{m_{\mathrm{K,D}}}$	0.2	6.4	28.3	−19.2
$m_{\mathrm{Ca,T},\infty}$	67.1	−7.2	$\tau_{m_{\mathrm{Ca,T}}}$	21.7	21.3	68.1	−20.5
$h_{\mathrm{Ca,T},\infty}$	80.1	5.5	$\tau_{h_{\mathrm{Ca,T}}}$	410	179.6	55	−16.9
$m_{\mathrm{H},\infty}$	80.0	6.0	$\tau_{m_{\mathrm{H}}}$	272	−1149	42.2	−8.73

Table D.2: Dynamics parameters of the ionic channels.

Features used to describe calcium dynamics

Throughout the thesis, different calcium-based plasticity rules are described. Here, I aimed first at reviewing key features to describe calcium dynamics in a neuron model. Then, I further detailed the model of Shouval et al. (Shouval et al., 2002) using the text from the Supplementary Materials of (Jacquerie et al., 2022).

Calcium is often used as the key driver to induce synaptic change. The correspondence between the change in calcium and the related pre- and postsynaptic spiking is implemented in several manners. Here, I list some common modeling practices (Table D.3). First, the *calcium source* must be explicit such as NMDAr (Houben and Keil, 2020; Kumar and Mehta, 2011) or voltage dependent calcium channels (VDCC) (Chen et al., 2013) or their sum (Karmarkar and Buonomano, 2002). It can also come from more complex mechanisms such as intracellular stores such as endoplasmic reticulum (Berridge, 1998; Griffith et al., 2014). Calcium is also released via activation of metabotropic glutamate receptors. Others calcium-dependent mechanisms can be integrated such as calcium-extrusion mechanisms, including membrane pumps, intake and uptake into intracellular calcium-stores. Or by contrast, calcium can be abstract and explicitly described by a mathematical variable directly translating the neuronal activity without intermediate terms (Graupner et al., 2016). Second, calcium from NMDAr is frequently used, the *description of NMDAr* is also various. It can be expressed by a simple synaptic variable equation (Shouval et al., 2002), a more complex detailed equations of its kinetics (Saudargienė and Graham, 2015) or relatively simple by converting the spike timing activity (Griffith et al., 2014; Graupner et al., 2016). Finally, the *calcium dynamics* provides the time-evolution of the calcium that is affecting the synaptic strength. Several descriptions exist. For example, a differential equation converts the calcium from NMDAr or NMDAr and VDCC into a calcium fluctuation (Shouval et al., 2002). Once again, its dynamics can be also expressed very abstractly (Graupner et al., 2016) or with a lot of intermediate terms to mimic the whole complex process (Rubin et al., 2005).

Table D.3 provides the overview of the different calcium modeling practices. Conceptual equations are presented. Each article might adapt the equation form for example by adding scaling factors.

Feature	Notation	Description
Calcium source		
	I_{NMDA}	$I_{\text{NMDA}} = g_{\text{NMDA}}\, s_{\text{NMDA}} B(V_{\text{post}})(V_{\text{post}} - E_{\text{NMDA}})$ g_{NMDA}: NMDA conductance s_{NMDA}: gating variable $B(V_{\text{post}})$: voltage-dependent magnesium blocker dynamics
	$I_{\text{NMDA}} + I_{\text{VDCC}}$	sum of the two currents
	Others	eg: buffers, diffusion terms, pumps, ...
	NMDA(t_{spk})	Decreasing exponential at each postsynaptic spikes.
NMDA model		
	Time	Pre- or postsynaptic spike times govern the NMDA equation
	Voltage	Pre- and postsynaptic voltages govern the NMDA equation
	Kinetics	NMDAr is described by kinetic equations
	/	No biological current
	Others	More complex process describe the NMDAr
Calcium dynamics		
	NMDA	$\tau_{\text{Ca}}\dot{\text{Ca}} = \alpha I_{\text{NMDA}} - \text{Ca}$ α: current-to-concentration factor
	NMDA + VDCC	$\tau_{\text{Ca}}\dot{\text{Ca}} = (\alpha I_{\text{NMDA}} + \beta I_{\text{VDCC}}) - \text{Ca}$ α, β: current-to-concentration factors
	$\delta(t_{\text{spk}})$	Simplified equation converting spike times into calcium variation
	Others / Process	More biophysical description of the calcium change

Table D.3: Model features used to implement calcium in a neuron model. There are various sources of calcium that can be considered. The implementation of the NMDA receptor dynamics varies between model. Calcium dynamics can be governed by calcium current sources or more abstract translating spike time activity.

APPENDIX E

Calcium-based model from (Shouval et al., 2002)

The model of Graupner was inspired by the Shouval's work in Shouval et al. (2002). The synaptic change follows a typical first-order differential equation:

$$\dot{w} = \frac{1}{\tau_w([\mathrm{Ca}])} \left(\Omega([\mathrm{Ca}]) - w\right), \tag{E.1}$$

where the time constant $\tau_w([\mathrm{Ca}])$ and the steady-state value $\Omega([\mathrm{Ca}])$ are calcium-dependent. This steady state value is defined by two sigmoids in order to build the U-shape for Ω:

$$\Omega([\mathrm{Ca}]) = a_0 - a_0 \exp\left(\frac{b_1([\mathrm{Ca}] - a_1)}{1 + \exp(b1([\mathrm{Ca}] - a_1))}\right) + m_2 \exp\left(\frac{b_2([\mathrm{Ca}] - a_2)}{1 + \exp(b_2([\mathrm{Ca}] - a_2))}\right) \tag{E.2}$$

This expression relies on five parameters:

- a_0 is the ordinate at low levels of calcium,
- a_1 is the abscissa where the ordinate a_0 is divided by 2. It dictates the place along the x-axis where the first sigmoid is decreasing.
- b_1 governs the sharpness of the decrease around a_1. The bigger, the flatter the slope.
- m_2 the converging value at high calcium level.
- a_2 is the x-value where Ω equal $m_2/2$.
- b_2 is similar as b_1; it dictates the sharpness of the slope.

The time-constant is also calcium-dependent and it is given by Shouval et al. (2002)

$$\tau_w([\mathrm{Ca}]) = P_4 + \frac{P_1}{P_2 + [\mathrm{Ca}]^{P_3}}$$

P_1, P_2, P_3 and P_4 are fitted parameters to describe the calcium-dependent time constant. The different parameters were identified to reproduce the different potentiation and depression levels provided by the previous model for the frequency-dependency protocol.

The presented synaptic rule is driven by a more elaborated calcium dynamics considering the back-propagation action potential or a more complex calcium dynamic. However, in this paper, the synaptic rule of Shouval can be adapted to the chosen calcium dynamics.

Bibliography

Abarbanel HD, Gibb L, Huerta R, Rabinovich MI (2003) Biophysical model of synaptic plasticity dynamics. *Biological Cybernetics* 89:214–226.

Abbott LF (2003) Balancing homeostasis and learning in neural circuits. *Zoology* 106:365–371.

Abbott LF, Nelson SB (2000) Synaptic plasticity: Taming the beast. *Nature Neuroscience* 3:1178–1183.

Abraham WC (2008) Metaplasticity: Tuning synapses and networks for plasticity. *Nature Reviews Neuroscience* 9:387–399.

Abraham WC, Bear MF (1996) Metaplasticity: the plasticity of synaptic plasticity. *Trends in Neurosciences* 19:126–130.

Abraham WC, Jones OD, Glanzman DL (2019) Is plasticity of synapses the mechanism of long-term memory storage? *npj Science of Learning* 4 Publisher: Springer US.

Acharya J, Basu A, Legenstein R, Limbacher T, Poirazi P, Wu X (2022) Dendritic Computing: Branching Deeper into Machine Learning. *Neuroscience* 489:275–289.

Adams WB (1985) Slow depolarizing and hyperpolarizing currents which mediate bursting in Aplysia neurone R15. *The Journal of Physiology* 360:51–68.

Alonso LM, Marder E (2019) Visualization of currents in neural models with similar behavior and different conductance densities. *eLife* 8:1–28.

Amano R, Nakao M, Matsumiya K, Miwakeichi F (2022) A computational model to explore how temporal stimulation patterns affect synapse plasticity. *PLOS ONE* 17:e0275059.

Amarillo Y, Mato G, Nadal MS (2015) Analysis of the role of the low threshold currents IT and Ih in intrinsic delta oscillations of thalamocortical neurons. *Frontiers in Computational Neuroscience* 9:1–9.

Ang GWY, Tang CS, Hay YA, Zannone S, Paulsen O, Clopath C (2021) The functional role of sequentially neuromodulated synaptic plasticity in behavioural learning. *PLOS Computational Biology* 17:e1009017.

Anirudhan A, Narayanan R (2015) Analogous synaptic plasticity profiles emerge from disparate channel combinations. *Journal of Neuroscience* 35:4691–4705.

Artola A, Bröcher S, Singer W (1990) Different voltage-dependent thresholds for inducing long-term depression and long-term potentiation in slices of rat visual cortex. *Nature* 347:69–72.

Artola A, Singer W (1993) Long-term depression of excitatory synaptic transmission and its relationship to long-term potentiation. *Trends in Neurosciences* 16:480–487.

Avery MC, Krichmar JL (2017) Neuromodulatory Systems and Their Interactions: A Review of Models, Theories, and Experiments. *Frontiers in Neural Circuits* 11:108.

Babadi B, Abbott LF (2016) Stability and Competition in Multi-spike Models of Spike-Timing Dependent Plasticity. *PLoS Computational Biology* 12.

Bacak BJ, Segaran J, Molkov YI (2016) Modeling the effects of extracellular potassium on bursting properties in pre-Bötzinger complex neurons. *Journal of Computational Neuroscience* 40:231–245.

Bading H (2013) Nuclear calcium signalling in the regulation of brain function. *Nature Reviews Neuroscience* 14:593–608.

Badoual M, Zou Q, Davison AP, Rudolph M, Bal T, Frégnac Y, Destexhe A (2006) Biophysical and phenomenological models of multiple spike interactions in spike-timing dependent plasticity. *International Journal of Neural Systems* 16:79–97.

Baltaci SB, Mogulkoc R, Baltaci AK (2019) Molecular Mechanisms of Early and Late LTP. *Neurochemical Research* 44:281–296.

Bannon NM, Chistiakova M, Chen JY, Bazhenov M, Volgushev M (2017) Adenosine shifts plasticity regimes between associative and homeostatic by modulating heterosynaptic changes. *Journal of Neuroscience* 37:1439–1452.

Bannon NM, Chistiakova M, Volgushev M (2016) Homeostatic Role of Heterosynaptic Plasticity. *Homeostatic Control of Brain Function* pp. 124–142.

Bazhenov M, Timofeev I, Steriade M, Sejnowski TJ (2002) Model of thalamocortical slow-wave sleep oscillations and transitions to activated states. *Journal of Neuroscience* 22:8691–8704.

Bazzari A, Parri H (2019) Neuromodulators and Long-Term Synaptic Plasticity in Learning and Memory: A Steered-Glutamatergic Perspective. *Brain Sciences* 9:300.

Bear MF, Connors BW, Paradiso MA (2016) *Neuroscience: exploring the brain* Fourth edition. Philadelphia : Wolters Kluwer Issue: International Edition.

Benuskova L, Abraham WC (2007) STDP rule endowed with the BCM sliding threshold accounts for hippocampal heterosynaptic plasticity. *Journal of Computational Neuroscience* 22:129–133.

Berridge MJ (1998) Neuronal Calcium Signaling. *Neuron* 21:13–26.

Berridge MJ (2014) Calcium regulation of neural rhythms, memory and alzheimer's disease. *Journal of Physiology* 592:281–293.

Bertram R, Rhoads J, Cimbora WP (2008) A Phantom Bursting Mechanism for Episodic Bursting. *Bulletin of Mathematical Biology* 70:1979–1993.

Beurrier C, Congar P, Bioulac B, Hammond C (1999) Subthalamic Nucleus Neurons Switch from Single-Spike Activity to Burst-Firing Mode. *The Journal of Neuroscience* 19:599–609.

Bevan M (2002) Move to the rhythm: oscillations in the subthalamic nucleus–external globus pallidus network. *Trends in Neurosciences* 25:525–531.

Bezanson J, Edelman A, Karpinski S, Shah VB (2017) Julia: A Fresh Approach to Numerical Computing. *SIAM Review* 59:65–98.

Bi GQ, Poo MM (1998) Synaptic modifications in cultured hippocampal neurons: Dependence on spike timing, synaptic strength, and postsynaptic cell type. *Journal of Neuroscience* 18:10464–10472.

Bi Gq, Poo Mm (2001) Synaptic Modification by Correlated Activity: Hebb's Postulate Revisited. *Annual Review of Neuroscience* 24:139–166.

Bienenstock E, Cooper L, Munro P (1982) Theory for the development of neuron selectivity: orientation specificity and binocular interaction in visual cortex. *The Journal of Neuroscience* 2:32–48.

Billings G, van Rossum MCW (2009) Memory Retention and Spike-Timing-Dependent Plasticity. *Journal of Neurophysiology* 101:2775–2788.

Bin Ibrahim MZ, Benoy A, Sajikumar S (2022) Long-term plasticity in the hippocampus: maintaining within and 'tagging' between synapses. *The FEBS Journal* 289:2176–2201.

Blesneac I, Chemin J, Bidaud I, Huc-Brandt S, Vandermoere F, Lory P (2015) Phosphorylation of the Cav3.2 T-type calcium channel directly regulates its gating properties. *Proceedings of the National Academy of Sciences* 112:13705–13710.

Bliss TVP, Lømo T (1973) Long-lasting potentiation of synaptic transmission in the dentate area of the anaesthetized rabbit following stimulation of the perforant path. *The Journal of Physiology* 232:331–356.

Bliss TV, Cooke SF (2011) Long-term potentiation and long-term depression: a clinical perspective. *Clinics* 66:3–17.

Bloss EB, Cembrowski MS, Karsh B, Colonell J, Fetter RD, Spruston N (2018) Single excitatory axons form clustered synapses onto CA1 pyramidal cell dendrites. *Nature Neuroscience* 21:353–363.

Bonilla-Quintana M, Rangamani P (2022) Can biophysical models of dendritic spines be used to explore synaptic changes associated with addiction? *Physical Biology* 19:041001.

Borczyk M, Śliwińska MA, Caly A, Bernas T, Radwanska K (2019) Neuronal plasticity affects correlation between the size of dendritic spine and its postsynaptic density. *Scientific Reports* 9:1693.

Born J, Rasch B, Gais S (2006) Sleep to remember. *Neuroscientist* .

Bourjaily MA, Miller P (2011) Excitatory, Inhibitory, and Structural Plasticity Produce Correlated Connectivity in Random Networks Trained to Solve Paired-Stimulus Tasks. *Frontiers in Computational Neuroscience* 5.

Bouvier G, Higgins D, Spolidoro M, Carrel D, Mathieu B, Léna C, Dieudonné S, Barbour B, Brunel N, Casado M (2016) Burst-Dependent Bidirectional Plasticity in the Cerebellum Is Driven by Presynaptic NMDA Receptors. *Cell Reports* 15:104–116.

Bozelos P, Poirazi P (2017) Impact of Structural Plasticity on Memory Capacity In *The Rewiring Brain*, pp. 319–341. Elsevier.

Brader JM, Senn W, Fusi S (2007) Learning Real-World Stimuli in a Neural Network with Spike-Driven Synaptic Dynamics. *Neural Computation* 19:2881–2912.

Bradley C, Nydam AS, Dux PE, Mattingley JB (2022) State-dependent effects of neural stimulation on brain function and cognition. *Nature Reviews Neuroscience* 23:459–475.

Brokaw K, Tishler W, Manceor S, Hamilton K, Gaulden A, Parr E, Wamsley EJ (2016) Resting state EEG correlates of memory consolidation. *Neurobiology of Learning and Memory* 130:17–25.

Brown P, Williams D (2005) Basal ganglia local field potential activity: Character and functional significance in the human. *Clinical Neurophysiology* .

Brzosko Z, Mierau SB, Paulsen O (2019) Neuromodulation of Spike-Timing-Dependent Plasticity: Past, Present, and Future. *Neuron* 103:563–581 Publisher: Elsevier Inc.

Brzosko Z, Zannone S, Schultz W, Clopath C, Paulsen O (2017) Sequential neuromodulation of Hebbian plasticity offers mechanism for effective reward-based navigation. *eLife* 6:e27756.

Bush D, Jin Y (2012) Calcium control of triphasic hippocampal STDP. *Journal of Computational Neuroscience* 33:495–514.

Butson CR (2012) Computational Models of Neuromodulation. *International Review of Neurobiology* 107:5–22.

Butts DA, Kanold PO, Shatz CJ (2007) A Burst-Based "Hebbian" Learning Rule at Retinogeniculate Synapses Links Retinal Waves to Activity-Dependent Refinement. *PLoS Biology* 5:e61.

Butz M, van Ooyen A (2013) A Simple Rule for Dendritic Spine and Axonal Bouton Formation Can Account for Cortical Reorganization after Focal Retinal Lesions. *PLoS Computational Biology* 9:e1003259.

Buzsáki G (2009) *Rhythms of the Brain* Oxford University Press Publication Title: Rhythms of the Brain.

Byrne JH, Heidelberger R, Waxham MN, editors (2014) *From molecules to networks: an introduction to cellular and molecular neuroscience* Elsevier/AP, Academic Press is an imprint of Elsevier, Amsterdam ; Boston, third edition edition.

Cai Y, Gavornik JP, Cooper LN, Yeung LC, Shouval HZ (2007) Effect of stochastic synaptic and dendritic dynamics on synaptic plasticity in visual cortex and hippocampus. *Journal of Neurophysiology* 97:375–386.

Cain SM, Snutch TP (2010) Contributions of T-type calcium channel isoforms to neuronal firing. *Channels* 4:475–482.

Cajal R (1888) Estructura de los centros nerviosos de las aves. *Revista Trimestral de His-tología Normal y Patológica,* 1.

Cannon J, Mccarthy MM, Lee S, Lee J, Börgers C, Whittington MA, Kopell N (2014) Neurosystems: Brain rhythms and cognitive processing. *European Journal of Neuroscience* 39:705–719.

Capone C, Pastorelli E, Golosio B, Paolucci PS (2019) Sleep-like slow oscillations improve visual classification through synaptic homeostasis and memory association in a thalamo-cortical model. *Scientific Reports* 9:1–11.

Carlson KD, Giordano N (2011) Interplay of the magnitude and time-course of postsynaptic Ca2 + concentration in producing spike timing-dependent plasticity. *Journal of Computational Neuroscience* 30:747–758.

Carvalho TP, Buonomano DV (2011) A novel learning rule for long-term plasticity of short-term synaptic plasticity enhances temporal processing. *Frontiers in Integrative Neuroscience* 5:1–11.

Castro-Alamancos MA (2004) Dynamics of sensory thalamocortical synaptic networks during information processing states. *Progress in Neurobiology* .

Castro-Alamancos MA, Connors BW (1997) Distinct forms of short-term plasticity at excitatory synapses of hippocampus and neocortex. *Proceedings of the National Academy of Sciences* 94:4161–4166.

Caverzasio S, Amato N, Manconi M, Prosperetti C, Kaelin-Lang A, Hutchison WD, Galati S (2018) Brain plasticity and sleep: Implication for movement disorders. *Neuroscience and biobehavioral reviews* 86:21–35 Place: United States Publisher: Elsevier Ltd.

Chemin J, Monteil A, Perez-Reyes E, Bourinet E, Nargeot J, Lory P (2002) Specific contribution of human T-type calcium channel isotypes (a-1G, a-1H and a-1l) to neuronal excitability. *Journal of Physiology* 540:3–14.

Chemin J, Siquier-Pernet K, Nicouleau M, Barcia G, Ahmad A, Medina-Cano D, Hanein S, Altin N, Hubert L, Bole-Feysot C, Fourage C, Nitschké P, Thevenon J, Rio M, Blanc P, Vidal C, Bahi-Buisson N, Desguerre I, Munnich A, Lyonnet S, Boddaert N, Fassi E, Shinawi M, Zimmerman H, Amiel J, Faivre L, Colleaux L, Lory P, Cantagrel V (2018) De novo mutation screening in childhood-onset cerebellar atrophy identifies gain-of-function mutations in the CACNA1G calcium channel gene. *Brain* 141:1998–2013.

Chen JY, Lonjers P, Lee C, Chistiakova M, Volgushev M, Bazhenov M (2013) Heterosynaptic plasticity prevents runaway synaptic dynamics. *Journal of Neuroscience* 33:15915–15929.

Chen Y, Parker WD, Wang K (2014) The Role of T-Type Calcium Channel Genes in Absence Seizures. *Frontiers in Neurology* 5.

Chindemi G, Abdellah M, Amsalem O, Benavides-Piccione R, Delattre V, Doron M, Ecker A, Jaquier AT, King J, Kumbhar P, Monney C, Perin R, Rössert C, Tuncel AM, Van Geit W, DeFelipe J, Graupner M, Segev I, Markram H, Muller EB (2022) A calcium-based plasticity model for predicting long-term potentiation and depression in the neocortex. *Nature Communications* 13:3038.

Chistiakova M, Bannon NM, Bazhenov M, Volgushev M (2014) Heterosynaptic plasticity: Multiple mechanisms and multiple roles. *Neuroscientist* 20:483–498.

Choi S, Yu E, Lee S, Llinás RR (2015) Altered thalamocortical rhythmicity and connectivity in mice lacking $Ca_v 3.1$ T-type Ca^{2+} channels in unconsciousness. *Proceedings of the National Academy of Sciences* 112:7839–7844.

Chrol-Cannon J, Jin Y (2014) Computational modeling of neural plasticity for self-organization of neural networks. *Biosystems* 125:43–54.

Cichon J, Wasilczuk AZ, Looger LL, Contreras D, Kelz MB, Proekt A (2023) Ketamine triggers a switch in excitatory neuronal activity across neocortex. *Nature Neuroscience* 26:39–52.

Cirelli C (2017) Sleep, synaptic homeostasis and neuronal firing rates. *Current Opinion in Neurobiology* 44:72–79 Publisher: Elsevier Ltd.

Citri A, Malenka RC (2008) Synaptic plasticity: Multiple forms, functions, and mechanisms. *Neuropsychopharmacology* 33:18–41.

Clapham DE, Garbers DL (2005) International Union of Pharmacology. L. Nomenclature and structure-function relationships of CatSper and two-pore channels. *Pharmacological Reviews* 57:451–454.

Clopath C (2019) Long-Term Plasticity, Biophysical Models. *Encyclopedia of Computational Neuroscience* pp. 1–12.

Clopath C, Büsing L, Vasilaki E, Gerstner W (2010) Connectivity reflects coding: A model of voltage-based STDP with homeostasis. *Nature Neuroscience* 13:344–352 Publisher: Nature Publishing Group.

Clopath C, Gerstner W (2010) Voltage and spike timing interact in STDP - a unified model. *Frontiers in Synaptic Neuroscience* 2:1–11.

Clopath C, Ziegler L, Vasilaki E, Büsing L, Gerstner W (2008) Tag-trigger-consolidation: A model of early and late long-term-potentiation and depression. *PLoS Computational Biology* 4.

Contreras D, Steriade M (1995) Cellular basis of EEG slow rhythms: a study of dynamic corticothalamic relationships. *The Journal of Neuroscience* 15:604–622.

Costa RP, Froemke RC, Sjöström PJ, van Rossum MC (2015) Unified pre- and postsynaptic long-term plasticity enables reliable and flexible learning. *eLife* 4:e09457.

Coulter DA, Huguenard JR, Prince DA (1989) Calcium currents in rat thalamocortical relay neurones: kinetic properties of the transient, low-threshold current. *The Journal of Physiology* 414:587–604.

Crandall S, Cruikshank S, Connors B (2015) A Corticothalamic Switch: Controlling the Thalamus with Dynamic Synapses. *Neuron* 86:768–782.

Dahan L, Astier B, Vautrelle N, Urbain N, Kocsis B, Chouvet G (2007) Prominent Burst Firing of Dopaminergic Neurons in the Ventral Tegmental Area during Paradoxical Sleep. *Neuropsychopharmacology* 32:1232–1241.

Daoudal G, Debanne D (2003) Long-Term Plasticity of Intrinsic Excitability: Learning Rules and Mechanisms. *Learning & Memory* 10:456–465.

Dastgheib M, Kulanayagam A, Dringenberg HC (2022) Is the role of sleep in memory consolidation overrated? *Neuroscience & Biobehavioral Reviews* 140:104799.

De Franceschi G, Barkat TR (2021) Task-induced modulations of neuronal activity along the auditory pathway. *Cell Reports* 37:110115.

Debanne D, Gahwiler BH, Thompson SM (1994) Asynchronous pre- and postsynaptic activity induces associative long-term depression in area CA1 of the rat hippocampus in vitro. *Proceedings of the National Academy of Sciences* 91:1148–1152.

Debanne D (2010) Spike-timing dependent plasticity beyond synapse - pre- and post-synaptic plasticity of intrinsic neuronal excitability. *Frontiers in Synaptic Neuroscience* .

Debanne D, Inglebert Y, Russier M (2019) Plasticity of intrinsic neuronal excitability. *Current Opinion in Neurobiology* 54:73–82 Publisher: Elsevier Ltd.

Deger M, Helias M, Rotter S, Diesmann M (2012) Spike-Timing Dependence of Structural Plasticity Explains Cooperative Synapse Formation in the Neocortex. *PLoS Computational Biology* 8:e1002689.

Deisseroth K, Bito H, Schulman H, Tsien RW (1995) Synaptic Plasticity: A molecular mechanism for metaplasticity. *Current Biology* 5:1334–1338.

Delamare G, Feitosa Tomé D, Clopath C (2022) Intrinsic neural excitability induces time-dependent overlap of memory engrams preprint, Neuroscience.

Delattre V, Keller D, Perich M, Markram H, Muller EB (2015) Network-timing-dependent plasticity. *Frontiers in cellular neuroscience* 9:220–220 Place: Switzerland Publisher: Frontiers Research Foundation.

Deperrois N, Graupner M (2020) Short-term depression and long-term plasticity together tune sensitive range of synaptic plasticity. *PLoS Computational Biology* 16:1–25.

Desai NS (2003) Homeostatic plasticity in the CNS: Synaptic and intrinsic forms. *Journal of Physiology Paris* 97:391–402.

Desai NS, Walcott EC (2016) Homeostatic Synaptic Scaling at Central Synapses. *Homeostatic Control of Brain Function* pp. 108–123.

Desroches M, Rinzel J, Rodrigues S (2022) Classification of bursting patterns: A tale of two ducks. *PLOS Computational Biology* 18:e1009752.

Destexhe A (1998) Spike-and-Wave Oscillations Based on the Properties of GABA $_b$ Receptors. *The Journal of Neuroscience* 18:9099–9111.

Destexhe A, Contreras D, Steriade M (1998) Mechanisms Underlying the Synchronizing Action of Corticothalamic Feedback Through Inhibition of Thalamic Relay Cells. *Journal of Neurophysiology* 79:999–1016.

Destexhe A, Contreras D, Steriade M, Sejnowski TJ, Huguenard JR (1996) In vivo, in vitro, and computational analysis of dendritic calcium currents in thalamic reticular neurons. *Journal of Neuroscience* 16:169–185.

Destexhe A, Mainen ZF, Sejnowski TJ (1994) Synthesis of models for excitable membranes, synaptic transmission and neuromodulation using a common kinetic formalism. *Journal of Computational Neuroscience* 1:195–230.

Destexhe A, Marder E (2004) Circuit Computations. *Nature* 431:789–795.

Destexhe A, Neubig M, Ulrich D, Huguenard J (1998) Dendritic low-threshold calcium currents in thalamic relay cells. *Journal of Neuroscience* 18:3574–3588.

Dias I, Levers MR, Lamberti M, Hassink GC, van Wezel R, le Feber J (2021) Consolidation of memory traces in cultured cortical networks requires low cholinergic tone, synchronized activity and high network excitability. *Journal of Neural Engineering* 18:046051.

Ding F, O'Donnell J, Xu Q, Kang N, Goldman N, Nedergaard M (2016) Changes in the composition of brain interstitial ions control the sleep-wake cycle. *Science* 352:550–555.

Ding Y, Wang Y, Cao L (2022) A Simplified Plasticity Model Based on Synaptic Tagging and Capture Theory: Simplified STC. *Frontiers in Computational Neuroscience* 15:798418.

Drion G (2013) Regulation of excitability, pacemaking and bursting: insights from dopamine neuron electrophysiology Ph.D. diss., University of Liege.

Drion G, Dethier J, Franci A, Sepulchre R (2018) Switchable slow cellular conductances determine robustness and tunability of network states. *PLoS Computational Biology* 14:1–20.

Drion G, Franci A, Dethier J, Sepulchre R (2015) Dynamic input conductances shape neuronal spiking. *eNeuro* 2:1–15.

Drion G, Franci A, Sepulchre R (2019) Cellular switches orchestrate rhythmic circuits. *Biological Cybernetics* 113:71–82.

Drion G, Franci A, Seutin V, Sepulchre R (2012) A novel phase portrait for neuronal excitability. *PLoS ONE* 7:1–14.

Dudek SM, Bear MF (1992) Homosynaptic long-term depression in area CA1 of hippocampus and effects of N-methyl-D-aspartate receptor blockade. *Proceedings of the National Academy of Sciences* 89:4363–4367.

Ebner C, Clopath C, Jedlicka P, Cuntz H (2019) Unifying Long-Term Plasticity Rules for Excitatory Synapses by Modeling Dendrites of Cortical Pyramidal Neurons. *Cell Reports* 29:4295–4307.e6 Publisher: ElsevierCompany.

El Boustani S, Yger P, Fregnac Y, Destexhe A (2012) Stable Learning in Stochastic Network States. *Journal of Neuroscience* 32:194–214.

Engert F, Bonhoeffer T (1999) Dendritic spine changes associated with hippocampal long-term synaptic plasticity. *Nature* 399:66–70.

Esser SK, Hill S, Tononi G (2009) Breakdown of effective connectivity during slow wave sleep: Investigating the mechanism underlying a cortical gate using large-scale modeling. *Journal of Neurophysiology* 102:2096–2111.

Fanselow EE, Sameshima K, Baccala LA, Nicolelis MAL (2001) Thalamic bursting in rats during different awake behavioral states. *Proceedings of the National Academy of Sciences* 98:15330–15335.

Farries MA, Fairhall AL (2007) Reinforcement Learning With Modulated Spike Timing–Dependent Synaptic Plasticity. *Journal of Neurophysiology* 98:3648–3665.

Fauth M, Tetzlaff C (2016) Opposing Effects of Neuronal Activity on Structural Plasticity. *Frontiers in Neuroanatomy* 10.

Fauth MJ, Van Rossum MC (2019) Self-organized reactivation maintains and reinforces memories despite synaptic turnover. *eLife* 8:1–19.

Feldman DE (2012) The Spike-Timing Dependence of Plasticity. *Neuron* 75:556–571.

Feldman DE (2020) Spike timing–dependent plasticity. *Neural Circuit and Cognitive Development* pp. 127–141 Publisher: Elsevier Inc.

Field RE, D'amour JA, Tremblay R, Miehl C, Rudy B, Gjorgjieva J, Froemke RC (2020) Heterosynaptic Plasticity Determines the Set Point for Cortical Excitatory-Inhibitory Balance. *Neuron* pp. 1–13 Publisher: Elsevier Inc.

Fiete IR, Senn W, Wang CZ, Hahnloser RH (2010) Spike-Time-Dependent Plasticity and Heterosynaptic Competition Organize Networks to Produce Long Scale-Free Sequences of Neural Activity. *Neuron* 65:563–576.

Foncelle A, Mendes A, Jedrzejewska-Szmek J, Valtcheva S, Berry H, Blackwell KT, Venance L (2018) Modulation of spike-timing dependent plasticity: Towards the inclusion of a third factor in computational models. *Frontiers in Computational Neuroscience* 12:1–21.

Fourcaud-Trocmé N (2014) Integrate and Fire Models, Deterministic In Jaeger D, Jung R, editors, *Encyclopedia of Computational Neuroscience*, pp. 1–9. Springer New York, New York, NY.

Franci A, Drion G, Sepulchre R (2012) An organizing center in a planar model of neuronal excitability. *SIAM Journal on Applied Dynamical Systems* 11:1698–1722.

Franci A, Drion G, Sepulchre R (2014) Modeling the modulation of neuronal bursting: A singularity theory approach. *SIAM Journal on Applied Dynamical Systems* 13:798–829.

Franci A, Drion G, Sepulchre R (2018) Robust and tunable bursting requires slow positive feedback. *Journal of Neurophysiology* 119:1222–1234.

Franci A, Drion G, Seutin V, Sepulchre R (2013) A Balance Equation Determines a Switch in Neuronal Excitability. *PLoS Computational Biology* 9.

Franks KM, Sejnowski TJ (2002) Complexity of calcium signaling in synaptic spines. *BioEssays* 24:1130–1144.

Frazier CJ, Serrano JR, George EG, Yu X, Viswanathan A, Perez-Reyes E, Jones SW (2001) Gating kinetics of the a-1I T-type calcium channel. *Journal of General Physiology* 118:457–470.

Fremont R, Calderon DP, Maleki S, Khodakhah K (2014) Abnormal High-Frequency Burst Firing of Cerebellar Neurons in Rapid-Onset Dystonia-Parkinsonism. *Journal of Neuroscience* 34:11723–11732.

Frey U, Huang YY, Kandel ER (1993) Effects of cAMP Simulate a Late Stage of LTP in Hippocampal CA1 Neurons. *Science* 260:1661–1664.

Frey U, Morris RGM (1997) Synaptic tagging and long-term potentiation. *Nature* 385:533–536.

Frey U, Morris RG (1998) Synaptic tagging: implications for late maintenance of hippocampal long-term potentiation. *Trends in Neurosciences* 21:181–188.

Froemke RC (2015) Plasticity of Cortical Excitatory-Inhibitory Balance. *Annual Review of Neuroscience* 38:195–219.

Froemke RC, Dan Y (2002) Spike-timing-dependent synaptic modification induced by natural spike trains. *Nature* 416:433–438.

Froemke RC, Tsay IA, Raad M, Long JD, Dan Y (2006) Contribution of individual spikes in burst-induced long-term synaptic modification. *Journal of Neurophysiology* 95:1620–1629.

Frémaux N, Gerstner W (2015) Neuromodulated spike-timing-dependent plasticity, and theory of three-factor learning rules. *Frontiers in Neural Circuits* 9.

Frémaux N, Sprekeler H, Gerstner W (2013) Reinforcement Learning Using a Continuous Time Actor-Critic Framework with Spiking Neurons. *PLoS Computational Biology* 9:e1003024.

Fröhlich F, Bazhenov M (2006) Coexistence of tonic firing and bursting in cortical neurons. *Physical Review E - Statistical, Nonlinear, and Soft Matter Physics* 74:1–7.

Fuchsberger T, Clopath C, Jarzebowski P, Brzosko Z, Wang H, Paulsen O (2022) Postsynaptic burst reactivation of hippocampal neurons enables associative plasticity of temporally discontiguous inputs. *eLife* 11:e81071.

Fusi S, Abbott LF (2007) Limits on the memory storage capacity of bounded synapses. *Nature Neuroscience* 10:485–493.

Gabbiani F, Krapp HG (2006) Spike-Frequency Adaptation and Intrinsic Properties of an Identified, Looming-Sensitive Neuron. *Journal of Neurophysiology* 96:2951–2962.

Gallinaro JV, Gašparović N, Rotter S (2022) Homeostatic control of synaptic rewiring in recurrent networks induces the formation of stable memory engrams. *PLOS Computational Biology* 18:e1009836.

Gallinaro JV, Rotter S (2018) Associative properties of structural plasticity based on firing rate homeostasis in recurrent neuronal networks. *Scientific Reports* 8:3754.

Garg N, Balafrej I, Stewart TC, Portal JM, Bocquet M, Querlioz D, Drouin D, Rouat J, Beilliard Y, Alibart F (2022) Voltage-dependent synaptic plasticity: Unsupervised probabilistic Hebbian plasticity rule based on neurons membrane potential. *Frontiers in Neuroscience* 16 Publisher: arXiv Version Number: 5.

Gatev P, Darbin O, Wichmann T (2006) Oscillations in the basal ganglia under normal conditions and in movement disorders. *Movement Disorders* 21:1566–1577.

Gerkin RC, Bi GQ, Rubin JE (2010) A phenomenological calcium-based model of STDP. *Springer* pp. pp. 571–591.

Gerstner W, Kempter R, Van Hemmen JL, Wagner H (1996) A neuronal learning rule for sub-millisecond temporal coding. *Nature* 383:76–78.

Gerstner W (2011) Hebbian Learning and Plasticity. *From neuron to cognition via computational neuroscience* pp. 1–25.

Gerstner W, Kistler WM (2002) Mathematical formulations of Hebbian learning. *Biological Cybernetics* 87:404–415.

Gerstner W, Kistler WM, Naud R, Paninski L (2014) *Neuronal dynamics: from single neurons to networks and models of cognition* Cambridge University Press, Cambridge, United Kingdom.

Gerstner W, Lehmann M, Liakoni V, Corneil D, Brea J (2018) Eligibility Traces and Plasticity on Behavioral Time Scales: Experimental Support of NeoHebbian Three-Factor Learning Rules. *Frontiers in Neural Circuits* 12:1–16.

Gilly WF, Gillette R, McFarlane M (1997) Fast and slow activation kinetics of voltage-gated sodium channels in molluscan neurons. *Journal of Neurophysiology* .

Gjorgjieva J, Clopath C, Audet J, Pfister JP (2011) A triplet spike-timing-dependent plasticity model generalizes the Bienenstock-Cooper-Munro rule to higher-order spatiotemporal correlations. *Proceedings of the National Academy of Sciences of the United States of America* 108:19383–19388.

Gjorgjieva J, Drion G, Marder E (2016a) Computational implications of biophysical diversity and multiple timescales in neurons and synapses for circuit performance. *Current Opinion in Neurobiology* 37:44–52 Publisher: Elsevier Ltd.

Gjorgjieva J, Evers JF, Eglen SJ (2016b) Homeostatic activity-dependent tuning of recurrent networks for robust propagation of activity. *Journal of Neuroscience* 36:3722–3734.

Gjorgjieva J, Toyoizumi T, Eglen SJ (2009) Burst-time-dependent plasticity robustly guides ON/OFF segregation in the lateral geniculate nucleus. *PLoS Computational Biology* 5.

Glasgow SD, McPhedrain R, Madranges JF, Kennedy TE, Ruthazer ES (2019) Approaches and Limitations in the Investigation of Synaptic Transmission and Plasticity. *Frontiers in Synaptic Neuroscience* 11:20.

Goaillard JM, Marder E (2021) Ion Channel Degeneracy, Variability, and Covariation in Neuron and Circuit Resilience. *Annual Review of Neuroscience* 44:335–357.

Golbert DC, Souza AC, Almeida-Filho DG, Ribeiro S (2017) Sleep, Synaptic Plasticity, and Memory In Byrne JH, editor, *Learning and Memory: A Comprehensive Reference*, pp. 539–562. Academic Press, Oxford, second edition.

Goldman MS, Golowasch J, Marder E, Abbott LF (2000) Dependence of firing pattern on intrinsic ionic conductances: Sensitive and insensitive combinations. *Neurocomputing* 32-33:141–146.

Golomb D, Wang XJ, Rinzel J (1994) Synchronization properties of spindle oscillations in a thalamic reticular nucleus model. *Journal of neurophysiology* 72:1109–1126.

Golowasch J, Goldman MS, Abbott LF, Marder E (2002) Failure of averaging in the construction of a conductance-based neuron model. *Journal of Neurophysiology* 87:1129–1131.

González OC, Sokolov Y, Krishnan GP, Delanois JE, Bazhenov M (2020) Can sleep protect memories from catastrophic forgetting? *eLife* 9.

González-Rueda A, Pedrosa V, Feord RC, Clopath C, Paulsen O (2018) Activity-Dependent Downscaling of Subthreshold Synaptic Inputs during Slow-Wave-Sleep-like Activity In Vivo. *Neuron* 97:1244–1252.e5.

Graupner M (2017) Synaptic Plasticity : Spike-timing dependent plasticity (STDP) Synaptic Plasticity : Spike-timing dependent plasticity (STDP).

Graupner M, Brunel N (2007) STDP in a bistable synapse model based on CaMKII and associated signaling pathways. *PLoS Computational Biology* 3:2299–2323.

Graupner M, Brunel N (2010) Mechanisms of induction and maintenance of spike-timing dependent plasticity in biophysical synapse models. *Frontiers in Computational Neuroscience* 4.

Graupner M, Brunel N (2012) Calcium-based plasticity model explains sensitivity of synaptic changes to spike pattern, rate, and dendritic location. *Proceedings of the National Academy of Sciences of the United States of America* 109:3991–3996.

Graupner M, Wallisch P, Ostojic S (2016) Natural firing patterns imply low sensitivity of synaptic plasticity to spike timing compared with firing rate. *Journal of Neuroscience* 36:11238–11258.

Greiner HM, Horn PS, Tenney JR, Arya R, Jain SV, Holland KD, Leach JL, Miles L, Rose DF, Fujiwara H, Mangano FT (2016) Preresection intraoperative electrocorticography (ECoG) abnormalities predict seizure-onset zone and outcome in pediatric epilepsy surgery. *Epilepsia* 57:582–589.

Griffith T, Mellor J, Tsaneva-Atanasova K (2014) Spike Timing-Dependent Plasticity (STDP), Biophysical Models In Jaeger D, Jung R, editors, *Encyclopedia of Computational Neuroscience*, pp. 1–5. Springer New York, New York, NY.

Grillner S, Kozlov A (2021) The CPGs for Limbed Locomotion–Facts and Fiction. *International Journal of Molecular Sciences* 22:5882.

Gu Q (2002) Neuromodulatory transmitter systems in the cortex and their role in cortical plasticity. *Neuroscience* 111:815–835.

Guillery RW, Sherman SM (2002) Thalamic relay functions and their role in corticocortical communication: Generalizations from the visual system. *Neuron* 33:163–175.

Gurunathan A, Iyer LR (2020) Spurious learning in networks with Spike Driven Synaptic Plasticity In *International Conference on Neuromorphic Systems 2020*, pp. 1–8, Oak Ridge TN USA. ACM.

Gütig R, Aharonov R, Rotter S, Sompolinsky H (2003) Learning Input Correlations through Nonlinear Temporally Asymmetric Hebbian Plasticity. *The Journal of Neuroscience* 23:3697–3714.

Hagen E, Næss S, Ness TV, Einevoll GT (2018) Multimodal Modeling of Neural Network Activity: Computing LFP, ECoG, EEG, and MEG Signals With LFPy 2.0. *Frontiers in Neuroinformatics* 12:92.

Haley JA, Hampton D, Marder E (2018) Two central pattern generators from the crab, Cancer borealis, respond robustly and differentially to extreme extracellular pH. *eLife* 7:e41877.

Hansel D, Mato G (2013) Short-Term Plasticity Explains Irregular Persistent Activity in Working Memory Tasks. *The Journal of Neuroscience* 33:133.

Harnett MT, Bernier BE, Ahn KC, Morikawa H (2009) Burst-Timing-Dependent Plasticity of NMDA Receptor-Mediated Transmission in Midbrain Dopamine Neurons. *Neuron* 62:826–838.

Hartley M, Taylor N, Taylor J (2006) Understanding spike-time-dependent plasticity: A biologically motivated computational model. *Neurocomputing* 69:2005–2016.

Hebb DO (1949) *The organization of behavior : a neuropsychological theory* A Wiley book in clinical psychology. John Wiley, New York, NY.

Hedrick T, Waters J (2012) Effect of temperature on spiking patterns of neocortical layer 2/3 and layer 6 pyramidal neurons. *Frontiers in Neural Circuits* 6.

Heidelberger R, Shouval H, Zucker RS, Byrne JH (2014) Synaptic Plasticity In *From Molecules to Networks: An Introduction to Cellular and Molecular Neuroscience: Third Edition*, pp. 533–561. Elsevier Inc.

Helias M (2008) Structural plasticity controlled by calcium based correlation detection. *Frontiers in Computational Neuroscience* 2.

Herculano-Houzel S (2009) The human brain in numbers: a linearly scaled-up primate brain. *Frontiers in Human Neuroscience* 3.

Herrington J, Lingle CJ (1992) Kinetic and pharmacological properties of low voltage-activated Ca2+ current in rat clonal (GH3) pituitary cells. *Journal of Neurophysiology* 68:213–232 _eprint: https://doi.org/10.1152/jn.1992.68.1.213.

Higgins D, Graupner M, Brunel N (2014) Memory Maintenance in Synapses with Calcium-Based Plasticity in the Presence of Background Activity. *PLoS Computational Biology* 10.

Hill S, Tononi G (2005) Modeling sleep and wakefulness in the thalamocortical system. *Journal of Neurophysiology* 93:1671–1698.

Hille B (2001) *Ion channels of excitable membranes* Sinauer, Sunderland, Mass, 3rd ed edition.

Hiratani N, Fukai T (2017) Detailed dendritic excitatory/inhibitory balance through heterosynaptic spike-timing-dependent plasticity. *Journal of Neuroscience* 37:12106–12122.

Hodgkin AL, Huxley AF (1952) A quantitative description of membrane current and its application to conduction and excitation in nerve. *The Journal of Physiology* 117:500–544.

Honnuraiah S, Narayanan R (2013) A Calcium-Dependent Plasticity Rule for HCN Channels Maintains Activity Homeostasis and Stable Synaptic Learning. *PLoS ONE* 8.

Houben AM, Keil MS (2020) A calcium-influx-dependent plasticity model exhibiting multiple STDP curves. *Journal of Computational Neuroscience* 48:65–84.

Huc S, Monteil A, Bidaud I, Barbara G, Chemin J, Lory P (2009) Regulation of T-type calcium channels: Signalling pathways and functional implications. *Biochimica et Biophysica Acta (BBA) - Molecular Cell Research* 1793:947–952.

Huguenard JR, McCormick DA (1992) Simulation of the currents involved in rhythmic oscillations in thalamic relay neurons. *Journal of Neurophysiology* 68:1373–1383.

Humphries M (2012) Dopaminergic control of the exploration-exploitation trade-off via the basal ganglia. *Frontiers in Neuroscience* 6.

Huxley A (2001) Sir Alan Hodgkin, 5 February 1914. 20 December 1998. *Proceedings of the American Philosophical Society* 145:98–105 Publisher: American Philosophical Society.

Iannella N, Launey T, Abbott D, Tanaka S (2014) A nonlinear cable framework for bidirectional synaptic plasticity. *PLoS ONE* 9:1–14.

Inglebert Y, Aljadeff J, Brunel N, Debanne D (2021) Synaptic plasticity rules with physiological calcium levels. *Proceedings of the National Academy of Sciences of the United States of America* 117:33639–33648.

Izhikevich EM (2007) Solving the distal reward problem through linkage of STDP and dopamine signaling. *Cerebral Cortex* 17:2443–2452.

Izhikevich EM, Hoppensteadt F (2004) Classification of bursting mappings. *International Journal of Bifurcation and Chaos* 14:3847–3854.

Jacquerie K, Drion G (2021) Robust switches in thalamic network activity require a timescale separation between sodium and T-type calcium channel activations. *PLOS Computational Biology* 17:e1008997.

Jacquerie K, Minne C, Ponnet J, Benghalem N, Sacré P, Drion G (2022) Switches to rhythmic brain activity lead to a plasticity-induced reset in synaptic weights preprint, Neuroscience.

Jedrzejewska-Szmek J, Damodaran S, Dorman DB, Blackwell KT (2017) Calcium dynamics predict direction of synaptic plasticity in striatal spiny projection neurons. *European Journal of Neuroscience* 45:1044–1056.

Jehasse K, Jacquerie K, de Froidmont A, Lemoine C, Grisar T, Stouffs K, Lakaye B, Seutin V (2021) Functional analysis of the F337C mutation in the *CLCN1* gene associated with dominant *myotonia congenita* reveals an alteration of the macroscopic conductance and voltage dependence. *Molecular Genetics & Genomic Medicine* 9:1–6.

Jeong J (2012) Bursting dynamics in the brain.

Jeong J, Shi WX, Hoffman R, Oh J, Gore JC, Bunney BS, Peterson BS (2012) Bursting as a source of non-linear determinism in the firing patterns of nigral dopamine neurons: Deterministic bursts in nigral DA neurons. *European Journal of Neuroscience* 36:3214–3223.

Ji H, Hougaard C, Herrik KF, Strøbaek D, Christophersen P, Shepard PD (2009) Tuning the excitability of midbrain dopamine neurons by modulating the Ca^{2+} sensitivity of SK channels. *European Journal of Neuroscience* 29:1883–1895.

Johnson SW, Seutin V, North RA (1992) Burst Firing in Dopamine Neurons Induced by *N* -Methyl-D-aspartate: Role of Electrogenic Sodium Pump. *Science* 258:665–667.

Kandel ER (1979) *Behavioral biology of Aplysia: a contribution to the comparative study of opisthobranch molluscs* A Series of books in psychology. W. H. Freeman, San Francisco.

Karabanov A, Ziemann U, Hamada M, George MS, Quartarone A, Classen J, Massimini M, Rothwell J, Siebner HR (2015) Consensus paper: Probing homeostatic plasticity of human cortex with non-invasive transcranial brain stimulation. *Brain Stimulation* 8:993–1006 Publisher: Elsevier.

Karmarkar UR, Buonomano DV (2002) A model of spike-timing dependent plasticity: One or two coincidence detectors? *Journal of Neurophysiology* 88:507–513.

Kirchner JH, Gjorgjieva J (2021) Emergence of local and global synaptic organization on cortical dendrites. *Nature Communications* 12:4005.

Kirchner JH, Gjorgjieva J (2022) Emergence of synaptic organization and computation in dendrites. *Neuroforum* 28:21–30.

Kirkwood A (2007) Neuromodulation of Cortical Synaptic Plasticity In Tseng KY, Atzori M, editors, *Monoaminergic Modulation of Cortical Excitability*, pp. 209–216. Springer US, Boston, MA.

Klöckner U, Lee JH, Cribbs LL, Daud A, Hescheler J, Pereverzev A, Perez-Reyes E, Schneider T (1999) Comparison of the Ca2+ currents induced by expression of three cloned a-1 subunits, a-1G, a-1H and α-1I, of low-voltage-activated T-type Ca2+ channels. *European Journal of Neuroscience* .

Komendantov AO, Venkadesh S, Rees CL, Wheeler DW, Hamilton DJ, Ascoli GA (2019) Quantitative firing pattern phenotyping of hippocampal neuron types. *Scientific Reports* 9:17915.

Konerding WS, Froriep UP, Kral A, Baumhoff P (2018) New thin-film surface electrode array enables brain mapping with high spatial acuity in rodents. *Scientific Reports* 8:3825.

Kornijcuk V, Kim D, Kim G, Jeong DS (2020) Simplified calcium signaling cascade for synaptic plasticity. *Neural Networks* 123:38–51.

Kotaleski JH, Blackwell KT (2010) Modelling the molecular mechanisms of synaptic plasticity using systems biology approaches. *Nature Reviews Neuroscience* 11:239–251.

Krieg D, Triesch J (2014) A unifying theory of synaptic long-term plasticity based on a sparse distribution of synaptic strength. *Frontiers in Synaptic Neuroscience* 6.

Kringelbach ML, Deco G (2020) Brain States and Transitions: Insights from Computational Neuroscience. *Cell Reports* 32:108128.

Krishnan GP, Chauvette S, Shamie I, Soltani S, Timofeev I, Cash SS, Halgren E, Bazhenov M (2016) Cellular and neurochemical basis of sleep stages in the thalamocortical network. *eLife* 5:1–29.

Krug M, Lössner B, Ott T (1984) Anisomycin blocks the late phase of long-term potentiation in the dentate gyrus of freely moving rats. *Brain Research Bulletin* 13:39–42.

Kubota S, Kitajima T (2008) A model for synaptic development regulated by NMDA receptor subunit expression. *Journal of Computational Neuroscience* 24:1–20.

Kubota S, Rubin JE (2011) NMDA-induced burst firing in a model subthalamic nucleus neuron. *Journal of Neurophysiology* 106:527–537.

Kucyi A, Davis KD (2017) The Neural Code for Pain: From Single-Cell Electrophysiology to the Dynamic Pain Connectome. *The Neuroscientist* 23:397–414.

Kumar A, Mehta MR (2011) Frequency-dependent changes in NMDAR-dependent synaptic plasticity. *Frontiers in Computational Neuroscience* 5.

Kühn AA, Williams D, Kupsch A, Limousin P, Hariz M, Schneider GH, Yarrow K, Brown P (2004) Event-related beta desynchronization in human subthalamic nucleus correlates with motor performance. *Brain* 127:735–746.

Lacaux C, Izabelle C, Santantonio G, De Villèle L, Frain J, Lubart T, Pizza F, Plazzi G, Arnulf I, Oudiette D (2019) Increased creative thinking in narcolepsy. *Brain* 142:1988–1999.

Lambert R, Bessaih T, Leresche N (2008) Modulation of Neuronal T-Type Calcium Channels. *CNS & Neurological Disorders - Drug Targets* 5:611–627.

Lamprecht R, LeDoux J (2004) Structural plasticity and memory. *Nature Reviews Neuroscience* 5:45–54.

Lappalainen J, Herpich J, Tetzlaff C (2019) A theoretical framework to derive simple, firing-rate-dependent mathematical models of synaptic plasticity. *Frontiers in Computational Neuroscience* 13:1–13.

LeCun Y, Cortes C, Burges C (1998) MNIST handwritten digit database.

Lee HK, Kirkwood A (2019) Mechanisms of Homeostatic Synaptic Plasticity in vivo. *Frontiers in cellular neuroscience* 13:520–520 Place: Switzerland Publisher: Frontiers Research Foundation.

Lee SH, Dan Y (2012) Neuromodulation of Brain States. *Neuron* 76:209–222 Publisher: Elsevier Inc.

Legenstein R, Pecevski D, Maass W (2008) A learning theory for reward-modulated spike-timing-dependent plasticity with application to biofeedback. *PLoS Computational Biology* 4.

Legenstein RA, Maass W (2005) A Criterion for the Convergence of Learning with Spike Timing Dependent Plasticity In *NIPS 2005*, p. 8, Vancouver, Canada.

Lehr AB, Luboeinski J, Tetzlaff C (2022) Neuromodulator-dependent synaptic tagging and capture retroactively controls neural coding in spiking neural networks. *Scientific Reports* 12:17772.

LeMasson G, Marder E, Abbott LF (1993) Activity-Dependent Regulation of Conductances in Model Neurons. *Science* 259:1915–1917.

Lerner TN, Kreitzer AC (2011) Neuromodulatory control of striatal plasticity and behavior. *Current Opinion in Neurobiology* 21:322–327.

Letzkus JJ, Kampa BM, Stuart GJ (2006) Learning Rules for Spike Timing-Dependent Plasticity Depend on Dendritic Synapse Location. *Journal of Neuroscience* 26:10420–10429.

Li Y, Kulvicius T, Tetzlaff C (2016) Induction and consolidation of calcium-based homo- and heterosynaptic potentiation and depression. *PLoS ONE* 11:1–23.

Lisman J (1997) Bursts as a unit of neural information: making unreliable synapses reliable. *Trends in Neurosciences* 20:38–43.

Lisman J, Grace AA, Duzel E (2011) A neoHebbian framework for episodic memory; role of dopamine-dependent late LTP. *Trends in Neurosciences* 34:536–547.

Lisman J, Spruston N (2010) Questions about STDP as a general model of synaptic plasticity. *Frontiers in Synaptic Neuroscience* 2:1–5.

Liu H, Song Y, Xue F, Li X (2015) Effects of bursting dynamic features on the generation of multi-clustered structure of neural network with symmetric spike-timing-dependent plasticity learning rule. *Chaos: An Interdisciplinary Journal of Nonlinear Science* 25:113108–113108.

Liu Z, Golowasch J, Marder E, Abbott LF (1998) A Model Neuron with Activity-Dependent Conductances Regulated by Multiple Calcium Sensors. *The Journal of Neuroscience* 18:2309–2320.

Luboeinski J, Tetzlaff C (2021) Memory consolidation and improvement by synaptic tagging and capture in recurrent neural networks. *Communications Biology* 4:275.

Madadi Asl M, Vahabie AH, Valizadeh A (2018) Dopaminergic Modulation of Synaptic Plasticity, Its Role in Neuropsychiatric Disorders, and Its Computational Modeling. *Basic and Clinical Neuroscience Journal* .

Magee JC, Grienberger C (2020) Synaptic Plasticity Forms and Functions. *Annual Review of Neuroscience* 43:95–117 Publisher: Annual Reviews.

Mahajan G, Nadkarni S (2019) Intracellular calcium stores mediate metaplasticity at hippocampal dendritic spines. *Journal of Physiology* 597:3473–3502.

Manninen T, Hituri K, Kotaleski JH, Blackwell KT, Linne ML (2010) Postsynaptic Signal Transduction Models for Long-Term Potentiation and Depression. *Frontiers in Computational Neuroscience* 4.

Marder E (2003) Plateau properties in pain pathways. *Nature Neuroscience* 6:210–212.

Marder E (2011) Variability, compensation, and modulation in neurons and circuits. *Proceedings of the National Academy of Sciences* 108:15542–15548.

Marder E (2012) Neuromodulation of Neuronal Circuits: Back to the Future. *Neuron* 76:1–11 Publisher: Elsevier Inc.

Marder E, Abbott LF, Turrigiano GG, Liu Z, Golowasch J (1996) Memory from the dynamics of intrinsic membrane currents. *Proceedings of the National Academy of Sciences of the United States of America* 93:13481–13486.

Marder E, Bucher D (2007) Understanding Circuit Dynamics Using the Stomatogastric Nervous System of Lobsters and Crabs. *Annual Review of Physiology* 69:291–316.

Marder E, O'Leary T, Shruti S (2014) Neuromodulation of Circuits with Variable Parameters: Single Neurons and Small Circuits Reveal Principles of State-Dependent and Robust Neuromodulation. *Annual Review of Neuroscience* 37:329–346.

Marder E, Prinz AA (2002) Modeling stability in neuron and network function: The role of activity in homeostasis. *BioEssays* 24:1145–1154.

Marder E, Rue MC (2021) From the Neuroscience of Individual Variability to Climate Change. *The Journal of Neuroscience* 41:10213–10221.

Marder E, Taylor AL (2011) Multiple models to capture the variability in biological neurons and networks. *Nature Neuroscience* 14:133–138 Publisher: Nature Publishing Group.

Markram H, Gerstner W, Sjöström PJ (2012) Spike-timing-dependent plasticity: A comprehensive overview. *Frontiers in Synaptic Neuroscience* 4:2–5.

Markram H, Gerstner W, Sjöström PJ (2011) A history of spike-timing-dependent plasticity. *Frontiers in Synaptic Neuroscience* 3:1–24.

Markram H, Lübke J, Frotscher M, Sakmann B (1997) Regulation of Synaptic Efficacy by Coincidence of Postsynaptic APs and EPSPs. *Science* 275:213–215.

Markram H, Muller E, Ramaswamy S, Reimann M, Abdellah M, Sanchez C, Ailamaki A, Alonso-Nanclares L, Antille N, Arsever S, Kahou G, Berger T, Bilgili A, Buncic N, Chalimourda A, Chindemi G, Courcol JD, Delalondre F, Delattre V, Druckmann S, Dumusc R, Dynes J, Eilemann S, Gal E, Gevaert M, Ghobril JP, Gidon A, Graham J, Gupta A, Haenel V, Hay E, Heinis T, Hernando J, Hines M, Kanari L, Keller D, Kenyon J, Khazen G, Kim Y, King J, Kisvarday Z, Kumbhar P, Lasserre S, Le Bé JV, Magalhães B, Merchán-Pérez A, Meystre J, Morrice B, Muller J, Muñoz-Céspedes A, Muralidhar S, Muthurasa K, Nachbaur D, Newton T, Nolte M, Ovcharenko A, Palacios J, Pastor L, Perin R, Ranjan R, Riachi I, Rodríguez JR, Riquelme J, Rössert C, Sfyrakis K, Shi Y, Shillcock J, Silberberg G, Silva R, Tauheed F, Telefont M, Toledo-Rodriguez M, Tränkler T, Van Geit W, Díaz J, Walker R, Wang Y, Zaninetta S, DeFelipe J, Hill S, Segev I, Schürmann F (2015) Reconstruction and Simulation of Neocortical Microcircuitry. *Cell* 163:456–492.

Mazzoni A, Lindén H, Cuntz H, Lansner A, Panzeri S, Einevoll GT (2015) Computing the Local Field Potential (LFP) from Integrate-and-Fire Network Models. *PLOS Computational Biology* 11:e1004584.

McCormick DA, Huguenard JR (1992) A model of the electrophysiological properties of thalamocortical relay neurons. *Journal of Neurophysiology* 68:1384–1400.

McCormick DA, Bal T (1997) Sleep and arousal: Thalamocortical mechanisms. *Annual Review of Neuroscience* 20:185–215.

McCormick DA, Salkoff DB (2015) Brain State Dependent Activity in the Cortex and Thalamus. *Current Opinion in Neurobiology* 31:133–140.

McGinley MJ, Vinck M, Reimer J, Batista-Brito R, Zagha E, Cadwell CR, Tolias AS, Cardin JA, McCormick DA (2015) Waking State: Rapid Variations Modulate Neural and Behavioral Responses. *Neuron* 87:1143–1161 Publisher: Elsevier.

Mei J, Muller E, Ramaswamy S (2022) Informing deep neural networks by multiscale principles of neuromodulatory systems. *Trends in Neurosciences* 45:237–250.

Meriney SD, Fanselow EE (2019) Chapter 14 - Synaptic Plasticity In Meriney SD, Fanselow EE, editors, *Synaptic Transmission*, pp. 287–329. Academic Press.

Miehl C, Gjorgjieva J (2022) Stability and learning in excitatory synapses by nonlinear inhibitory plasticity. *PLOS Computational Biology* 18:e1010682.

Miehl C, Onasch S, Festa D, Gjorgjieva J (2022) Formation and computational implications of assemblies in neural circuits. *The Journal of Physiology* p. JP282750.

Molnár B, Sere P, Bordé S, Koós K, Zsigri N, Horváth P, Lőrincz ML (2021) Cell Type-Specific Arousal-Dependent Modulation of Thalamic Activity in the Lateral Geniculate Nucleus. *Cerebral Cortex Communications* 2:tgab020.

Morrison A, Diesmann M, Gerstner W (2008) Phenomenological models of synaptic plasticity based on spike timing. *Biological Cybernetics* 98:459–478.

Murakami M, Kashiwadani H, Kirino Y, Mori K (2005) State-Dependent Sensory Gating in Olfactory Cortex. *Neuron* 46:285–296.

Murray Sherman S (2001) Tonic and burst firing: Dual modes of thalamocortical relay ISSN: 01662236 Publication Title: Trends in Neurosciences.

Mäki-Marttunen T, Iannella N, Edwards AG, Einevoll GT, Blackwell KT (2020) A unified computational model for cortical post-synaptic plasticity. *eLife* 9:e55714.

Nadim F, Bucher D (2014) Neuromodulation of neurons and synapses. *Current Opinion in Neurobiology* 29:48–56.

Nakano T, Doi T, Yoshimoto J, Doya K (2010) A kinetic model of dopamine- and calcium-dependent striatal synaptic plasticity. *PLoS Computational Biology* 6.

Nere A, Hashmi A, Cirelli C, Tononi G (2013) Sleep-dependent synaptic down-selection (I): modeling the benefits of sleep on memory consolidation and integration. *Frontiers in neurology* 4:143–143 Place: Switzerland Publisher: Frontiers Media S.A.

Neuromatch (2021) Youtube link \url{https://www.youtube.com/watch?v=p848349hPyw}.

Nevian T, Sakmann B (2006) Spine Ca2+ signaling in spike-timing-dependent plasticity. *Journal of Neuroscience* 26:11001–11013.

Ngezahayo A, Schachner M, Artola A (2000) Synaptic Activity Modulates the Induction of Bidirectional Synaptic Changes in Adult Mouse Hippocampus. *The Journal of Neuroscience* 20:2451–2458.

O'Donnel C, Nolan MF, van Rossum MC (2011) Dendritic spine dynamics regulate the long-term stability of synaptic plasticity. *Journal of Neuroscience* 31:16142–16156.

Oja E (1982) Simplified neuron model as a principal component analyzer. *Journal of Mathematical Biology* 15:267–273.

Okuda K, Højgaard K, Privitera L, Bayraktar G, Takeuchi T (2021) Initial memory consolidation and the synaptic tagging and capture hypothesis. *European Journal of Neuroscience* 54:6826–6849.

Olcese U, Esser SK, Tononi G (2010) Sleep and synaptic renormalization: A computational study. *Journal of Neurophysiology* 104:3476–3493.

O'Leary T, Sutton AC, Marder E (2015) Computational models in the age of large datasets. *Current Opinion in Neurobiology* 32:87–94 Publisher: Elsevier Ltd.

O'Leary T, Williams AH, Franci A, Marder E (2014) Cell Types, Network Homeostasis, and Pathological Compensation from a Biologically Plausible Ion Channel Expression Model. *Neuron* 82:809–821 Publisher: Elsevier Inc.

Olypher AV, Calabrese RL (2007) Using constraints on neuronal activity to reveal compensatory changes in neuronal parameters. *Journal of Neurophysiology* 98:3749–3758.

Paludo Silveira JA, Protachevicz PR, Viana RL, Batista AM (2021) Effects of burst-timing-dependent plasticity on synchronous behaviour in neuronal network. *Neurocomputing* 436:126–135.

Park Y, Choi W, Paik SB (2017) Symmetry of learning rate in synaptic plasticity modulates formation of flexible and stable memories. *Scientific Reports* 7:5671.

Pawlak V, Kerr JND (2008) Dopamine Receptor Activation Is Required for Corticostriatal Spike-Timing-Dependent Plasticity. *Journal of Neuroscience* 28:2435–2446.

Pawlak V (2010) Timing is not everything: neuromodulation opens the STDP gate. *Frontiers in Synaptic Neuroscience* 2.

Payeur A, Guerguiev J, Zenke F, Richards BA, Naud R (2020) Burst-dependent synaptic plasticity can coordinate learning in hierarchical circuits preprint, Neuroscience.

Pedrosa V, Clopath C (2017) The role of neuromodulators in cortical plasticity. A computational perspective. *Frontiers in Synaptic Neuroscience* 8:38–38.

Perez-Reyes E (2003) Molecular Physiology of Low-Voltage-Activated T-type Calcium Channels. *Physiological Reviews* 83:117–161.

Petousakis K, Apostolopoulou AA, Poirazi P (2022) The impact of Hodgkin–Huxley models on dendritic research. *The Journal of Physiology* p. JP282756.

Pfister JP, Gerstner W (2006) Triplets of spikes in a model of spike timing-dependent plasticity. *Journal of Neuroscience* 26:9673–9682.

Poirazi P, Kastellakis G (2017) . . . with Love, from Post to Pre. *Neuron* 96:9–10.

Poirazi P, Mel BW (2001) Impact of Active Dendrites and Structural Plasticity on the Memory Capacity of Neural Tissue. *Neuron* 29:779–796.

Poirazi P, Papoutsi A (2020) Illuminating dendritic function with computational models. *Nature Reviews Neuroscience* 21:303–321.

Polack PO, Friedman J, Golshani P (2013) Cellular mechanisms of brain state–dependent gain modulation in visual cortex. *Nature Neuroscience* 16:1331–1339.

Pospischil M, Toledo-Rodriguez M, Monier C, Piwkowska Z, Bal T, Frégnac Y, Markram H, Destexhe A (2008) Minimal Hodgkin–Huxley type models for different classes of cortical and thalamic neurons. *Biological Cybernetics* 99:427–441.

Prinz AA, Abbott LF, Marder E (2004) The dynamic clamp comes of age. *Trends in Neurosciences* 27:218–224.

Prinz AA, Billimoria CP, Marder E (2003) Alternative to Hand-Tuning Conductance-Based Models: Construction and Analysis of Databases of Model Neurons. *Journal of Neurophysiology* 90:3998–4015.

Prinz AA, Bucher D, Marder E (2004) Similar network activity from disparate circuit parameters. *Nature Neuroscience* pp. 1345–1352.

Purves D (2014) *Neuroscience, 3rd Edition* Sinauer Associates.

Rackham OJ, Tsaneva-Atanasova K, Ganesh A, Mellor JR (2010) A Ca2+-based computational model for NDMA receptor-dependent synaptic plasticity at individual post-synaptic spines in the hippocampus. *Frontiers in Synaptic Neuroscience* 2:1–12.

Ramcharan EJ, Gnadt JW, Sherman SM (2000) Burst and tonic firing in thalamic cells of unanesthetized, behaving monkeys. *Visual Neuroscience* 17:55–62.

Ramirez JM, Koch H, Garcia AJ, Doi A, Zanella S (2011) The role of spiking and bursting pacemakers in the neuronal control of breathing. *Journal of Biological Physics* 37:241–261.

Rasmussen R, Jensen MH, Heltberg ML (2017) Chaotic Dynamics Mediate Brain State Transitions, Driven by Changes in Extracellular Ion Concentrations. *Cell Systems* 5:591–603.e4.

Reckziegel G, Beck H, Schramm J, Elger CE, Urban BW (1998) Electrophysiological characterization of Na+ currents in acutely isolated human hippocampal dentate granule cells. *Journal of Physiology* 509:139–150.

Redondo RL, Morris RGM (2011) Making memories last: the synaptic tagging and capture hypothesis. *Nature Reviews Neuroscience* 12:17–30.

Redondo RL, Okuno H, Spooner PA, Frenguelli BG, Bito H, Morris RGM (2010) Synaptic Tagging and Capture: Differential Role of Distinct Calcium/Calmodulin Kinases in Protein Synthesis-Dependent Long-Term Potentiation. *The Journal of Neuroscience* 30:4981–4989.

Reimer J, Froudarakis E, Cadwell C, Yatsenko D, Denfield G, Tolias A (2014) Pupil Fluctuations Track Fast Switching of Cortical States during Quiet Wakefulness. *Neuron* 84:355–362.

Roffman RC, Norris BJ, Calabrese RL (2012) Animal-to-animal variability of connection strength in the leech heartbeat central pattern generator. *Journal of Neurophysiology* 107:1681–1693.

Rubin J, Lee DD, Sompolinsky H (2001) Equilibrium Properties of Temporally Asymmetric Hebbian Plasticity. *Physical Review Letters* 86:364–367.

Rubin JE, Gerkin RC, Bi GQ, Chow CC (2005) Calcium time course as a signal for spike-timing-dependent plasticity. *Journal of Neurophysiology* 93:2600–2613.

Rubin JE, Terman D (2004) High frequency stimulation of the subthalamic nucleus eliminates pathological thalamic rhythmicity in a computational model. *Journal of Computational Neuroscience* 16:211–235.

Rule ME, O'Leary T, Harvey CD (2019) Causes and consequences of representational drift. *Current Opinion in Neurobiology* 58:141–147.

Rush ME, Rinzel J (1994) Analysis of bursting in a thalamic neuron model. *Biological Cybernetics* 71:281–291.

Salgado H, Köhr G, Treviño M (2012) Noradrenergic 'Tone' Determines Dichotomous Control of Cortical Spike-Timing-Dependent Plasticity. *Scientific Reports* 2:417.

Saudargienė A, Graham BP (2015) Inhibitory control of site-specific synaptic plasticity in a model CA1 pyramidal neuron. *Biosystems* 130:37–50.

Schultz W (2006) Behavioral Theories and the Neurophysiology of Reward. *Annual Review of Psychology* 57:87–115.

Schultz W (2007) Behavioral dopamine signals. *Trends in Neurosciences* 30:203–210.

Schulz DJ, Goaillard JM, Marder E (2006) Variable channel expression in identified single and electrically coupled neurons in different animals. *Nature Neuroscience* 9:356–362.

Sehgal M, Song C, L. Ehlers V, Moyer J (2013) Learning to learn – intrinsic plasticity as a metaplasticity mechanism for memory formation. *Neurobiology of Learning and Memory* 105:186–99.

Seibt J, Frank MG (2019) Primed to sleep: The dynamics of synaptic plasticity across brain states. *Frontiers in Systems Neuroscience* 13:1–19.

Senn W, Group TN (2020) Spike-Timing-Dependent Plasticity: learning rules. *Encyclopedia of Computational Neuroscience* pp. 1–10.

Seol GH, Ziburkus J, Huang S, Song L, Kim IT, Takamiya K, Huganir RL, Lee HK, Kirkwood A (2007) Neuromodulators Control the Polarity of Spike-Timing-Dependent Synaptic Plasticity. *Neuron* 55:919–929.

Sepulchre R (2020) Noble use of feedback. *IEEE Control Systems* 40:3–4.

Shah NT, Yeung LC, Cooper LN, Cai Y, Shouval HZ (2006) A biophysical basis for the inter-spike interaction of spike-timing- dependent plasticity. *Biological Cybernetics* 95:113–121.

Shao J, Liu Y, Gao D, Tu J, Yang F (2021) Neural Burst Firing and Its Roles in Mental and Neurological Disorders. *Frontiers in Cellular Neuroscience* 15:741292.

Shepherd JD, Rumbaugh G, Wu J, Chowdhury S, Plath N, Kuhl D, Huganir RL, Worley PF (2006) Arc/Arg3.1 Mediates Homeostatic Synaptic Scaling of AMPA Receptors. *Neuron* 52:475–484.

Sherman SM (2001) Tonic and burst firing: dual modes of thalamocortical relay. *Trends in neurosciences* 24:122–6.

Sherman SM, Guillery RW (1996) Functional organization of thalamocortical relays. *Journal of Neurophysiology* 76:1367–1395.

Shine JM, Müller EJ, Munn B, Cabral J, Moran RJ, Breakspear M (2021) Computational models link cellular mechanisms of neuromodulation to large-scale neural dynamics. *Nature Neuroscience* 24:765–776.

Shouval HZ (2007) Models of synaptic plasticity. *Scholarpedia* .

Shouval HZ (2011) What is the appropriate description level for synaptic plasticity? *Proceedings of the National Academy of Sciences of the United States of America* 108:19103–19104.

Shouval HZ, Bear MF, Cooper LN (2002) A unified model of NMDA receptor-dependent bidirectional synaptic plasticity. *Proceedings of the National Academy of Sciences of the United States of America* 99:10831–10836.

Shouval HZ, Castellani GC, Blais BS, Yeung LC, Cooper LN (2002) Converging evidence for a simplified biophysical model of synaptic plasticity. *Biological Cybernetics* 87:383–391.

Shouval HZ, Kalantzis G (2005) Stochastic properties of synaptic transmission affect the shape of spike time-dependent plasticity curves. *Journal of Neurophysiology* 93:1069–1073.

Sjöström J, Gerstner W (2010) Spike-timing dependent plasticity. *Scholarpedia* 5:1362–1362.

Sjöström PJ, Häusser M (2006) A Cooperative Switch Determines the Sign of Synaptic Plasticity in Distal Dendrites of Neocortical Pyramidal Neurons. *Neuron* 51:227–238.

Sjöström PJ, Turrigiano GG, Nelson SB (2001) Rate, Timing, and Cooperativity Jointly Determine Cortical Synaptic Plasticity. *Neuron* 32:1149–1164.

Smith GD, Cox CL, Sherman SM, Rinzel J (2000) Fourier Analysis of Sinusoidally Driven Thalamocortical Relay Neurons and a Minimal Integrate-and-Fire-or-Burst Model. *Journal of Neurophysiology* 83:588–610.

Smolen P (2007) A Model of Late Long-Term Potentiation Simulates Aspects of Memory Maintenance. *PLoS ONE* 2:e445.

Smolen P, Baxter DA, Byrne JH (2006) A Model of the Roles of Essential Kinases in the Induction and Expression of Late Long-Term Potentiation. *Biophysical Journal* 90:2760–2775.

Smolen P, Baxter DA, Byrne JH (2020) Comparing Theories for the Maintenance of Late LTP and Long-Term Memory: Computational Analysis of the Roles of Kinase Feedback Pathways and Synaptic Reactivation. *Frontiers in Computational Neuroscience* 14:569349.

Soffe S (1993) Two distinct rhythmic motor patterns are driven by common premotor and motor neurons in a simple vertebrate spinal cord. *The Journal of Neuroscience* 13:4456–4469.

Song S, Miller KD, Abbott LF (2000) Competitive Hebbian learning through spike-timing-dependent synaptic plasticity. *Nature Neuroscience* 3:919–926.

Standage D, Trappenberg T, Blohm G (2014) Calcium-dependent calcium decay explains STDP in a dynamic model of hippocampal synapses. *PLoS ONE* 9.

Steriade M, Amzica F, Nunez A (1993) Cholinergic and noradrenergic modulation of the slow (approximately 0.3 Hz) oscillation in neocortical cells. *Journal of Neurophysiology* 70:1385–1400.

Steriade M, Timofeev I, Grenier F (2001) Natural waking and sleep states: A view from inside neocortical neurons. *Journal of Neurophysiology* 85:1969–1985.

Strogatz a S (2015) *Nonlinear dynamics and chaos : with applications to physics, biology, chemistry, and engineering* Second edition. Boulder, CO : Westview Press, a member of the Perseus Books Group, [2015].

Swann N, Poizner H, Houser M, Gould S, Greenhouse I, Cai W, Strunk J, George J, Aron AR (2011) Deep Brain Stimulation of the Subthalamic Nucleus Alters the Cortical Profile of Response Inhibition in the Beta Frequency Band: A Scalp EEG Study in Parkinson's Disease. *Journal of Neuroscience* 31:5721–5729.

Takahashi K, Lin JS, Sakai K (2006) Neuronal Activity of Histaminergic Tuberomammillary Neurons During Wake-Sleep States in the Mouse. *Journal of Neuroscience* 26:10292–10298.

Takeuchi T, Duszkiewicz AJ, Morris RGM (2014) The synaptic plasticity and memory hypothesis: encoding, storage and persistence. *Philosophical Transactions of the Royal Society B: Biological Sciences* 369:20130288.

Tantirigama MLS, Zolnik T, Judkewitz B, Larkum ME, Sachdev RNS (2020) Perspective on the Multiple Pathways to Changing Brain States. *Frontiers in Systems Neuroscience* 14:23.

Tatsuki F, Sunagawa GAA, Shi S, Susaki EAA, Yukinaga H, Perrin D, Sumiyama K, Ukai-Tadenuma M, Fujishima H, Ohno Ri, Tone D, Ode KLL, Matsumoto K, Ueda HR (2016) Involvement of Ca2+-Dependent Hyperpolarization in Sleep Duration in Mammals. *Neuron* 90:70–85 Publisher: Elsevier Inc.

Telenczuk B, Telenczuk M, Destexhe A (2020) A kernel-based method to calculate local field potentials from networks of spiking neurons. *Journal of Neuroscience Methods* 344:108871.

Terman D, Rubin JE, Yew AC, Wilson CJ (2002) Activity Patterns in a Model for the Subthalamopallidal Network of the Basal Ganglia. *The Journal of Neuroscience* 22:2963–2976.

Tetzlaff C, Kolodziejski C, Timme M, Tsodyks M, Wörgötter F (2013) Synaptic Scaling Enables Dynamically Distinct Short- and Long-Term Memory Formation. *PLoS Computational Biology* 9:e1003307.

Timofeev I, Chauvette S (2019) Sleep-Wake and Cortical Synaptic Plasticity. *Handbook of Behavioral Neuroscience* 30:443–454.

Titley HK, Brunel N, Hansel C (2017) Toward a Neurocentric View of Learning. *Neuron* 95:19–32.

Traboulsie A, Chemin J, Chevalier M, Quignard JF, Nargeot J, Lory P (2007) Subunit-specific modulation of T-type calcium channels by zinc: Zn $^{2+}$ modulation of T-type Ca $^{2+}$ channels. *The Journal of Physiology* 578:159–171.

Tsai HC, Zhang F, Adamantidis A, Stuber GD, Bonci A, de Lecea L, Deisseroth K (2009) Phasic Firing in Dopaminergic Neurons Is Sufficient for Behavioral Conditioning. *Science* 324:1080–1084.

Tupikov Y, Jin DZ (2021) Addition of new neurons and the emergence of a local neural circuit for precise timing. *PLOS Computational Biology* 17:e1008824.

Turrigiano G, LeMasson G, Marder E (1995) Selective regulation of current densities underlies spontaneous changes in the activity of cultured neurons. *The Journal of Neuroscience* 15:3640–3652.

Turrigiano GG (2012) Homeostatic synaptic plasticity: Local and global mechanisms for stabilizing neuronal function. *Cold Spring Harbor Perspectives in Biology* 4:1–18.

Turrigiano GG, Abbott LF, Marder E (1994) Activity-dependent changes in the intrinsic properties of cultured neurons. *Science* 264:974–977.

Turrigiano GG, Nelson SB (2000) Hebb and homeostasis in neuronal plasticity. *Current Opinion in Neurobiology* 10:358–364.

Turrigiano GG, Nelson SB (2004) Homeostatic plasticity in the developing nervous system. *Nature Reviews Neuroscience* 5:97–107.

Tyree S, Luis De Lecea (2017) Optogenetic Investigation of Arousal Circuits. *International Journal of Molecular Sciences* 18:1773.

Udakis M, Pedrosa V, Chamberlain SE, Clopath C, Mellor JR (2020) Interneuron-specific plasticity at parvalbumin and somatostatin inhibitory synapses onto CA1 pyramidal neurons shapes hippocampal output. *Nature Communications* 11 Publisher: Springer US.

Uhlhaas PJ, Singer W (2006) Neural Synchrony in Brain Disorders: Relevance for Cognitive Dysfunctions and Pathophysiology. *Neuron* 52:155–168.

Urakubo H, Honda M, Froemke RC, Kuroda S (2008) Requirement of an Allosteric Kinetics of NMDA Receptors for Spike Timing-Dependent Plasticity. *Journal of Neuroscience* 28:3310–3323.

URL Image from \url{https://dagemti.com/dage-mti-ir-1000-real-time-infrared-microscopy-camera/}.

URL Image from \url{https://en.wikipedia.org/wiki/Default_mode_network}.

URL Image from \url{https://www.amazon.com.be/dp/B001CIZX0G?psc=1&ref_=cm_sw_r_cp_ud_dp_4HCAGNQD4EVX8SDNBNN1

URL Image from \url{https://www.coolled.com/technical-resources/app-notes/epifluorescence-imaging-and-optogenetic-stimulation-for-in-vitro-electrophysiology/}.

URL Image from \url{https://www.enmieux.be/actualite/inauguration-l-irm-7-tesla-l-universite-liege}.

URL Image from \url{https://www.myndlift.com/post/how-does-our-brain-work-different-brainwaves}.

URL Image from \url{https://www.programmes.uliege.be/cocoon/20222023/en/formations/bref/A2UBIO01.html}.

URL of the website https://www.science.gov/topicpages/r/reward-modulated+spike-timing-dependent+plasticity.html.

URL Youtube video \url{https://www.youtube.com/watch?v=JzlsvFN_5HI}.

Van Ooyen A, Van Pelt J, Corner M (1995) Implications of activity dependent neurite outgrowth for neuronal morphology and network development. *Journal of Theoretical Biology* 172:63–82.

Van Pottelbergh T, Drion G, Sepulchre R (2018) Robust modulation of integrate-and-fire models. *Neural Computation* 30:987–1011.

van Rossum MCW, Shippi M, Barrett AB (2012) Soft-bound Synaptic Plasticity Increases Storage Capacity. *PLoS Computational Biology* 8:e1002836.

Van Rossum MC, Bi GQ, Turrigiano GG (2000) Stable Hebbian learning from spike timing-dependent plasticity. *Journal of Neuroscience* 20:8812–8821.

Van Rossum MC, Shippi M (2013) Computational modelling of memory retention from synapse to behaviour. *Journal of Statistical Mechanics: Theory and Experiment* 2013.

Vecoven N, Ernst D, Wehenkel A, Drion G (2020) Introducing neuromodulation in deep neural networks to learn adaptive behaviours. *PLoS ONE* 15:1–62.

Vignoud G, Venance L, Touboul JD (2018) Interplay of multiple pathways and activity-dependent rules in STDP. *PLOS Computational Biology* 14:e1006184.

Wang HX, Gerkin RC, Nauen DW, Bi GQ (2005) Coactivation and timing-dependent integration of synaptic potentiation and depression. *Nature Neuroscience* 8:187–193.

Wang XJ (1994) Multiple dynamical modes of thalamic relay neurons: Rhythmic bursting and intermittent phase-locking. *Neuroscience* 59:21–31.

Wang XJ, Rinzel J, Rogawski MA (1991) A model of the T-type calcium current and the low-threshold spike in thalamic neurons. *Journal of Neurophysiology* 66:839–850.

Wang XJ (2010) Neurophysiological and Computational Principles of Cortical Rhythms in Cognition. *Physiological Reviews* 90:1195–1268.

Watson CJ, Lydic R, Baghdoyan HA (2011) Sleep duration varies as a function of glutamate and GABA in rat pontine reticular formation: Glutamate, GABA, and sleep episode duration. *Journal of Neurochemistry* 118:571–580.

Wei Y, Krishnan GP, Bazhenov M (2016) Synaptic mechanisms of memory consolidation during sleep slow oscillations. *Journal of Neuroscience* 36:4231–4247.

Weimann JM, Marder E, Evans B, Calabrese RL (1993) The effects of SDRNFLRFamide and TNRNFLRFamide on the motor patterns of the stomatogastric ganglion of the crab cancer borealis. *The Journal of Experimental Biology* 181:1–26.

Williams A, O'Leary T, Marder E (2013) Homeostatic Regulation of Neuronal Excitability. *Scholarpedia* 8:1656–1656.

Wittenberg GM, Wang SSH (2006) Malleability of Spike-Timing-Dependent Plasticity at the CA3-CA1 Synapse. *Journal of Neuroscience* 26:6610–6617.

Wu YK, Hengen KB, Turrigiano GG, Gjorgjieva J (2020) Homeostatic mechanisms regulate distinct aspects of cortical circuit dynamics. *Proceedings of the National Academy of Sciences of the United States of America* 117:24514–24525.

Wu YK, Miehl C, Gjorgjieva J (2022) Regulation of circuit organization and function through inhibitory synaptic plasticity. *Trends in Neurosciences* 45:884–898.

Yang JW, Reyes-Puerta V, Kilb W, Luhmann HJ (2016) Spindle Bursts in Neonatal Rat Cerebral Cortex. *Neural Plasticity* 2016:1–11.

Yang Y, Cui Y, Sang K, Dong Y, Ni Z, Ma S, Hu H (2018) Ketamine blocks bursting in the lateral habenula to rapidly relieve depression. *Nature* 554:317–322.

Yeung LC, Blais BS, Cooper LN, Shouval HZ (2003) Selectivity and metaplasticity in a unified calcium-dependent model. *Advances in Neural Information Processing Systems* .

Yeung LC, Shouval HZ, Blais BS, Cooper LN (2004) Synaptic homeostasis and input selectivity follow from a calcium-dependent plasticity model. *Proceedings of the National Academy of Sciences of the United States of America* 101:14943–14948.

Yger P, Gilson M (2015) Models of metaplasticity: A review of concepts. *Frontiers in Computational Neuroscience* 9:1–14.

Yu FH, Yarov-Yarov V, Gutman G, Catterall WA (2005) Overview of Molecular Relationships in the. *Pharmacological Reviews* 57:387–395.

Yu X, Shouval HZ, Knierim JJ (2008) A biophysical model of synaptic plasticity and metaplasticity can account for the dynamics of the backward shift of hippocampal place fields. *Journal of Neurophysiology* 100:983–992.

Zagha EM D (2014) Neural Control of Brain State. *Current Opinion in NeurobiologyBiology* 0:178–186 ISBN: 6176321972 _eprint: NIHMS150003.

Zagha E, McCormick DA (2014) Neural control of brain state. *Current Opinion in Neurobiology* 29:178–186 Publisher: Elsevier Ltd.

Zamponi GW, Striessnig J, Koschak A, Dolphin AC (2015) The Physiology, Pathology, and Pharmacology of Voltage-Gated Calcium Channels and Their Future Therapeutic Potential. *Pharmacological Reviews* 67:821–870.

Zannone S, Brzosko Z, Paulsen O, Clopath C (2018) Acetylcholine-modulated plasticity in reward-driven navigation: a computational study. *Scientific Reports* 8:1–20.

Zeldenrust F, Wadman WJ, Englitz B (2018) Neural Coding With Bursts—Current State and Future Perspectives. *Frontiers in Computational Neuroscience* 12:48.

Zenke F, Agnes EJ, Gerstner W (2015) Diverse synaptic plasticity mechanisms orchestrated to form and retrieve memories in spiking neural networks. *Nature Communications* 6.

Zenke F, Gerstner W (2017) Hebbian plasticity requires compensatory processes on multiple timescales. *Philosophical Transactions of the Royal Society B: Biological Sciences* 372.

Zenke F, Hennequin G, Gerstner W (2013) Synaptic Plasticity in Neural Networks Needs Homeostasis with a Fast Rate Detector. *PLoS Computational Biology* 9:e1003330.

Zhang JC, Lau PM, Bi GQ (2009) Gain in sensitivity and loss in temporal contrast of STDP by dopaminergic modulation at hippocampal synapses. *Proceedings of the National Academy of Sciences* 106:13028–13033.

Zhang W, Linden DJ (2003) The other side of the engram: experience-driven changes in neuronal intrinsic excitability. *Nature Reviews Neuroscience* 4:885–900.

Zheng P, Dimitrakakis C, Triesch J (2013) Network Self-Organization Explains the Statistics and Dynamics of Synaptic Connection Strengths in Cortex. *PLoS Computational Biology* 9:e1002848.

Zhou JF, Yuan WJ, Chen D, Wang BH, Zhou Z, Boccaletti S, Wang Z (2019) Synaptic modifications driven by spike-timing-dependent plasticity in weakly coupled bursting neurons. *Physical Review E* 99:1–6 Publisher: American Physical Society.

Ziegler L, Zenke F, Kastner DB, Gerstner W (2015) Synaptic consolidation: From synapses to behavioral modeling. *Journal of Neuroscience* 35:1319–1334.

Zucker RS, Regehr WG (2002) Short-term synaptic plasticity. *Annual Review of Physiology* 64:355–405.

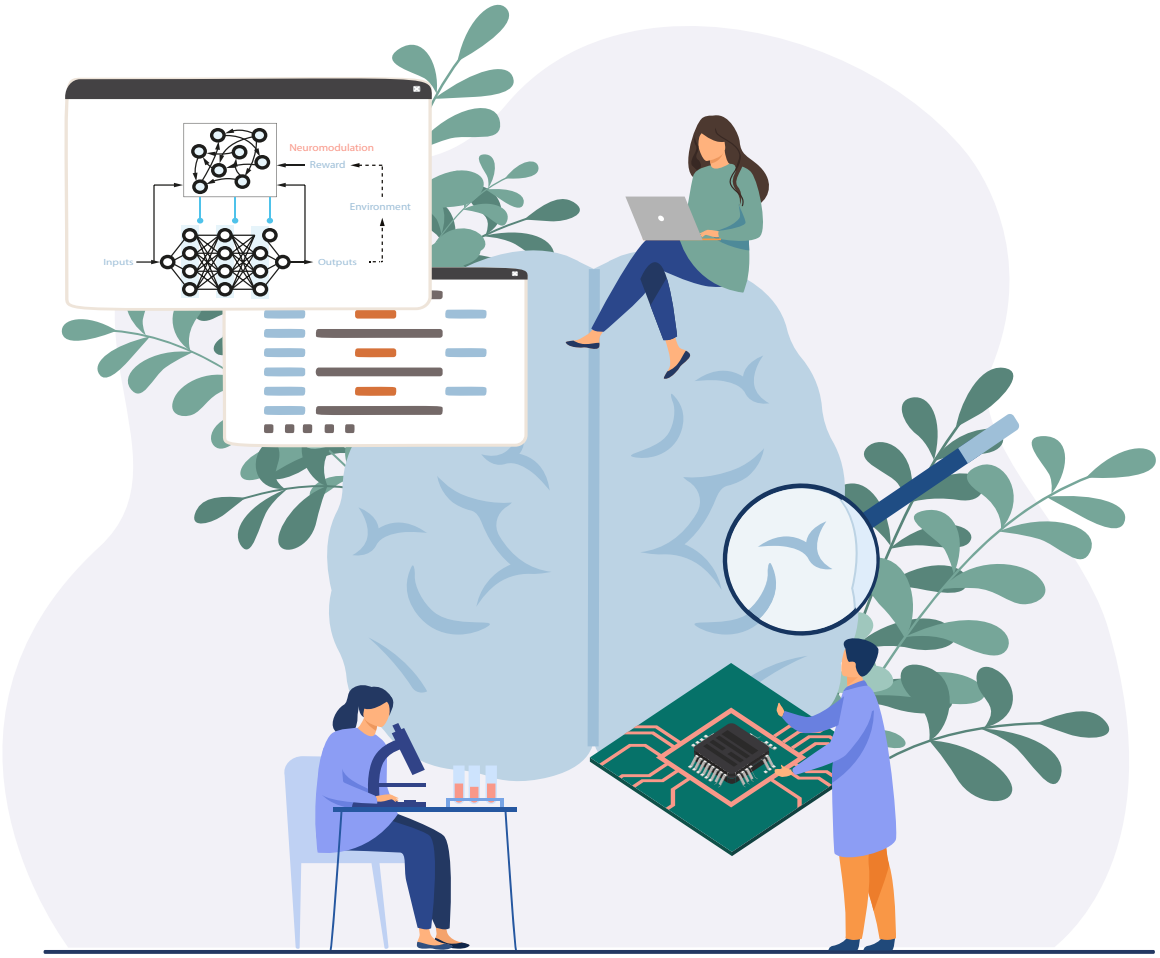
Neuromodulation
Reward
Environment
Inputs
Outputs